New Functional Poly(2-alkyl-2-oxazoline)s and Alternatives to PEG in Protein Stabilization

Zur Erlangung des akademischen Grades eines

DOKTORS DER NATURWISSENSCHAFTEN

(Dr. rer. nat.)

Karlsruher Instituts für Technologie (KIT)

Fakultät für Chemie und Biowissenschaften

genehmigte

DISSERTATION

von

Gabriela Gil Alvaradejo

aus

Mexico City, Mexico

Referent: Dr. Guillaume Delaittre

Korreferent: Prof. Dr. Patrick Théato

Tag der mündlichen Prüfung: 16.04.2018

Die vorliegende Arbeit wurde im Zeitraum von Oktober 2014 bis April 2018 unter Anleitung von Dr. Guillaume Delaittre und Prof. Dr. Christopher Barner-Kowollik am Karlsruher Institut für Technologie - Universitätbereich angefertigt.

Hiermit bestätige ich wahrheitsgemäß, dass ich die vorliegende Arbeit im Rahmen der Betreuung durch Dr. Guillaume Delaittre und Prof. Dr. Christopher Barner-Kowollik selbstständig verfasst und keine anderen Quellen und Hilfsmittel als die angegebenen verwendet habe. Wörtlich oder inhaltlich übernommene Stellen sind als solche kenntlich gemacht und die Satzung des Karlsruher Instituts für Technologie (KIT) zur Sicherung guter wissenschaftlicher Praxis wurde beachtet. Des Weiteren erkläre ich, dass ich mich derzeit in keinem weiteren laufenden Promotionsverfahren befinde und keine vorausgegangenen Promotionsversuche unternommen habe.

Karlsruhe

Gabriela Gil Alvaradejo

Dedicated to my family

"Happiness can be found in the darkest of times,

if one only remembers to turn on the light."

-Albus Percival Wulfric Brian Dumbledore

Abstract

Synthetic polymers represent a versatile class of biomaterials applied for tissue engineering, drug delivery, and biosensors. Among the polymer systems developed, polyethylene glycol (PEG) is the gold standard in the field thanks to its excellent biocompatibility, high water solubility, and low toxicity. Despite its popularity, health concerns originating from the presence of PEG antibodies in humans have increased the interest in alternative polymers for biomedical applications. Among these, poly(oligo(ethylene glycol) methyl ether methacrylate) (POEGMA), poly(*N*-acryloyl morpholine) (PNAM), and poly(2-alkyl-2-oxazoline)s (PAOx) were investigated in the present thesis.

The first two parts of the thesis describe the α- or ω-end chain functionalization of PAOx during initiation or termination of the cationic ring-opening polymerization (CROP) of 2-ethyl-2-oxazoline (EtOx). In Chapter 3, new nosylate initiators were synthesized and used to obtain maleimide- or thiol-functional PAOx. After respective optimization of the reaction conditions, well-defined polymers with molar masses relevant for either bioconjugation to a model protein or surface patterning were obtained from the synthesized initiators. Chapter 4 describes the synthesis of the first PEtOx-based macromonomers (MM) for ring-opening metathesis polymerization (ROMP) to develop a metal-free PEtOx-based MRI probe. PEtOx MM were obtained by termination of the CROP of EtOx with norbornene moieties. Bivalent alkyne-PEtOx MM were functionalized with a paramagnetic nitroxide**,** used as MRI contrast enhancement agent, by CuAAC click reaction. The synthesis of bottlebrush polymers and BASPs from linear and nitroxide-functionalized PEtOx MMs by graft-through ROMP was carried out with nearly quantitative conversion. The new PEtOx-based MRI probe showed an improved transverse relaxivity (r_2) of up to ∼13.5 times higher when compared to common nitroxides, indicating potential for further development as an alternative to the previously reported PEG-based MRI probes.

In the last part of the thesis, a method to evaluate the influence of polymer type, molar mass, and conjugation degree on the physicochemical properties of polymer-conjugated lysozyme

was developed. Low molar mass (3 kDa) mono-conjugates (both PNAM and POEGMA) showed an increased or equal activity to that of the native protein, combined with an increased equilibrium solubility in high salt concentrations at pH 3 compared to native lysozyme. $POEGMA_{7.5kDa}$ showed the highest increase in solubility of all tested conjugates, but also a minimal activity (less than 10%). The results obtained indicate that depending on the desired application for the conjugate, a compromise should be found between enhanced solubility and activity. The high-throughput method developed allows the potential extrapolation to assess the physicochemical properties of other available biocompatible polymers.

Zusammenfassung

Synthetische Polymere stellen eine vielseitige Klasse von Biomaterialien dar, die im Bereich des Tissue Engineering, der Wirkstoffabgabe und Biosensoren eingesetzt werden. Unter den entwickelten Polymersystemen stellt Polyethylenglykol (PEG) dank seiner ausgezeichneten Biokompatibilität, hohen Wasserlöslichkeit und geringen Toxizität den (Gold)Standard auf diesem Gebiet dar. Trotz seiner Popularität haben gesundheitliche Bedenken, aufgrund der Anwesenheit von PEG-Antikörpern bei Menschen, das Interesse an alternativen Polymeren für biomedizinische Anwendungen erhöht. Zwei von ihnen sind Poly(oligo(ethylen glykol)methylethermethacrylat) (POEGMA), Poly(*N*-acryloylmorpholin) (PNAM) und Poly(2-alkyl-2-oxazolin) (PAOx) welche in der vorliegenden Arbeit untersuchtwurden.

Die ersten beiden Kapitel der Doktorarbeit beschäftigen sich mit der α- oder ω-Endkettenfunktionalisierung von PAOx während der Initiierung oder Terminierung der kationischen Ringöffnungspolymerisation (CROP) von 2-Ethyl-2-oxazolin (EtOx). In Kapitel 3 wurden neue Nosylat-Initiatoren synthetisiert und verwendet, um PAOx mit Maleimid- oder Thiolfunktionalität zu erhalten. Nach entsprechender Optimierung der Reaktionsbedingungen wurde aus den synthetisierten Initiatoren wohldefinierte Polymere erhalten, dessen Molmassen entweder für eine Biokonjugation an ein Modellprotein oder eine Oberflächenstrukturierung relevant sind. Kapitel 4 beschreibt die Synthese einer ringöffnenden Metathese-Polymerisation (ROMP), die erstmalig auf PEtOX Makromonomeren (MM) basiert, für die Entwicklung einer metallfreien PEtOx-basierten Magnetresonanztomographie-Sonde (MRT). PEtOx-MM wurden durch Terminierung der CROP von EtOx mit Norbornen erhalten. Bivalente Alkin-PEtOx-MM wurden mit dem paramagnetischen Nitroxid, das als MRT-Kontrastverstärkungsmittel verwendet wurde, durch CuAAC im Rahmen der Click-Chemie funktionalisiert. Die Synthese von „Bottlebrush“-Polymeren und BASPs aus linearen und Nitroxid-funktionalisierten PEtOx-MM durch graft-through ROMP wurde mit nahezu quantitativem Umsatz durchgeführt. Die neue PEtOx-basierte MRT-Sonde wies eine verbesserte transversale Relaxivität (r_2) von bis zum ca. 13-Fachen im Vergleich zu Nitroxid CP-3 auf, was auf

eine mögliche Weiterentwicklung als Alternative zu den bisher beschriebenen PEG-basierten MRT-Sonden hinweist.

Im letzten Kapitel der Arbeit wurde eine Methode zur Bestimmung des Einflusses von Polymertyp, Molmasse und Konjugationsgrad auf die physikalisch-chemischen Eigenschaften von PNAM- und POEGMA-konjugiertem Lysozym entwickelt. Der Satz von Monokonjugaten mit niedriger Molmasse (3 kDa) (sowohl PNAM als auch POEGMA) zeigte eine erhöhte oder gleiche Aktivität zu der des nativen Proteins, kombiniert mit einer erhöhten Gleichgewichtslöslichkeit in hohen Salzkonzentrationen bei pH 3 im Vergleich mit nativem Lysozym. $POEGMA_{7.5kDa}$ zeigte den höchsten Anstieg der Löslichkeit aller getesteten Konjugate, aber auch eine minimale Aktivität (weniger als 10%). Abhängig von der gewünschten Anwendung des Konjugats sollte ein Kompromiss zwischen erhöhter Löslichkeit und Aktivität gefunden werden. Die entwickelte Hochdurchsatzmethode erlaubt die mögliche Extrapolation andere verfügbare biokompatible Polymere zu bewerten.

Contents

1

Introduction

The use of synthetic polymers to develop biomaterials such as scaffolds for tissue engineering, drug-delivery vehicles, or biomedical sensors, has encountered significant advance during the last decades.[1–3] Polyethylene glycol (PEG) is the most widely investigated polymer system and the gold standard in the field. PEG exhibits a number of excellent properties such as biocompatibility, high water solubility, and low toxicity and immunogenicity.[4] Thanks to its approval by the Food and Drug Administration (FDA) as food additive and in medicine, PEG has been widely used not only as drug carriers, but also for the fabrication of implants, as tablet surface coatings, and for daily use products such as oral hygiene products and cosmetics.[5–8] The popularity of this polymer has led not only to research on further biomedical applications, but also deeper understanding of the side effects PEG has on the human body. For instance, cases of hypersensitivity and allergic reactions to PEG have been reported with increasing frequency.[9] Immunogenicity studies show that PEGylated proteins can induce the formation of PEG antibodies.[10–12] In fact, in 2009, antibodies against PEG were found in 25% of healthy blood donors, compared to 0.2% only 20 years before.[13] This can be attributed to the better detection methods recently developed, but also to the large exposure of humans to PEG. Another

controversial aspect is the non-biodegradability of PEG, that can result in accumulation in the body as vacuoles in organs such as kidneys, liver, or spleen.[14]

Unequivocally, PEG has the advantage of decades of research, and a number of PEGylated drugs already in the market to back it up.[15] However, the findings on adverse side effects of PEG have increased the interest in alternative polymer systems that could serve in the biomedical field.[13,16] In addition, recent advances on polymerization techniques provide the possibility to develop polymer systems with tunable properties by careful selection of (co)monomers, the availability of a number of functionalization strategies, and access to different architectures with well-defined polymer sizes, as well as the possibility to obtain narrow dispersities.[17–20] Among the pool of hydrophilic biocompatible polymers already being investigated are poly(amino acid)s,[21] poly(oligo(ethylene glycol) methyl ether methacrylate) (POEGMA),[22–24] poly(*N*-acryloyl morpholine) (PNAM),[25] polyglycerol (PG),[26] poly(*N*-(2-hydroxypropyl)methacrylamide) (PHPMA),[27] poly(vinylpyrrolidone) (PVP),[28] and poly(2-alkyl-2-oxazoline)s (PAOx).[29] Among these, PAOx, POEGMA, and PNAM are of utter relevance for the development of this thesis.

Although PAOx were first reported in 1966,[30–33] it is only in the last couple of decades that the interest in these polymers has increased, proved by an exponential growth in published reports and patents of PAOx with promising applications in biomedical fields. PAOx share some characteristics with PEG such as high solubility in water, biocompatibility, and low toxicity, but with the great advantage of synthetic versatility that comes from the polymerization mechanism.[34,35] PAOx are synthesized by living cationic ring-opening polymerization (CROP), which allows the tailoring of the properties of the resulting polymer depending on the choice of 2-oxazoline monomers, and the addition of functional groups at the α or ω end chains, depending on the initiator and terminating agent used.[36] The polymerization mechanism also allows the formation of random and block copolymers, and a variety of architectures, with well-defined polymer sizes and narrow distributions.[37] In the scope of the present thesis, a number of end-functionalized PAOx were synthesized taking advantage of the living CROP mechanism.

Chapter 3 describes the design and synthesis of maleimide- and thiol- α-functionalized PAOx, obtained using novel functional initiators for the CROP of 2-ethyl-2-oxazoline (EtOx) (**Figure 1**). The synthesis and characterization of the new initiators are presented, as well as kinetic studies of the polymerization of EtOx with the newly synthesized initiators. The resulting polymers were characterized to prove end-group fidelity and reactivity with model molecules. For each initiator, an application relevant to the potential of PAOx either as polymer-protein conjugate or as passivating materials for surfaces is presented.

Chapter 4 deals with the synthesis of new PAOx macromonomers for ring-opening metathesis polymerization (ROMP), to produce a new type of organic-radical based magnetic resonance imaging (MRI) contrast agent as alternative to PEG. The new macromonomers were developed using the termination step as a functionalization strategy to introduce either norbornene or dual norbornene-alkyne groups, for further functionalization (**Figure 1**). The macromonomers were characterized and used for the first time for the formation of bottlebrush polymers and brush-arm star polymers by ROMP. The reduction-resistant spirocyclohexyl nitroxide **chex**, which provides MRI contrast enhancement, was incorporated to the macromonomers by click reaction, resulting in a PAOx-based metal-free MRI probe. Relaxivity studies were carried out to test its potential use as an alternative to already existing PEG-based MRI probes.

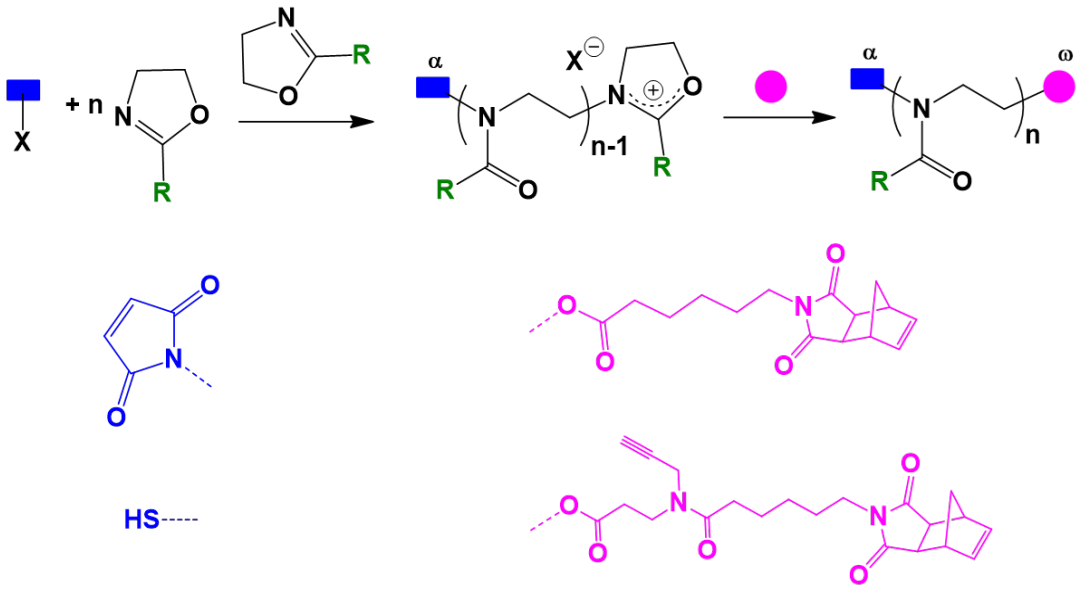

Figure 1. General strategies for the functionalization of PAOx and aim of the project.

Chapter 5 describes the synthesis and conjugation of the biocompatible polymers POEGMA and PNAM to a model protein, for the evaluation of the influence of a series of parameter on the physicochemical properties of the resulting conjugates. The conjugation of polymers to proteins, generally brings advantages such as better solubility and longer circulation times *in vivo*. However, there is no available tool to evaluate the influence of parameters such as polymer type, molar mass, or the number of chains attached to the conjugate on physicochemical properties. Here, sets of POEGMA and PNAM of different molar masses were synthesized, characterized, and conjugated to lysozyme. A systematic assessment of the effects of polymer size and conjugation degree on aggregation behavior, solubility, and remaining activity was performed (**Figure 2**).

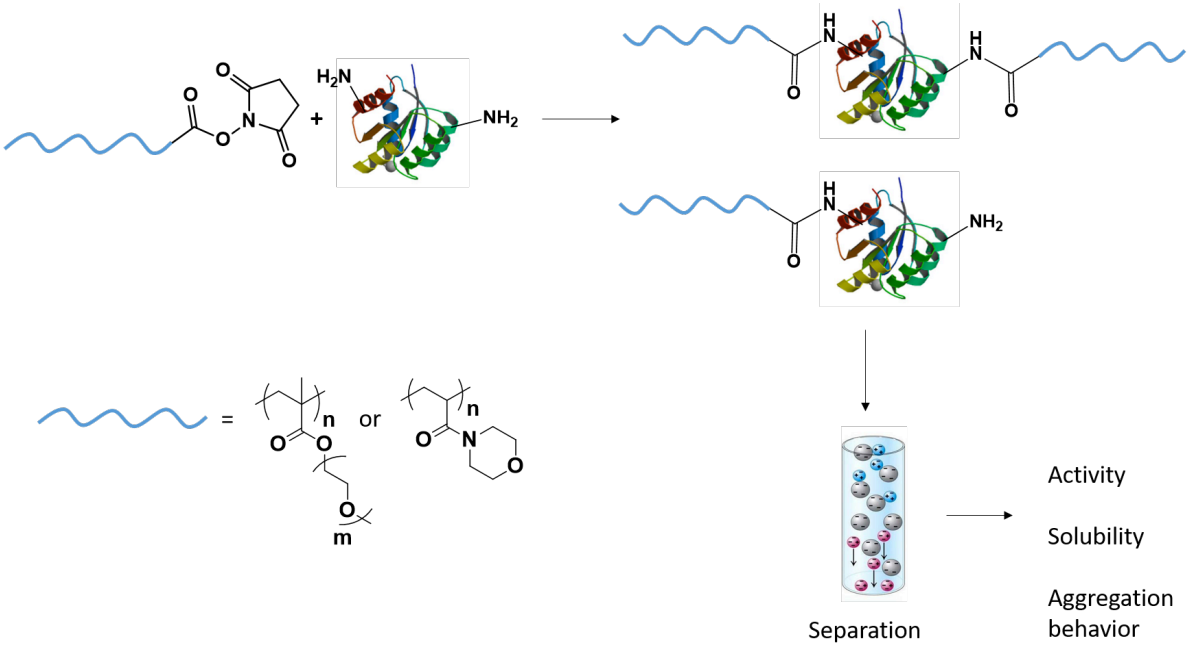

Figure 2. Strategy for the formation of polymer-protein conjugates and its separation for high-throughput screening of physicochemical properties.

2

Theory and Background

2.1. Biocompatible polymers: Poly(ethylene glycol) and alternatives

Synthetic biocompatible polymers enable the development of materials for modern biomedical applications such implants, biosensors, drug delivery, gene therapy, and regenerative medicine.[3,38] To achieve this, stimuli-responsive polymers, water-soluble polymers, or polymer conjugates have to be developed.[39] Considering the advances on living polymerization techniques, it is possible to obtain highly defined materials with the necessary functionalities for the desired application.

Polymers for drug delivery are used in a number of ways, including the formation of drug complexes by direct attachment to the pharmaceutical active,[40] lipid-polymer conjugates to become part of the liposomal delivery system,[41] or nucleic acid-polymer complexes attached via cationic interactions.[42,43] These polymer carriers provide a shielding effect on the drug to avoid fast recognition by the immune system and clearance from the body. The suppression of interactions with blood components in the body is known as the stealth effect.[44,45] Other advantages of the use of a polymer for conjugation include protection against degradation by enzymes, an increased solubility in water, and selective tumor accumulation.[46]

Structural parameters of the polymer, such as molar mass and dispersity have an influence on the biological and stabilizing effects of the polymer carrier, affecting biocompatibility and stealth behavior.[47] For instance, a low dispersity (*Đ*) is desired for most biomedical applications since it provides the homogeneity necessary to ensure reproducibility in body-residence time and immunogenicity.

Examples of synthetic biocompatible polymers tested for drug-delivery applications include poly(ethylene glycol) (PEG),[48] polylactic acid (PLA),[49] polysialic acid (PSA),[50] *N*-(2-hydroxypropyl) methacrylamide (HPMA),[27] polyglutamic acid (PGA),[21] and polyvinylpyrrolidone (PVP).[28] Among these, poly(ethylene glycol) (PEG) is the most widely used non-ionic, hydrophilic polymer with stealth behavior. PEG is considered the gold standard in polymer-based biomedical applications. Despite its success, it has relevant limitations that have recently raised concerns regarding its use, and there is an ongoing search for potential synthetic polymer alternatives.[3,47]

In this section, a description of the main characteristics of PEG will be addressed, as well as the main raised concerns of its use in therapeutics. Examples of synthetic polymers that have shown potential to be alternatives to PEG in biomedical applications will be given.

2.1.1. Advantages and disadvantages of PEG

PEG is the most studied and applied synthetic polymer in the biomedical field. Among the many advantages of PEG claimed so far are its nontoxicity and low immunogenicity.[51] In addition, the anionic polymerization of ethylene oxide can provide defined polymers with narrow dispersities showing $Đ < 1.1$. Its high solubility in both organic and aqueous solvents make end-group modifications possible while at the same time ensuring biocompatibility.[47]

In 1977, the first covalent attachment of PEG to bovine serum albumin (BSA) and liver catalase was reported.[52] It was found that the attachment of the polymeric chain increased the circulation time in blood vessels and decreased the immunogenicity of the proteins, while retaining the activity of the enzymes. PEG conjugates show high water solubility, physical and

thermal stability, reduced aggregation, less immunogenicity, and long storage capability.[44] Pharmacokinetic studies of PEG in humans have shown that gastrointestinal absorption of PEG decreases as the molar mass increases, with excretion in humans of 85% and 96% in 12 h after intravenous injection of 1 g of 1 kDa and 6 kDa PEG, respectively. Toxicology tests, carcinogen studies, and mutagen assays did not show adverse effects from low molar mass PEG.[53]

In 1990, Adagen was the first PEGylated protein to be approved by the FDA.[15] This conjugate is used for enzyme replacement therapy in the treatment of severe combined immunodeficiency disease. Over 40 years after the first PEGylation, a number of PEG conjugated proteins, DNA, RNA, and polypeptides have been developed, showing more stable and efficient performances when compared to using only to the pharmaceutical active. **Table 1** summarizes some of the FDA-approved PEG conjugates already available on the market.[54]

Table 1. Examples of FDA approved PEGylated drug carriers.

PEGylated protein	Molar mass	Protein name
Adagen	5 kDa	Adenosine deaminase
Cimzia	40 kDa	Antibody TNF
Neulasta	20 kDa	Filgrastim G-CSF
Oncaspar	5 kDa	*L*-asparaginase
PEGASYS	40 kDa	Interferon alfa-2a
PEG-INTRON	12 kDa	Interferon alfa-2b
Somavert	5 kDa	Human growth hormone receptor antagonist B2036
Krystexxa	10 kDa	Mammalian urate oxidase
Mircera	30 kDa	Continuous erythropoietin receptor activator

The mentioned characteristics make PEG useful for a number of applications besides drug carrier. PEG is currently used for blood and organ storage,[55] the fabrication of stents,[56] and as

excipient for nasal and ocular applications.[57] On daily use products, PEG can be found in shampoos, fragrances, cleansing agents, and contact lenses, among many others.

The large and continuous exposure to PEG in cosmetics, food processing, and pharmaceuticals that has taken place for a few decades now, has also lead to more findings regarding unfavorable side effects of PEG carriers.

The non-immunogenicity of PEG is one of the controversial aspects surrounding the use of PEG conjugates.[10] Studies have shown that the use of PEGylated proteins such as uricase, or ovalbumin, can induce the formation of antibodies against PEG (anti-PEG).[58] In the human body, the main consequence of anti-PEG presence is limiting the efficacy of the peptide, protein or drug used, or reducing the tolerance to the conjugate. However, keeping in mind that most proteins or drugs used are immunogenic themselves, the use of PEG can mask the immune system response to these therapeutics.[48] An important consequence of the constant exposure of humans to PEG for the last decades is evident in a study conducted in 2009, where in 25% of healthy blood donors PEG antibodies were found, whereas only 20 years before the occurrence was only 0.2%.[11]

The non-biodegradability of PEG is another disadvantage in biomedical applications. Control over the molar mass of the polymer dictates toxicity and excretion of the body.[59] For certain applications, the size requirements of the polymer include exceeding the renal clearance limit to increase the circulation time of the drug. However, the longer circulation of these polymers results in their excretion through the liver or deposition in other tissues, inducing the formation of vacuoles in the liver, kidneys, or spleen.[14] On the other hand, polymers below 400 Da are found toxic. These small size PEG chains can go through oxidative degradation by alcohol and aldehyde dehydrogenase and produce diacid and hydroxyl acid metabolites.[60]

The toxicity of the side products obtained during PEG synthesis is another concern. Both the remaining ethylene oxide of the polymerization, and 1,4-dioxane, the main side product, are considered carcinogenic in humans. Therefore, strict content limits of the mentioned compounds in PEG are required for biomedical applications.[47]

The described limitations have boosted efforts to find other potential polymers that can be used for therapeutics, either by addressing the disadvantages previously described, or by bringing additional benefits to the function of the formed conjugates. Some of the relevant results and possibilities of synthetic polymeric systems will be described in the following section.

2.1.2. Alternatives to PEG

2.1.2.1. Degradable polymers

Poly(glutamic acid) (PGA),[61] poly(hydroxyethyl-*L*-asparagine) (PHEA),[62] poly(hydroxyethyl-*L*-glutamine) (PHEG),[63] and poly(sarcosine) (pSar),[64] are some poly(amino acid)s currently being tested as alternatives to PEG (**Figure 3A-D**). The biodegradability of these polymers into their corresponding amino acids, which can then be metabolized in the body, represents the major advantage over other biocompatible polymers.[61,65,66] Out of the mentioned poly(amino acid)s, PGA has already been approved to use as thickener in food, wetting agent for cosmetics, and additive for fertilizers.[61] Importantly, a PGA conjugate for cancer treatment is currently on phase III of clinical trials. On preliminary studies, the paclitaxel-PGA conjugate showed high water solubility, improved safety, enhanced antitumor efficacy, and produced less side effects, when compared to native paclitaxel.[67]

Poly(oligo(ethylene glycol) methyl ether methacrylate) (POEGMA), a hydrophilic, PEG-based comb-like polymer, has been extensively studied for potential biomedical applications (**Figure 3E**). POEGMA can be synthesized by reversible-deactivation radical polymerization (RDRP) techniques such as atom transfer radical polymerization (ATRP), or reversible addition-fragmentation chain transfer (RAFT) polymerization. The resulting polymers not only present defined sizes and narrow dispersities, but can be modified to add special functionalities to the polymeric chain depending on the initiator or transfer agent used.[22–24] POEGMA has been grafted from model proteins using modified ATRP initiators in aqueous medium with high yields and low dispersities.[23,68,69] The resulting conjugates have the advantage of specificity on the

conjugation site (either *N* or *C* terminus). In addition, *in vivo* studies of the conjugates showed an increased circulation time of 15-50 times, as well as increased tumor accumulation when compared to the native protein.[13] POEGMA brushes are degradable, since these are linked through a methacrylate backbone, connected by ester bonds that are susceptible to hydrolysis and enzymatic breakdown.

Among other relevant degradable synthetic polymers studied as potential alternatives to PEG are poly(zwitterions), such as poly(carboxybetaine methacrylate) (PCBMA) and poly(sulfobetaine methacrylate) (PSBMA) (**Figure 3F-G**). Either as self-assembled monolayers, or as brush copolymers on surfaces, this type of polymers show protein resistant properties.[70,71] Conjugation of PCBMA to a model enzyme showed an increased stability similar to PEGylation, but with an improvement in the binding affinity.[72] This can be achieved thanks to the properties of zwitterionic polymers to regulate ionic structuring of water. By drawing water molecules away from hydrophobic regions of the protein, which is generally the catalytic site, protein-substrate interactions are enhanced. Similar to POEGMA, when the backbone of the polymer brushes studied is methacrylate-based, degradability is possible. However, the biocompatibility *in vivo* of the degradation products, e.g., polymethacrylic acid, should also be considered.

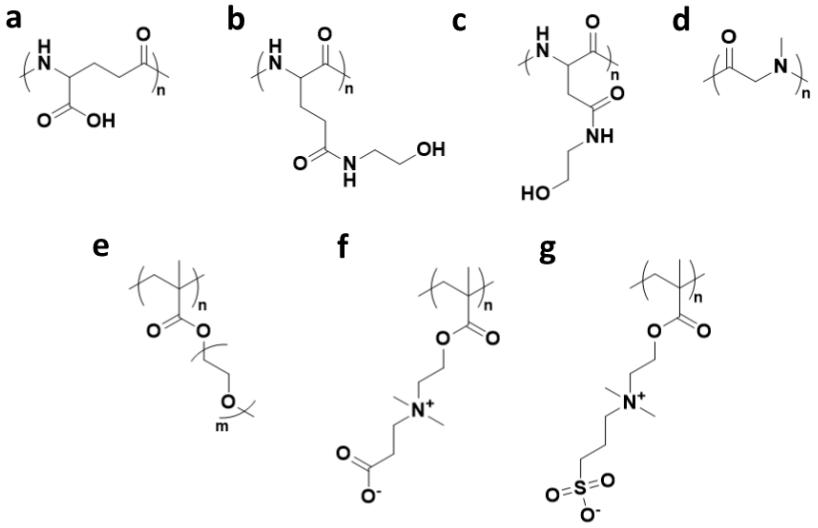

Figure 3. Structures of a) poly(glutamic acid) (PGA), b) poly(hydroxyethyl-*L*-glutamine) (PHEG), c) poly(hydroxyethyl-*L*-asparagine) (PHEA), d) poly(sarcosine) (pSar), e) poly(oligo(ethylene glycol) methyl

ether methacrylate) (POEGMA) f) poly(carboxybetaine methacrylate) (PCBMA), and g) poly(sulfobetaine methacrylate) (PSBMA).

2.1.2.2. Nondegradable polymers

Polyglycerol (PG) is structurally very similar to PEG and, as expected, its properties are also very similar, including an excellent biocompatibility (**Figure 4A**). However, PG also shares the disadvantage of non-degradability with PEG. An advantage of PG is the possibility to synthesize a number of architectures, including linear and hyperbranched polymers, with a wide range of defined molar masses and added functionalities.[26] A study of linear and hyperbranched PG showed superior blood and cell compatibility and longer circulation times from both PG architectures, when compared to PEG.[73] The first PG-protein conjugate was developed by grafting branched PG to the model protein BSA,[74] and since then conjugates using different architectures of PG have been reported. An activity comparison among linear, mid-functional, hyperbranched, and linear hyperbranched architectures conjugated to lysozyme, showed the linear PG conjugate showed the lowest remaining activity among the set of conjugates.[75]

Poly(*N*-(2-hydroxypropyl)methacrylamide) (PHPMA) is a non-toxic, neutral, hydrophilic, biocompatible polymer (**Figure 4B**).[76] It has been investigated for over four decades for biomedical applications, since its characteristics make it suitable for drug delivery. After the synthesis of well-defined PHPMA was reported,[77] the number of PHPMA-protein conjugates developed has been increasing. Promising conjugates include a 28 kDa PHPMA-doxorubicin copolymer and a 25 kDa PHPMA-platinate, which are already on clinical trials.[47]

Poly(*N*-acryloylmorpholine) (PNAM) is a bi-substituted acrylamide derivative with properties including solubility in water and other polar solvents, and low toxicity (**Figure 4C**). It has been synthesized by RAFT polymerization and modified for selective attachment to surfaces, as well as enzymes, showing a reduced immunogenicity.[78] For instance, drug-PNAM conjugates have been reported for doxorubicin and amoxicillin, although without further evaluation.[79] In addition, PNAM conjugation to the enzyme Candida lipase resulted in conjugates with a higher

solubility in organic solvents and higher remaining activity when compared to its reported PEG analogue.[79]

Polyvinylpyrrolidone (PVP) is a commercially available polymer, already used for a wide range of applications including adhesives, coatings, photoresists, photography, and textiles (**Figure 4D**).[47,80] Until recently, PVP was synthesized by free radical polymerization. The possibility to synthesize defined molecular weight PVP with narrow dispersities opened a number of possibilities for pharmaceutical applications.[81] PVP has been tested for drug-delivery systems, where it has shown increased circulation time, as well as higher solubility and stability towards denaturation.[82]

Poly(2-alkyl-2-oxazoline)s (PAOx) are synthetic polymers which have gathered increasing popularity in the last couple of decades, especially in the biomedical field (**Figure 4E**). The interest in PAOx comes from their versatility, since properties such as solubility and thermoresponsiveness can be tuned depending on the 2-alkyl substituent selected.[36,37] Another advantage of PAOx over PEG is the easy access to copolymers, allowing the introduction of functional groups on the side chain.[35] Poly(2-methyl-2-oxazoline) (PMeOx) and poly(2-ethyl-2-oxazoline) (PEtOx) are the most popular PAOx, thanks to their high water solubility, biocompatibility, and non-cytotoxicity.[34] Despite the very recently renewed interest in PAOx, the first PEtOx conjugate for treatment of Parkinson's disease already entered phase II of clinical trials.[83] A more detailed description of the polymerization mechanism, different approaches to functionalization, and recent advances of its use on biomedical research will be addressed in the following section.

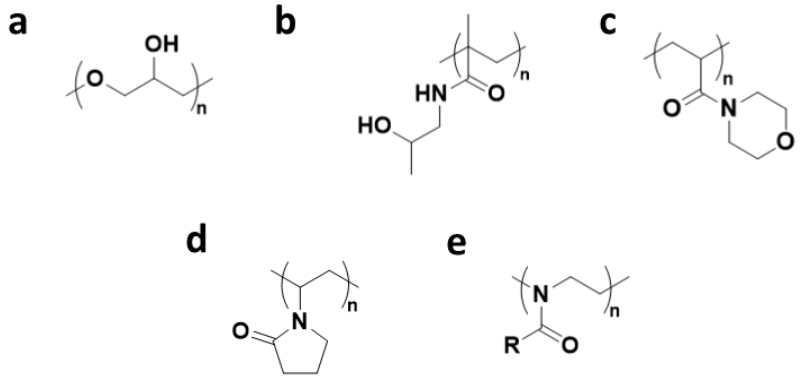

Figure 4. a) Polyglycerol (PG), b) poly(*N*-(2-hydroxypropyl)methacrylamide) (PHPMA), c) poly(*N*-acryloylmorpholine) (PNAM), d) poly(vinylpyrrolidone) (PVP), and e) poly(2-alkyl-2-oxazoline)s (PAOx).

2.2. Poly(2-oxazoline)s

The synthesis of poly(2-alkyl/aryl-2-oxazoline)s (PAOx) by polymerization of 2-oxazolines was first described in the 1960s by four independent groups.[30–33] However, it is only in recent years that interest in these polymers has rapidly increased, thanks to their potential biomedical applications[29,34,84,85] and the thermoresponsive properties of certain PAOx.[86,87] Particularly, PMeOx and PEtOx share properties such as biocompatibility, low toxicity, and anti-fouling behavior with PEG, the gold standard for stealth polymers.[88,89]

PAOx are a type of synthetic polyamides with a structure that is isomeric to natural peptides,[90] and are therefore considered pseudo polypeptides (**Figure 5**).

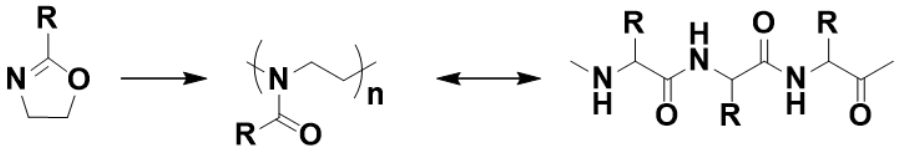

Figure 5. Structures of 2-alkyl-2-oxazoline, its corresponding polymer, and a polypeptide.

2.2.1. Cationic ring-opening polymerization of 2-oxazolines

PAOx are prepared by cationic ring-opening polymerization (CROP). This type of polymerization enables access to polymers with functional end groups by the utilization of functional initiators or terminating agents, as well as block copolymers by the sequential addition of different monomers.[91] The versatility of this method allows the preparation of well-defined polymers with tunable properties. The CROP of 2-oxazolines follows a chain-growth polymerization mechanism, where the main steps are initiation, propagation, and termination, as shown in **Scheme 1**.

Under the appropriate conditions, the CROP of 2-oxazolines can proceed in a living manner, which means that no chain transfer or undesired termination should occur during the

polymerization.[36] To achieve this living character, the purity and dryness of all components of the system is of utter importance.

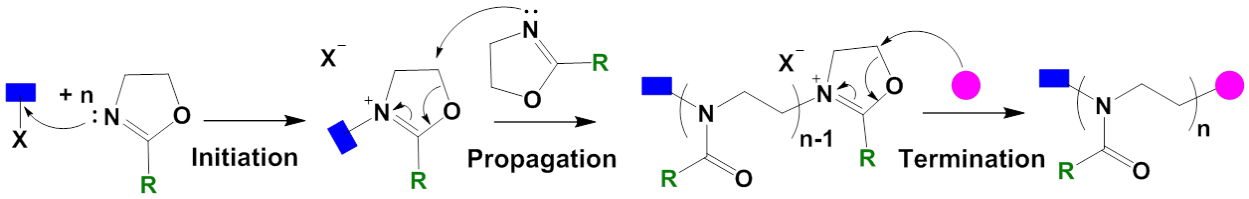

Scheme 1. General mechanism of the cationic ring-opening polymerization of 2-alkyl-2-oxazolines.

The initiation step occurs by a nucleophilic attack of the cyclic imino ether to the electrophilic initiator resulting in the formation of an oxazolinium cation (**Scheme 1**). When initiation is incomplete or slow, it leads to a deviation of the desired first-order kinetics. This results in broad molar mass distributions and high dispersities.[36] The CROP of 2-oxazolines has been reported using a variety of initiators including Lewis acids such as boron trifluoride, trihalogenobismuthine,[92] and zirconium/tris(pentafluorophenyl)borate; alkyl esters such as tosylates,[18] triflates,[18] nosylates;[19] and halides including chlorides,[16] bromides,[16] and iodides.[17] Some of the most commonly used initiators are alkylating agents, such as methyl triflate, methyl tosylate, methyl iodide, and benzyl bromide. Among these possibilities, methyl tosylate is the most popular and preferred initiator for the CROP of 2-oxazolines due to its higher stability, low price, and commercial availability. When modifying the initiator, alkyl tosylates may show slow initiation, and in these cases it is best to use an alternative counter ion. Although triflates provide the fastest initiation when compared to tosylates and nosylates, its inherent instability, along with a problematic synthesis and purification become a relevant disadvantage.[93] In such cases, nosylates become a more suitable possibility for the design of functional initiators due to their stability and easier synthesis.

The propagation step occurs in a two-step fashion (**Scheme 2**). The first (and rate determining) step is the addition of the first monomer to the product of initiation ($k_{p,1}$). After that, the propagation rate constant (k_p) increases dramatically because of a neighboring, intra-molecular

dipole-ion polarization effect that results in the stabilization of the transition state.[94] The k_p for the CROP of 2-oxazolines depends on a number of parameters such as monomer structure, monomer concentration, solvent used, and temperature.[95,96] Optimized conditions for the CROP of 2-oxazolines are 140 °C in acetonitrile using a microwave reactor. At this temperature, it was shown that theoretical and experimental values of molecular weight were almost perfectly close.[97] However, microwave irradiation is not necessary, and similar results can be obtained using superheated conditions in pressure reactors or flow reactors.[98,99]

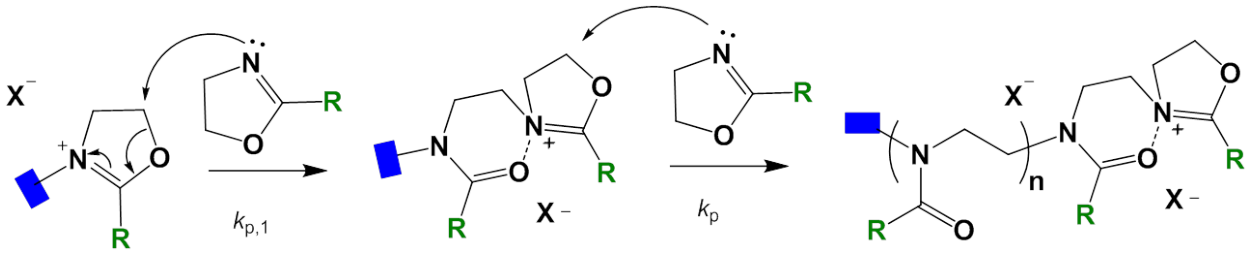

Scheme 2. Propagation mechanism for the CROP of 2-oxazolines.

As previously mentioned, one of the conditions of a living polymerization is that no side reactions occur. For the CROP of 2-oxazolines, however, two possible chain transfer reactions are known to happen (**Scheme 3**).[100] The main side reaction is a β-elimination process, with an imine-enamine rearrangement that results in the formation of two species: a proton-initiated oxazolinium cation, and an enamine ether-terminated polymer chain. The second possible chain transfer reaction is only relevant at higher conversion, where the enamine ether-terminated chain can act as nucleophile leading to chain coupling and the formation of branching points.[101] The main problem with the proton-initiated oxazolinium cation created during chain transfer is the creation of a new growing center. More growing chains present result in lower molar mass polymers. This additional and unwanted polymer population can be detected using mass spectrometry, for example. It has been reported that chain transfer constants are 200 to 800 times smaller than propagation constants, depending on the conditions and monomer used.[94] This means chain transfer occurs at a much slower rate than propagation, and low dispersities, as well as end group fidelity, are still achievable.

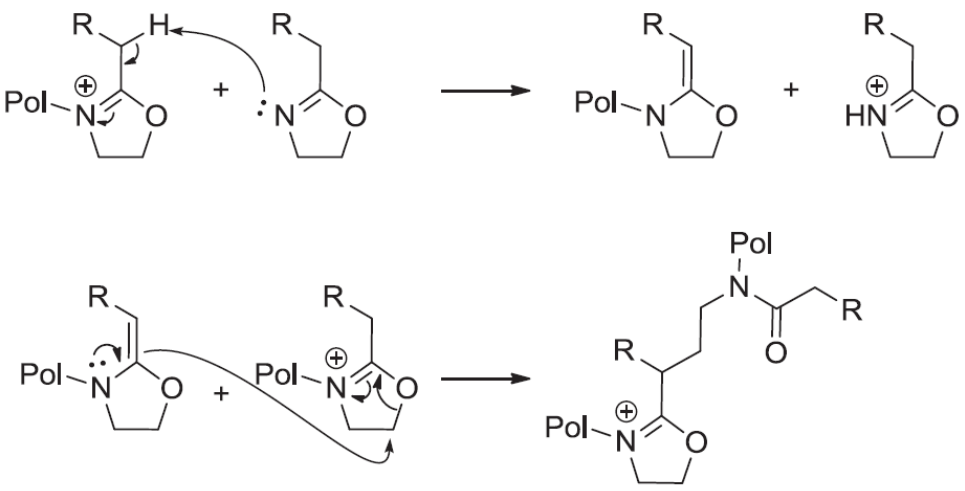

Scheme 3. Chain transfer reaction via β-elimination. Top: enamine-functionalized chain and a proton-initiated growing center. Bottom: Coupling of a living polymer chain to an enamine-functionalized chain. Adapted from reference 36 with permission from Elsevier.

To terminate the polymerization, a nucleophilic agent is required to stop the propagation of the oxazolinium ion (**Scheme 4**). There are two possible termination mechanisms: the attack on the 2-position of the oxazolinium ring that yields the kinetic product, or the nucleophilic attack on position 5, which is thermodynamically controlled.[102,103]

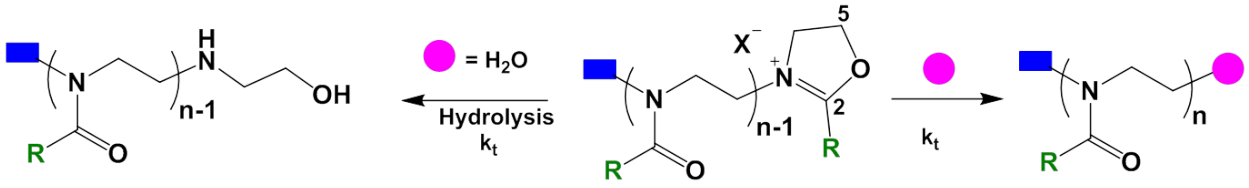

Scheme 4. Termination possibilities for the CROP of 2-oxazolines. Left: Kinetic product obtained by termination with water. Right: Thermodynamic product by nucleophilic attack on position 5.

Terminating agents based on oxygen, nitrogen, and sulfur are normally used. One of the most widely used terminating agent is water, that attacks on the 2-position of the oxazolinium ions to form an amine ester end group that is then hydrolyzed to afford the hydroxyl-terminal

kinetically controlled product.[104] An alternative strategy for the introduction of a primary alcohol end group is the use of a methanolic potassium or sodium hydroxide solution, which gives the termination on the 5-position.[105] The nucleophilic character of amines makes them suitable for the termination reaction, as well. Primary, secondary, and tertiary amines, as well as ammonia and azides have been reported to terminate the polymerization.[106–109] Although the use of some amines can possibly terminate more than one chain per terminating agent, this can be suppressed using a large excess of the terminating molecule. Aniline,[110] long aliphatic amines,[108] derivatives of piperidine,[111] piperazine,[112] pyrrole,[113] among others have been reported as terminating agents for PAOx. Carboxylic acids such as maleic acid,[114] glutaric acid,[115] cinnamic acid,[116] among others have also been used to terminate the CROP of 2-oxazolines,[43,117,118] as well as sulfur-based derivatives such as sodium thiolates, that introduce terminal carboxylic acid end groups.[119]

2.2.2. Functionalization of poly(2-oxazoline)s

Depending on the desired application for the polymer, it is possible to tune a number of parameters. Physical properties, architecture, size, added functionalities, among other properties, can be modified to achieve the established goal. The versatility of PAOx allows the use of different functionalization strategies, whether that means modifying end groups or the side chain. Examples of these strategies are described in the following section.

2.2.2.1. Functional initiators

A relevant advantage of the polymerization mechanism is that during initiation, an α-terminal functionality can be incorporated into the PAOx chains using a functional initiator. The desired functionality needs to be compatible with the CROP of 2-oxazolines to provide fast initiation and ensure the living character of the polymerization. Otherwise, protection strategies for the functionality can be utilized.

A number of initiators bearing functional moieties been reported. Among these functionalities are allyl[120] and alkyne groups,[121] for the possibility to introduce functional blocks by click reactions. For instance, an α-alkyne PMeOx was used to form graft copolymers of poly(ε-caprolactone)-*graft*-poly(2-MeOx) by copper-catalyzed azide–alkyne cycloaddition (CuAAC) for potential application as drug carriers.[122] Initiators that add amine,[123] hydroxyls,[124] or carboxylic acid based on esters,[125] and other specific functionality to the polymeric chain allow for further functionalization. Other types of initiators introduce functionality by structure, containing moieties such as lipids, porphyrins, or saccharides.[35,85] Some examples of functional initiators are shown in **Figure 6**.

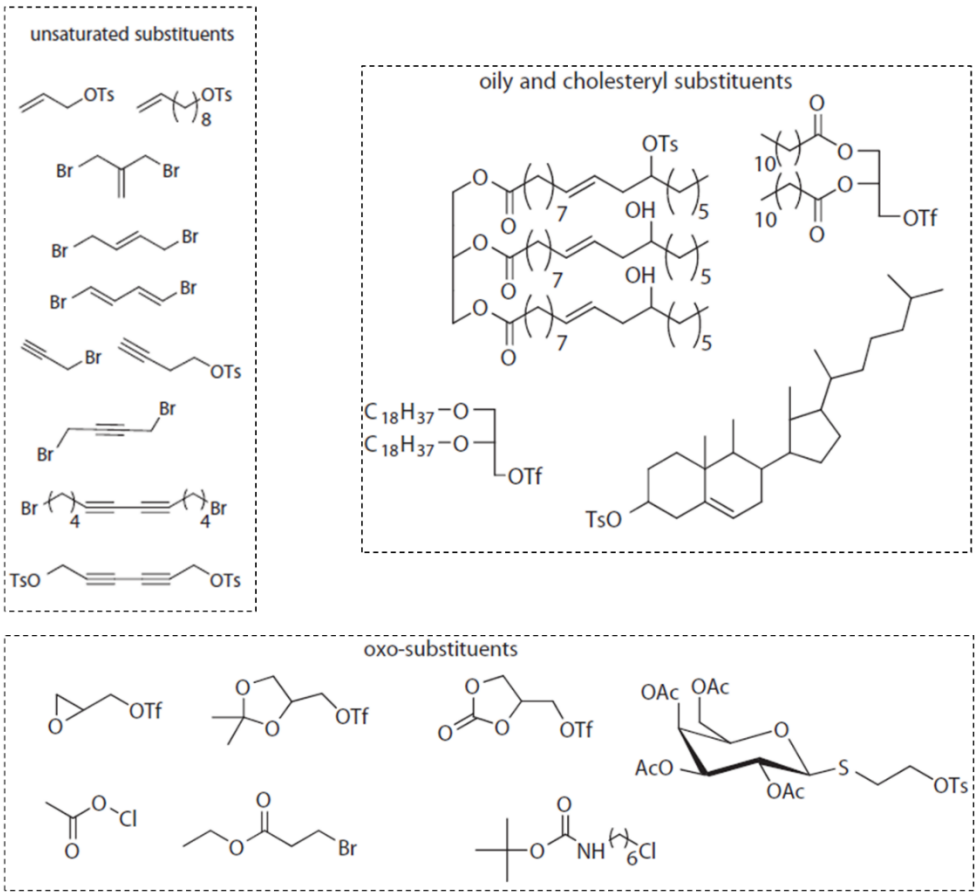

Figure 6. Functionalized initiators for the CROP of 2-alkyl-2-oxazolines (Adapted from reference 92 with permission from John Wiley and Sons).

An initiator with antimicrobial activity (*N,N*-dimethyldodecylammonium bromide) was also used for the polymerization of MeOx, proving that the PAOx system can be used as an alternative to PEGylated antimicrobial polymers.[126] The one-step synthesis of amphiphilic block copolymers with narrow molar masses was done using a dual RAFT-CROP initiator 4- cyano-4-(dodecylthiocarbonothioylthio)pentyl-4-methylbenzenesulfonate (CDPS).[127] This dual initiator allows the possibilities to tune the hydrophobic block depending on the monomer used, keeping a biocompatible hydrophilic PEtOx block. Functional initiators also open the possibility to synthesize polymers with different architectures. For example, a tetratosylate initiator, with a porphyrin core was synthesized and used to produce well-defined star-shaped PEtOx.[128]

Many common end-chain functionalization methods make use of the ω end chain, since incompatible functionalities can be added once the polymerization is over. However, the use of functional initiators brings the advantage that ideally one functional group will initiate one polymeric chain, and there is no need to add an excess of the functional moiety. In addition, functional initiators can give direct access to heterotelechelic PAOx, when combined with an appropriate termination strategy.

2.2.2.2. Functionalization of the R-group

The choice of R-group of the 2-alkyl-2-oxazoline has an impact on the solubility, mechanical properties, and thermal properties of the resulting polymer. The possibility to tune the properties of the polymer based on the type of monomer used, along with the use of R functional pendant groups is one of the most important advantages of PAOx over PEG.[92]

Hydrophilicity can be tuned depending on the size of the R substituent used. PMeOx and PEtOx are the most popular monomers for biomedical applications, since both are very hydrophilic. By increasing the length of the R groups or using aromatic groups, the hydrophobic character of the resulting polymer is increased.

In general terms, the lower critical solution temperature (LCST) of PAOx depends on a) the molar mass, and b) the addition of comonomers to influence the balance of hydrophobicity and

hydrophilicity.[129–131] Finely tuned LCSTs can be obtained by the random or gradient copolymerization of monomers with different R groups. For instance, a study varying the composition and molar mass of three different 2-oxazoline monomers, with either ethyl, isopropyl, or *n*-propyl side chains, whose homopolymer exhibits a different LCST (60 °C, 36 °C, and 24 °C, respectively),[132–134] showed that it is possible to obtain a range of LCSTs from 24 °C to 97 °C, depending on the molar mass and composition of the polymer system.[135,136] These copolymers could potentially be used in biomedical applications for the preparation of thermosensitive bioconjugates.

The addition of unsaturated monomers such as 2-isopropenyl-2-oxazoline,[137] 2-(9-decenyl)-2-oxazoline,[138] soy-based 2-oxazoline,[139] and 2-oxazolines bearing cycloaliphatic R-side chains and aromatic systems have been reported.[140–143] Monomers that bear nitrogen-containing groups on the pendant chain such as azetidinyl, azepanyl, piperidine, 1-azocanyl, 1-morpholine, 1-pyrrolidinyl, and pyrrolidonylethyl have also been reported.[144–146] Hydroxyl- end groups on the pendant chains can be obtained using esters or acetals as protecting groups.[147,148] Modified 2-oxazolines with polystyrene or poly(ethylene oxide) as the R group can be used as macromonomers for the synthesis of graft copolymers.[149,150]

Taking advantage of the possibility to directly copolymerize 2-ethyl-2-oxazoline with functional side chain monomers such as 2-methoxycarbonylethyl-2-oxazoline,[151] that can be easily modified to add bioactive molecules (or other specific groups), creates the possibility to develop functional biocompatible polymers, such as drug carriers or conjugates.[83]

2.2.2.3. Functional terminating agents

During the termination step, a variety of functionalities can be added on the ω-chain end. Adding a functionality during termination has the advantage that the addition of groups that are not compatible with the polymerization mechanism is possible, since these are added at the end of the reaction.

Some functional terminating agents include silane-containing amines for surface functionalization,[152,153] sodium azide,[107] and hexynoic acid[154] for click reactions. Carboxylate derivatives to add polymerizable end groups such as styrenics,[155] acrylates,[156] and methacrylates[118] have also been reported for the synthesis of macromonomers for graft copolymerization by free radical polymerization (**Figure 7**).

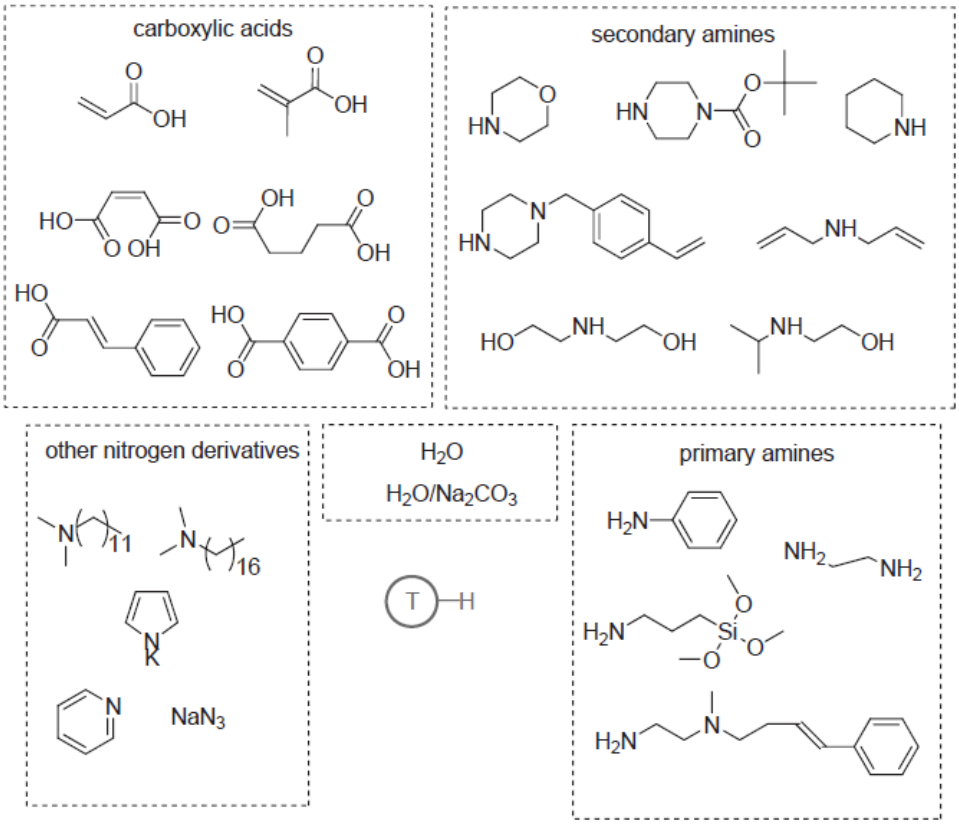

Figure 7. Terminating agents for the CROP of 2-alkyl-2-oxazolines (Adapted from reference 92 with permission from John Wiley and Sons).

Other examples of functional terminating groups, such as carboxylic acid-containing RAFT agents, or norbornene, transform PAOx into macromonomers for the synthesis of graft copolymers.

2.2.3. Poly(2-oxazoline)s as biomaterials

A number of PAOx have already been studied to use as drug carriers in the form of polymer-protein conjugates,[119,157] polymer-drug conjugates,[83] or polymeric micelles.[158,159] PAOx hydrogels for tissue engineering, and PAOx grafted onto surfaces to obtain a protein and cell repelling effect have also been developed. Currently, PEtOx is approved by the FDA, yet only as an indirect food additive. However, recently, the first PAOx-drug conjugate entered phase II clinical trials. Although the necessary *in vivo* research has to verify the safety of PAOx in the human body, the amount of available data gathered in such relatively short amount of time provides promising results.

Poly(2-oxazoline)s, as homopolymers or copolymers, have been conjugated to a number of proteins, giving similar resulting properties as PEG conjugates.[119,157] An extensive study, made by Veronese and coworkers, compared the biological and chemical properties of PAOx, and its conjugates with model proteins, to the PEG analogues.[43] Three monomers with different R groups were used (methyl, ethyl, and propyl), with hydroxyl or carboxylic acid end groups for further functionalization via activation with *p*-nitrophenylchloroformate, disuccinimidylcarbonate, or *N*-hydroxysuccinimide. In all cases, as expected, defined polymer sizes with narrow distributions were produced and functionalized for protein conjugation. The repeatability and ease of functionalization of the polymer were highlighted, and the lower viscosity shown in all PAOxs, compared to PEG. Important finding of this study include a lower immune response by the PAOx conjugates (**Figure 8**, right), a similar activity, and better pharmacokinetics as observed from longer circulation times of the PAOx-conjugate *in vivo* (**Figure 8**, left).

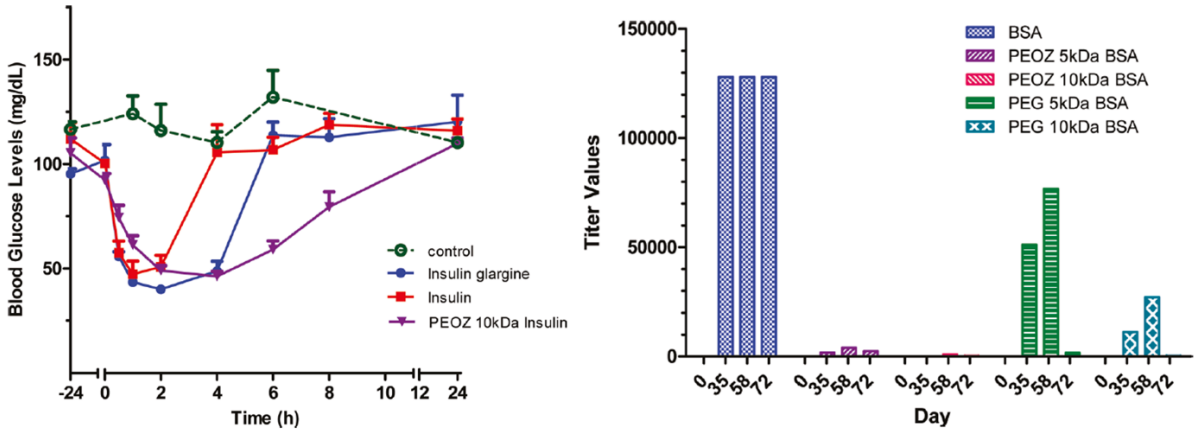

Figure 8. Left: Effect of subcutaneous injection of insulin, insulin glargine, and 10kDa PEtOx-insulin on the blood glucose levels in male Sprague–Dawley rats. Right: Relative immunogenicity of BSA, PEG-BSA, and PEtOx-BSA in rabbits, measured by anti-BSA antibody levels. Adapted from reference 43. Copyright 2018 American Chemical Society.

Polymer-drug conjugates represent a strategy to increase the solubility of drugs in water, as well as to improve the drug pharmacokinetics.[160] Although the number of PAOx-drug conjugates is reduced, compared to PEG, a significant advance has been achieved. A very recent and relevant report was the development of the first anti-cancer drug-PAOx conjugate.[83] In this study, taking advantage of the living character of the CROP of 2-oxazolines, copolymers of mainly 2-ethyl-2-oxazoline and the functional 2-methoxycarboxyethyl-2-oxazoline, terminated with methanolic ammonia were synthesized with defined molar masses and narrow distributions. The selected anti-cancer drug, doxorubicin, was loaded using an acid-degradable hydrazone linker attached to the functional side chain (**Figure 9**). Additionally, a radiolabel was attached after functionalization of the ω-chain end. *In vivo* experiments in mice showed prolonged blood circulation, increased tumor accumulation and enhanced antitumor efficacy of the PEtOx conjugate. An *in vivo* comparison to the PHPMA-doxorubicin analogue, did not show substantial differences in biodistribution and antitumor efficacy. This report is a clear example of the versatility of the synthesis of PAOx, and the possibility of tuning the properties of the system depending on the desired application.

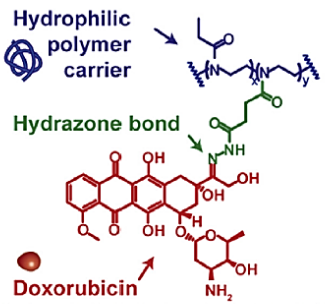

Figure 9. Structure of the studied PEtOx-doxorubicin conjugate. Adapted from reference 83 with permission from Elsevier.

Polymeric micelles based on PAOx have also been used as effective delivery systems for anti-cancer drugs. Micelles with a hydrophilic PEtOx shell and hydrophobic drug core (doxorubicin) for controlled released by pH changes have been developed.[158] In another contribution, a pH-sensitive copolymer of poly(2-ethyl-2-oxazoline)-*b*-poly(*D*,*L*-lactide) was used to load the hydrophobic drug paclitaxel into the micellar core by non-covalent hydrophobic interactions.[159] In both cases, the drug-loaded micelles demonstrated effective antitumor effect *in vivo* over the free drug, also showing low toxicity.

The functionalization of surfaces is another approach to tackle biomedical challenges. Biofouling of proteins, cells, or bacteria on surfaces represents a major problem in devices such as stents, catheters, and joint implants, among many others. Coatings provide a stealth effect to these materials, making the surface undetectable by the organism and preventing infections.[161] PEtOx has been photo-immobilized on surfaces widely used in analytical devices such as silicon wafers, glass slides, and Au films.[162] The protein-resistant properties of the films were evaluated by treatment with BSA, providing the expected repealing effect.

The exceptional properties of PAOx, such as biocompatibility, high stability, structural and functional diversity, along with the possibility to obtain high controlled and defined polymers, make this class of polymers an attractive option to develop biomaterials and polymer therapeutics. Over the last 20 years, publications and patents of PAOx for biomedical applications have exponentially increased, positioning this polymeric system as an emerging alternative to PEG.

2.3. Living ring-opening metathesis polymerization

Ring-opening metathesis polymerization (ROMP) is a powerful and broadly applicable method for the synthesis of macromolecular materials with unique architectures and useful functions. The origin of ROMP can be traced to 1955, when the first carbon-carbon double bond rearrangement reaction in polymerization of norbornene, catalyzed by titanium, was reported by Anderson and Merckling.[163] About ten years later, this metal-catalyzed redistribution of carbon-carbon double bonds was named olefin metathesis.[164] Initially, olefin metathesis was regarded as an odd reaction, but since then it has been established as one of the most powerful transformations in chemical synthesis of a wide variety of useful products, both in industry and academia.[165,166] The development of defined catalysts enabled the synthesis of a wide range of polymers with complex architectures and useful applications.[167]

In this section, a description of the ROMP mechanism will be provided, as well as a brief history of a variety of relevant catalysts that have been used for olefin metathesis.

2.3.1. Mechanism

ROMP is a chain-growth polymerization that converts cyclic olefins into linear polymers containing olefinic bonds in the main chain as shown in **Figure 10**. The polymerization mechanism is based on a metal-mediated carbon–carbon (C–C) double bond exchange processes.[168] Contrary to other olefin addition polymerizations, in ROMP the unsaturation of the monomer is conserved as it is converted to a polymer.

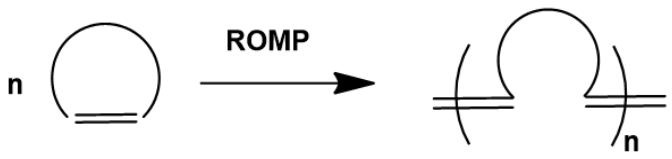

Figure 10. The general ROMP reaction.

In 1970, Chauvin proposed the commonly accepted ROMP mechanism, illustrated in **Scheme 5.**[169] The initiation step involves the coordination of a cyclic olefin to a metal alkylidene complex. A [2+2] cycloaddition produces a metallacyclobutane intermediate that forms the beginning of a growing polymer chain. This intermediate undergoes cycloreversion to obtain a new metal alkylidene. As monomers are incorporated to the chain, the size of the resulting complex increases. Despite the size increase, its reactivity toward cyclic olefins remains similar to the initiator. Thus, during propagation, analogous steps are repeated until either a) all monomer is consumed, b) a reaction equilibrium is reached, or c) the reaction is terminated. ROMP is commonly quenched by the addition of a reagent, e.g. ethyl vinyl ether (EVE), which reacts with the metal carbene species of the growing polymer chain end, and removes the metal from the polymer.[170,171]

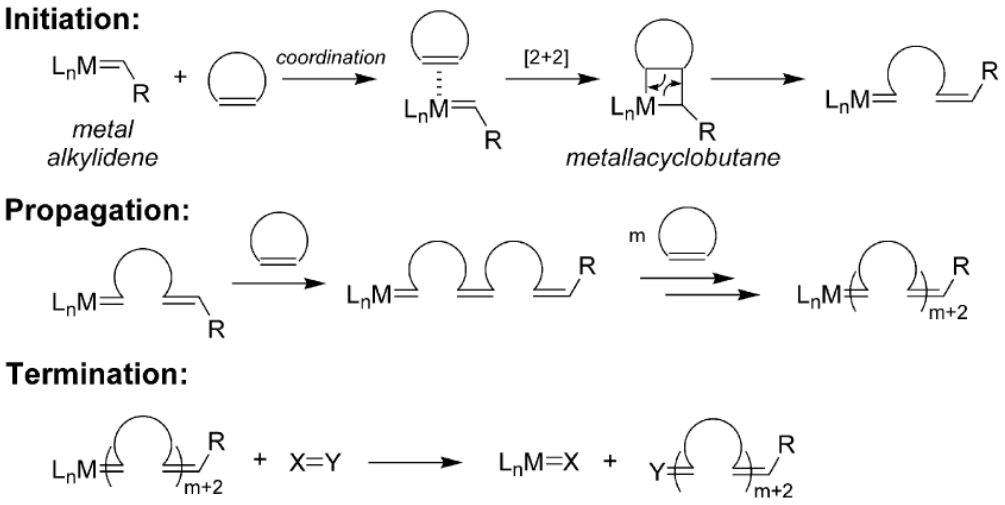

Scheme 5. General mechanism of the ROMP reaction (Adapted from reference 170 with permission from Elsevier).

In addition to the general ROMP mechanism already illustrated in **Scheme 5**, inter and intramolecular chain-transfer reactions can occur, also considered secondary metathesis reactions (**Scheme 6**).[170,167] In an intermolecular chain transfer, a polymer chain that contains the active metal alkylidene on its terminus, can react with an olefin along the backbone of another polymer chain. This intermolecular reaction keeps the number of polymer chains

unchanged, however, there is a change in molar mass of the individual chains involved in the reaction. The intramolecular chain-transfer reaction, also known as backbiting, occurs when the active terminus of a polymer chain reacts with itself to form a cyclic polymer chain with a reduced molar mass. Overall, both types of chain-transfer reactions broaden the molar mass distribution of the system.

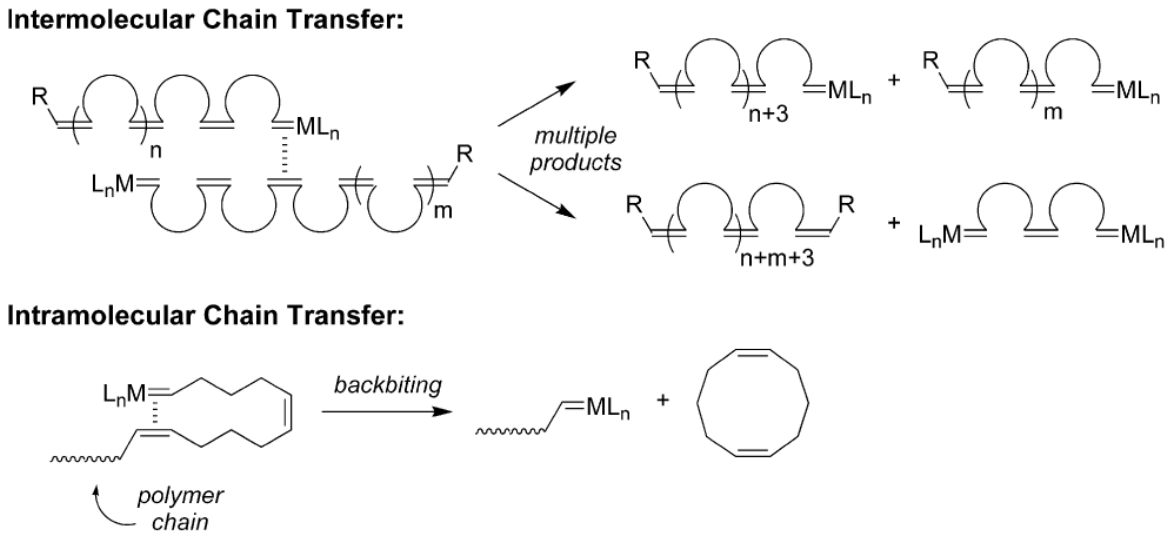

Scheme 6. Secondary metathesis reactions in ROMP. (Adapted from reference 170 with permission from Elsevier).

The ROMP reaction is driven by a decrease in entropy that comes from the release of strain of the cyclic olefin as it goes from monomer to polymer. Strained cyclic olefins that do not contain bulky groups around the double bond are commonly used as monomers for ROMP (**Figure 11**). These include cyclobutene, cyclopentene, cis-cyclooctene, and norbornene. All of these have a degree of strain > 5 kcal mol^{-1}.[172] Cyclohexene, for instance, has a lower ring strain, which makes it an exception of polymerizable monomers by ROMP. Norbornene and its derivatives are the most commonly used monomers due to their high reactivity for ROMP, and relatively easy functionalization for further applications.

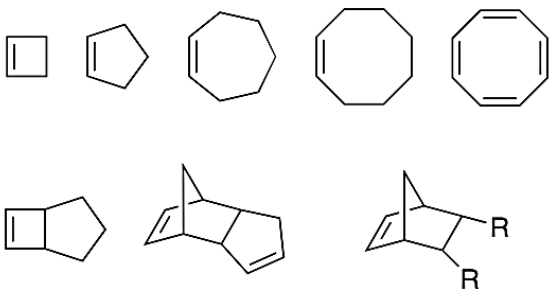

Figure 11. Examples of ROMP monomers.

2.3.2. Catalysts

The requirements of a living polymerization include the rapid consumption of initiating species, a linear relation between the degree of polymerization and monomer consumption, and low dispersities (*Đ*).[173] Evidently, the catalysts developed for ROMP must satisfy these conditions. Progress on the development of metal-based catalysts has led to catalyst systems that exhibit fast initiation kinetics, reduce the occurrence of intramolecular or intermolecular chain transfer reactions, show solubility in a wide range of organic (or even aqueous) solvents, show stability towards air, moisture, and some organic functional groups, and can be used at room temperature. These advances are the result of decades of research dedicated to the development of robust catalytic systems suitable for olefin metathesis.

Since the discovery of olefin metathesis many decades ago, extensive work was put to identify, isolate, and characterize the key intermediates involved in the metathesis, metal-carbene complexes and metallacyclobutanes.[168] The first reported catalysts were based on mixtures of a range of transition metals. A heterogeneous catalyst mixture of Ti and W halides with Al co-catalysts was used to obtain a high molar mass polymers from norbornene for the first time.[174,168] Soon after, the development of homogeneous catalyst systems that polymerized a wider variety of monomers (i.e. cyclobutene, cycloheptene, cyclooctene, and norbornene), showed the potential of this type of polymerization to synthesize new macromolecules.[175,176] These first investigations required demanding conditions (e.g. moisture- and air-free), and did not completely satisfy the living polymerization conditions.

Single-component catalysts allowed for the first time the possibility to define the relation between structure and reactivity. Catalyst systems that provide a living character to ROMP are developed based on titanium, tantalum, tungsten, molybdenum, or ruthenium.[177] Titanium-based catalysts were the first to add a living character to the polymerization,[178] also providing the possibility to add functional end groups during initiation and termination,[179] and the formation of block copolymers.[180] However, its low reactivity soon focused the attention on the more reactive tantalum-based catalysts. For instance, a tantalum-based catalyst with bulky, electron-rich ligands was used to successfully polymerized norbornene to high conversion with dispersity values below 1.1.[181,182] Despite these advances, the high oxidation state and reactivity towards functional groups with heteroatoms and carbonyls limited the living character of the ROMP reaction.

A significant advance was made by Schrock in the preparation of tungsten and molybdenum catalysts.[183–185] Especially relevant, the molybdenum-based alkylidenes, shown in **Figure 12** brought advantages such as a relatively simple synthesis and higher stability towards decomposition.[185] Importantly, these catalysts were tolerant to monomers containing a variety of functionalities including amide, ketal, cyano, ester, trifluoromethyl, halogen, and imide groups, and were able to provide stereoregular polymers. The activity of these catalysts could be tuned through modification of the alkoxide ligand. Fluorinated derivatives, for example, showed increased activities and were found to rapidly isomerize 2-pentene and other acyclic olefins.[186] It was also found that molybdenum-based catalysts are able to polymerize a wider range of cyclic olefins with varying degrees of ring strain and functionality such as norbornene, cyclopentene, cyclobutenes, and cyclopropenes.[187,188] The great disadvantage of these catalysts is the high oxophilicity of the metal center, which makes it sensitive to oxygen and moisture.

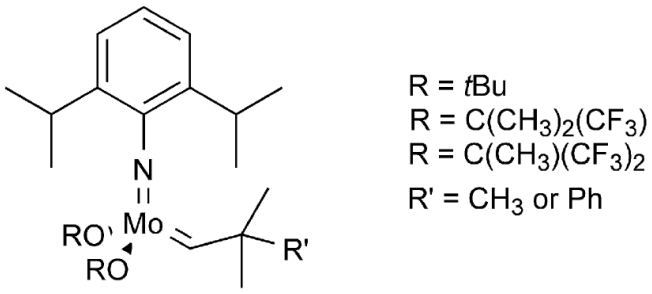

Figure 12. Molybdenum-based alkylidenes (Adapted from reference 170 with permission from Elsevier).

The field of olefin metathesis was for a really long time dominated by the Schrock catalysts, until another breakthrough was made by Grubbs in 1992, when he synthesized a group of Ru-based catalysts with unique properties (**Figure 13**).[189,190] The first generation of this catalyst system, Grubbs 1 or G1, allowed the polymerization reactions to happen in the presence of oxygen, but with the disadvantage of a lower activity compared to Schrock's catalysts. The change of one of the phosphine ligands in G1 for an *N*-heterocyclic carbene produced the second generation Grubbs catalyst, G2. In this case, Grubbs 2 has a higher tolerance to functional groups when compared to G1, but with a rather slower initiation. The 3rd generation of Grubbs catalysts contains strongly ligating *N*-heterocyclic carbenes with weakly coordinating pyridines. These catalysts display extremely high activities and fast initiation kinetics. A wide range of monomers can be polymerized with this catalyst resulting in polymers with low dispersities. Additionally, the catalyst can initiate metathesis in the presence of alcohol, water, and carboxylic acids, and is also stable in air.

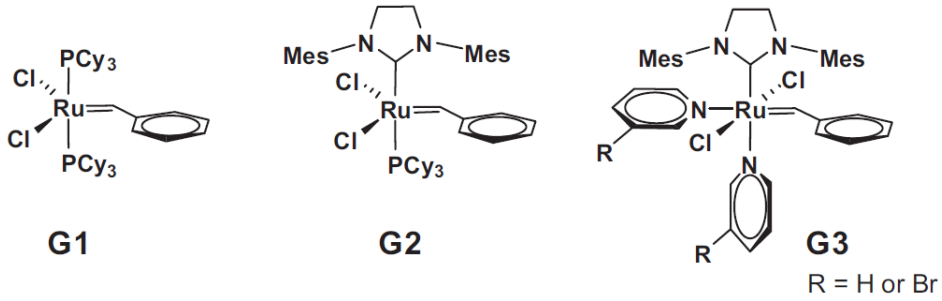

Figure 13. Ruthenium-based ROMP catalysts (Adapted from reference 191 with permission from Elsevier).

2.3.3. Applications of polymers synthesized by ROMP

ROMP is capable of producing functionally diverse and structurally complex polymers from a diverse range of monomers through the implementation of well-defined catalysts. The architectures of polymers synthesized using ROMP generally fall under four broad categories: linear, cross-linked, branched, and dendritic.[192] The wide range of polymers that can be synthesized with unique architectures and useful functions make ROMP a relevant tool in industry, as well in academia, in fields like life sciences, optics and electronics, sensors, or energy storage.[167,193]

ROMP can be used to synthesize defined bioactive polymers with structural features optimized for the biologically relevant applications. The developed polymers have diverse functions, including inhibitors of receptor–ligand interactions, novel drug delivery agents, innovative imaging agents, and incisive mechanistic probes of multivalent interactions.[193–198]

The nanoscopic size and multivalence of bottlebrushes, bivalent bottlebrushes, and dendronized polymers synthesized using a graft-through ROMP make them attractive for *in vivo* drug delivery applications.[3,199] For instance, a bivalent-brush polymer for use in chemotherapy delivery reported by the Grubbs group was synthesized by graft-through ROMP of poly(ethylene glycol) (PEG) based macromonomers (MMs) that were loaded with photo cleavable anticancer drugs doxorubicin (DOX) and camptothecin (CT) (**Figure 14**).[194] The graft-through ROMP approach has the advantage that it ensures that the weight percentage of drug loaded onto the brush polymers is the same as the weight percentage of drug on the MM.

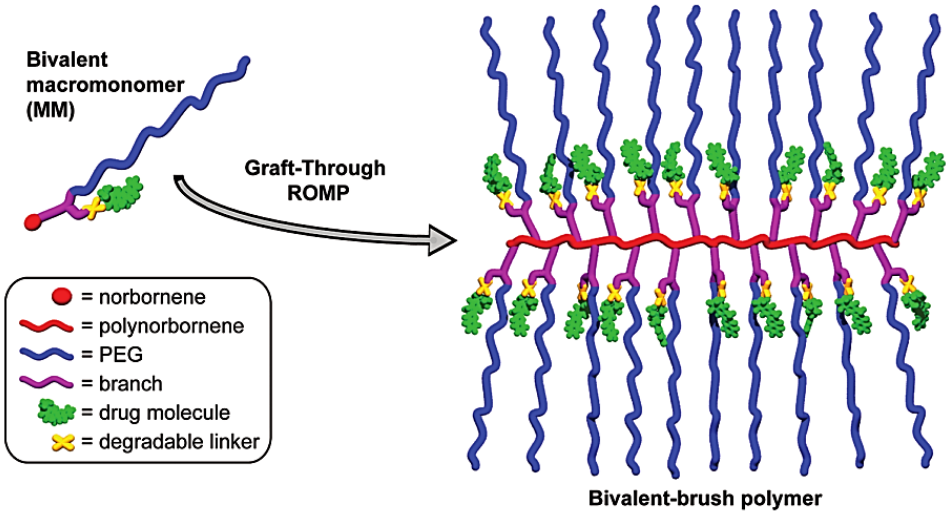

Figure 14. Bivalent macromonomer and bivalent-brush polymer. Adapted from reference 194. Copyright 2018 American Chemical Society.

In diagnostic imaging, for example, polymers can exhibit enhanced sensitivity. The relaxivity of an MRI contrast agent can be augmented through its incorporation into a polymer.[200,201] Likewise, polymers can bear many copies of an imaging agent, which can lead to signal enhancement. ROMP is an ideal polymerization method for this purpose because it can give rise to polymers with multiple sites that can be simultaneously functionalized with contrast agents, or targeting probes. In 2006, a monomer for ROMP that also functions as a portion of a Gd^{III} chelating moiety for an MRI contrast agent was developed.[196] An increase in relaxivity per Gd^{III} was shown upon transition from monomer to polymer, and extremely large molecular relaxivities were achieved through incorporation of multiple Gd^{III} ions per polymer. In another contribution, the Johnson group reported a metal-free nitroxide-based MRI probe that showed increased relaxivity per nitroxide (up to 44 times higher) compared to common nitroxides, higher stability, and low toxicity.[197] The probe was synthesized by ROMP of functionalized branched PEG macromonomers containing the nitroxide, to form brush-arm star polymers (BASP) (**Figure 15**). The particular architecture of the BASP, with a dense layer of nitroxides at the interface of a rigid polyacetal core and a hydrophilic PEG shell, resulted in the improved performance for MRI.

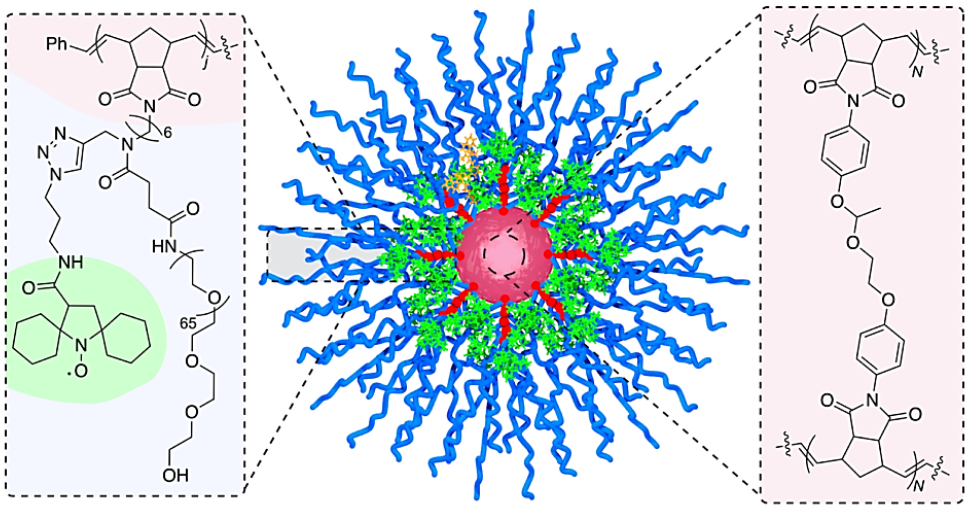

Figure 15. Schematic representation of a PEG-based MRI probe synthesized by ROMP. Branched macromonomers functionalized with a nitroxide are combined with an acetal crosslinker (Adapted from reference 197).

Another relevant application of polymers synthesized by ROMP is its use to mimic the molecular architecture and activity of natural antimicrobial peptides (NAP). NAPs are one of the first compounds produced after an infection, and vital components of the immune system. The natural amphiphilicity of antimicrobial peptides was mimicked using ROMP copolymers made of amphiphilic oxanorbornene-capped macromonomers (**Figure 16**).[195] Through ROMP, the hydrophilic and hydrophobic components were varied independently, which produced an extensive library of antibacterial polymers.

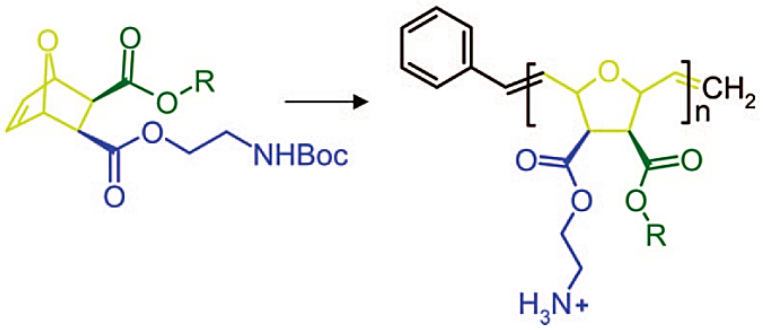

Figure 16. The synthetic approach allows the combination of a hydrophilic (blue), a hydrophobic (green), and a polymerizable (yellow) part of the monomer, producing an extensive library of antimicrobial polymers. Adapted from reference 195. Copyright 2018 American Chemical Society.

Applications of polymers synthesized by ROMP are providing new materials for understanding and tuning biological responses. Further advances in ROMP will undoubtedly fuel new and imaginative applications of bioactive polymers.

2.4. Radical polymerization

Radical polymerization is generally used for the commercial production of high molar mass polymers, due to its ability to polymerize a wide variety of monomers on flexible conditions at an industrial scale.[19] However, the lack of control on the architecture of the produced polymer was a disadvantage for many years. The development of reversible-deactivation radical polymerization (RDRP) led to the possibility to synthesize advanced materials with precise control of the molecular architecture.[202] In this section, an overview on free radical polymerization, and three approaches to control radical polymerization will be given.

2.4.1. Free-radical polymerization

Free-radical polymerization is the chosen method for many industrial applications due to its ability to polymerize a large variety of monomers (e.g. acrylates, methacrylates, acrylamides, methacrylamides, styrenes, dienes, and vinyl monomers), its tolerance to many functional groups and reaction conditions, and the relative simplicity to implement this process compared to other technologies.[20]

The mechanism of free-radical polymerization involves a chain polymerization, where initiation occurs by radicals, formed by an initiator, added to the monomer. Subsequent addition of monomer units to the radicals formed occurs, until the propagating radicals react with each other, terminating the reaction (**Scheme 7**). In conventional radical polymerization, the process involves polymer chains continuously forming, propagating, and terminating. These chains grow for 5–10 s before terminating.[20] At early stages of the polymerization, high molar mass chains are formed, and as conversion progresses, the molar mass will decrease due to monomer depletion. In the end, the size and distribution of the resulting polymers are determined by statistical factors, where dispersity is broad ($Đ > 1.5$).[203]

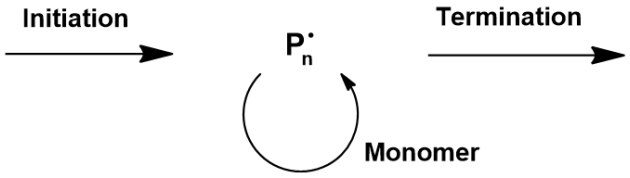

Scheme 7. Free radical polymerization mechanism.

2.4.2. Reversible-deactivation radical polymerization (RDRP)

For over two decades after its discovery in 1956 by Szwarc,[204] anionic living polymerization was the only example of a living polymerization process. After its discovery, it facilitated major developments in synthetic polymer chemistry with advantages that included the high degree of control over the macromolecular structure, particularly, the molar mass distribution, composition, and architecture. However, living anionic polymerizations present demanding reaction conditions such as the use of ultrapure reagents, and high vacuum to minimize traces of moisture and air.

One of the most relevant contributions in polymer science was the development of RDRP, the general name for a family of pseudo-living radical polymerization techniques. In a living polymerization, in general, all chains should initiate at the beginning of the reaction, and grow at the same rate, without the occurrence of chain transfer reactions or termination, by establishing an equilibrium between active and dormant species.[91]

In RDRP, the propagating species is a free radical, and there is a dynamic equilibrium between active radicals and dormant species (**Figure 17**). The success of this polymerization is based on the decrease of irreversible termination by having the propagating polymer chains in the dormant state most of the time. This can be achieved using reagents that react with the propagating radicals by reversible deactivation or reversible chain transfer. Contrary to conventional radical polymerization, the lifetime of active chains in RDRP is much lower, allowing a rapid shift in the equilibrium from dormant to active species. As a result of this equilibrium, all chains grow at the same rate throughout the polymerization, which means the

molar mass increases linearly with conversion, resulting in polymers with predetermined degree of polymerization and narrow molar mass distribution.[20]

RDRP is of particular interest in the synthesis of advanced architectures such as block copolymers, comb-shaped polymers, multi-armed polymers, cyclic polymers, telechelic polymers, and gradient copolymers.[17]

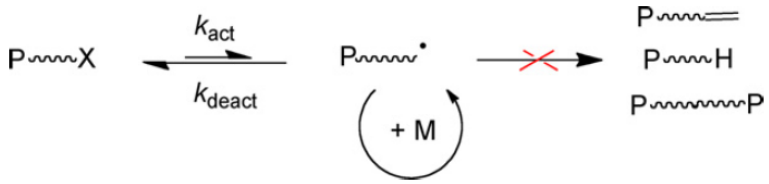

Figure 17. General mechanism of RDRP techniques (Adapted from reference 205 with permission from Elsevier).

Derived from these concepts, there are well-defined techniques of RDRP: reversible addition-fragmentation chain transfer (RAFT) polymerization, nitroxide-mediated polymerization (NMP), and atom-transfer radical polymerization (ATRP).

2.4.2.1. Nitroxide-mediated polymerization

NMP is historically the first discovered RDRP technique and synthetically perhaps the easiest of them to apply. Before the development of NMP, it was known that nitroxides efficiently trap carbon-centered radicals to form alkoxyamines. Nitroxides were used as radical traps in polymerization reactions of some monomers, such as acrylates and styrene.[206] It was observed that under some conditions the trapping of propagating radicals by the nitroxide was reversible, which led to the exploration of alkoxyamines as polymerization initiators. In 1985, the first report of NMP as a living polymerization technique was published.

The NMP mechanism is based on the reversible termination between a growing propagating radical chain and a nitroxide, that acts as a control agent, to yield the dormant and predominant species, an alkoxyamine-terminated chain (**Scheme 8**).[203] When an external

stimulus is applied, tipically heat, a homolytic cleavage of the dormant species regenerates a propagating radical chain and the nitroxide. This way, an equilibrium between dormant and active species, also described as the activation–deactivation equilibrium, is established with constants k_{act} and k_{deac}. The advantage of this equilibrium over other RDRP techniques, is the thermal nature of the process, where no catalyst is required. The polymerization kinetics is governed by both the activation–deactivation equilibrium and the persistent radical effect (PRE).

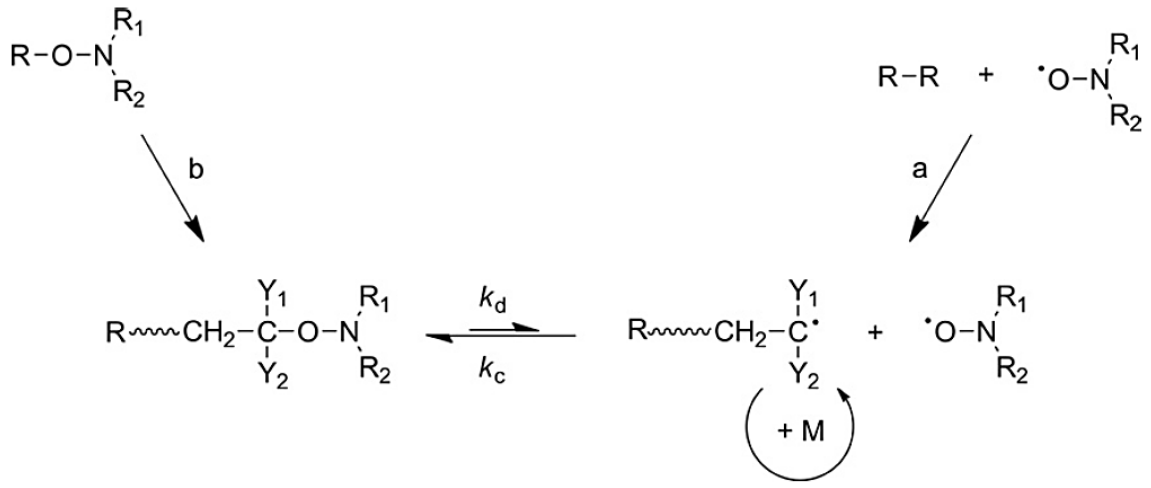

Scheme 8. Activation – deactivation mechanism of NMP, from either a mono- or bicomponent system (Adapted from reference 205 with permission from Elsevier).

The PRE is based on the occurrence of termination reaction at early stages of the polymerization, and can be explained considering a compound that can decompose in a transient radical and a persistent radical. At the beginning of the reaction, the initial concentration of both radicals is zero and increases with time in a linear fashion. As more radicals are formed, at some point radical-radical termination will happen, either terminating transient radicals irreversibly, or combining the transient and persistent radicals in a reversible manner. Irreversible termination of transient radicals leads to an increase in concentration of the persistent radicals, making the recombination of persistent and transient radicals more favored. After some time, the concentration of transient radicals will decrease to zero, and only

the persistent radicals will be controlling the reaction.[205] **Scheme 9** provides a simple explanation.

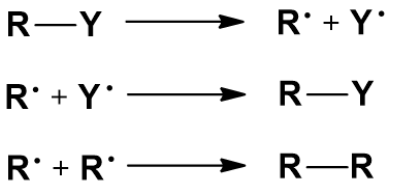

Scheme 9. Persistent radical effect. The termination of transient radicals (R•) increases the concentration of persistent radicals (Y•), favoring the recombination of transient and persistent species (R-Y).

A wide variety of nitroxides and alkoxyamines have been exploited in NMP, using two different strategies, either with a one- or two-component setup. This means the initiator can be either an alkoxyamine, or a thermal initiator that is mixed with a free nitroxide to form the alkoxyamine *in situ*.

Studies on the influence of the structure of the nitroxide or alkoxyamine over the kinetics and mechanism of NMP have been conducted with a number of initiators to improve their performance. TEMPO is one of the most common nitroxides used for the polymerization of styrene. However, it is not efficient for acrylates. By tuning the structure of TEMPO, a broader range of monomers can be polymerized.[207] Some NMP initiators are shown in **Figure 18**.

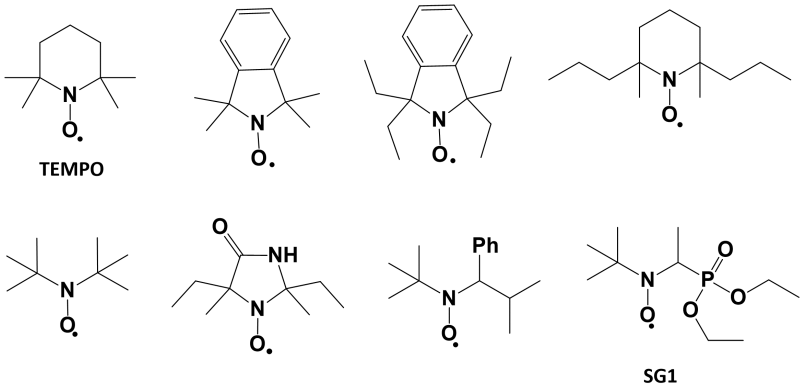

Figure 18. Examples of nitroxides used for NMP.

The limitation on the number of monomers that can be polymerized using NMP, makes other polymerization techniques, such as ATRP and RAFT, somewhat more attractive options to obtain a wider range of polymers. However, the synthetic simplicity of NMP, along with the mono component system, and no extra steps required for purification still make NMP a plausible option to obtain certain functional and defined polymers. Furthermore, research is still ongoing to develop novel nitroxides which can give access to a broader monomer range.[208]

2.4.2.2. Atom-transfer radical polymerization (ATRP)

Since its discovery in 1995, ATRP has become a powerful and versatile RDRP technique.[209] In ATRP, the catalyst used for initiation and chain growth is a complex of a transition metal, generally copper, and more rarely ruthenium, iron, osmium, or nickel.[210] In this technique, the chain growth is controlled by an equilibrium between a low concentration of macroradicals and a large number of dormant species, mainly in the form of initiating alkyl halides. Transition-metal complexes mediate the generation of radicals through a reversible redox process.

In the ATRP mechanism, the dormant species periodically react with transition-metal complexes in their lower oxidation state, M_t^n-Y, acting as activators to intermittently form propagating radicals ($R_n\bullet$). Deactivation occurs when transition-metal complexes in their higher oxidation state, coordinated with halide ligands X−M_t^{m+1}-Y, react with the propagating radical in a reverse reaction to re-form the dormant species and the transition metal complex in its lower oxidation state (**Scheme 10**).[211,212] This process occurs with rate constants of activation k_{act} and deactivation k_{deact}. The concentration of radicals for ATRP is kept low, due to the persistent radical effect (similar to NMP), resulting in well-defined polymers. Termination reactions can occur in ATRP, through radical coupling. However, due to the low concentration of macroradicals and large amount of dormant species, termination is minimized.[19]

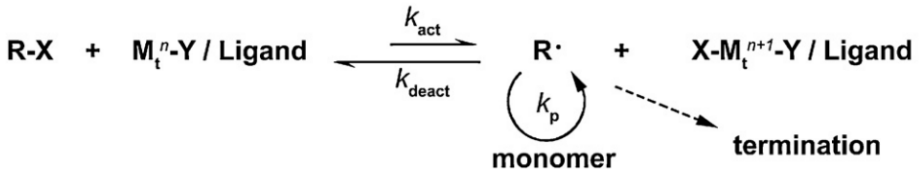

Scheme 10. Mechanism of ATRP (adapted from reference 212 with permission from Elsevier).

ATRP provides a number of advantages, similar to those of the other RDRP techniques: it enables precise control on molar mass, narrow dispersities, and the possibility to introduce functionalities. In addition, reactions can be prepared in a variety of different solvents and conditions, including water and room temperature, and is tolerant to most functional groups.[213] Depending on the reaction conditions and parameters, control over reaction kinetics can be achieved. An important feature is that polymers can be grown from almost any surface or material that has an attached ATRP initiator, including proteins for the formation of conjugates, and organic or inorganic materials, such as nanoparticles.[214] Particularly, many alkyl halides (i.e. potential ATRP initiators) are commercially available and can easily be modified.

2.4.2.3. Reversible addition-fragmentation chain transfer (RAFT) polymerization

Contrary to NMP and ATRP, where control over the polymerization is achieved via reversible deactivation of propagating macroradicals by atom-transfer or radical-radical reactions, and the dormant species are also the radicals source, in RAFT polymerization, deactivation–activation equilibria are chain-transfer reactions, and an external component is the source of radicals to start the polymerization.

RAFT is one of the most convenient and versatile polymerization methods, applicable to the majority of monomers that can undergo radical polymerization. In the mid-1980s, the first report on the use of addition-fragmentation reactions to control polymerization was published.[215] In 1998, CSIRO reported the living radical polymerization using thicarbonylthio compounds, namely dithioesters and trithiocabonates, followed by a patent in 1999, where

they used xanthate and dithiocarbamate compounds as RAFT agents, also called chain transfer agents (CTA).[216,217] Since then, many other CTA variations became available, and RAFT developed into one of the most used methods of living polymerization.

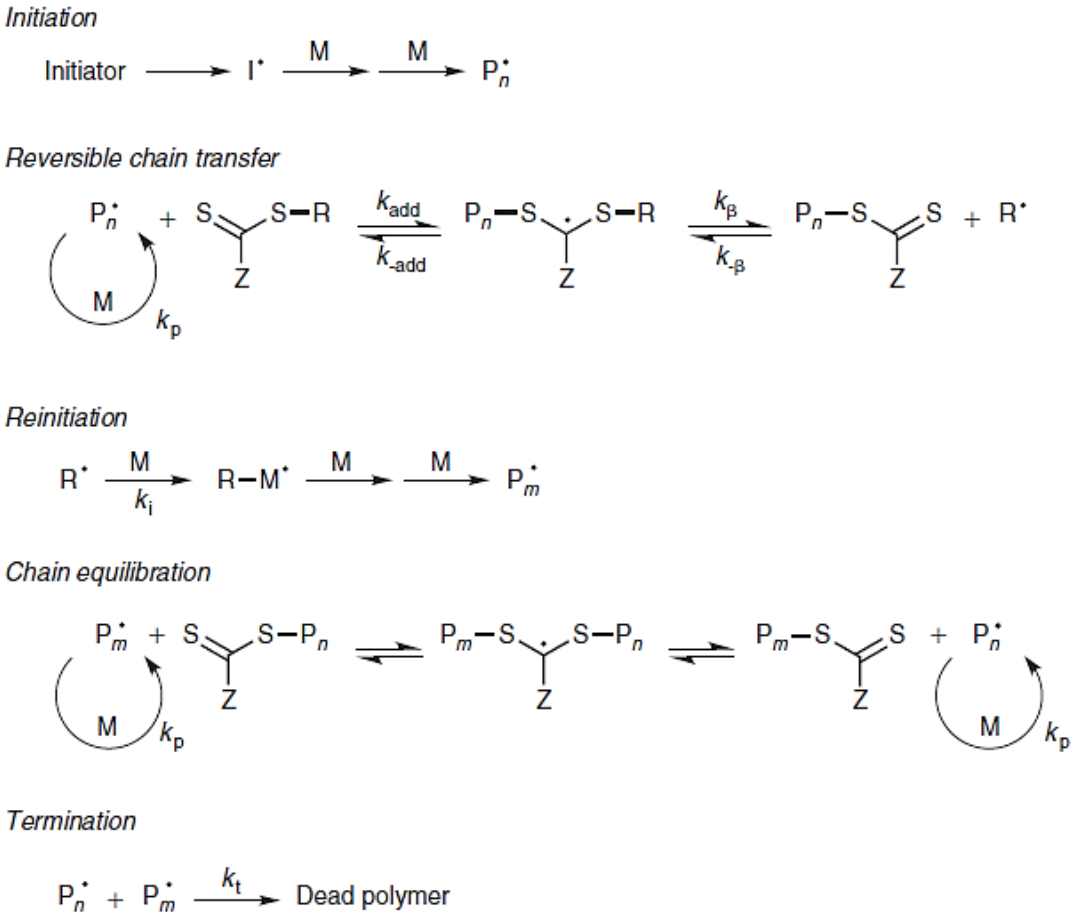

Scheme 11. RAFT polymerization mechanism (adapted from reference 218 with permission from Elsevier).

The process of RAFT polymerization is based on addition-fragmentation equilibria that establish control over the radical polymerization. The mechanism, shown in **Scheme 11**, starts with the generation of radicals through the decomposition of an initiator, that add onto monomer units and lead to propagation. In this process, the addition of a growing polymer chain to the initial CTA, yields a new chain-transfer agent and a free radical for propagation, R•. Re-initiation by the free radical creates a new propagating radical. A rapid equilibrium between both

propagating species, distributes equally the propagation probability among all polymer chains, resulting in the production of polymers with narrow dispersities. Importantly, once the reaction is complete, the majority of chains retain the thiocarbonylthio end group, which can subsequently be used for the synthesis of block copolymers, be removed, or used for a post polymerization modification to add a functionality.[216]

Transfer agents are unsaturated compounds that can undergo a two-step addition-fragmentation mechanism, and have the general structure shown in **Figure 19**. The effectiveness of the RAFT agent depends on the substituents R and Z, and on the monomer to polymerize. The Z group determines the reactivity toward propagating radicals and the stability of the intermediate radicals. The leaving group R has to be capable of efficiently re-initiating the polymerization.

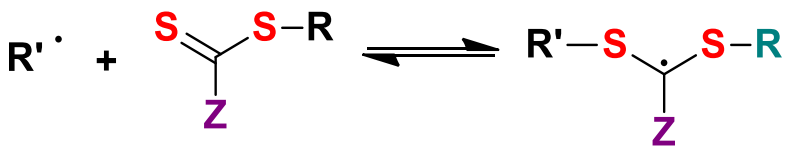

Figure 19. General structure of RAFT agents.

When designing chain transfer agents, the R group must have a balance of re-initiation efficiency and good homolytic leaving group ability. In the most effective RAFT agents, R is a tertiary cyanoalkyl or cumyl.[18,216] The Z group influences the rate of addition of radicals to the C=S double bond. In a general trend, this rate is higher for dithiobenzoates and decreases for trithiocarbonates, dithioalkanoates, dithiocarbonates, and lastly dithiocarbamates. A set of guidelines to aid on the selection of the appropriate CTA to use with respect to the monomer is shown in **Figure 20**. In the end, the compatibility with reaction media, desired end-group functionality, and polymer architecture dictate the choice of the RAFT agent.

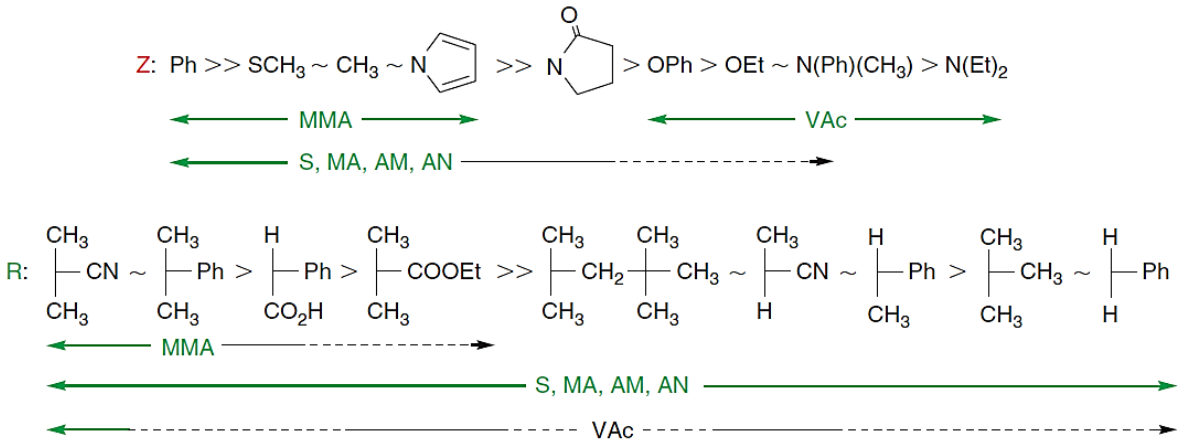

Figure 20. Guidelines for selection of RAFT agents for various polymerizations. MMA = methyl methacrylate; VAc = vinyl acetate; S = styrene; MA = methyl acrylate; AM = acrylamide; AN = acrylonitrile (Adapted from reference 218).

One significant advantage of RAFT polymerization and other RDRP methods over other processes for living polymerization is its compatibility with protic solvents and other functionalities present in the monomer or the RAFT agent. This makes the technique suitable for the synthesis of end-functional polymers by incorporating the functionality into the Z or R groups of the RAFT agent. Alternatively, to add an end functionality, the transformation or removal of the thiocarbonylthio group via aminolysis, thermal elimination, and hydrolysis, among many others techniques, has been widely used.

RAFT polymerization is potentially universal and can be applied to a wide range of functional monomers (styrenics, alkyl(meth)acrylates, acrylic acid, vinyl acetate, etc.), allowing the preparation of polymers with precisely controlled structural parameters such as random, block, gradient, graft, and star copolymers. RAFT polymerization can be performed in homogeneous media (bulk and solution) as well as in ionic liquids and aqueous dispersed systems.[213]

2.5. Protein conjugation

The conjugation of polymers to proteins results in higher physical and thermal stabilities, reduced immunogenicity, and improved solubility of the biomolecule. In the case of therapeutic proteins, the improved pharmacokinetics allow the possibility to reduce the amount and frequency of the doses used for patients. A number of biocompatible polymers, such as PEG, HPMA, PLGA, and PEtOx are already used for clinical research. Already a variety of polymer-protein conjugates, mainly using PEG, have been approved by the FDA and are used in the treatment of diabetes, cancer, and hepatitis C.[16,213]

Important aspects in the design of a polymer-protein conjugate include the specificity of the conjugation site, steric hindrance created by the polymer, and the enhancement of the reactivity of the drug.[76] Since the location of the polymer chain on the protein can potentially have an effect on the remaining activity of the protein, engineering of protein to have one binding site is a helpful strategy to achieve the required specificity.[219,220] However, in the case of already commercially available PEGylated proteins, non-specific binding nevertheless improved the pharmaceutical properties of the conjugate.[7]

The architecture, size, coupling strategy, and distribution of the polymer can also affect the performance of the conjugate. High molar mass linear polymers and dendrimers generally exhibit steric hindrance. It is important, therefore, to adjust the size of the polymer, as well as the number of incorporated chains, to ensure that the performance of the conjugate is improved.[76] An alternative strategy to avoid steric hindrance is the use of linkers, commonly polypeptides, between the polymer and the protein.[221]

A variety of strategies to form polymer-conjugate systems is available. The first approach (grafting onto) is the design of polymers with reactive groups towards either the *C*- or *N*-terminus or the amino acids along the protein chain. Alternatively, proteins can be modified to add initiators to the amino acid chain, becoming macro initiators for controlled polymerization techniques. In this approach (grafting from), the polymer grows from the protein (**Scheme 12**).

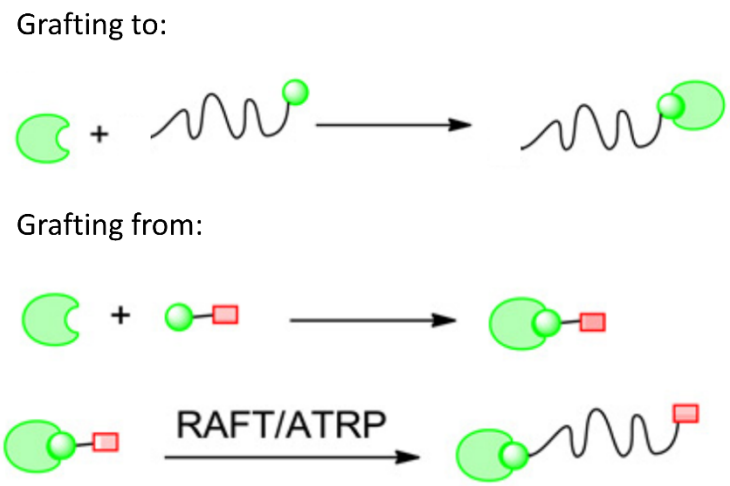

Scheme 12. General approaches used to synthesize protein-polymer conjugates (Adapted from reference 222 with permission from Elsevier).

Considering the first approach, where polymer chains are grafted to the protein, lysine residues are a highly popular target for the conjugation, due to the high reactivity of the amine side chain towards a number of functional groups including activated esters, thioimido esters, isocyanates, dichlorotriazines, ketones, and aldehydes.[6]

N-hydroxysuccinimide (NHS) ester activation on polymers is a widely used approach for further conjugation. NHS ester-activated compounds react with primary amines, in this case lysine residues, in physiological to slightly alkaline conditions (pH 7.2 to 9) to yield stable amide bonds, with simultaneous release of NHS (**Figure 21**). One disadvantage of this approach is the lack of site-specificity during conjugation, since most proteins contain more than one accessible lysine in their structure.

To obtain NHS-functionalized polymers, a strategy for polymers possessing hydroxyl groups, such as PEG, is to turn them into an acid functionality with succinic anhydride, with subsequent activation with *N*-hydroxysuccinimide.[6] Controlled polymerization techniques can also be used to obtained NHS functionalities on the end chain. For example, with an NHS ester-containing chain-transfer agent for RAFT polymerization, PVP was conjugated to lysozyme.[223] Using ATRP, NHS ester-terminated glycopolymers (glucofuranose and galactopyranose) were synthesized

and conjugated to small polypeptides.[224] The polymerization of *N*,*N*-dimethylacrylamide using a carboxylic acid-functionalized initiator for NMP that was then modified post polymerization to an NHS ester, and conjugated to lysozyme.[225]

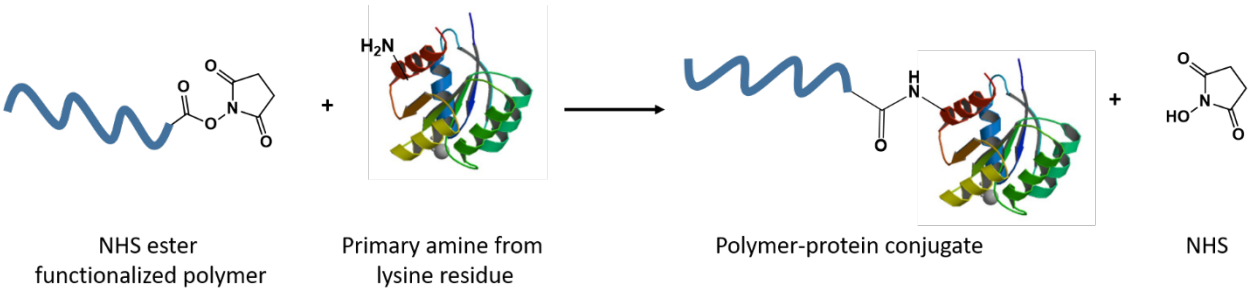

Figure 21. NHS ester reaction scheme for protein conjugation to a primary amine.

Other examples of conjugation to the lysine residues include the introduction of a thiazolidine-2-thione group using a functional chain-transfer agent for RAFT polymerization of HPMA,[226] and an aldehyde-containing POEGMA synthesized by ATRP.[227]

Cysteine residues are another attractive targets for the conjugation of polymers to proteins. The advantage over lysine residues is the rareness of free cysteine residues on the protein surface, which leads to a more site-specific conjugation. Alternatively, if the protein does not naturally contain free cysteine residues in its structure, a site-specific cysteine residue can be added using protein engineering without modifying the 3D structure of the protein or its activity.[228] Activated disulfides, haloacyl compounds, and maleimides, among others can react with cysteine for conjugation (**Figure 22**).[229] The common conjugation reaction is a Michael addition, or alternatively, reactions that create a disulfide bond can be used.[230]

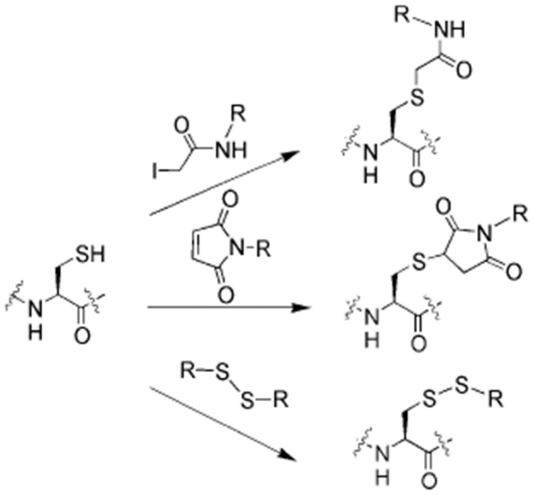

Figure 22. Coupling methods for cysteine residues (adapted from reference 229 with permission from John Wiley and Sons).

PEG derivatives for cysteine conjugation have been developed, including PEG-maleimide, vinylsulfone, iodoacetamide, and orthopyridyl disulfide, and are widely used with high conjugation efficiencies.[6,7] Among the possible reactive groups, maleimide is preferred due to its high reactivity towards cysteine. Protected maleimide functionalized chain-transfer agents for RAFT polymerization have been developed. For example, to furan-protected maleimido-poly(ethylene glycol acrylate) (PEGA) was synthesized, and after deprotection, conjugated to a model protein.[231] Protected maleimides can also be introduced to the end chain of polymers using functional ATRP initiators.[232] Other groups such as pyridyl disulfide and vinyl sulfones have also been used to functionalize either RAFT chain-transfer agents or ATRP initiators.[233–235]

Other possible target amino acids that can be used for conjugation are tyrosine, glutamine, tryptophan, aspartic acid, glutamic acid, arginine, and phenylalanine.[230] However, the low reactivity shown by some of these compared to lysine or cysteine, along with reaction conditions, that in some cases require enzymatic or organometallic catalysts, make them less convenient for conjugation.

The second strategy, that consists on modifying the protein so that the polymer grows from the protein, has the advantage that no excess of polymer chains is required. In this case, the selected amino acid is modified to become either a macromolecular chain-transfer agent for RAFT polymerization or a macroinitiator for ATRP. For instance, a biotinylated ATRP initiator was developed for conjugation to streptavidin for the polymerization of *N*-isopropylacrylamide (NIPAAm).[23] Similarly, maleimide or pyridyl disulfide ATRP initiators have been synthesized for conjugation to cysteine, forming an ATRP macroinitiator.[236] Via RAFT polymerization it is also possible to produce a protein-polymer conjugate *in situ*. In this case, the protein is attached to a pyridyl disulfide trithiocarbonate CTA for subsequent polymerization.[237] In all cases, it was proved that the proteins used for conjugation retained the activity after polymerization.

3

Maleimide- and Thiol-Functionalized Initiators for the Polymerization of 2-Oxazolines

3.1. Introduction[1]

As stated in **section 2.2**, the synthesis of PAOx can proceed via living CROP, a method that allows full control over molar mass, narrow distributions, and the possibility of tuning the properties of the polymer.[36,37,238] Taking advantage of the CROP mechanism, a number of functionalization strategies are available, depending on the choice of 2-oxazoline monomer or the use of functional initiators and terminating agents to obtain end-functionalized PAOx (**Scheme 13**).[35,92]

[1] Part of this chapter was done in collaboration with the group of Prof. Richard Hoogenboom at Gent University, in Belgium, and was adapted from reference 267. XPS analyses were performed by Vanessa Trouillet in KIT. Surface patterning was carried out by Dr. Sylwia Sekula-Neuner, at INT, in KIT.

In principle, the use of functional initiators provides an advantage in terms of stoichiometry, since one chain should grow per initiating molecule available. In contrast, the use of terminating agents requires an excess of the terminating molecule. Furthermore, using a functional initiator to introduce the functionality at the α chain end offers an interesting alternative, since it opens the possibility to create bifunctional (hetero)telechelic PAOx by terminating the reaction with a functional nucleophile.

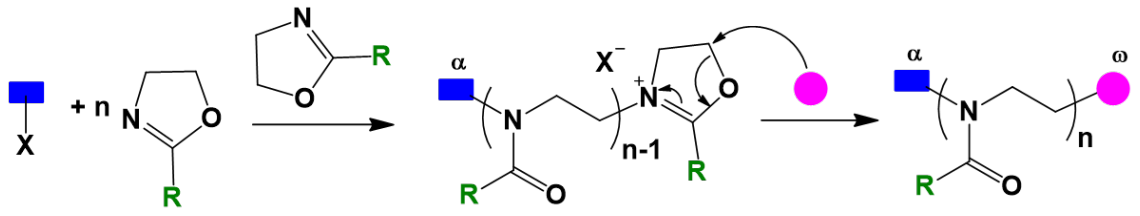

Scheme 13. General strategies for the functionalization of PAOx.

Generally used initiators for CROP include alkyl halides,[239-94] or alkyl sulfonates, such as tosylates,[240] nosylates,[241] and triflates.[240] The most commonly used initiator is methyl tosylate, however, available initiators that add specific functionalities to the polymeric chain or allow further functionalization include allyl,[120] amine,[123] hydroxyl,[124] or carboxylic acid,[125] in some cases requiring the protection of the functional group.[125]

In this chapter, the aim is to develop a strategy for the introduction of functional moieties at the α chain end of PAOx. Thiol and maleimide were chosen functionalities for this project since these can undergo a variety of reactions with multiple applications. For instance, the maleimide moiety can engage in a number of coupling reactions, such as Diels–Alder reactions,[242–245] dipolar cycloadditions,[246] and Michael-type additions,[246] and may react via radical copolymerization.[247] This versatility makes maleimides a convenient group for post-polymerization modification, protein conjugation, synthesis of block copolymers, surface functionalization, or network formation. On the other hand, thiol-based chemistry is versatile and powerful because the thiol group can be used as a nucleophilic agent,[248] a chain transfer agent in radical processes (radical addition[249] or radical polymerization[250]), or an electrophilic

reagent.[251] In addition, thiol-based reactions are usually very efficient and can be performed under a wide variety of conditions, usually without side reactions.[252] Post-polymerization modifications to introduce thiol groups at the chain end have been increasingly used to create functional polymers and architectures for biological and nanotechnology applications.[253]

Some examples of maleimide or thiol end-functionalized PAOx have been reported,[254–258] but mainly by adding the functionality on the ω end chain by termination, or post-polymerization modification. In the case of maleimide, the group of Schacher reported the introduction of the end group on the ω end chain by first capping with sodium azide and then performing an azide–alkyne cycloaddition with an alkyne-functionalized protected maleimide. The synthesis of the alkyne-protected maleimide compound used was developed using a three-step reaction, with an overall yield of 9%, that included a column chromatography purification step.[254] A second approach to add a maleimide functionality on the ω chain end was reported by the group of Luxenhofer,[257] where furan-protected maleimide was directly used as a terminating agent for the CROP of 2-oxazolines. The capping agent was obtained in a single step without a complex purification with a yield of 45%. Yet, the termination efficiency was 55%, followed by a deprotection step, with an 85% efficiency, to yield the maleimide-bearing PAOx.

PAOx presenting a thiol at the ω end chain have been synthesized by direct termination with a thiol,[259] a thioacetate,[260] or after the modification of functional terminating agents that include xanthate,[261,262] dithiocarbonates,[259] diallyl amine,[263] and maleimide.[264] A strategy to add thiols on the α end chain was developed by Ruehe and coworkers, who synthesized tosylates of ω,ω-dihydroxy alkyl disulfide initiators for the CROP of 2-oxazolines, with the aim of grafting the polymer on gold surfaces.[265] However, no extensive characterization of the polymers obtained was done.

Throughout this chapter, the synthesis of novel maleimide- and thiol-containing CROP initiators and their application to the synthesis of α-functional-PAOx is presented. In addition, the reactivity of both maleimide- and thiol-functional PAOx by coupling with small molecules is described, as well as in the formation of either protein-PAOx conjugates, for the maleimide-PAOx, or surface patterning, in the case of thiol-PAOx.

3.2. Synthesis of functional initiators for the CROP of 2-oxazolines

When designing a functional initiator for the polymerization of 2-oxazolines, an important parameter to consider is the compatibility of the chosen functional group with the CROP reaction. Functionalities that are incompatible with the CROP of 2-oxazolines can also be introduced during initiation, but in these cases, an appropriate protecting group strategy has to be utilized.

The protection of the maleimide by cycloaddition with furan is necessary during the CROP to avoid nucleophilic attacks and other potential side reactions. In the case of thiols, the protection in the form of thioacetates is required since thiols exhibit a high reactivity toward a large variety of substrates, and are sensitive to oxidation, which leads to the formation of disulfides.[266]

It was decided to use alkyl sulfonate initiators because these typically lead to faster polymerizations via exclusive cationic propagation,[240] and are easily synthesized from alcohol derivatives, typically with simple purification procedures.[128] While tosylate derivatives are significantly more popular, the utility of nosylate initiators was recently demonstrated.[93] In this project, both types of sulfonates for each functional group chosen were synthesized and characterized for the CROP of EtOx.

3.2.1. Synthesis of maleimide-functional initiators

The synthetic strategy followed to obtain the maleimide-functional initiators is depicted in **Scheme 14**. Maleic anhydride was used as the starting material to incorporate the activated ene group. Prior to further functionalization, the latter was protected through a classic Diels–Alder cycloaddition with furan. The cycloadduct **1** was ring-opened with ethanolamine and dehydrated, to produce the hydroxylated *N*-substituted protected maleimide **2**. Nucleophilic substitution of **2** with tosyl and nosyl chloride generated the corresponding tosylate **3** and nosylate **4**, respectively. The overall yield for these (non-optimized) 3-step syntheses were 17.5 and 8.1%, for **3** and **4**, respectively.

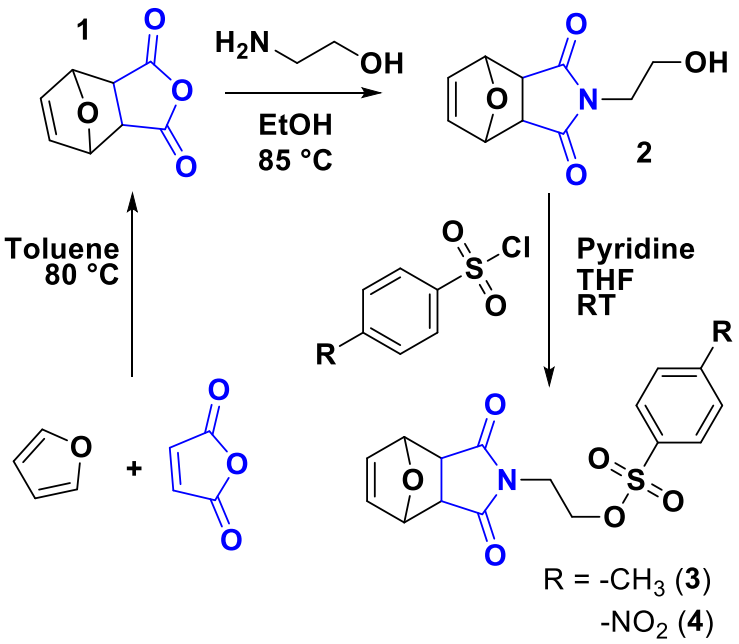

Scheme 14. Synthetic route for maleimide-functionalized tosylate and nosylate initiators for the CROP of 2-oxazolines (Adapted from 267).

It is worth highlighting that the starting materials for these syntheses are very cheap and no chromatographic step was required, in contrast to the previously mentioned synthetic strategies for maleimide end-functional PEtOx.[254,257] Analysis of both initiators by ^{1}H and ^{13}C NMR spectroscopy (**Figure 23**, **Figure 24**, **Figure 26**, and **Figure 27**), as well as ESI-MS (**Figure 25** and **Figure 28**) confirmed that the targeted structures were obtained with high purity. The nosylate initiator (**FurMalNos 4**) unfortunately showed a limited solubility in MeCN, the most commonly employed solvent for the CROP of 2-oxazolines.

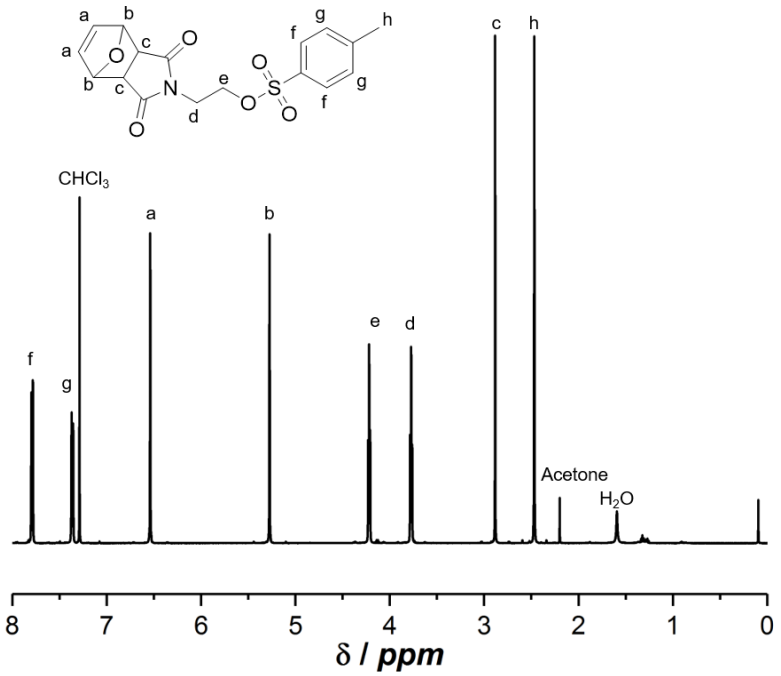

Figure 23. ^{1}H NMR spectrum of **FurMalTos 3** in $CDCl_3$ (Adapted from 267).

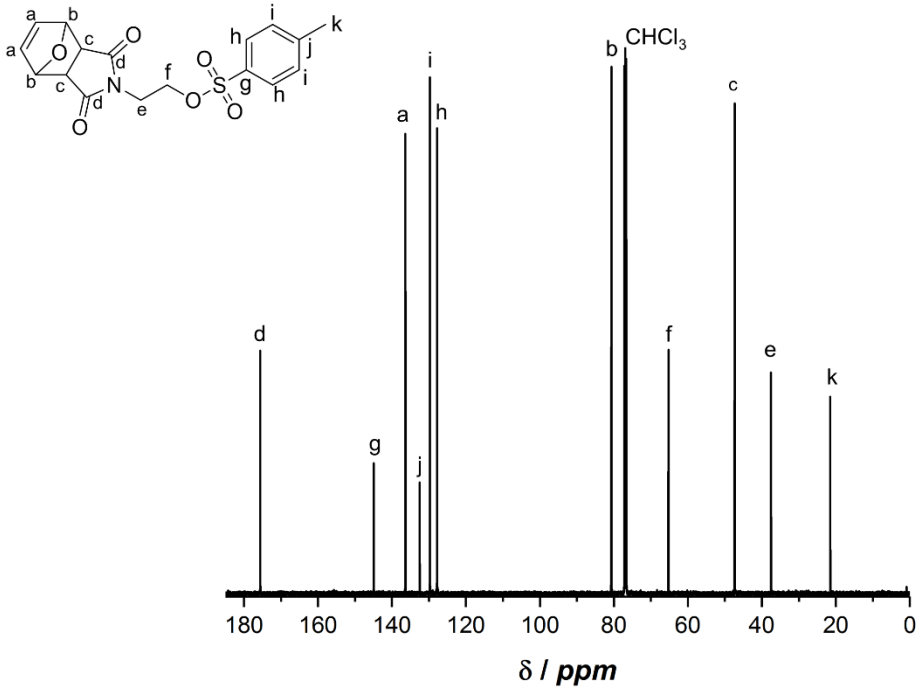

Figure 24. ^{13}C NMR spectrum of **FurMalTos 3** in $CDCl_3$ (Adapted from 267).

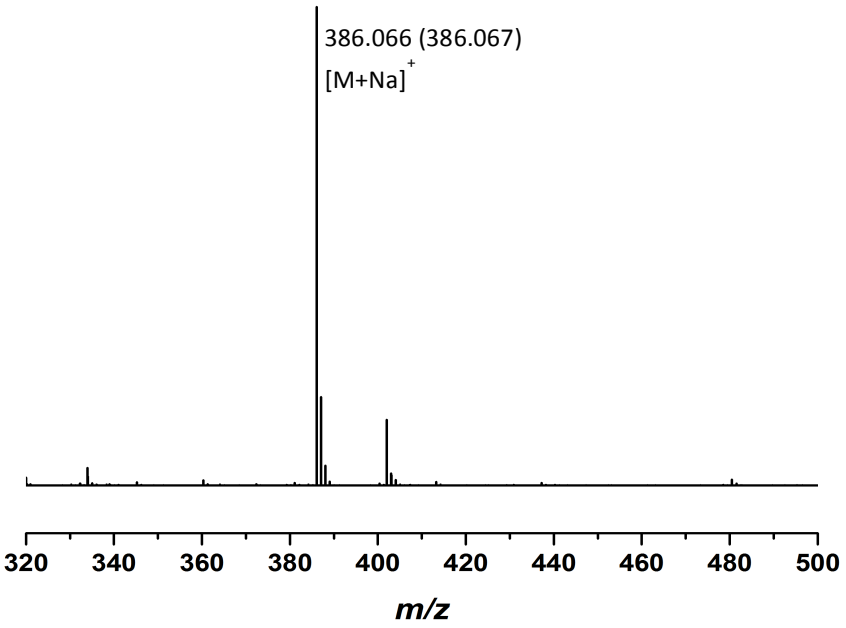

Figure 25. ESI mass spectrum of **FurMalTos 3** (Adapted from 267).

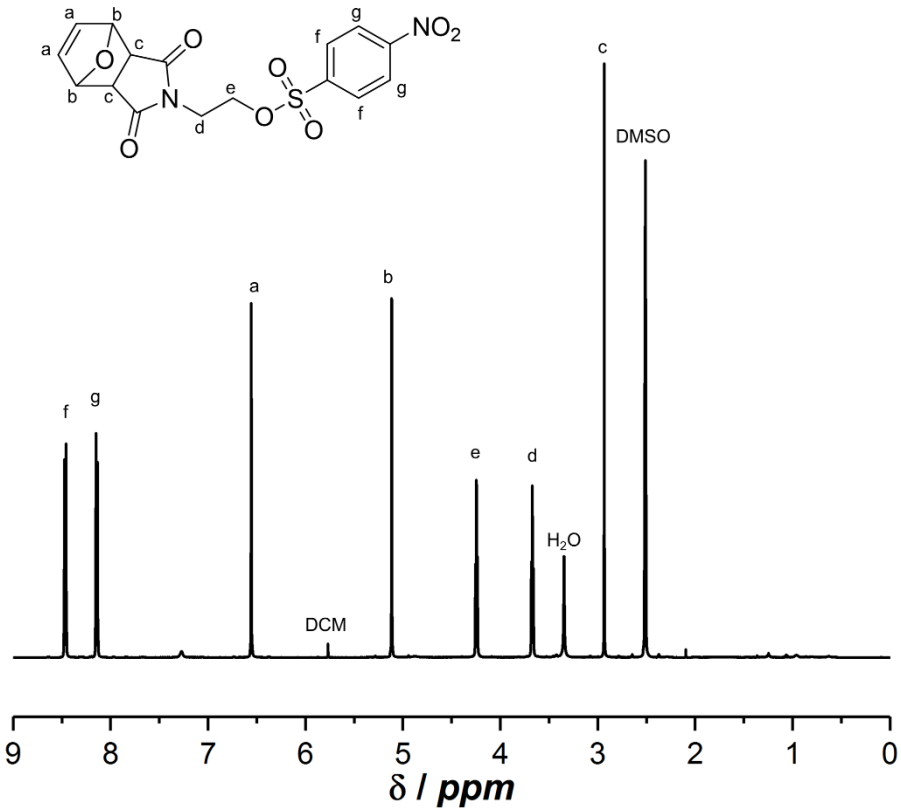

Figure 26. ^{1}H NMR spectrum of **FurMalNos 4** in DMSO-d6 (Adapted from 267).

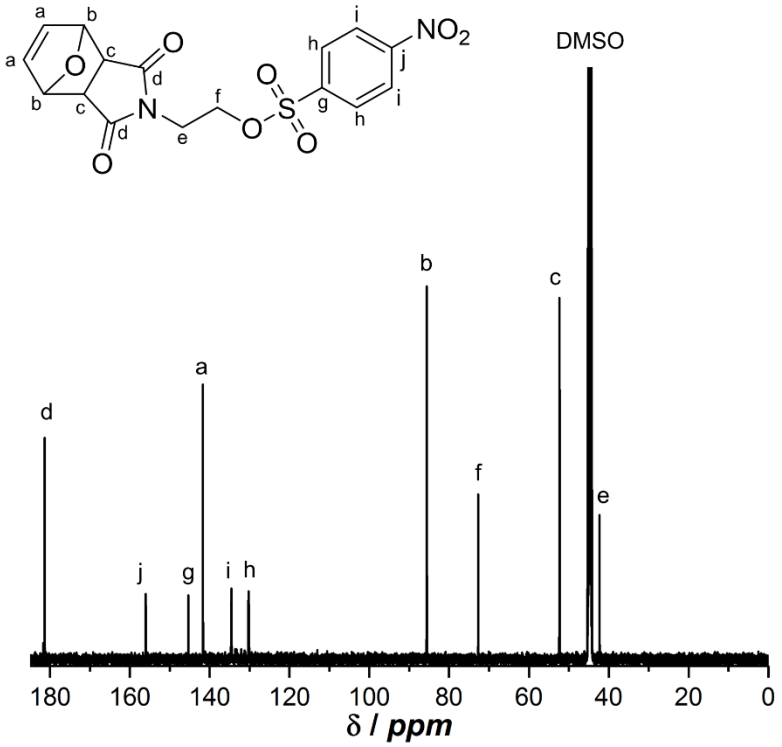

Figure 27. ^{13}C NMR spectrum of **FurMalNos 4** in DMSO-d6 (Adapted from 267).

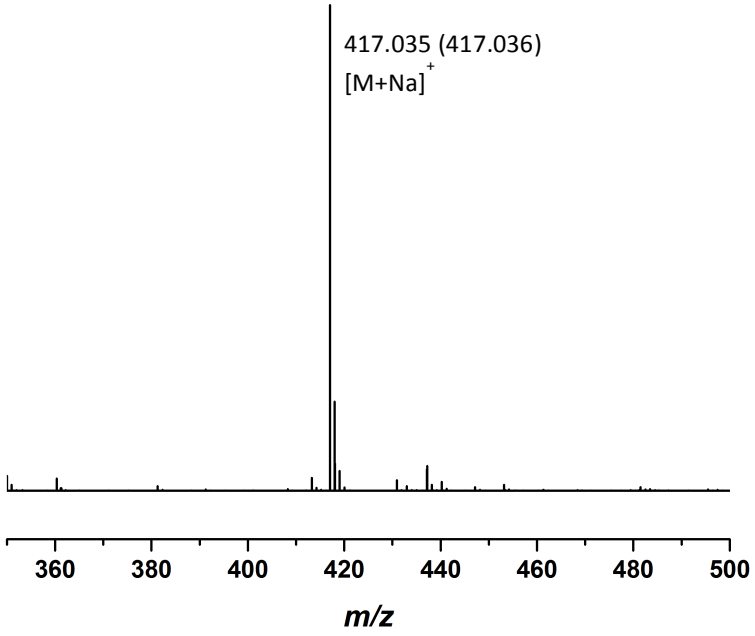

Figure 28. ESI mass spectrum of **FurMalNos 4** (Adapted from 267).

3.2.2. Synthesis of thiol-functional initiator

Two different synthetic strategies were developed to obtain the tosylate and nosylate versions of the thiol initiators, as depicted in **Scheme 15**. In the case of the tosylated initiator, **ThioAcTos 6**, the synthetic route started with the nucleophilic substitution of allyl alcohol with tosyl chloride to yield allyl tosylate **5**. The corresponding initiator **ThioAcTos 6** was obtained by photo thiol-ene addition of **5** with thioacetic acid with a 55% overall yield. An alternative route for the synthesis of the nosylate initiator was used, since purification of the products when following the previous strategy proved to be a more challenging task. **ThioAcNos 8** was obtained after the nosylation of the product of the photo thiol-ene addition of thioacetic acid and allyl alcohol. The product, **ThioAcNos 8**, was purified by recrystallization, avoiding chromatographic steps, with an overall yield of 60%.

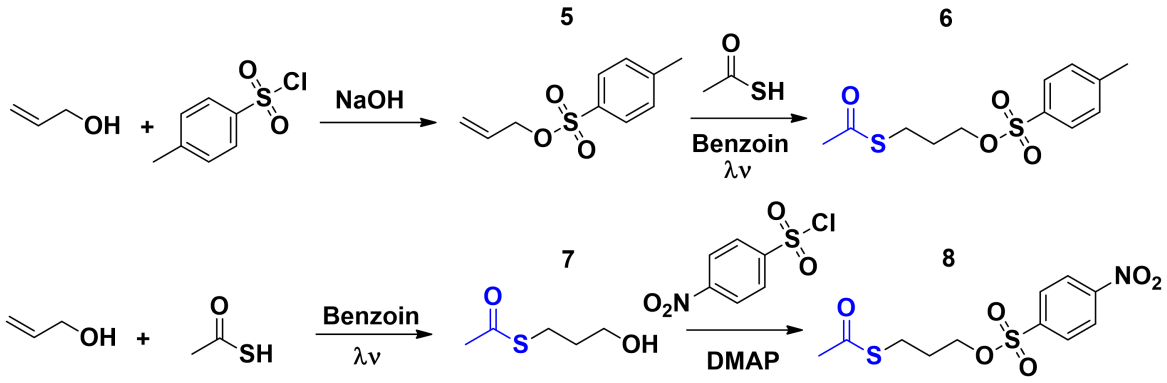

Scheme 15. Synthetic routes designed for thiol-functionalized tosylate and nosylate initiators for the CROP of 2-oxazolines.

Similar to the maleimide initiators described earlier, the low cost of the starting materials selected and the reasonable yields, combined with an uncomplicated synthesis, make this an advantageous methodology to obtain thiol-functionalized PEtOx. Analysis of both initiators by ^{1}H and ^{13}C NMR spectroscopy, as well as ESI-MS confirmed that the targeted structures were obtained with high purity (**Figure 29, Figure 30, Figure 31, Figure 32, Figure 33,** and **Figure 34**).

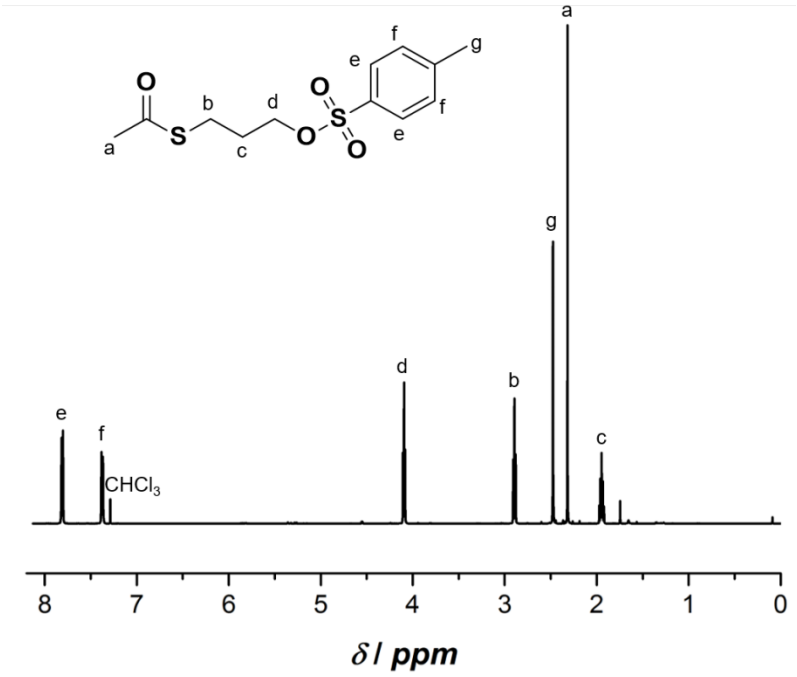

Figure 29. ^{1}H NMR spectrum of **ThioAcTos 6** in $CDCl_3$.

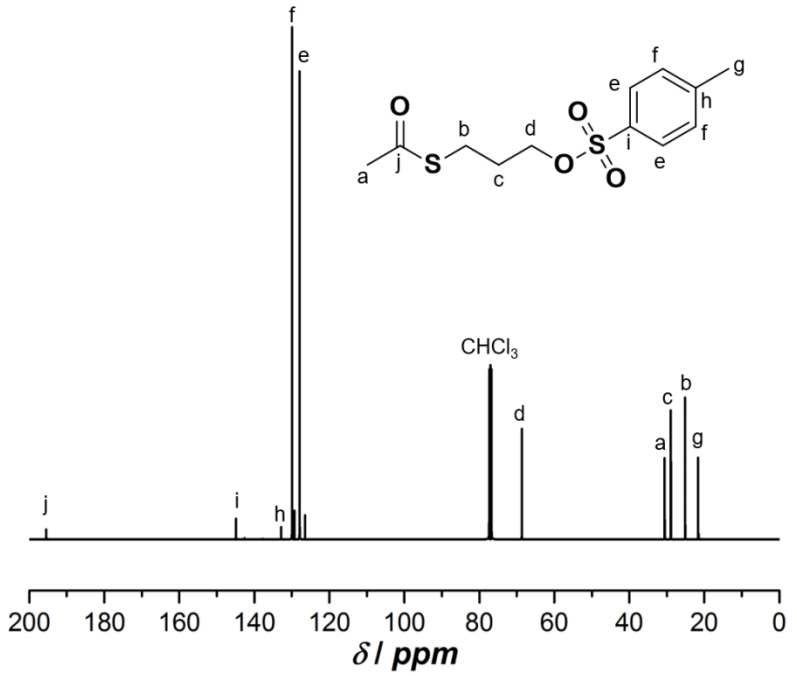

Figure 30. ^{13}C NMR spectrum of **ThioAcTos 6** in $CDCl_3$.

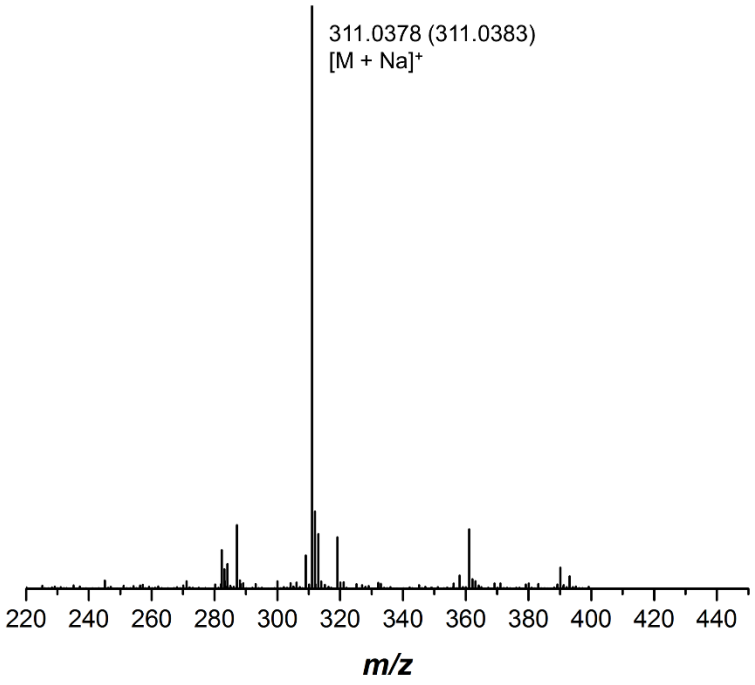

Figure 31. ESI mass spectrum of **ThioAcTos 6**.

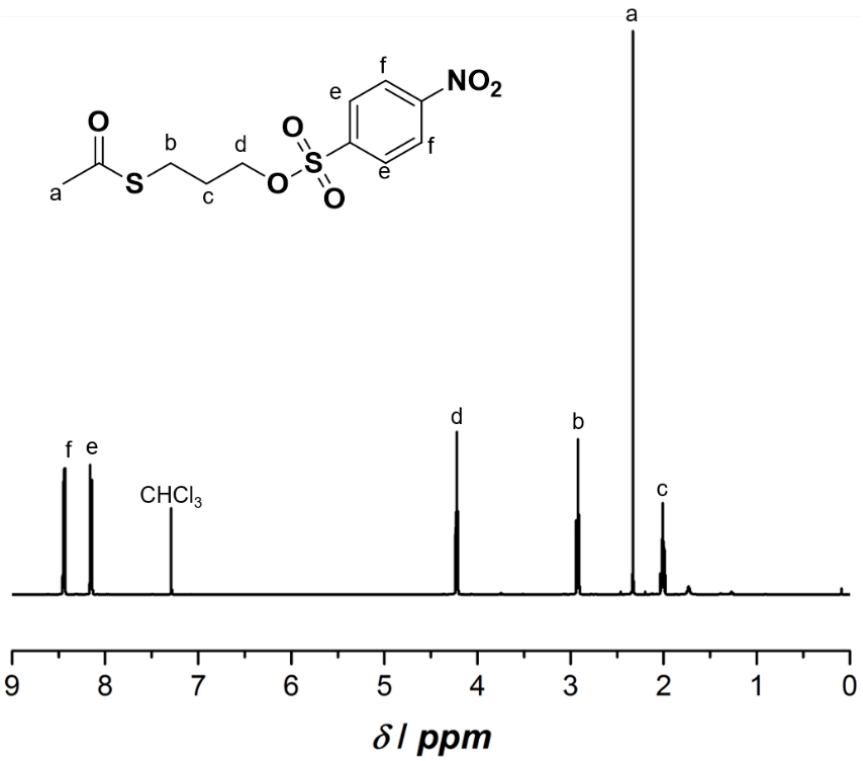

Figure 32. ^{1}H NMR spectrum of **ThioAcNos 8** in $CDCl_3$.

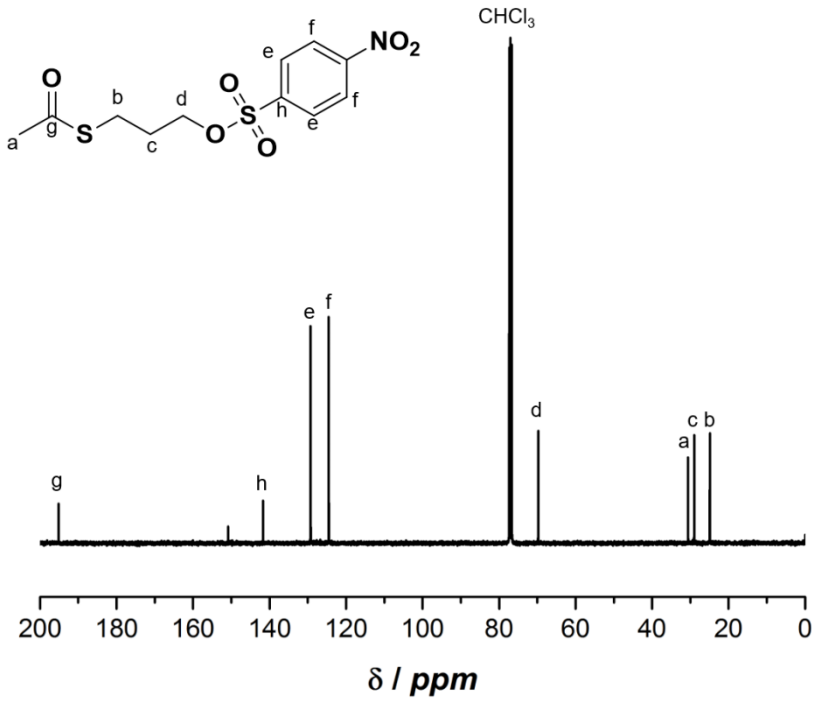

Figure 33. ^{13}C NMR spectrum of **ThioAcNos 8** in $CDCl_3$.

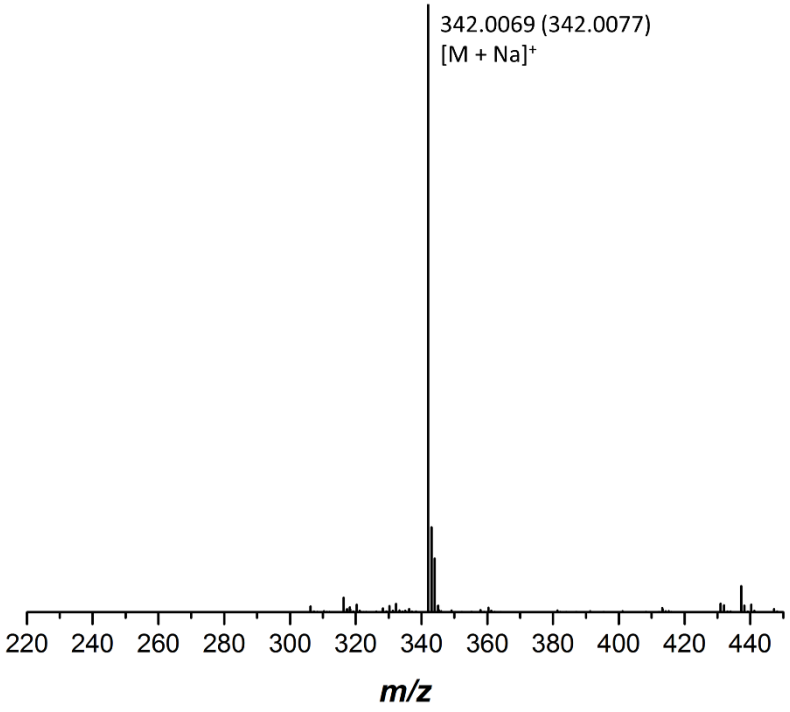

Figure 34. ESI mass spectrum of **ThioAcNos 8**.

3.3. Cationic ring-opening polymerization

For this project, the chosen monomer to polymerize using the new functional initiators was 2-ethyl-2-oxazoline. Compared to 2-methyl-2-oxazoline, PEtOx has a lower water-solubility due to the existence of an LCST at approximately 60 °C. In spite of this, it is still more convenient that PMeOx, that has a lower solubility in other solvents, including in the monomer itself.[258]

Reported optimized conditions for a very fast CROP of various 2-oxazolines, among them EtOx, are microwave-assisted polymerization in acetonitrile at 140 °C.[97] However, depending on the compatibility of the chosen initiator with these conditions, some modifications are necessary to achieve the living character of the polymerization.

In this section, the optimized conditions used, as well as analyses of the kinetic studies performed and the characterization of the resulting polymers using each functional initiator will be addressed.

3.3.1. Maleimide initiator

In the case of these new protected maleimide initiators, the high temperature used in the optimal polymerization conditions reported is not compatible, as it would lead to the deprotection of the maleimide group by cycloelimination. Consequently, lower temperatures were directly employed for preliminary experiments. Unfortunately, the microwave-assisted polymerization at 80 °C in acetonitrile already triggered the loss of the maleimide protecting group, as shown by ^{1}H NMR in **Figure 35**. Further polymerization tests performed at 80 °C with conventional heating displayed broad molar mass distributions in SEC ($Đ$ = 1.32–1.41), which indicates the loss of control over the polymerization (**Figure 36**). Therefore, the polymerization temperature was lowered to 50 °C using conventional heating to prevent the deprotection of the maleimide group and favor a controlled polymerization (**Scheme 16**).

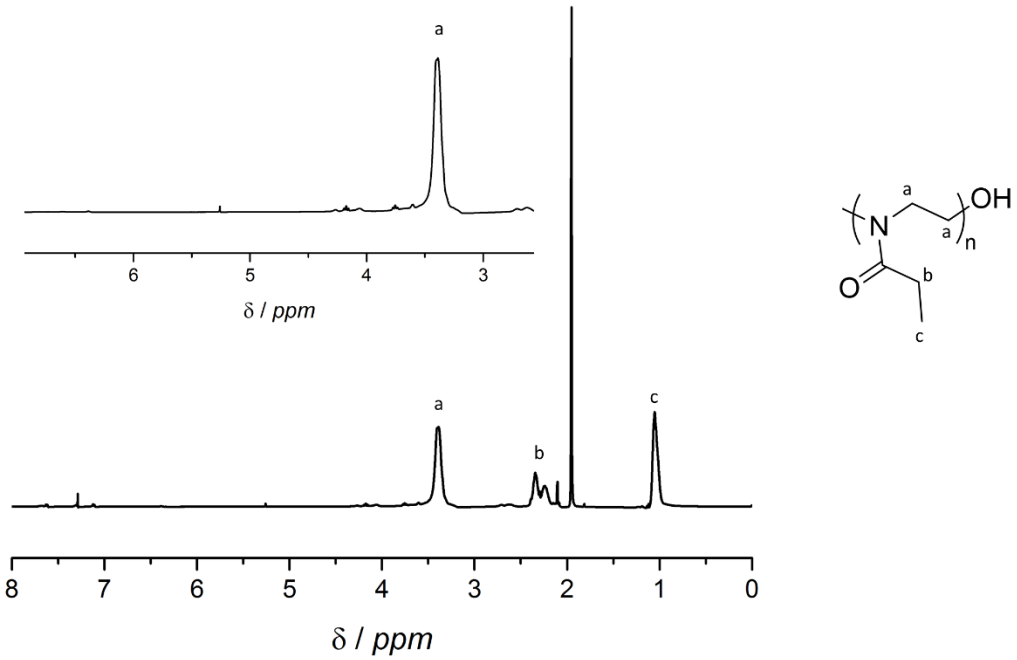

Figure 35. ^{1}H NMR spectrum of the crude polymer mixture after microwave-assisted polymerization of 2-ethyl-2-oxazoline using [EtOx]/[**FurMalTos 3**] = 40 at 80 °C for 50 minutes in acetonitrile. No end group signals remain (Adapted from 267).

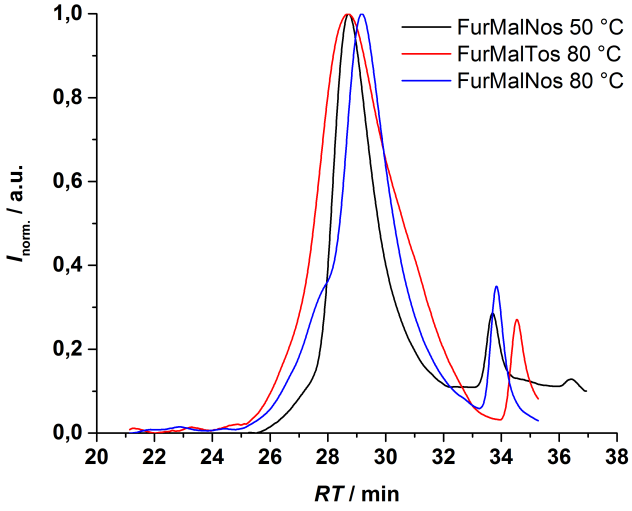

Figure 36. SEC traces of PEtOx obtained with either **FurMalNos 4** or **FurMalTos 3** as initiator and at either 50 °C for 75 h or 80°C for 3 hours. Polymers made at 80 °C show a broader distribution, indicating the loss of control over the polymerization at such temperature (Adapted from 267).

A first set of kinetic experiments to polymerize EtOx was performed in MeCN with [EtOx] = 4 M, in the case of **FurMalTos 3**, and [EtOx] = 1.5 M for **FurMalNos 4**. The monomer concentration for the polymerization using **FurMalNos 4** is significantly lower than what is typically encountered in the literature (the optimal monomer concentration is established as 4 M),[95] due to the previously mentioned solubility limits of **FurMalNos 4** in MeCN.

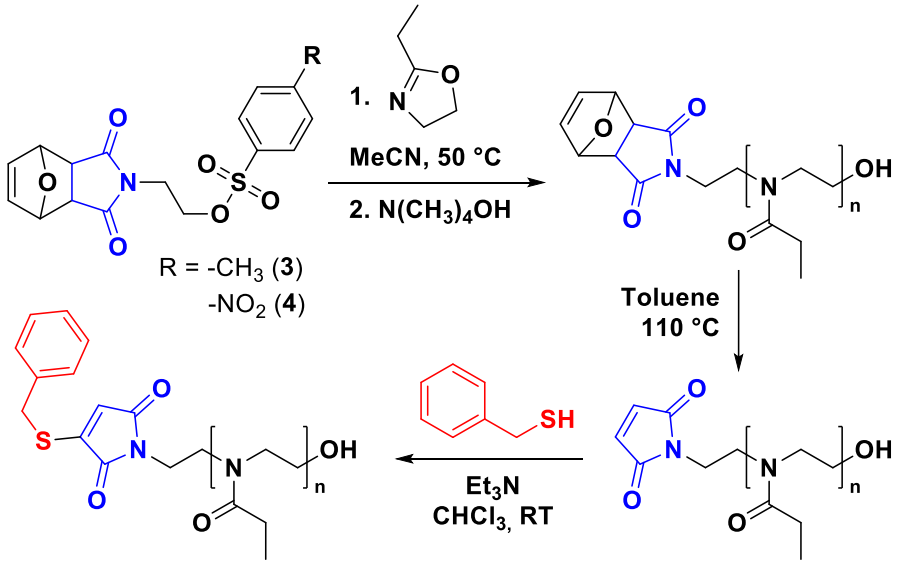

Scheme 16. Synthetic route for the synthesis of α-maleimido-PEtOx by polymerization of EtOx using functional initiators **3** and **4** and retro-Diels–Alder cycloelimination, followed by Michael addition with a model small molecule (Adapted from 267).

A preliminary assessment of the ability of the two protected maleimide-functionalized sulfonic esters to initiate the polymerization was performed at 50 °C, targeting a degree of polymerization (DP) of 50 at full conversion ([EtOx]/[initiator] = 50). After 74 hours, 72% conversion was achieved with the **FurMalNos 4**, whereas less than 10% was obtained for **FurMalTos 3,** as can been seen in **Figure 37**. Importantly, for the **FurMalNos 4** initiated polymerization, it was possible to observe the survival of the furan-maleimide at the end of the polymerization using ^{1}H NMR spectroscopy (**Figure 43**).

Recent studies on the CROP of 2-oxazolines in MeCN at 80 °C, report that, except for methyl tosylate, initiation with alkyl tosylates generally leads to slow initiation and propagation rates, as a consequence of low electrophilicity and relatively low leaving group ability.[93] It was also reported that the reactivity of ethyl nosylate is high enough to quantitatively initiate in the first instants of the polymerization. Considering the above mentioned facts, along with the experimental findings of the preliminary experiments, subsequent investigations were exclusively conducted with **FurMalNos 4** as initiator.

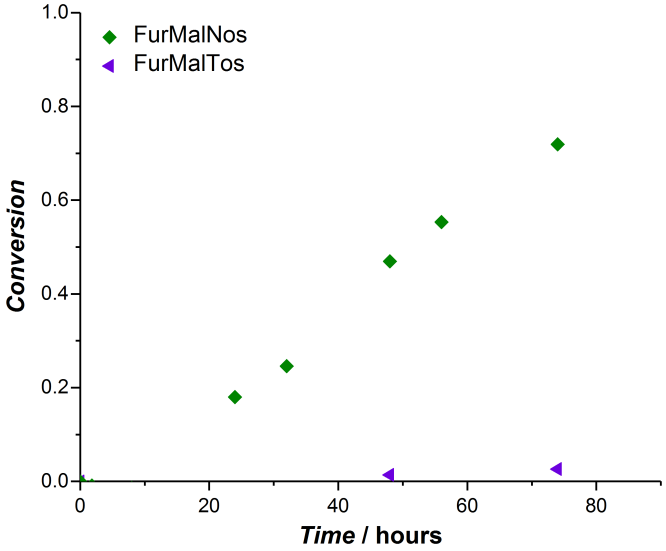

Figure 37. Monomer conversion as a function of time for the CROP of 2-ethyl-2-oxazoline at 50 °C in acetonitrile using **FurMalTos 3** and **FurMalNos 4** as initiators. [EtOx] = 1.5 M; [EtOx]/[Initiator] = 50 (Adapted from 267).

In order to evaluate the possibility of producing α-maleimido-PEtOx of various molar masses, a number of polymerizations varying monomer-to-initiator ratios were carried out (**Figure 39**). It was observed that when keeping all other parameters constant, faster polymerization rates are obtained when using a lower monomer-to-initiator ratio (**Figure 39A**).[240] Long polymerization times of up to 76 hours to reach 94% conversion in the case of DP 20 were required (**Figure 38**). The change in monomer concentration and the dramatic decrease of the reaction temperature had a significant effect on the polymerization rate. Despite these long polymerization times, all

kinetics showed a similar trend, i.e., a rather slow polymerization with two distinct regimes: first, a slow non-linear increase of *ln(1/(1-conversion))* with time at the beginning of the polymerization, followed by a linear behavior indicating a constant concentration of propagating species (**Figure 39**, top).

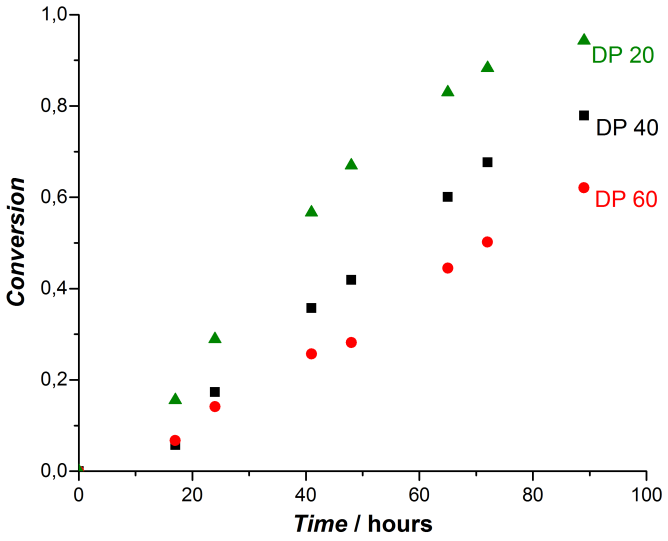

Figure 38. Monomer conversion as a function of time for the CROP of 2-ethyl-2-oxazoline at 50 °C in acetonitrile using **FurMalNos 4** as initiator at three distinct targeted degrees of polymerization (DP = [EtOx]/[**FurMalNos**]. [EtOx] = 1.5 M (Adapted from 267).

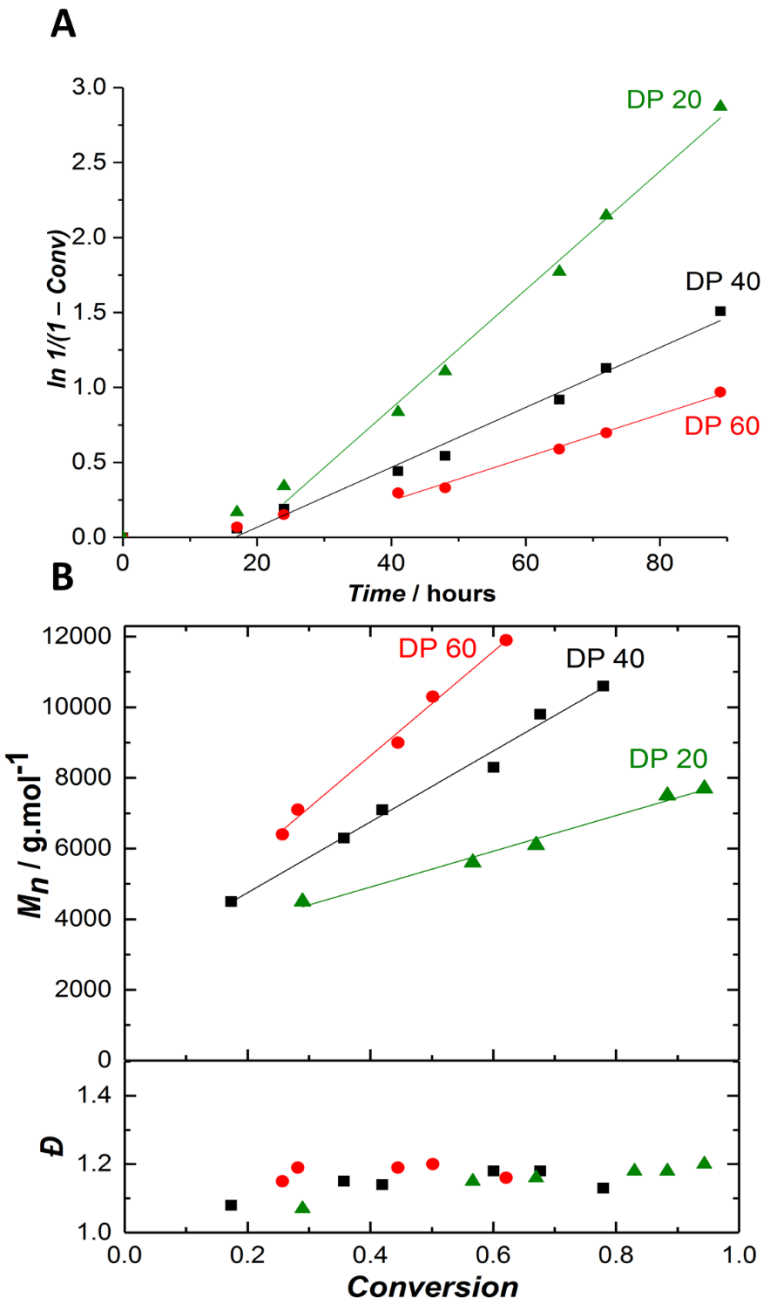

Figure 39. (A) First-order kinetic plots and (B) evolution of the number-average molar mass and dispersity vs conversion for the CROP of EtOx initiated by **FurMalNos 4** at various targeted degrees of polymerization (DP = [EtOx]/[**FurMalNos**]) in MeCN at 50 °C. [EtOx] = 1.5 M (Adapted from 267).

The apparent propagation rate constant values, k_p, were calculated for each kinetic run from **Figure 39** using the following equation:

$$-\frac{d[M]}{dt} = k_p \cdot [P^*] \cdot [M]$$

where [M] and [P*] are the monomer and propagating species concentrations, respectively. Assuming that all initiators react simultaneously upon heating, and therefore that $[P^*] = [I]_0$ (initial initiator concentration), the integration of the previous equation leads to:

$$\ln\frac{[M]_0}{[M]} = k_p \cdot [I]_0 \cdot t$$

The k_p values obtained are shown in **Table 2** and appear to be independent of the initial monomer-to-initiator ratio, as observed in previous studies.[240] The observed two stages of the polymerization can be explained by a relatively slow initiation reaction that results in a slow build-up of the concentration of propagating species. This phenomenon can be attributed to the different polymerization conditions that include lower temperature and lower monomer concentration, in comparison to classic EtOx polymerization conditions.

Table 2. Estimated polymerization rate constant k_p of the polymerization of PEtOx with **FurMalNos 4** using three different monomer-to-initiator ratios (Adapted from 267).

[EtOx]/[FurMalNos]	k_p (10^{-6} L mol^{-1} s^{-1})
20:1	158
40:1	166
60:1	160

As conversion increased, all SEC traces shifted towards lower retention times (**Figure 40**, **Figure 41** and **Figure 42**). In addition, number-average molar masses (M_n) increased linearly, while dispersity values remained confined between 1.1 and 1.2 (**Figure 39B**), evidence of a polymerization with living character. It is important to mention that to obtain the M_n and $Đ$ values from the chromatogram, the integration of the polymer peak was selected from low

elution times to approximately 33 minutes because of an overlap with an SEC system peak. Therefore, M_n and $Đ$ can be considered estimates. Nevertheless, at high conversions the values obtained can be considered quite accurate since minimal overlap is observed.

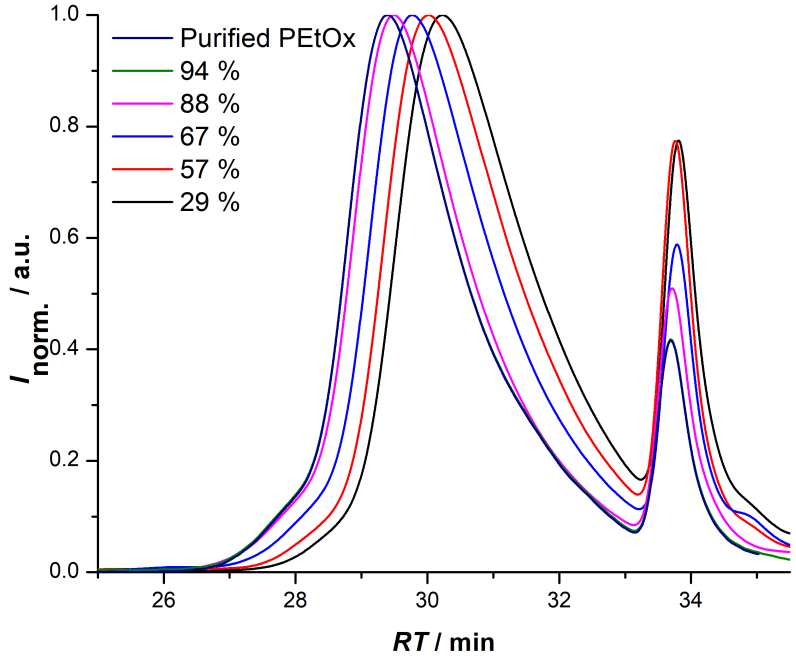

Figure 40. Overlay of SEC traces for the CROP of 2-ethyl-2-oxazoline at 50 °C in acetonitrile using **FurMalNos 4** as initiator. [EtOx] = 1.5 M. [EtOx]/[**FurMalNos**] = 20 (Adapted from 267).

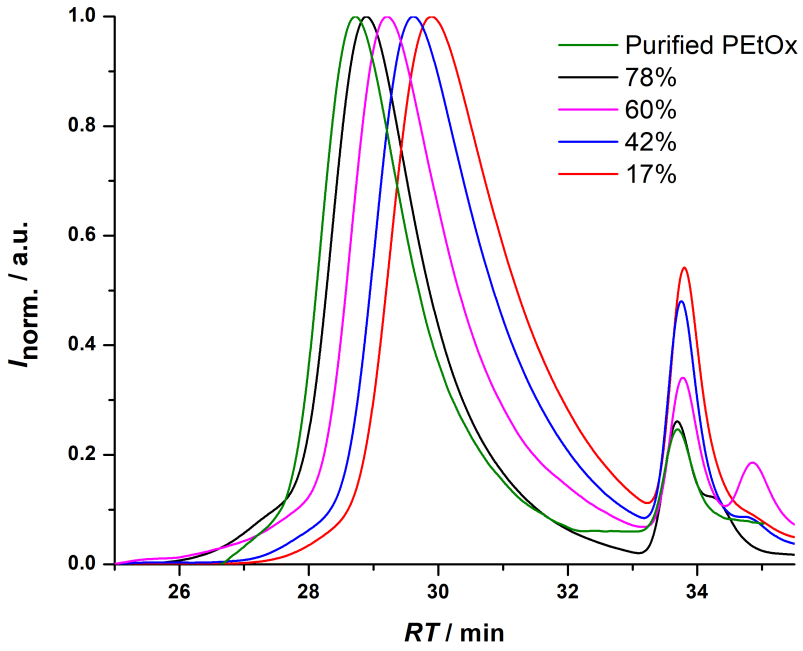

Figure 41. Overlay of SEC traces for the CROP of 2-ethyl-2-oxazoline at 50 °C in acetonitrile using **FurMalNos 4** as initiator. [EtOx] = 1.5 M. [EtOx]/[**FurMalNos**] = 40 (Adapted from 267).

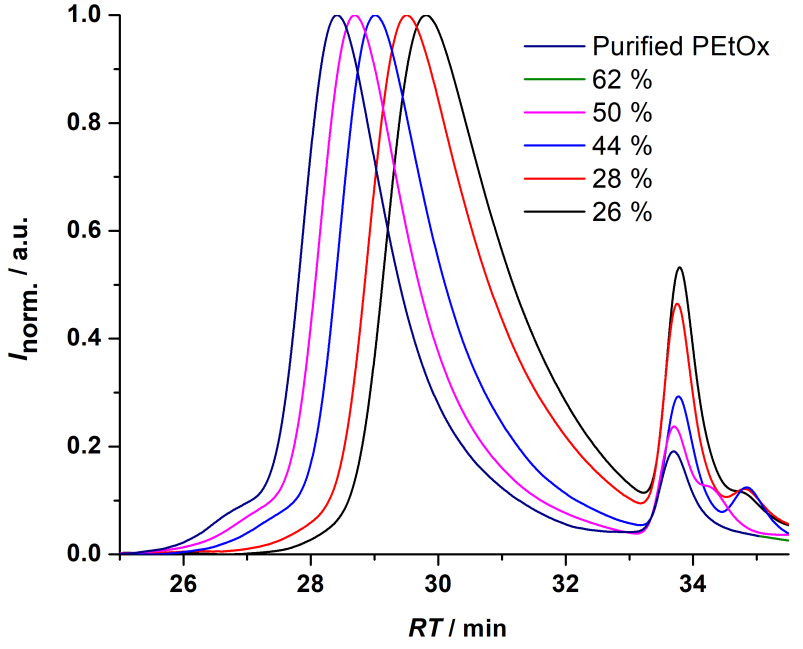

Figure 42. Overlay of SEC traces for the CROP of 2-ethyl-2-oxazoline at 50 °C in acetonitrile using **FurMalNos 4** as initiator. [EtOx] = 1.5 M. [EtOx]/[**FurMalNos**] = 60 (Adapted from 267).

The linear increase of M_n values with conversion, along with low $Đ$, demonstrates that **FurMalNos 4** enables the synthesis of well-defined polymers, despite the signs of slow initiation. The M_n values obtained from SEC are significantly higher than the expected theoretical ones, another evidence suggesting the slow initiating nature of reaction. However, the difference in the values is also partly caused by M_n values calculated with a calibration based on poly(methyl methacrylate) standards, which results in an overestimation.[268] To calculate molar masses for final samples after purification, ^{1}H NMR spectroscopy was used. The end group signals from the protected maleimide, found at 5.2 and 6.5, were compared to the signals corresponding to the side chain and backbone of the polymer (**Figure 43A**). A summary of the obtained M_n values, and the relevant characteristics of the polymers obtained is provided in **Table 3**. The $M_{n,NMR}$ values obtained were significantly closer to the theoretical ones, in contrast to the SEC results. For instance, for the α-furan-maleimide-PEtOx sample prepared with DP 40 ([EtOx]/[**FurMalNos**] = 40), after 78% conversion, the $M_{n,SEC}$ value obtained was 10600 g mol^{-1}, whereas $M_{n,NMR}$ was 6100 g mol^{-1}. Although the value obtained with ^{1}H NMR is significantly closer, it is still higher than the theoretical one. This corroborates the slow initiation that would result in a higher effective monomer-to-initiator ratio throughout a significant part of the polymerization. Another possible explanation for the discrepancy between experimental and theoretical values, can also involve a low initiator efficiency. In this case, the difference between the expected and NMR-calculated degrees of polymerization of the resulting polymer would lead to a 53% initiator efficiency. However, even when there may be a low initiator efficiency, it does not have implications on the actual functionalization of the α end chain of the polymer.

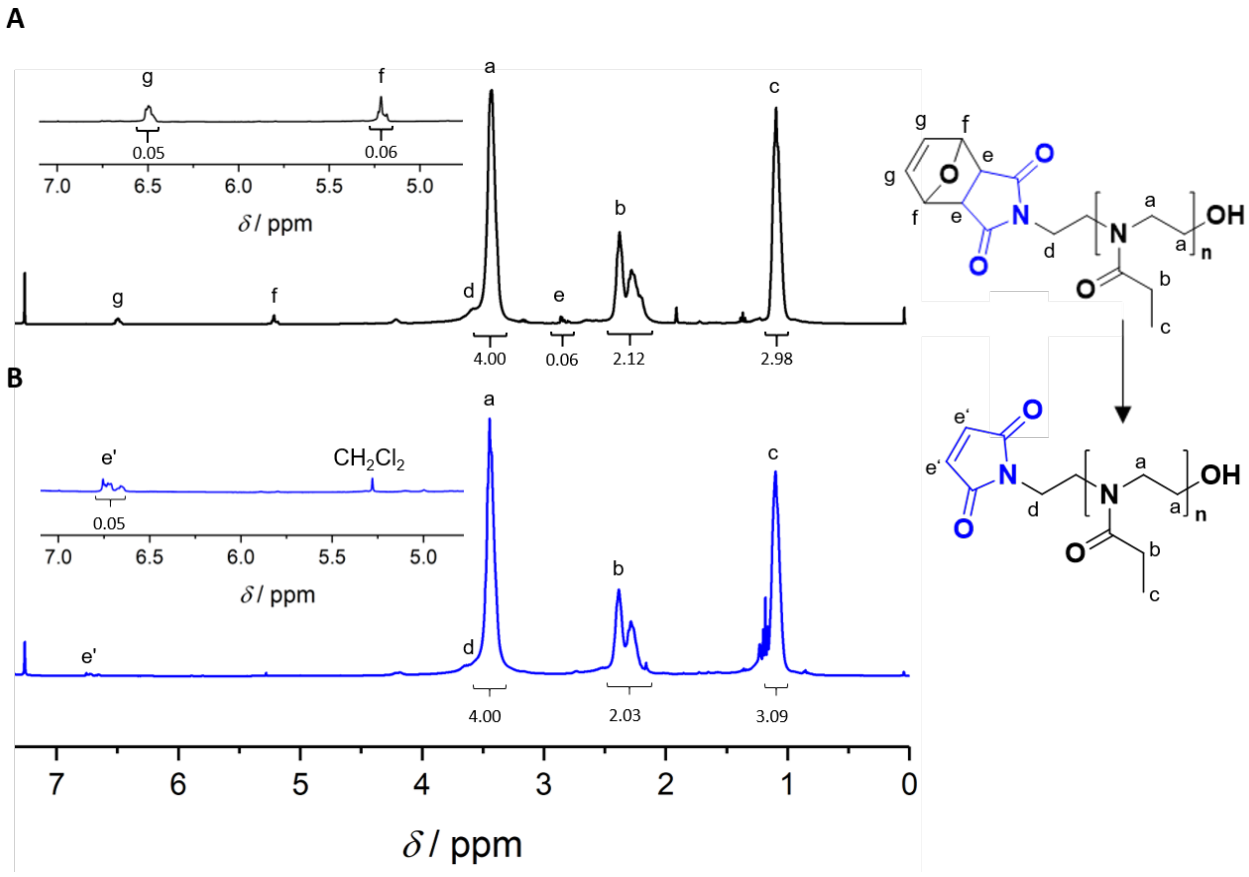

Figure 43. ^{1}H NMR spectra of a poly(2-ethyl-2-oxazoline) **FurMal-PEtOx** obtained through **FurMalNos 4** initiation ([EtOx]/[**FurMalNos**] = 20; $M_{n,SEC}$ = 6500 g mol^{-1}, $Đ$ = 1.20; $M_{n,NMR}$ = 4400 g mol^{-1}) before (A) and after (B) deprotection of the maleimide group by retro-Diels–Alder cycloelimination (Adapted from 267).

Table 3. Summary of the characterization of the final purified products of the polymerization of EtOx with **FurMalNos 4** as the initiator (Adapted from 267).

[EtOx]/ [FurMalNos]	Conversion (%)	$M_{n,theo}$ (g mol^{-1})	$M_{n,NMR}$ (g mol^{-1})	$M_{n,SEC}$* (g mol^{-1})	$Đ$
20	94	2190	4400	6500	1.20
40	78	4172	6100	10600	1.13
60	62	6153	6700	11900	1.16

*Relative to PMMA standards

3.3.1.1. Bifunctional heterotelechelic PEtOx

The functionalization of PAOx using the initiation approach provides the possibility to produce a bifunctional polymer by addition of a moiety on the ω end chain by termination. The successful polymerization with **FurMalNos 4** led to preliminary tests to form a PEtOx-based macro-CTA by termination with the deprotonated version of a pentanoic acid-bearing dithiobenzoate RAFT agent (**Figure 44**). PEtOx-based macro CTAs can be used for the synthesis of block copolymers and the formation of maleimide-functionalized nanoparticles by polymerization induced self-assembly (PISA).

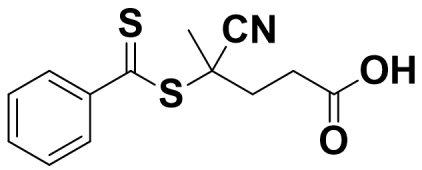

Figure 44. RAFT agent used in the present study 4-cyano-4-(phenylcarbonothioylthio)pentanoic acid.

The CROP initiated by **FurMalNos 4** was performed using similar reaction conditions described in previous experiments, except the termination was carried out using 1.5 equivalents of the selected RAFT agent (DTB) deprotonated *in situ* with TEA. The produced polymers, with DPs 20 and 40, were characterized by ^{1}H NMR, SEC, and ESI-MS to confirm the introduction of both functional groups at the end chain (**Figure 45**, **Figure 46**, and **Figure 47**). ^{1}H NMR shows the characteristic signals of the protected maleimide at 5.2 and 6.5 and the successful introduction of the CTA observed by the signals of the dithiobeozoate group between 7.3 and 8 ppm (**Figure 45**). A comparison between the integral values of the end groups shows a lower proportion of CTA protons than expected, indicating the termination was not quantitative. Calculated $M_{n,NMR}$ values obtained by comparing the integrals of the protected maleimide signals to polymer backbone are in close agreement to those calculated for **FurMalPEtOx** from previous experiments. ESI-MS spectra of both synthesized polymers (**Figure 46**) show that the most prominent population can be assigned to the FurMalPEtOx-DTB structure. Although the

presence of other signals with lower intensity is observed, these could not be assigned. SEC traces, in **Figure 47**, show a broader distribution compared to **FurMalPEtOx**. This can be an indication of possible side reaction during termination, since it has been proved that narrow distributions can be achieved with initiator **FurMalNos 4**. Optimization of this synthesis to achieve well-defined polymers can lead to a number of applications depending on the co-monomer of choice.

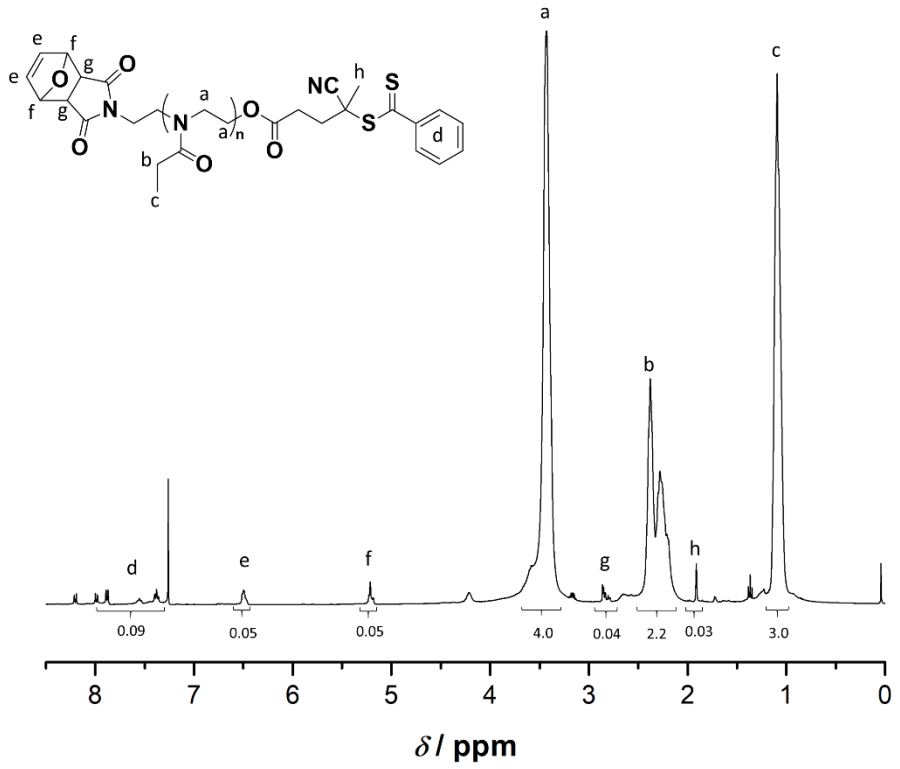

Figure 45. ^{1}H NMR spectrum of **FurMal-PEtOx-DTB** obtained after CROP of EtOx initiated by **FurMalNos 4** and terminated by **DTB** RAFT agent using [EtOx]/[**FurMalNos**] = 20.

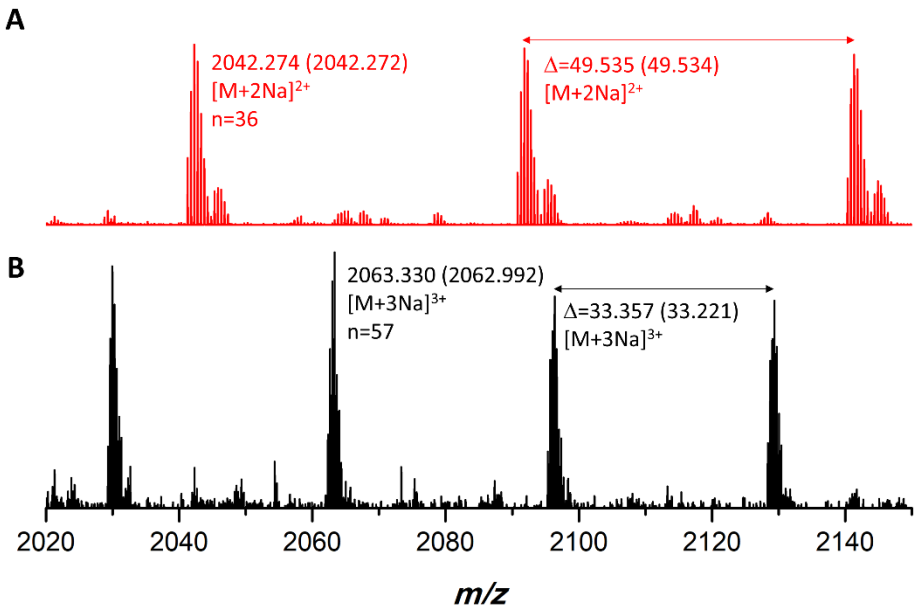

Figure 46. ESI-MS spectra of **FurMal-PEtOx-DTB** obtained after CROP of EtOx initiated by **FurMalNos 4** terminated by **DTB** RAFT agent using [EtOx]/[**FurMalNos**] = 20 (A) and 40 (B).

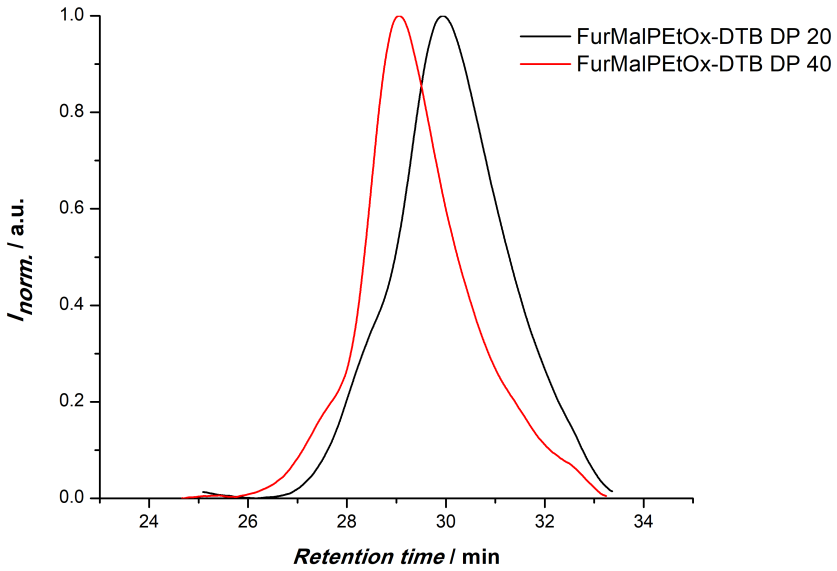

Figure 47. SEC traces of **FurMal-PEtOx-DTB** obtained after CROP of EtOx initiated by **FurMalNos 4** terminated by **DTB** RAFT agent using [EtOx]/[**FurMalNos**] 20 and 40. The polymers show a broader distribution indicating a certain loss of control of the polymerization.

A summary of the obtained M_n values, and the relevant characteristics of the polymers obtained is provided in **Table 4**.

Table 4. Summary of the characterization of the products of the polymerization of EtOx initiated by **FurMalNos 4** and terminated by DTB RAFT agent

[EtOx]/ [FurMalNos]	$M_{n,theo}$ (g mol^{-1})	$M_{n,NMR}$ (g mol^{-1})	$M_{n,SEC}$* (g mol^{-1})	$Đ$
20	2450	4400	6600	1.25
40	4430	6100	8700	1.26

*Relative to PMMA standards

3.3.2. Thiol initiator

Contrary to the polymerization initiated with the protected maleimide initiators, the CROP of 2-ethyl-2-oxazoline using the synthesized thiol-functional initiators was performed using optimized microwave conditions,[97] at 140 °C and with acetonitrile as reaction solvent, since in principle, no thermal incompatibility is expected (**Scheme 17**).

To assess the ability of both alkyl sulfonate esters to start the polymerization, a first set of experiments was carried out with [EtOx] = 4 M and a degree of polymerization of 50. After 7.5 minutes under microwave irradiation, the SEC traces of the polymers obtained revealed dispersities of 1.20 and 1.10 for **ThioAcTos 6** and **ThioAcNos 8**, respectively (**Figure 48**). Although both dispersity values are good indication of a controlled polymerization, the broader molar mass distribution, and the shape of the signal that shows some tailing on the SEC traces obtained when initiating the polymerization with **ThioAcTos 6,** indicate a lack of control on the polymerization, compared to the very low $Đ$ value (1.1) of the polymers initiated with **ThioAcNos 8**. For this reason, only the latter was used for subsequent experiments.

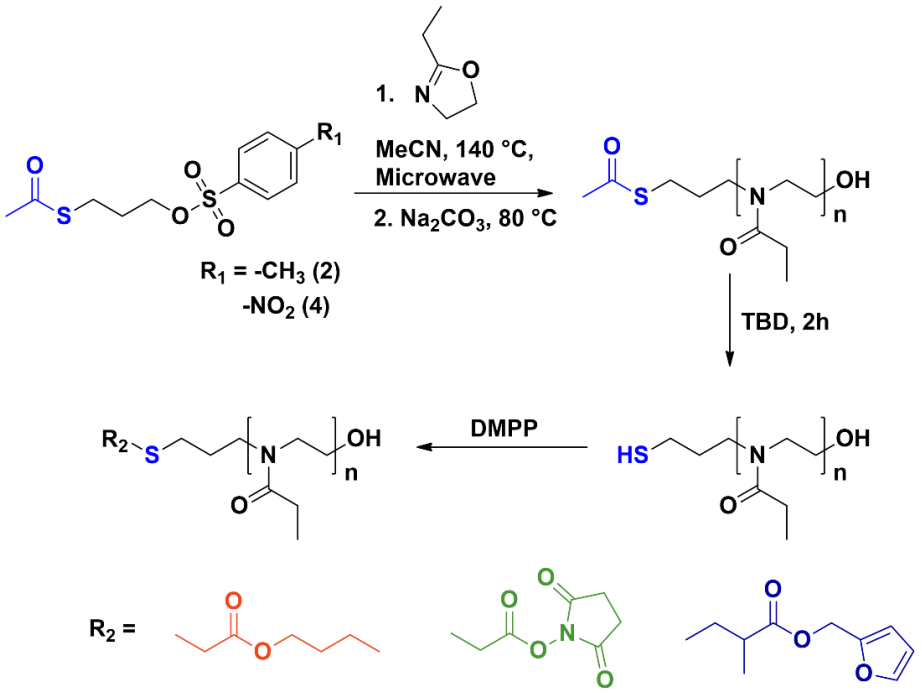

Scheme 17. Synthetic route for the synthesis of **α-Thiol-PEtOx** by polymerization of EtOx using functional initiators **6** and **8**, followed by deprotection, and subsequent Michael addition with three model molecules.

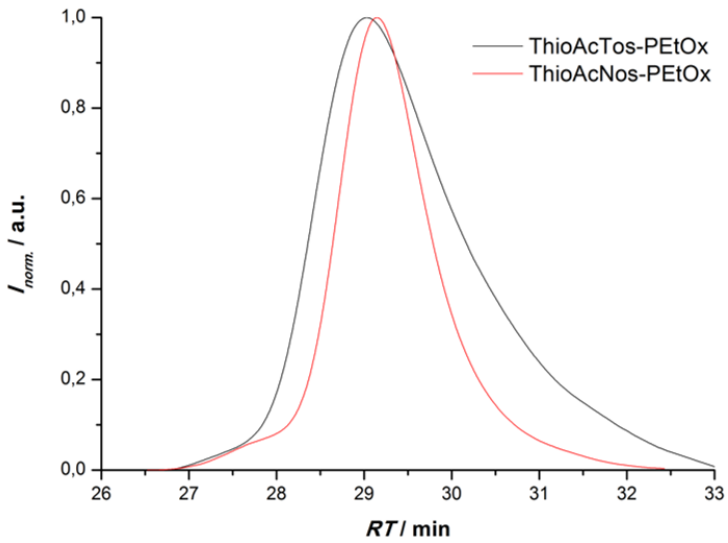

Figure 48. SEC traces of PEtOx obtained with either **ThioAcTos 6** or **ThioAcNos 8** as initiator. Microwave assisted polymerization at 140 °C in acetonitrile for 7.5 minutes. Polymers made with **ThioAcTos 6** show a broader distribution and tailing, indicating the loss of control over the polymerization.

Kinetic studies of a set of polymers with three different monomer to initiator ratios (20, 40, and 60) were carried out (**Figure 50**). As expected, the polymerization proceeds faster when a lower monomer-to-initiator ratio is used (**Figure 50A**).[240] It is worth highlighting the advantages of the compatibility of this initiator with the use of a single-mode microwave reactor. Compared to the previously described **FurMalNos 4** initiated reaction, where polymerization reactions took over 70 hours to get to a high conversion, with the **ThioAcNos 8** initiator the reaction rate was enhanced so that in less than 150 seconds, high conversions were already achieved in all cases (**Figure 49**).

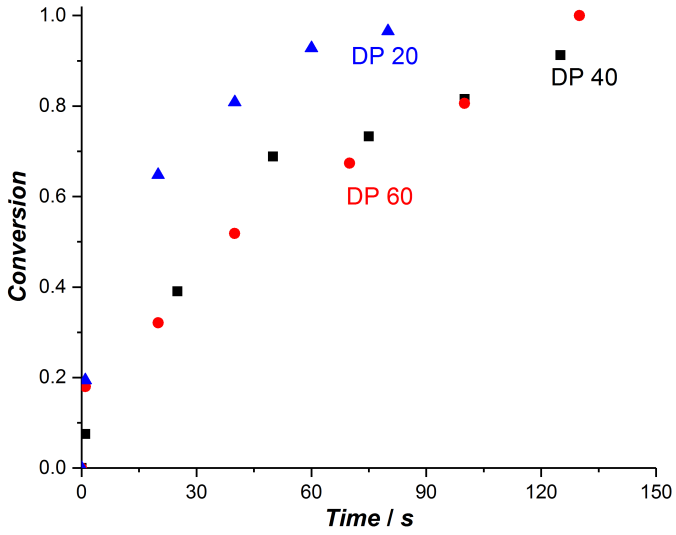

Figure 49. Monomer conversion as a function of time for the CROP of 2-ethyl-2-oxazoline at 140 °C in acetonitrile using **ThioAcNos 8** as initiator at three distinct targeted degrees of polymerization DP = [EtOx]/[**ThioAcNos**].

All kinetic experiments performed show a linear increase of *ln(1/1-conversion)* as conversion progressed, which indicates a constant concentration of the propagating species, a requirement to obtain the living character of a polymerization (**Figure 50**). The propagation constants were calculated for the three different DPs used, according to the same procedure described for **FurMalNos 8** in section **0**. The obtained values, shown in **Table 5**, are quite similar, which shows

the k_p obtained is independent of the DP used. Compared to the k_p calculated for the polymerization using **FurMalNos 4**, the k_p values of the polymerization performed with **ThioAcNos 8** are three orders of magnitude larger, further highlighting the advantages of higher temperatures enabled by microwave irradiation at enhancing the polymerization rate.

Table 5. Estimated polymerization rate k_p of the polymerization of PEtOx with **ThioAcNos 8** using three different monomer to initiator ratios.

[EtOx]/[ThioAcNos]	k_p (10^{-3} L mol^{-1} s^{-1})
20:1	200
40:1	190
60:1	225

Additionally, the SEC traces of the samples taken at time intervals show a linear increase of the number-average molar masses (M_n), dispersity values below 1.11 (**Figure 50B**), and a uniform shift to higher retention times as conversion increases (**Figure 51** and **Figure 52**). All of this is in agreement with living polymerization conditions. The difference between theoretical and experimental M_n values in this case, again comes from the calculation of the experimental values relative to poly(methyl methacrylate) standards which results in an overestimation.[268] Similar to the chromatograms obtained from the maleimide-functionalized polymers, the M_n and $Đ$ values can be considered estimates, since the integration was done in the same way for all samples (from low elution times to approximately 33 minutes due to overlap with an SEC system peak).

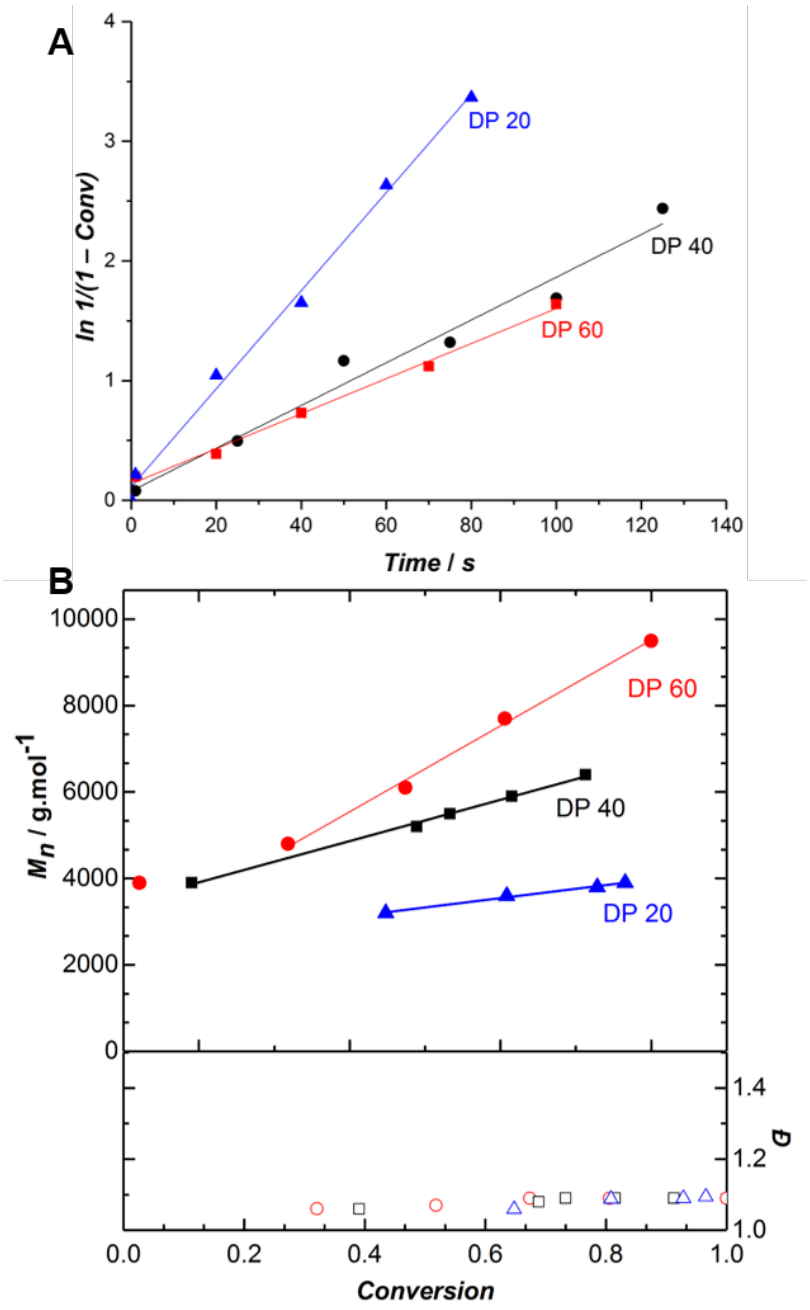

Figure 50. (A) First-order kinetic plots and (B) evolution of the number-average molar mass and dispersity vs conversion for the CROP of EtOx initiated by **ThioAcNos 4** at various targeted degrees of microwave-assisted polymerization (DP = [EtOx]/[**ThioAcNos**]) in MeCN at 140 °C. [EtOx] = 4 M.

The calculation of the molar masses of the purified samples obtained at the end of the polymerization was done using ^{1}H NMR spectroscopy. The visible end group signals of the initiator, found at 1.8, 2.8, and 4.4, were compared to the side chain and backbone of the polymer (**Figure 53**). A summary of the calculated results, along with other relevant features of the synthesized polymers, is shown in **Table 6**. The $M_{n,NMR}$ values obtained were significantly closer to the theoretical values, compared to the $M_{n,SEC}$ results. For instance, for the α-thioacetate-PEtOx sample prepared with DP 40 ([EtOx]/[**ThioAcNos**] = 40), after 91% conversion, the $M_{n,SEC}$ value obtained was 5800 g mol^{-1}, whereas $M_{n,NMR}$ was 4100 g mol^{-1}. The value obtained with ^{1}H NMR is very close to the expected theoretical value, which indicates a high efficiency of the initiator. Even when the obtained $M_{n,NMR}$ values are in the case of DP 20 and 40 slightly above what is expected, it is probably caused by a negligible amount of chain transfer reactions occurring during the polymerization, with proton-initiated chains as by-product. Nevertheless, the living polymerization requirements of linear increase in polymer chain size as conversion progresses, and low molar mass dispersities are still satisfied.

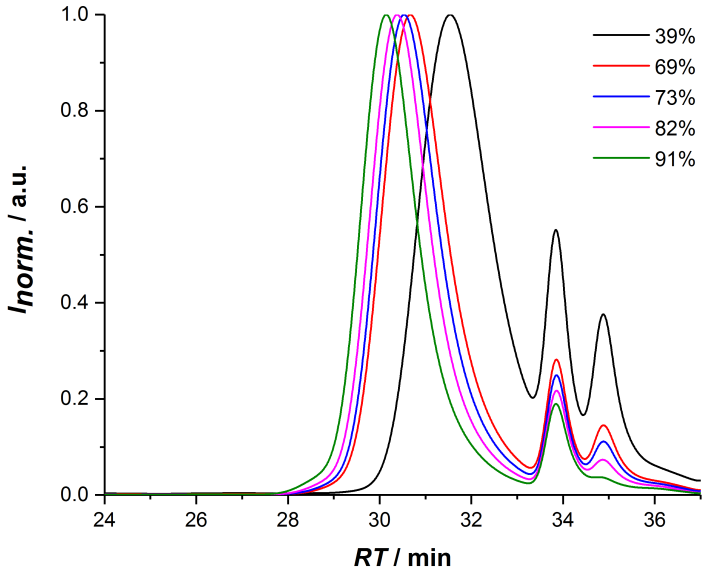

Figure 51. Overlay of SEC traces for the CROP of 2-ethyl-2-oxazoline at 140 °C in acetonitrile using **ThioAcNos 8** as initiator. [EtOx] = 4 M. [EtOx]/[**ThioAcNos**] = 40.

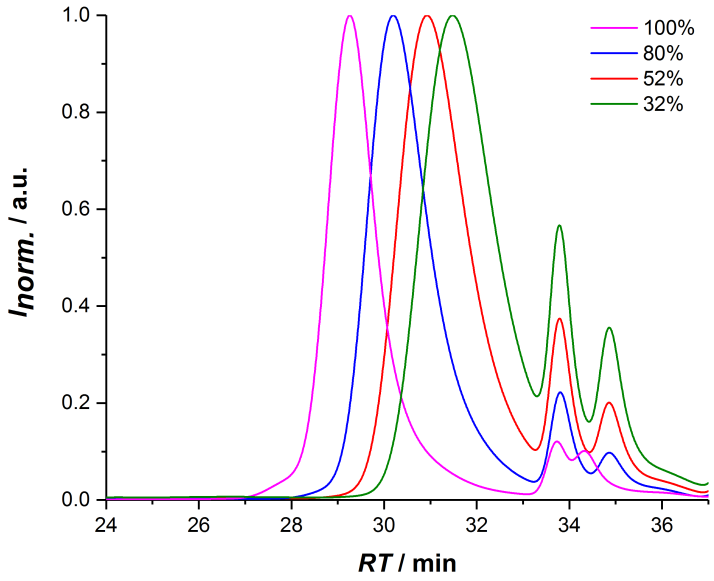

Figure 52. Overlay of SEC traces for the CROP of 2-ethyl-2-oxazoline at 140 °C in acetonitrile using **ThioAcNos 8** as initiator. [EtOx] = 4 M. [EtOx]/[**ThioAclNos**] = 60.

Table 6. Summary of the characterization of the final purified products of the polymerization of EtOx with **ThioAcNos 8** as the initiator.

[EtOx]/ [ThioAcNos]	Conversion (%)	Yield (%)	$M_{n,theo}$ (g mol^{-1})	$M_{n,\ NMR}$ (g mol^{-1})	$M_{n,\ SEC}$* (g mol^{-1})	$Đ$
20	97	89	2246	2700	3800	1.08
40	91	83	3909	4100	5800	1.09
60	100	87	6277	5500	9500	1.09

*Relative to PMMA standards

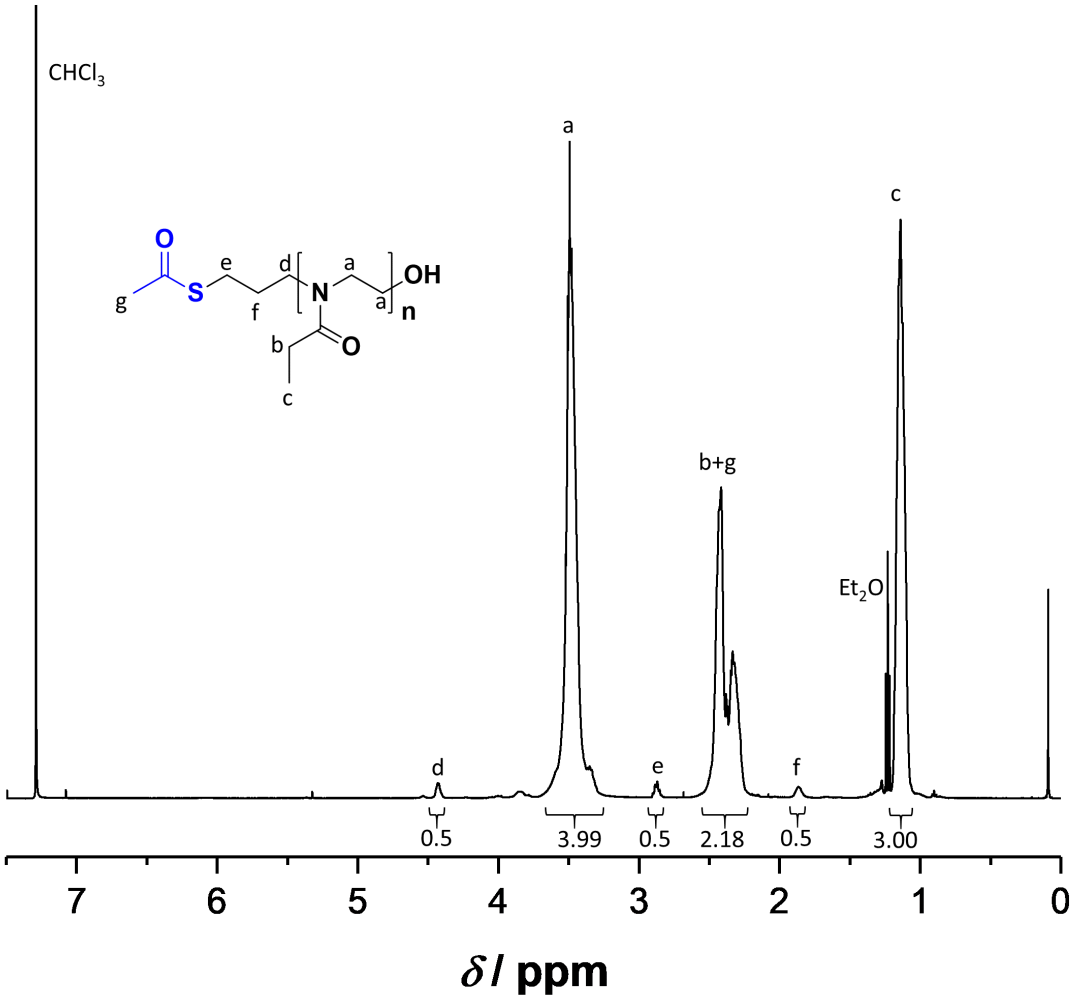

Figure 53. ^{1}H NMR spectra of a poly(2-ethyl-2-oxazoline) **ThioAc-PEtOx** obtained through **ThioAcNos 8** initiation ([EtOx]/[**ThioAcNos**] = 40; $M_{n,SEC}$ = 5800 g mol^{-1}, $Đ$ = 1.09; $M_{n,NMR}$ = 4100 g mol^{-1}).

The compatibility of the new initiator **ThioAcNos 8** with the polymerization conditions using a single-mode microwave reactor gave the reaction the advantages such as enhanced reaction rates and reduction of side reactions, while maintaining first-order kinetics of the monomer consumption and the livingness of the polymerization.[97]

3.4. Deprotection and reactivity assessment

3.4.1. Maleimide-PEtOx

A polymer **FurMal-PEtOx** obtained at 94% conversion ($M_{n,SEC}$ = 6500 g mol^{-1}, $Đ$ = 1.20; $M_{n,NMR}$ = 4400 g mol^{-1}) was purified to confirm the nature of the end groups, and was later used for coupling reactions. To evaluate the stability of the furan-protected maleimide throughout the polymerization and to monitor further modifications, ^{1}H NMR spectroscopy and ESI-MS were used (**Figure 43** and **Figure 54**). The ^{1}H NMR spectrum of **FurMal-PEtOx** shows the expected signals for the 6 methine protons (e–g) of the furan-maleimide Diels–Alder cycloadduct (**Figure 43A**). In addition, no signal corresponding to vinyl protons of deprotected maleimide was found (expected δ at approx. 6.7 ppm). The stability of the protecting group was corroborated by ESI-MS with the presence of a major population corresponding to chains having the initiating group and a hydroxyl moiety as the end groups (**Figure 54A**). The major side-product is a proton-initiated PEtOx, which is seen in most PAOx reports and originates from a chain transfer reaction via β-elimination described in section **2.2.1**.[101]

Thermal treatment in toluene at 110 °C for 4 h yielded the deprotected α-functional **Mal-PEtOx**. As shown in the ^{1}H NMR spectrum, the characteristic oxanorbornene signals of the cycloadduct quantitatively disappeared (**Figure 43B**), leaving new signals (e') corresponding to vinylic protons of an electron-deficient structure. When integrating the corresponding signals, the similar integration values obtained evidence the quantitative survival of the maleimide. To assess chain-end transformation, mass spectrometry was used. While the original signals assigned to **FurMal-PEtOx** vanished, a new set of peaks with a shift of about 34 amu (doubly charged species) corresponding to the loss of a furan molecule was observed after thermal treatment (**Figure 54B**).

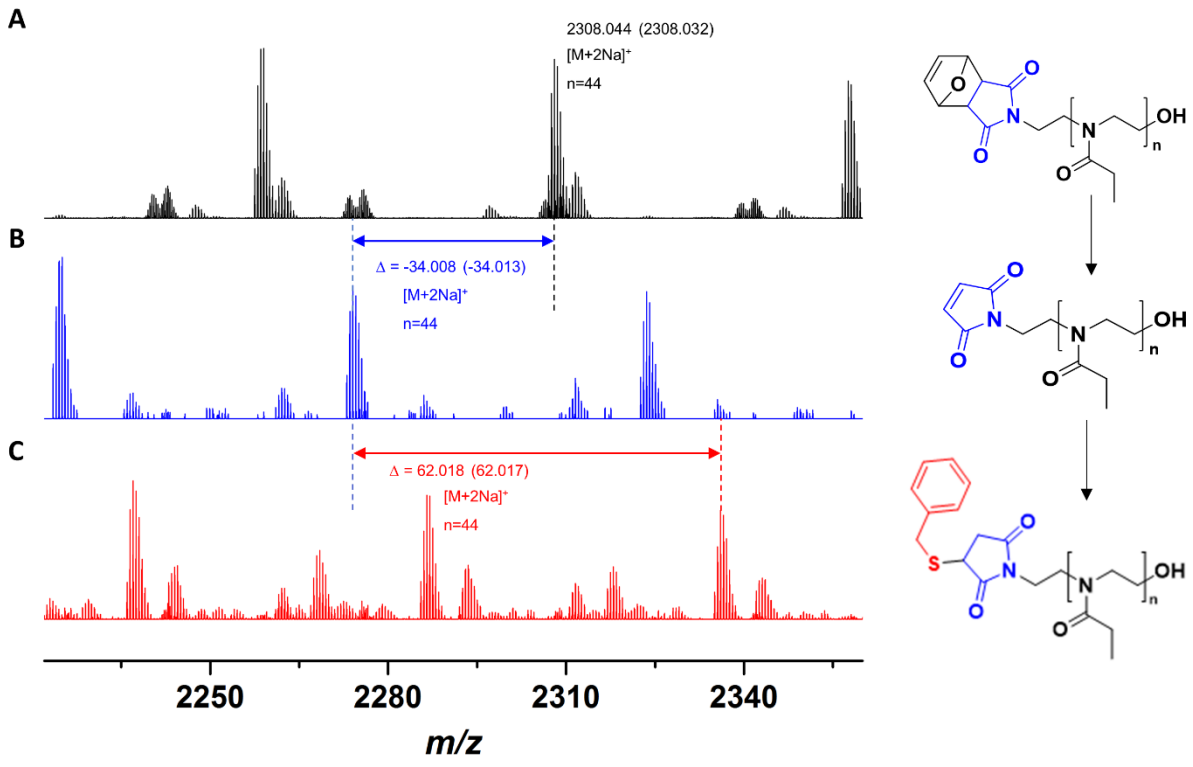

Figure 54. ESI-MS spectra of (A) **FurMal-PEtOx** as obtained after CROP of EtOx initiated by **FurMalNos**, (B) **Mal-PEtOx** obtained after thermal treatment of **FurMal-PEtOx**, and (C) the Michael addition product of **Mal-PEtOx** with benzyl mercaptans (BzSMal-PEtOx) (Adapted from 267).

The reactivity of the maleimide group of **Mal-PEtOx** was evaluated by trimethylamine-catalyzed Michael addition with a model thiol. In this case benzyl mercaptan was chosen. Again, the peak corresponding to the precursor polymer disappeared and a new main population appeared with a shift of approximately 62 amu considering double charges, which perfectly matches the addition of a benzyl mercaptan molecule, proving the reactivity of the maleimide at the α end of the polymeric chain (**Figure 54C**). Two by-products on the ESI MS spectrum are observed but it was not possible to identify them. The integrity of the polymer backbone during the successive transformations could be confirmed by SEC, where no significant difference in the molar mass distributions of **FurMal-PEtOx**, **Mal-PEtOx**, and **BzSMal-PEtOx** was observed (**Figure 55**; M_n = 6500–7000 g mol^{-1}, $Đ$ = 1.20–1.27).

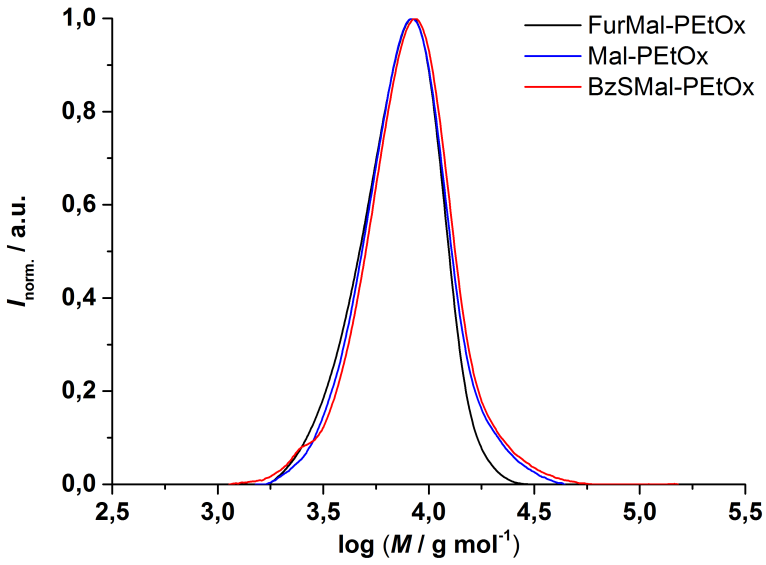

Figure 55. Overlay of SEC traces of **FurMal-PEtOx** ($M_{n,SEC}$ = 6500 g mol^{-1}, $Đ$ = 1.20), its deprotection **Mal-PEtOx** ($M_{n,SEC}$ = 6900 g mol^{-1}, $Đ$ = 1.24), and **BzSMal-PEtOx** ($M_{n,SEC}$ = 7000 g mol^{-1}, $Đ$ = 1.27) obtained by Michael addition with benzyl mercaptan (Adapted from 267).

3.4.2. Thiol-PEtOx

The purified polymer **ThioAc-PEtOx** (DP = 40, $M_{n,SEC}$ = 5800 g mol^{-1}, $Đ$ = 1.09 ; $M_{n,NMR}$ = 4100 g mol^{-1}) was used to confirm the nature of the end groups, and then for deprotection and modification with model molecules. The deprotection procedure was achieved using triazabicyclodecene (TBD), a mild base, and characterized via SEC (**Figure 57**) and ESI-MS (**Figure 56**). As shown in the ESI-MS spectra of the **ThioAcPEtOx** and its deprotected version, **Thiol-PEtOx**, the shift in the signals of 21 amu considering double charges matches the theoretical expected value. The presence of another polymer family is visible, since there are smaller signals from another distribution in the spectra. It corresponds to the product of chain-transfer reactions during the polymerization: proton-initiated chains, with a hydroxyl group on the ω end chain. Although ESI-MS is not a quantitative method, it can be assumed that the size of this secondary population is much smaller than the main and targeted polymer structure. These

proton-initiated chains, however, increase the calculated value $M_{n,NMR}$, and can explain the slightly higher $M_{n,NMR}$ value, compared to the theoretical M_n.

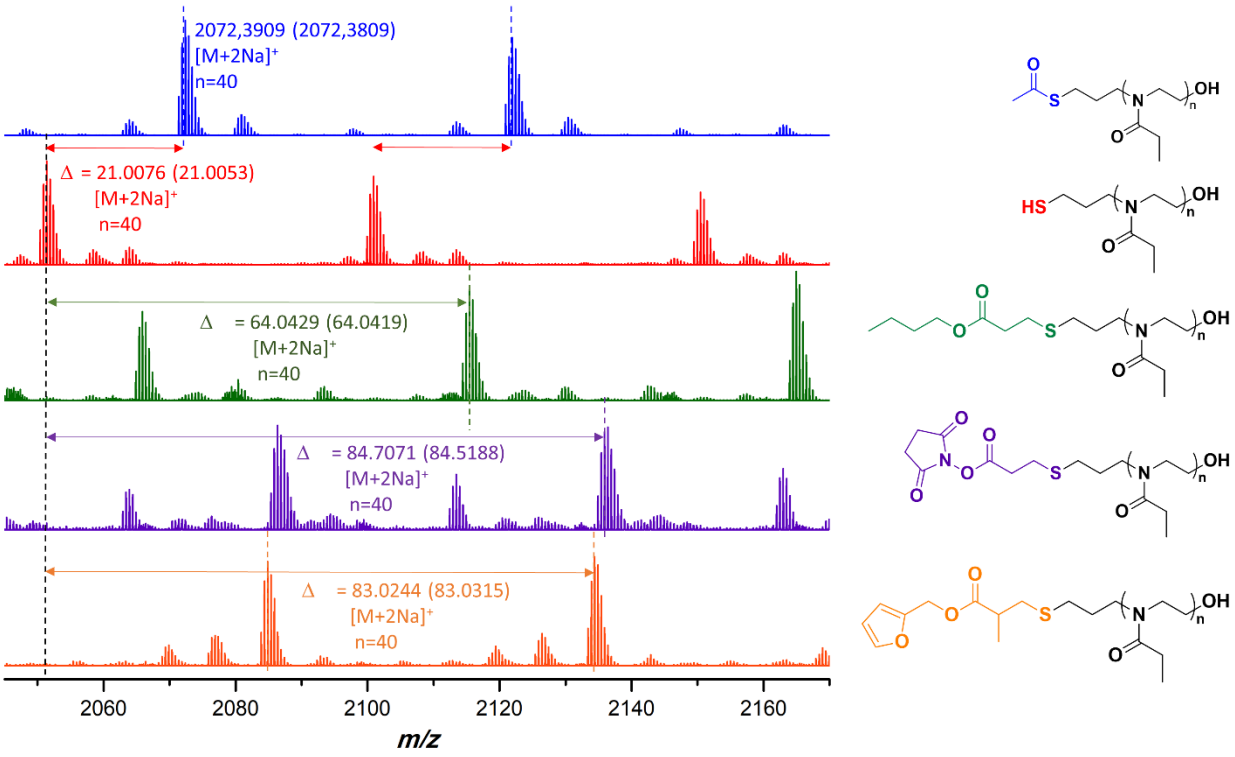

Figure 56. ESI-MS spectra of **ThioAc-PEtOx** as obtained after CROP of EtOx initiated by **ThioAcNos**, **Thiol-PEtOx** obtained after treatment of **ThioAc-PEtOx** with TBD, and the Michael addition products of **Thiol-PEtOx** with butylacrylate (**BA-thiol-PEtOx**), acrylic acid NHS (**NHS-thiol-PEtOx**), and furfuryl methacrylate (**FurfurylMA-thiol-PEtOx**).

As previously mentioned, the versatility of the thiol group allows a wide range of reactions. In this study, three different model molecules were attached to the polymer via Michael addition: *n*-butyl acrylate, acrylic acid NHS ester, and furfuryl methacrylate. In each case, in ESI-MS, the major population is shifted from the deprotected thiol signal to a value that corresponds to the change in molar mass expected from the addition of the chosen molecule (**Figure 56**). There is a number of smaller signals appearing after the Michael addition of the model molecules that have not been identified. It is assumed these correspond to the occurrence of side reactions.

Nevertheless, the SEC traces show the backbone structure of the polymer is conserved (**Figure 57**).

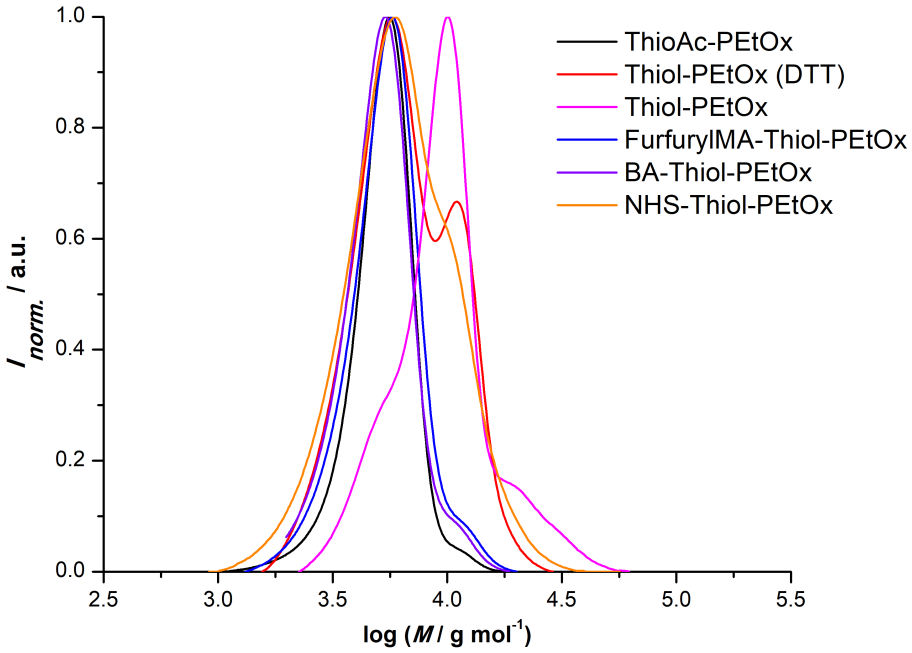

Figure 57. Overlay of SEC traces of **ThioAc-PEtOx** ($M_{n,SEC}$ = 5800 g mol^{-1}, $Đ$ = 1.09; $M_{n,NMR}$ = 4100 g mol^{-1}), its deprotection product **Thio-PEtOx** with and without a reducing agent (DTT), and the products of the Michael addition of furfuryl methacrylate **FurfurylMA-Thiol-PEtOx,** and butyl acrylate **BA-Thiol-PEtOx**.

3.5. Bioconjugation

As described in section **2.1.2.2**, PAOx have been discussed as a promising option for stealth polymers[88] and, as such, can be used for "PAOxylation" of proteins. Examples include the conjugation of PEtOx and PMeOx to model proteins such as catalase,[269] horseradish peroxidase,[270] bovine serum albumin,[43] uricase,[43] insulin,[43] and granulocyte colony stimulating factor.[119]

Considering the relatively low abundance of free cysteine residues in natural proteins, the maleimide-mediated functionalization with polymers can provide specificity to the conjugate, compared with other coupling strategies using lysine residues. The thiol addition to the activated double bond in aqueous conditions works best at neutral or mild alkaline pH (7.5–8.5).[51]

An experiment to conjugate a functional **Mal-PEtOx** ($M_{n,NMR}$ = 6100 g mol^{-1}) to BSA was performed. BSA was chosen as a model protein since it has one free cysteine exposed on its surface (Cys-34 residue) and available for conjugation.[271] The conjugation reaction ran overnight with three different polymer-to-protein molar ratios f (5, 10, and 15) in 100 mM phosphate buffer at pH 7.6. Under these pH conditions, it is ensured that no conjugation via the amino group of lysine residues happens, ensuring only attachment of the free cysteine present in BSA.[230]

The characterization of the resulting conjugate was performed using SDS-PAGE electrophoresis and MALDI spectrometry (**Figure 58**). For SDS-PAGE, in all lanes corresponding to the incubation of BSA with **Mal-PEtOx** a shift in the protein signal towards higher molar masses can be observed, indicating successful conjugation. The BSA signal broadened because only about 55 to 70 percents of commercial BSA actually contain the free cysteine residue,[258] which means this signal is a mixture of native and conjugated BSA. In addition, there was no shift observed when non-deprotected **FurMal-PEtOx** was incubated with BSA in identical conditions. To further characterize the conjugate, a preparative chromatographic separation was done and a sample collected at lower retention time than the BSA eluting time (highest intensity

considered) was analyzed by MALDI-ToF mass spectrometry. The spectrum of the conjugated sample (**Figure 58C**, bottom) shows a mixture of two species. First, a signal corresponding to the mass of pure BSA, which was expected since not all BSA molecules contain a free thiol available for conjugation, and a second population at higher *m/z* with a shift corresponding approximately to the mass of **Mal-PEtOx**. The second signal exhibits a significantly broader distribution than the protein, as expected from a synthetic polymer-protein conjugate.

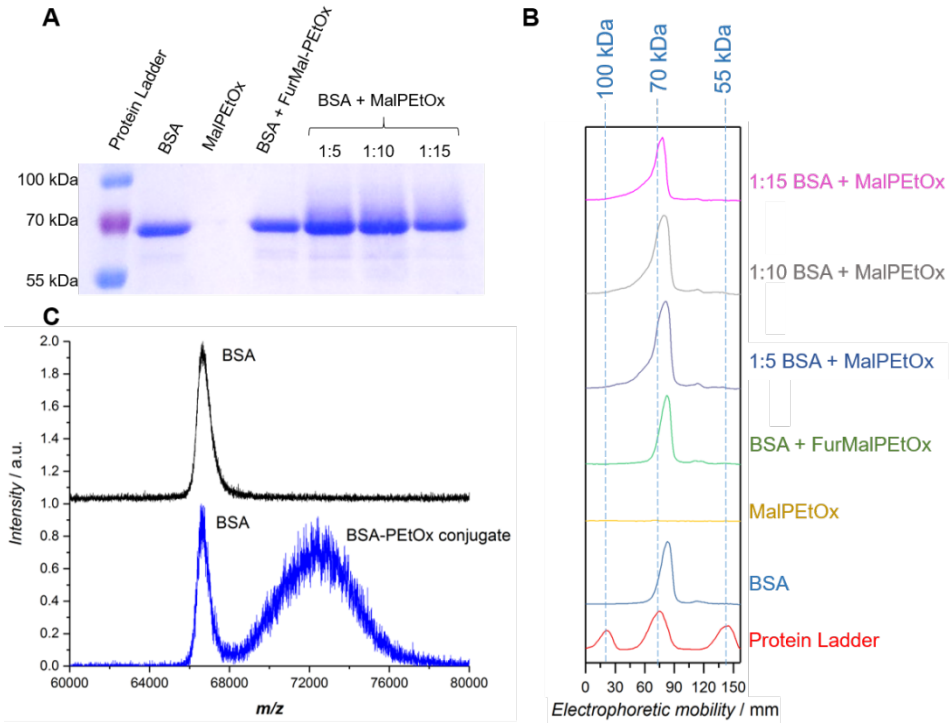

Figure 58. Protein conjugation experiment in 100 mM phosphate buffer at pH 7.6 for 18 hours at room temperature using three different [Mal-PEtOx]/[BSA] ratios. A) SDS-PAGE gel stained with Coomassie blue. B) Intensity of the signals from each lane as a function of electrophoretic mobility. C) MALDI-ToF spectra of (top) BSA and (bottom) the fraction collected after preparative FPLC of the PEtOx-BSA conjugate (Adapted from 267).

These results are an early proof that show the possibility of conjugation of the synthesized **Mal-PEtOx** to model proteins. Further investigations should be conducted to assess the ability of PEtOx to provide a stealth character similar to PEG.

3.6. Surface functionalization

Several strategies to graft PAOx on surfaces have been reported.[272,273] A simple and popular method uses α- or ω-functional PAOxs prepared with either a functional initiator, or a terminating agent, to add (directly or after modification) a coupling agent at the end chain.[273,272] Functionalities introduced by direct end-capping of the living polymer species to be used as anchors for the modification of substrates include silanes,[153,274] alkene,[153] xanthane,[261] and alkyne[275] groups. For similar surface immobilization purposes, allyl-,[153] disulfide-,[265] and alkyne-functional initiators[276] were used to produce α-functionalized PAOxs. Alternative strategies to graft PAOx on substrates include surface-initiated or -terminated polymerization,[265,277,278] photo-immobilization of the polymer at the backbone or the side chain,[273,272] and the use of graft copolymers bearing a coupling moiety.[273,272]

For this project, the synthesized α-**Thiol-PEtOx** using the initiator strategy were immobilized on acrylate-modified silicon substrates by Michael addition using micro-contact patterning (**Scheme 18**). The wafer functionalization with acrylate silane was carried out following reported protocols. The ink mixtures were prepared combining 1 µl **Thiol-PEtOx** solution (2.5 mg mL^{-1} in DMSO) with 0.2 µl of dimethylphenylphosphine (DMPP) as catalyst and 1 µl of glycerol to prevent the premature drying of the ink. A neat silicon wafer with a layer of silicon dioxide was patterned as control. Dots with a diameter of approximately 15 µm were patterned on the surfaces using a 30 µm spacing between each other. Unreacted material was removed from the surfaces by extensive washing with water and ethanol, and subsequently, the wafers were dried in a N_2 stream and analyzed by X-ray photoelectron spectroscopy (XPS). The surface with immobilized **Thiol-PEtOx** was compared to the patterned silicon wafer used as control, an acrylate-functionalized silicon wafer, and a piranha solution-activated silicon wafer (**Figure 59** and **Table 7**).

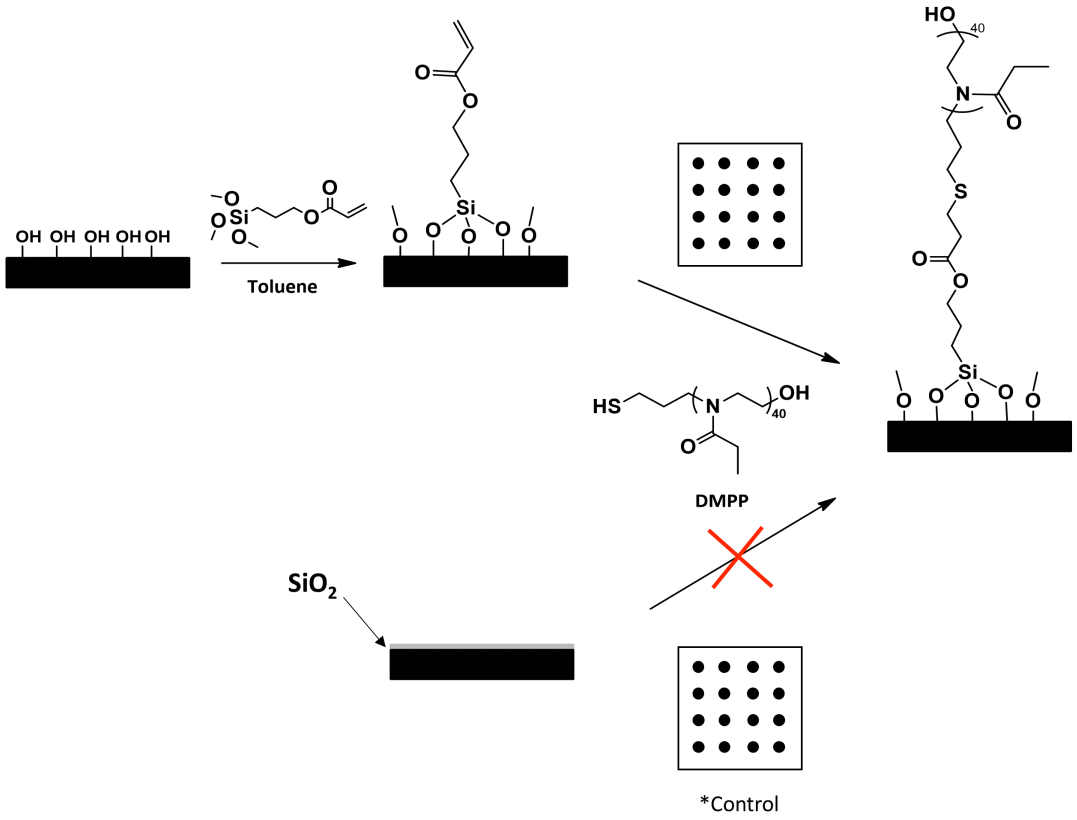

Scheme 18. General strategy for the immobilization of **Thiol-PEtOx** on acrylate-modified silicon wafers by micro-contact patterning.

XPS analysis of the activated wafer showed a total carbon content of 4.3 at% at the surface, attributed to contaminants (**Figure 59A**). After functionalization with acrylate, the total carbon content increased significantly to 19.7 at% and the appearance of a peak at 289.2 eV can be observed (**Figure 59B**), proving the presence of the O–C=O species with a contribution of 3.5 at%. Subsequently, an intensity decrease of this latter signal after **Thiol-PEtOx** patterning (1.1 at%), indicated successful surface modification (**Figure 59C**). Furthermore the appearance of an additional peak at 288.4 eV, attributed to amide carbons, was observed with a concentration of 0.5 at% (**Figure 59C**), proving functionalization with PEtOx. Additionally, the signal at 400.1 eV (0.5 at%) indicates the presence of nitrogen atoms on the surface with a 1 to 1 ratio to the amide carbon (**Table 7**). Signals at 288.0 eV and 400.1 eV were also detected for the control sample (0.3 %at in each case), attributed to potential adsorption of PEtOx to the silicon wafer

(**Figure 59D**) or other contaminants. Nevertheless, since the total carbon content on this control surface reaches only a concentration of 5.2 at%, this value is comparable to the carbon content of the activated surface and potential PEtOx adsorption is neglegible.

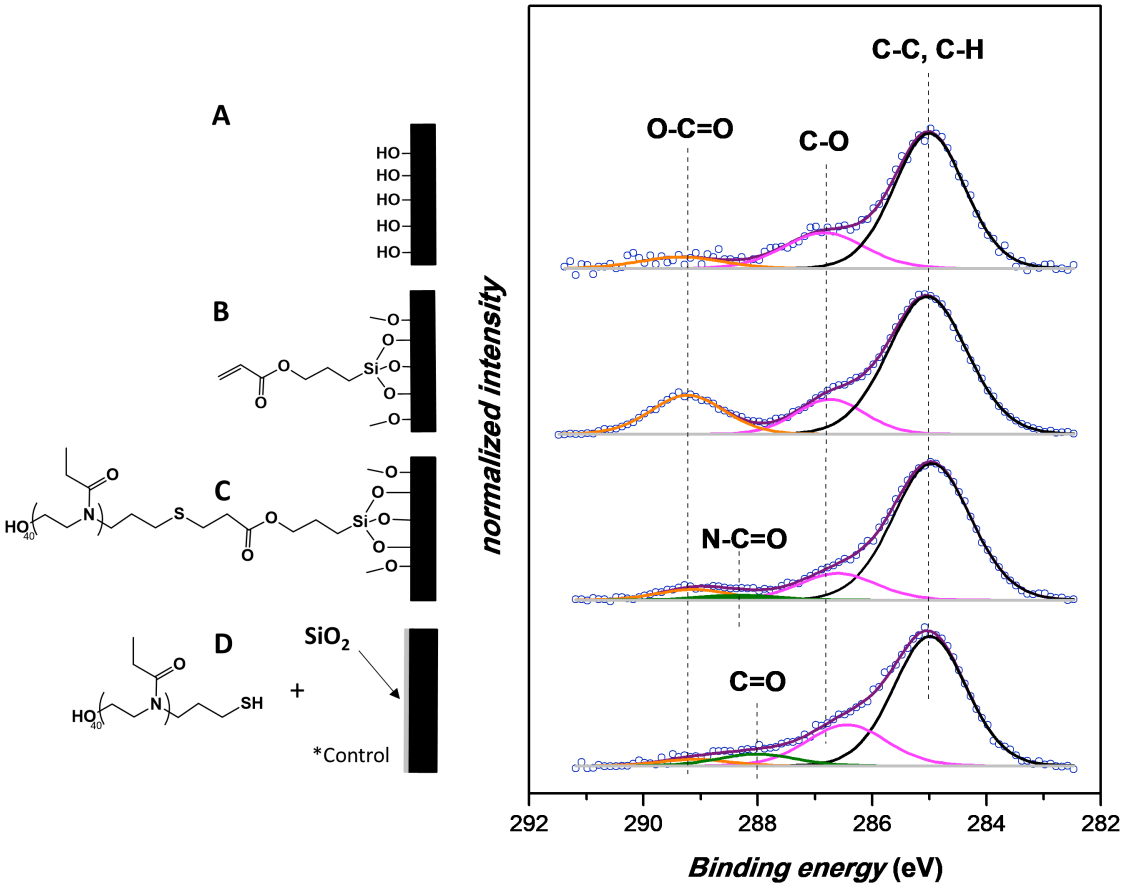

Figure 59. C 1s XP spectra of piranha solution-activated wafer (A), acrylate-functionalized wafer (B), **Thiol-PEtOx** functionalized Si wafer (C), and patterned Si wafer with a layer of SiO_2 as control (D). All intensities are normalized to the maximum of intensity.

Table 7. Atomic concentrations of carbon and nitrogen species calculated from XPS quantitative analysis of piranha solution-activated wafer (A), acrylate-functionalized wafer (B), **Thiol-PEtOx** functionalized Si wafer (C), and neat Si wafer with a layer of SiO_2 as control (D).

Binding energy (eV)	**Attribution**	**Atomic %**			
		A	**B**	**C**	**D**
285.0	C-C, C-H	3.1	13.3	14.5	3.5
286.6	C-O	0.9	2.9	2.8	1.2
288.0	C=O	-	-	-	0.3
288.4	N–C=O	-	-	0.5	-
289.2	O–C=O	0.3	3.5	1.1	0.2
	Total C	4.3	19.7	18.8	5.2
400.1	N	0.2	-	0.5	0.3

Further studies to evaluate the anti-fouling behavior of immobilized PEtOx on surfaces, as well and cytotoxicity studies, should be carried out to corroborate its potential for biomedical applications. In addition, functionalization of the ω- chain end of PEtOx with an appropriate moiety to link biomolecules can provide specific attachment to the surface of molecules of interest.

3.7. Conclusion

A novel, efficient route for the synthesis of maleimide and thiol end-functionalized PAOx was established using nosylate initiators bearing either a maleimide moiety protected in the form of a furan-based Diels–Alder adduct, or a thiol group in the form of tihoacetate for protection. In the case of **FurMalNos 4**, the limited solubility and thermal lability of the initiator required polymerization at a lower monomer concentration, and temperature. For **ThioAcNos 8**, the simple synthetic strategy, great solubility, along with the advantages of being compatible with microwave-assisted polymerization provided the possibility to synthesize well-defined polymers, available for post-polymerization modification, or direct surface functionalization. In both cases, molar masses relevant for bioconjugation or surface functionalization could be obtained. Although the functionalized initiator route (mainly in the case of **FurMalNos 4**) can lead to the presence of non-functionalized chains, via H transfer, or molar mass discrepancies caused by lower initiator efficiency, the combination of a straightforward synthesis with the availability of the ω chain end for further functionalization makes this route particularly attractive for advanced application in life sciences. We envision that this route would be practical for the development of bifunctional linkers for surface biofunctionalization, or antifouling surfaces, or for the construction of artificial protein dimers.

4

Poly(2-ethyl-2-oxazoline) macromonomers for the synthesis of functional bottlebrush polymers

4.1. Introduction[2]

PAOx is a polymer class with potential applications in the biomedical field thanks to its properties such as biocompatibility and stealth behavior.[84,279] Specifically, the water-soluble PEtOx and PMeOx are nontoxic and have high stability and low viscosity, which makes them potential alternatives to the gold standard polymer used for biomedical applications, PEG.[13,47] PAOxs are synthesized by living CROP, which provides synthetic versatility from the wide range of 2-oxazoline monomers available and the possibility to add functionalities at the chain ends depending on the initiator or terminating agent of choice.[36,92] Using the capping agent option for functionalization allows the facile introduction of ω end groups to the polymer chain that are incompatible with the polymerization reaction. For instance, termination of PAOx with

[2] The project described in this chapter was done in collaboration with the group of Prof. Jeremiah Johnson, at the Department of Chemistry of the Massachusetts Institute of Technology. EPR and relaxivity studies were experimentally carried out by Hung VanThanh Nguyen.

polymerizable units such as styrenics,[155,259,280,281] acrylates,[104,118,156,282,283] and methacrylates,[104,117,283,284] allows the formation of macromonomers (MM) to develop graft and comb copolymers by (controlled) radical polymerization. RAFT graft-through polymerization of methacrylate end-functionalized PEtOx MMs was used to obtain pH and temperature responsive comb or graft copolymers by incorporation of methyl methacrylate as comonomer.[117] In another contribution, PEtOx MMs obtained by direct end functionalization with *in situ* deprotonated acrylic acid, were polymerized by FRP, NMP, and RAFT graft-through polymerization. Kinetic studies of brush formation revealed an unusual behavior on the SEC traces with proceeding monomer consumption but with a limit to the reached molar mass of the comb polymer with narrow molar mass distributions. It was proposed that due to steric crowding effects the backbone DP did not exceed 25.[282]

Other than radical-based polymerization techniques, the graft-through ROMP approach has been recently applied for the synthesis of bottlebrush, bivalent bottlebrush, and dendronized polymers by direct polymerization of norbornene-functionalized macromonomers.[3,199] ROMP using ruthenium catalysts is particularly suited for the synthesis of side-chain functional polymers with controllable molar masses and low dispersities. For instance, graft-through ROMP of a macromonomer, followed by *in situ* crosslinking is a useful methodology for the synthesis of BASPs. These nanoparticles feature a unimolecular micelle-like structure with readily tunable core and shell functionalities that may contain a variety of polymer arms, drug molecules, and imaging agents. The brush-first ROMP method to form BASPs has been reported for the preparation of drug-loaded PEG-based BASPs,[285] two- and three-miktoarm BASPs,[198] and nitroxide-loaded PEG BASPs[197,286] that serve as metal-free MRI probes.

Organic-based MRI agents are an alternative to already existing metal-based MRI probes that may present toxicity concerns in some patients. Nitroxide radicals are organic molecules that have a single unpaired electron and have been extensively studied as potential contrast enhancing agents for MRI applications.[287–289] Paramagnetic nitroxides present low toxicity *in vivo*,[289] which makes them potential alternatives to metal-based MRI probes that may accumulate in biological tissue.[290] Commonly used nitroxides have the disadvantage of low ^{1}H

water relaxivities compared to contrast agents based on Gd^{3+} or Mn^{2+}, due to the number of unpaired electrons available (1 versus 7 or 5, respectively). Another challenge is the fast reduction *in vivo* (in the order of minutes) of commonly used nitroxides to form diamagnetic hydroxylamines.[291] Strategies to address these challenges include the use of poly(nitroxides), where relaxivity is multiplied by the number of available nitroxides, or the conjugation of the nitroxide radicals to a rigid scaffold to increase resistance to reduction.[197,201,292] Recently developed macromolecular nitroxide organic radical contrast agents (ORCAs) feature polymer chains conjugated to nitroxide radicals to form dendrimer scaffolds,[292] branched bottlebrush polymers,[201] or brush-arm star polymers (BASPs) from branched macromonomers.[197] For instance, a nitroxide-based MRI probe using a BASP nanostructure consisting of a dense layer of the paramagnetic nitroxide **chex** at the interface of a poly(acetal) core and a hydrophilic PEG shell, was reported to enhance relaxivity up to 44-fold when compared to common nitroxides, while maintaining stability *in vivo* for up to 20 hours after injection in mice.[197]

In this chapter, the first PEtOx macromonomers for ROMP were synthesized by ω functionalization via termination using a norbornene derivative of hexanoic acid. Bottlebrush copolymers of different MM-to-catalyst ratios were synthesized by graft-through ROMP, as well as BASPs by graft-through ROMP followed by *in situ* crosslinking with a bis-norbornene derivative. This MM approach was then combined with the previously reported strategy to form branched MMs, where an alkyne group from a bivalent norbornene MM is available for functionalization with a molecule of interest. The capability of the alkyne group to react by CuAAC click reaction allows the introduction of a number of azide-functionalized drugs or imaging agents to the macromonomer. For this project, the paramagnetic nitroxide **chex** was attached to the macromonomer to produce a new type of organic-radical based MRI contrast agent (**Figure 60**). In this project, the first PAOx MMs, and **chex**-branched MMs for ROMP were synthesized and characterized. The latter were used to produce an MRI probe that serves as an alternative to the previously reported structures.

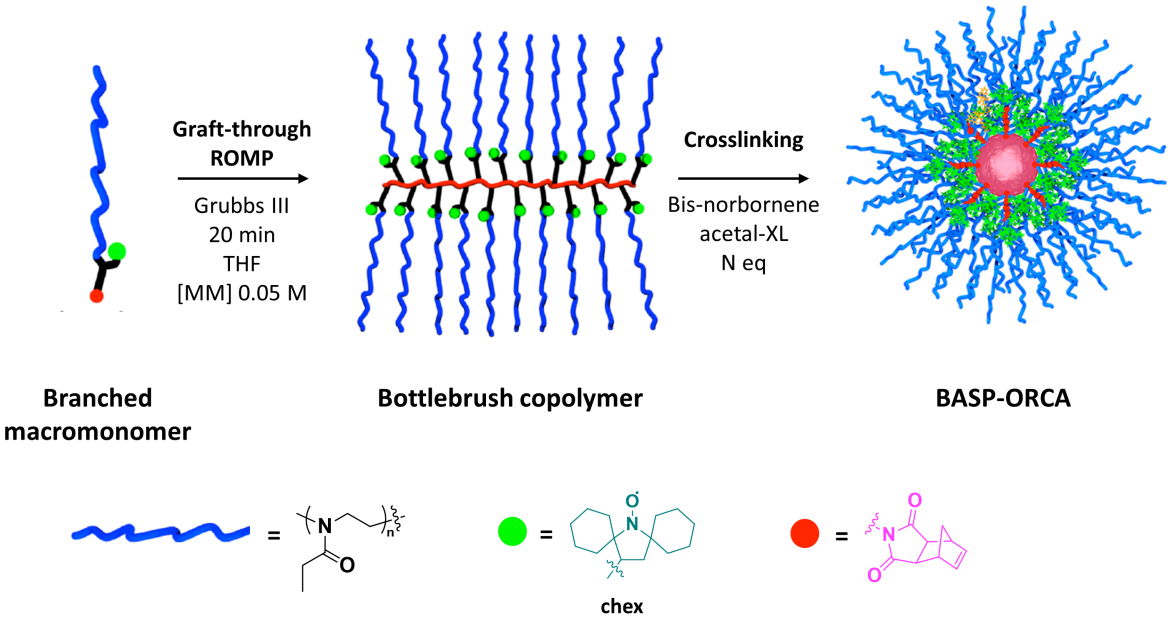

Figure 60. General procedure for the formation PEtOx-based BASP-ORCA. Graft-through ROMP of branched MMs functionalized with **chex** nitroxide exposed to Grubbs III catalyst produced living brushes, and subsequent addition of acetal-XL yielded BASP-ORCA (Adapted from reference [293] Copyright 2018 American Chemical Society).

4.2. Synthesis of norbornene-terminated PEtOx macromonomers

For this project, 2-ethyl-2-oxazoline was used as monomer since PEtOx is a biocompatible, water-soluble, non-toxic polymer with high stability and a suitable choice for potential applications in biomedical fields as an alternative to PEG. As initiator, methyl tosylate was chosen for its demonstrated efficient initiation for the polymerization of many 2-oxazolines, among them, 2-ethyl-2-oxazoline. Norbornene (as opposed to cyclobutene or cyclooctene) was selected as the polymerizable group due to its high ring strain, commercial availability, and the lack of chain transfer in ROMP.[294] Particularly, exo-norbornenes were utilized since these exhibit higher reactivity than their endo-norbornene analogues, due to reduced steric hindrance at the olefin site. The norbornene functionality was introduced to the PEtOx chain during the termination step in an effort to simplify the synthetic setup since neither initiator synthesis nor post-polymerization modification is required. Termination was carried out by addition of a carboxylic acid-functionalized norbornene molecule, mixed with TEA to deprotonate the carboxylic acid group, facilitating the nucleophilic attack. A five-carbon alkyl spacer between the norbornene moiety and the carboxylic acid group was selected to reduce the steric congestion during ROMP. It was also observed in the group of Jeremiah Johnson at MIT (collaborator in the present project) that the presence of polar moieties close to the polymerization site was detrimental for ROMP. The already optimized conditions for the CROP of EtOx reported in the literature (microwave-assisted polymerization at 140 °C in acetonitrile with monomer concentration 4 M) were used to produce polymers of various molar masses (**Scheme 19**).

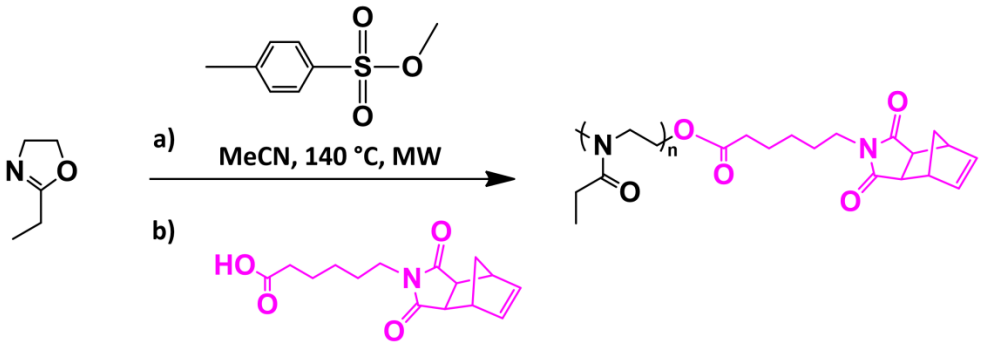

Scheme 19. Synthesis of **PEtOx MM**.

Polymers from three different monomer-to-initiator ratios were synthesized and characterized by ^{1}H NMR spectroscopy, SEC, and MALDI-ToF, to ensure end-group fidelity and confirm the production of polymers with well-defined molar masses and narrow distributions. SEC was performed in two sets with DMAc or THF as solvents (**Figure 61**). In all cases, the $M_{n,SEC}$ values obtained proportionally increased for each polymer depending on the target DP with $Đ$ < 1.16. However, the $M_{n,DMAc\text{-}SEC}$ values obtained are close to the theoretical values, which is unusual considering there generally exists an overestimation of values for PAOx when using PMMA as standard. In addition, the shape of the signal of **PEtOx MM 1.6kDa** shows a bimodal distribution, different from the monomodal distribution obtained from THF SEC. $M_{n,THF\text{-}SEC}$ values are significantly lower than $M_{n,theo}$. Polystyrene standards were used for the calculation of M_n and cannot be directly correlated to PEtOx. Nevertheless, narrowly dispersed polymers were obtained in all cases ($Đ$ < 1.15), sign of a controlled polymerization (**Figure 61**).

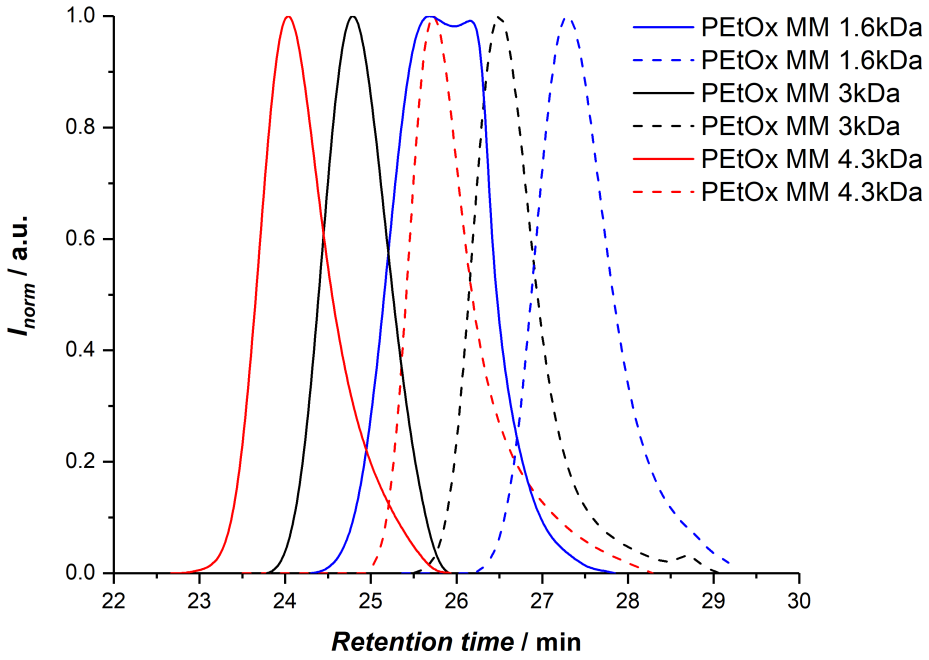

Figure 61. SEC traces of the **PEtOx MMs** obtained using DMAC SEC (solid) and THF SEC (dashed).

The end-group fidelity and success of the termination reaction were proved by ^{1}H NMR (**Figure 62**), where polymer backbone and side-chain signals were assigned, as well as end-chain signals. The ^{1}H NMR spectrum obtained from **PEtOx MM 3kDa** shows integration values of both end-group signals (found at 2.9 ppm for the α methyl group and at 6.2 ppm for the ω norbornene olefin moiety) of 2.4 and 2. The discrepancy displayed with respect to the expected 3 to 2 ratio of protons on each end group is potentially caused by proton initiated chains, product of transfer reactions. For all samples, the $M_{n,NMR}$ values were calculated using the norbornene olefin signal at 6.2 ppm and comparing it with the polymer backbone and side-chain signals at 3.4, 2.3, and 1.0 ppm, respectively. The calculated $M_{n,NMR}$ values are in close agreement with the theoretical value expected from the monomer-to-initiator ratio targeted on each case, indicating high degree of end group functionalization.

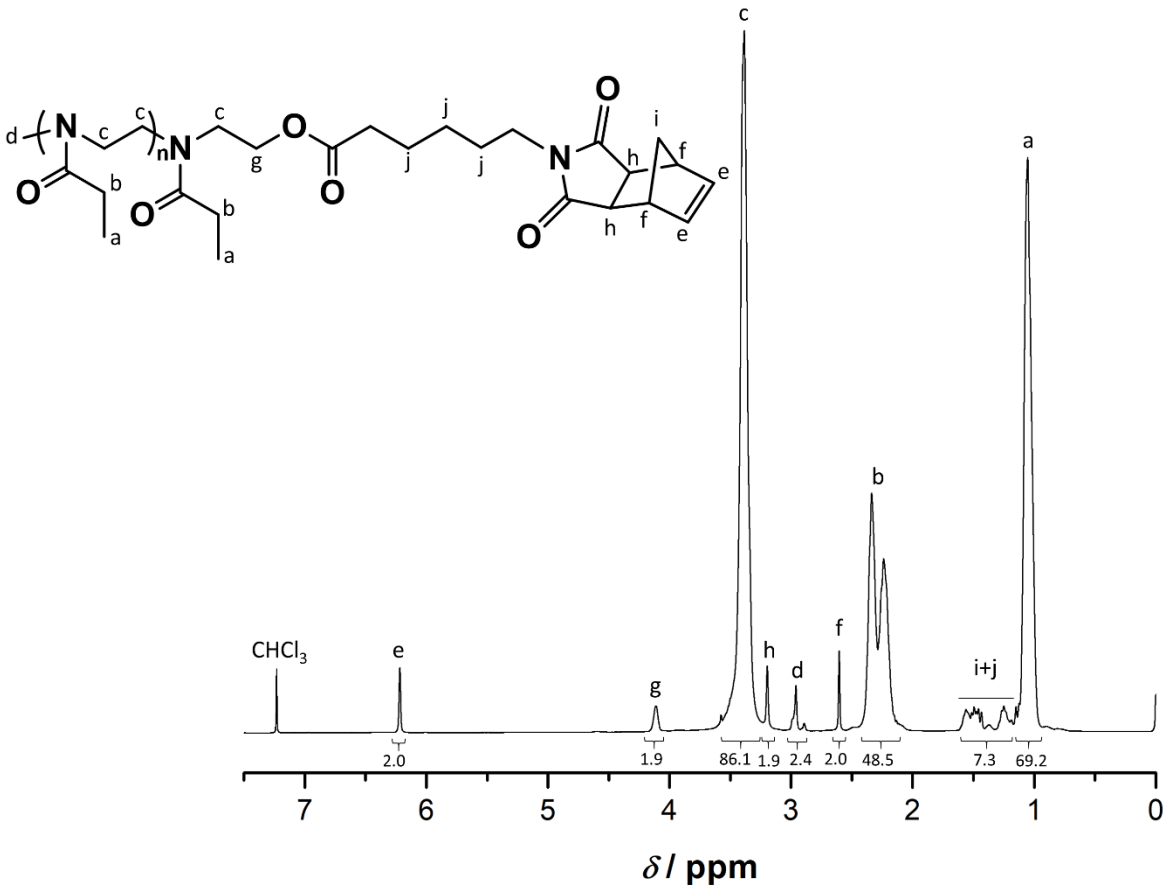

Figure 62. ^{1}H NMR spectrum of **PetOx MM 3kDa.**

MALDI-ToF analysis further confirmed the introduction of norbornene as end group during the termination reaction. The spectrum shows one main family of polymers, that corresponds to the polymer ionized with a proton, and the *m/z* values match the theoretical value calculated for the target structure (**Figure 63**). A second population with lower intensity is visible and corresponds to a lower molar mass polymer family. It was assigned to a proton-initiated PEtOx terminated with the norbornenyl molecule. Although this population is the product of chain transfer reactions, it carries the desired norbornene group and can be polymerized by ROMP. Additionally, the MALDI signals with highest intensity are in *m/z* range values that closely agree with the M_n value calculated by ^{1}H NMR and show a narrow distribution.

A summary of the characterization of the synthesized polymers is presented on **Table 8**.

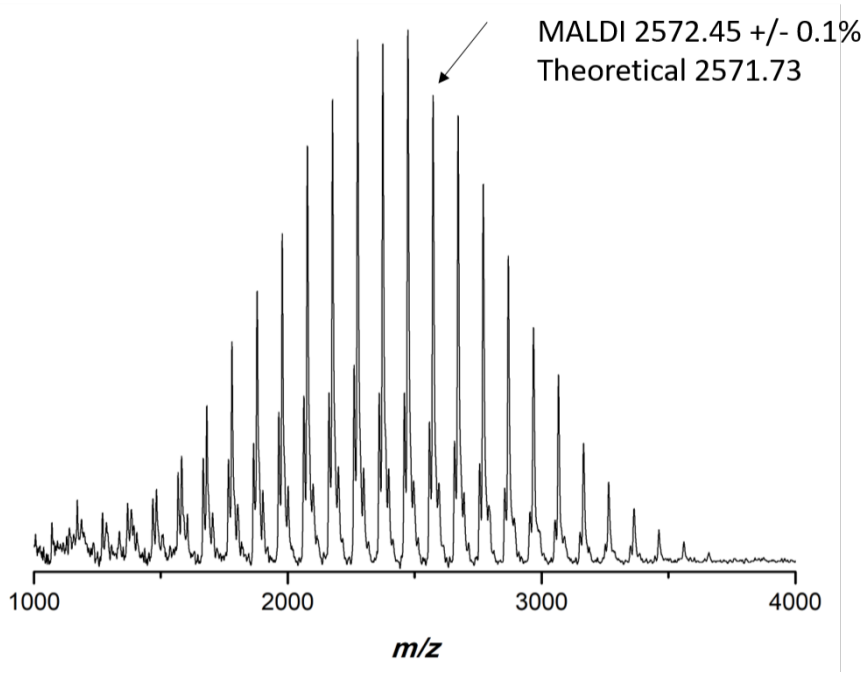

Figure 63. MALDI spectrum of **PEtOx MM 3kDa.**

Table 8. Summary of the characterization of **PEtOx MMs**.

Name	[EtOx]/ [MeOTs]	$M_{n,theo}$ (g mol^{-1})	$M_{n,NMR}$ (g mol^{-1})	$M_{n,DMAc\text{-}SEC}$ (g mol^{-1})	$Đ_{(DMAc)}$	$M_{n,THF\text{-}SEC}$ (g mol^{-1})	$Đ_{(THF)}$
PEtOx MM 1.6kDa	15	1780	1600	1400	1.15	1000	1.09
PEtOx MM 3kDa	30	3260	3000	3200	1.08	1600	1.11
PEtOx MM 4.3kDa	45	4750	4300	5100	1.14	2400	1.12

4.3. Synthesis of polymer bottlebrushes

The viability of the synthesized MMs, **PEtOx MM 3kDa** and **PEtOx MM 1.6kDa**, to carry out ROMP using Grubbs III (**G3**) bis-pyridin as catalyst was tested. This catalyst has been applied to the synthesis of bottlebrush, bivalent bottlebrush, and dendronized polymers by graft-through polymerization of functional norbornene macromomoners. Here, each **PEtOx MM** was dissolved in THF to a concentration of 0.05 M, and mixed with catalyst **G3** bis-pyridin (from a stock solution) at different **PEtOx MM**-to-**G3** ratios at room temperature (**Scheme 20**).

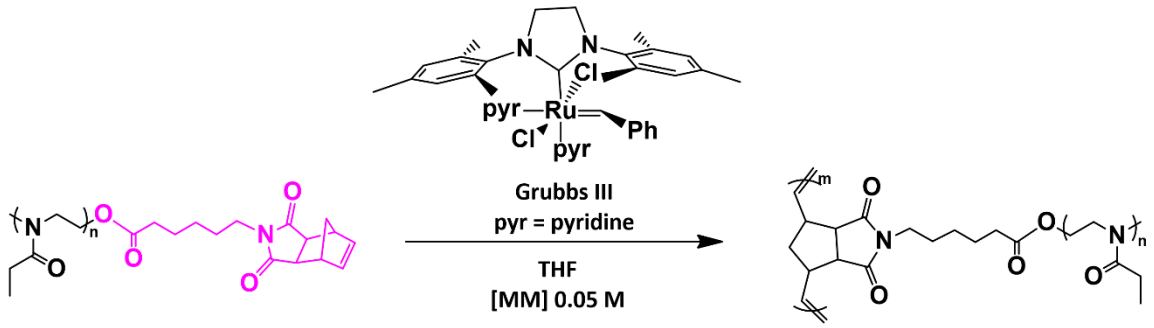

Scheme 20. Synthesis of brush copolymers from **PEtOx MM.**

The solutions were stirred overnight and quenched with excess ethyl vinyl ether (EVE). SEC traces in DMAc of the bottlebrush polymers produced from **PEtOx MM 3kDa**, in **Figure 64**, show a nearly quantitative conversion from MM to bottlebrush polymer in all cases, with a proportional increase in $M_{n,DMAc\text{-}SEC}$ and $Đ < 1.17$. The remaining signal at higher retention time can be attributed to non-functionalized or unreactive MM. The SEC traces of **PEtOx MM 1.6kDa** bottlebrush polymers in DMAc show for all screened DPs a bimodal distribution (**Figure 65**). At lower retention times, a signal with increasing M_n that corresponds to conversion from MM to bottlebrush is observed. However, the signal at higher retention time remains constant for all experiments. The proximity of the MM to the lower limit of the calibration curve may be causing this signal, since no other distributions or contaminants were observed during the characterization of the polymer using THF SEC, ^{1}H NMR spectroscopy, or MALDI-ToF mass

spectrometry. These same samples were analyzed by THF-SEC (**Figure 66**) where high conversion was observed (> 85%) for DPs 50 and below. The lowest conversion was achieved with DP 100, where a larger amount of MM remained unreactive.

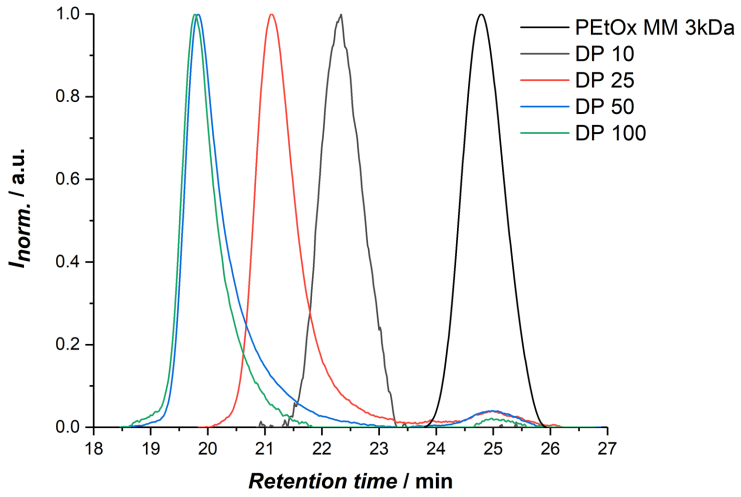

DP	$M_{n,\ DMAc\text{-}SEC}$ (g mol^{-1})	$Đ$
10	24100	1.11
25	48300	1.12
50	117900	1.16
100	141400	1.10

Figure 64. DMAc SEC traces of the polymers obtained after graft-through ROMP of **PEtOx MM 3kDa** with THF as solvent and [MM] 0.05 M, at various [MM]/[G3] ratios (= DP).

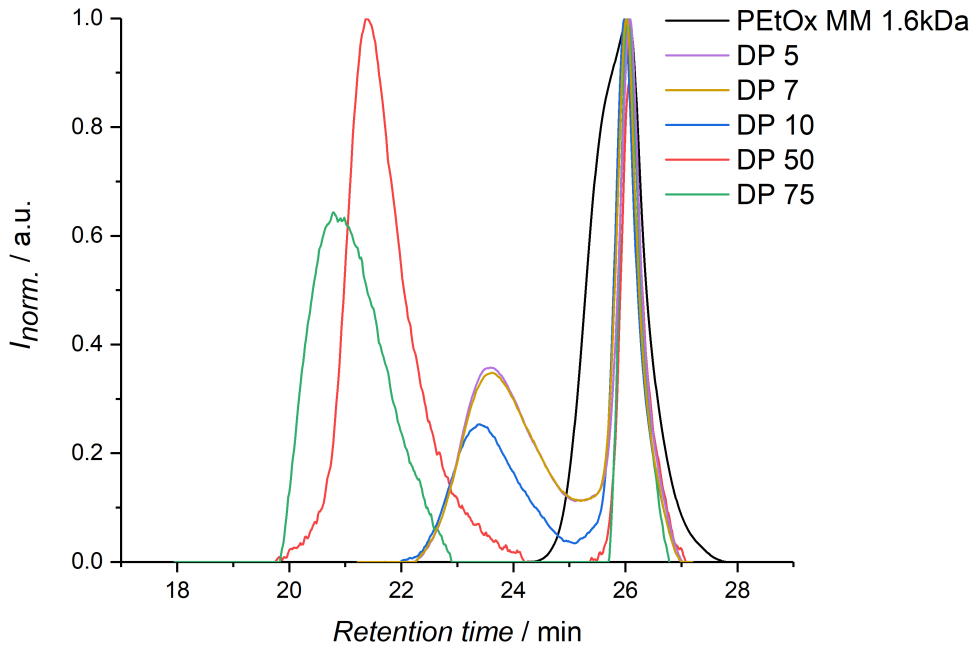

Figure 65. DMAc SEC traces of the products of the graft-through ROMP of **PEtOx MM 1.6kDa** at various targeted DPs with THF as solvent and [MM] 0.05 M.

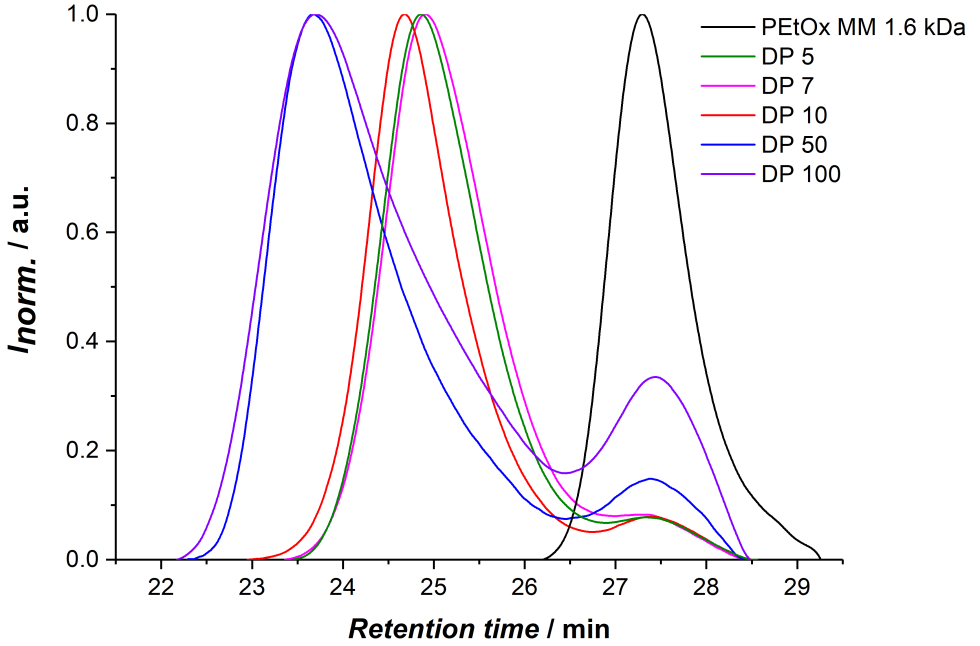

Figure 66. THF SEC traces of the products of the graft-through ROMP of **PEtOx MM 1.6kDa** at various targeted DPs with THF as solvent and [MM] 0.05 M.

Kinetic experiments of **PEtOx MM 3kDa** ROMP at DP 10 were performed using similar conditions as previous experiments. Samples were taken after 10, 15, and 20 minutes and quenched with EVE. SEC analysis in DMAc of the produced samples, in **Figure 67**, show that full conversion was achieved from the first sample taken at 10 minutes, indicating fast ROMP rates at low DP. These results indicate the potential of the produced bottlebrush polymers to form BASPs using the brush-first approach, where a bifunctional crosslinker is added to living polymer brushes of low DP to produce the micelle-like structure of BASPs.

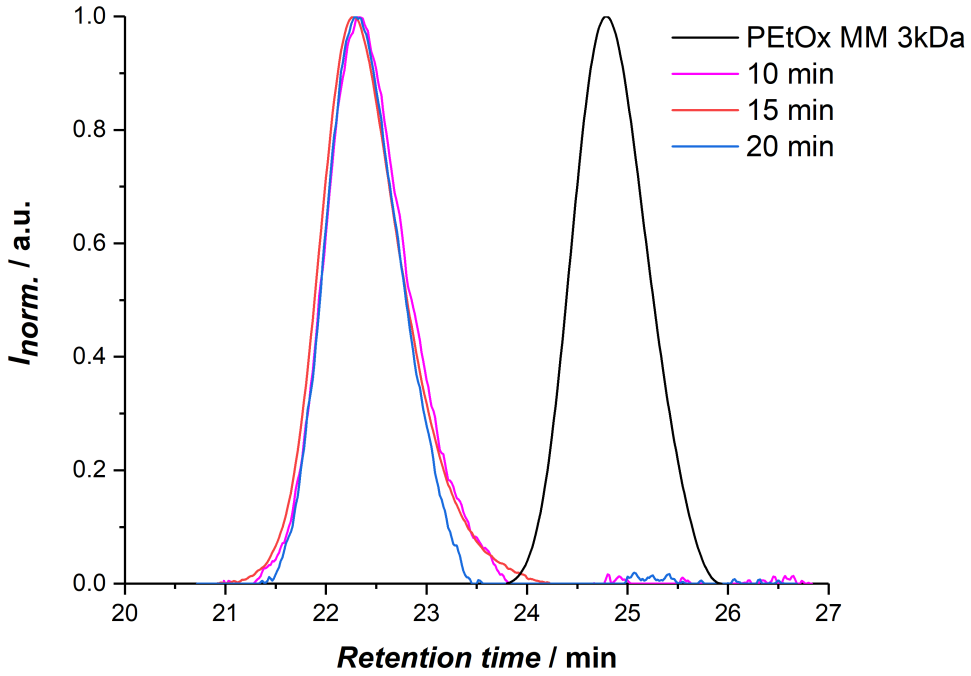

Figure 67. DMAc SEC traces of kinetic experiments of **PEtOx MM 3kDa** ROMP with targeted DP 10, using THF as solvent and [MM] 0.05 M.

To evaluate the potential incorporation of molecules of interest (e.g., drugs, imaging agents) to the polymer brush as random copolymers, **PEtOx MM 3kDa** was copolymerized with norbornene-functionalized hexanoic acid. The copolymerization experiments were carried out using similar conditions as previous experiments with MM-to-norbornene-carboxylic acid ratios of 1:4, 1:1, and 3:1. The resulting SEC traces show nearly quantitative conversion in all cases

with some remaining unreactive MM (**Figure 68**). The produced bottlebrushes reached M_n values in the range of 45700-49400 g mol^{-1} with $Đ$ < 1.16. These results are promising for the incorporation or functional molecules on the backbone of the polymer brush. However, this approach has the disadvantage of random addition to the bottlebrush without the possibility to control the amount of loaded molecule.

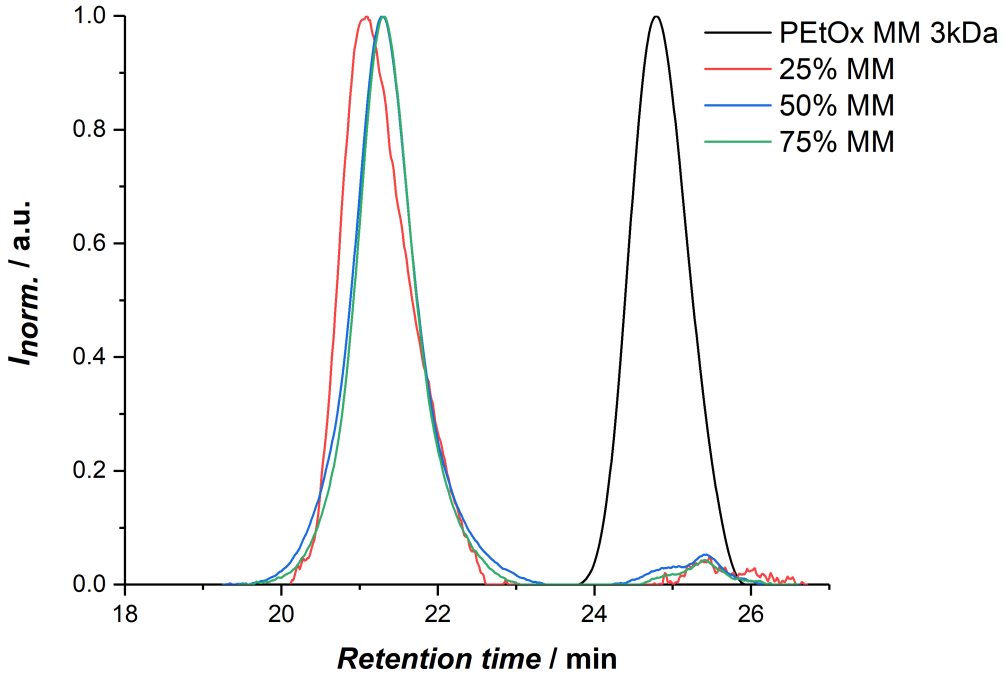

Figure 68. DMAc SEC traces of graft through copolymerization of **PEtOx MM 3kDa** : norbornene-hexanoic acid on 1:4, 1:1, and 3:1 ratios with targeted DP 25 and THF as solvent.

4.4. Synthesis of brush-arm star polymers (BASPs)

BASP synthesis provides a broadly useful methodology for nanoparticle synthesis with readily tunable core and shell functionality. For this project, the viability of BASP formation from **PEtOx MMs** was first tested. The BASPs were synthesized by graft-through ROMP of **PEtOx MM 3kDa** using **G3** bis-pyridine initiator with a MM-to-G3 ratio of 7 (m = 7) for 20 min. Subsequently, the living bottlebrush polymers were crosslinked by addition of 20 equivalents of bis-norbornene acetal crosslinker (**acetal-XL**) (N = 20) to the reaction mixture. The size of the BASP is determined by both m and N values. Samples of the resulting bottlebrush polymer and BASP were analyzed by SEC and DLS.

SEC revealed nearly quantitative MM-to-bottlebrush conversion, as well as high conversion to BASP from bottlebrush polymer (**Figure 69**). The unreactive species can potentially be assigned to either unfunctionalized or unreactive macromonomers.

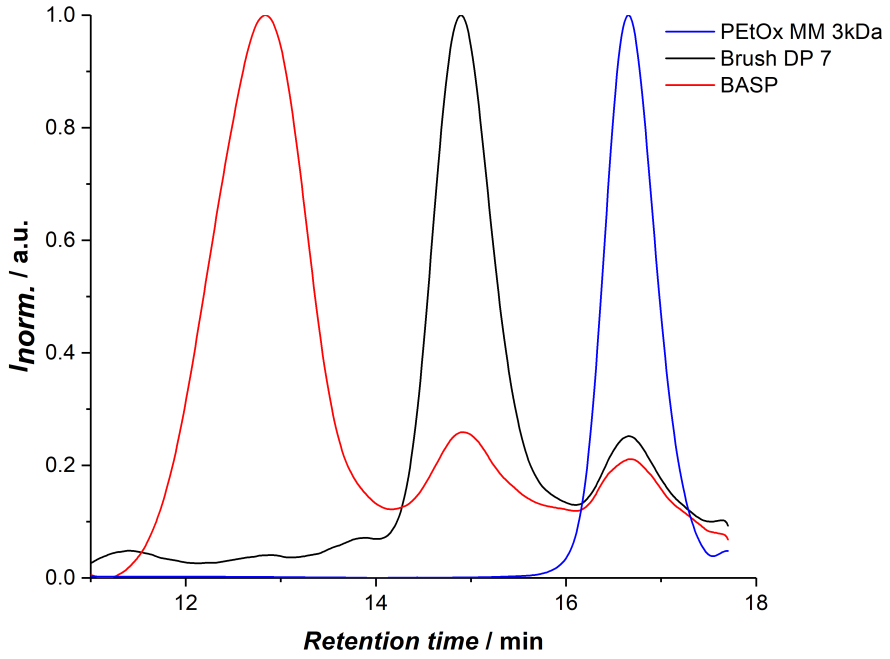

Figure 69. SEC traces in DMF of **Norbornene-PEtOx 3kDa,** the bottlebrush polymer, and BASPs obtained.

The diameters of bottlebrush polymer and BASP were determined by DLS in water at 25 °C, and are 5 nm and 17 nm, respectively (**Figure 70**). However, in the case of the bottlebrush polymer sample, the presence of particles with diameter of 144.5 nm was observed, which potentially correspond to the formation of aggregates. Nevertheless, a 3-fold size increase observed from the bottlebrush of DP 7, to the BASP formed with 20 equivalents of **acetal-XL**, indicates the successful formation of the BASPs.

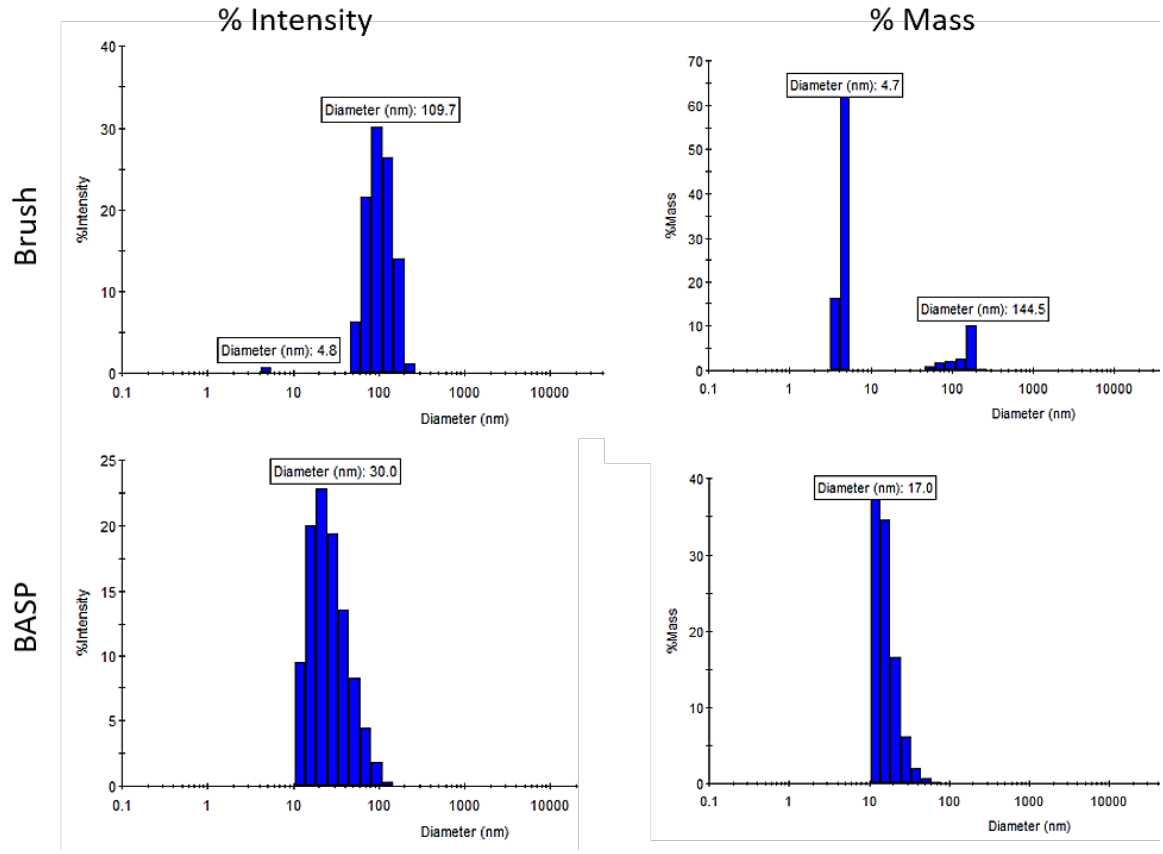

Figure 70. DLS analysis in water at 25 °C of living brush polymer and produced BASP.

The successful synthesis of bottlebrush polymers and BASPs from PEtOx MMs is a promising foundation to explore other functional PEtOx MM to form this architecture.

4.5. Synthesis of norbornene-branched-alkyne PEtOx macromonomers

The already described strategy to obtain bottlebrush copolymers and BASPs from PEtOx MM, was combined with a previously reported approach to synthesize branched MM with a pendant alkyne group, which allows the introduction of a functional molecule by CuAAC click reaction.[194] Using a branched MM provides the advantage that one molecule of interest is quantitatively integrated in one polymer chain. Consequently, the amount of loaded molecule is known and can be controlled.

The branched MMs (**alkyne-PEtOx MM**) were synthesized using similar conditions as **PEtOx MM**, except the termination step was carried out using 1.5 equivalents of norbornene-branched-alkyne hexanoic acid dissolved in DCM (**Scheme 21**). The synthesized polymers were analyzed by ^{1}H NMR spectroscopy, SEC, and MALDI-ToF mass spectrometry.

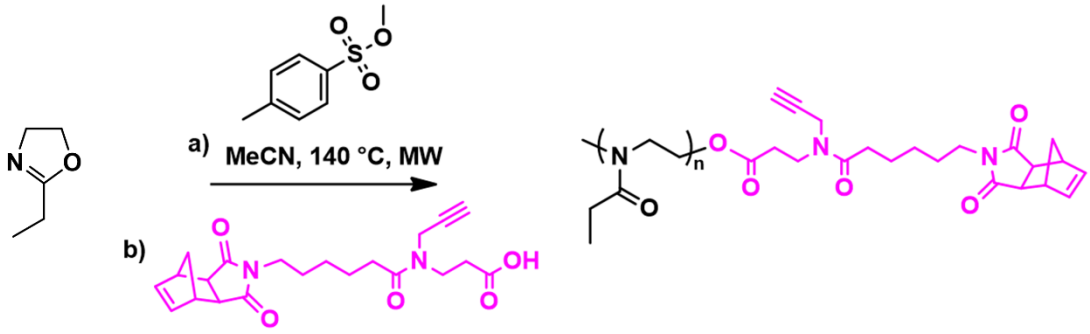

Scheme 21. Synthesis of **alkyne-PEtOx MM**.

SEC analyses show a proportional increase in $M_{n,SEC}$ to the target DP for each polymer. In general, the $M_{n,SEC}$ values are similar to $M_{n,theo}$, which is unusual considering that for PEtOx an over estimation in values is normally encountered when using PMMA standards. Nevertheless, the dispersity values obtained reflect a controlled polymerization, with $Đ$ values below 1.15 (**Figure 75**).

^{1}H NMR spectra of the synthesized polymers confirmed the quantitative presence of the terminating norbornene-branched-alkyne molecule. **Figure 71** shows the ^{1}H NMR obtained from **alkyne-PEtOx MM 3kDa**, where polymer backbone and side-chain signals are assigned and integrated, as well as end groups. The integration of both the α–methyl and ω–norbornene end group signals (d, at 2.9 ppm, and f at 6.2 ppm, respectively) corresponds to the expected proton ratio (3 to 2), indicating that both efficient initiation and termination occurred. Furthermore, the $M_{n,NMR}$ values were calculated similar to the **PEtOx MM** (using the norbornene signal at 6.2 ppm and comparing it to backbone and side chain signals at 4.0, 3.5, and 2.0 ppm, respectively). The values obtained are in agreement with the target DP in each case, a good indication of both efficient initiation and termination.

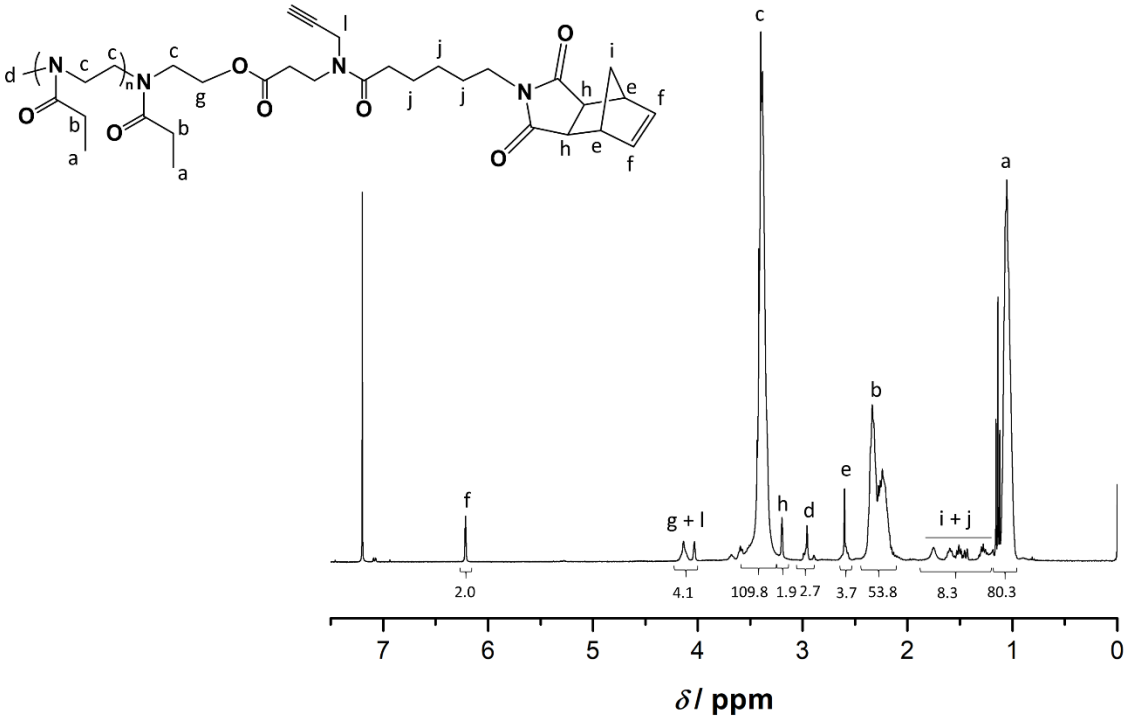

Figure 71. ^{1}H NMR spectrum of **alkyne-PEtOx 3kDa.**

MALDI-ToF analysis was also used to confirm the introduction of the branched norbornene as an end group during termination. The spectrum of **alkyne-PEtOx MM 3kDa** shows one main

family of polymers, that corresponds to the polymer structure ionized with a proton and has *m/z* values that match the theoretical *m/z* (**Figure 72**). Additionally, the signals with highest intensity are in close agreement with the M_n value calculated by ^{1}H NMR and show a narrow distribution.

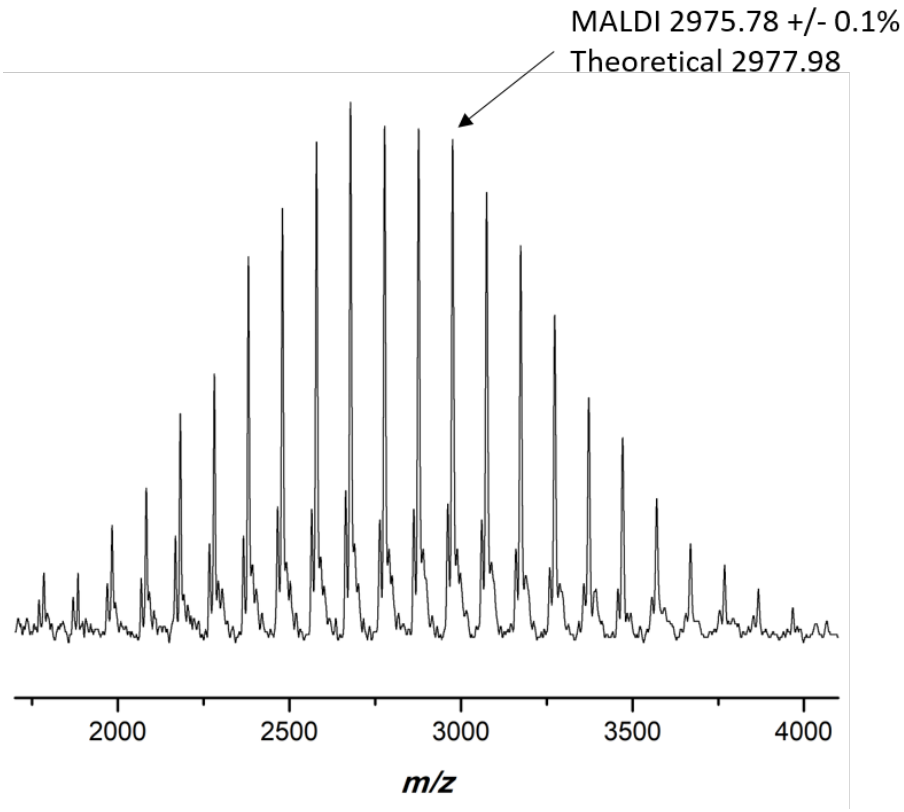

Figure 72. MALDI spectrum of **alkyne-PEtOx MM 3kDa.**

The values obtained after characterization of each polymer are summarized on **Table 9**.

Table 9. Summary of the characterization of **alkyne-PEtOx MMs**

Name	[EtOx]/ [MeOTs]	$M_{n,theo}$ (g mol^{-1})	$M_{n,NMR}$ (g mol^{-1})	$M_{n,DMAc\text{-}SEC}$ (g mol^{-1})	*Đ*
Alkyne-PEtOx 1.6kDa	15	1890	1600	1400	1.12
Alkyne-PEtOx 3kDa	30	3360	3100	2900	1.13

4.6. Synthesis of chex-PEtOx MM

Among the most widely used nitroxides as MRI contrast agents is 3-carboxy-2,2,5,5-tetramethyl-*L*-pyrrolidinyloxy (3-CP) and its derivatives (**Figure 73**). The half-life *in vivo* of these nitroxides is approximately 2 minutes in MRI mouse studies.[291,295] A reported alternative, **chex,** is a five-member ring (pyrrolidinyl) nitroxide that is sterically hindered by spirocyclohexyl groups (**Figure 73**). The shielding effect decreases the reduction rate of the nitroxide radical *in vivo*, and it was found that when conjugated to a dendrimer the longitudinal relaxitivy (r_1) increases to 0.44 mM^{-1} s^{-1}, when compared to r_1 = 0.15 mM^{-1} s^{-1} from the conjugate using the model nitroxide 3-CP.[292,296] The higher relaxivity values obtained by conjugation of **chex** to different polymer architectures make it a suitable choice for the development of nitroxide-PEtOx MM conjugates.

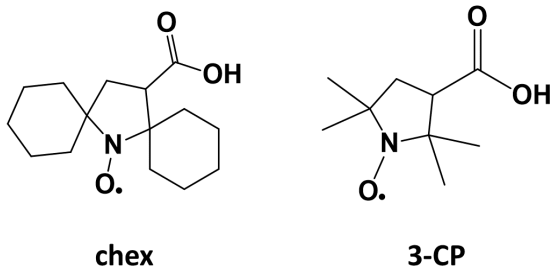

chex **3-CP**

Figure 73. Structures of nitroxides chex and 3-CP.

The introduction of nitroxide **chex** was carried out using azide-functionalized **chex**, for attachment to **alkyne-PEtOx MM 3kDa** by CuAAC click reaction (**Scheme 22**). The reaction was performed in a glove box using DCM as solvent. The resulting polymer, **chex-PEtOx MM**, was analyzed using MALDI-ToF mass spectrometry and SEC.

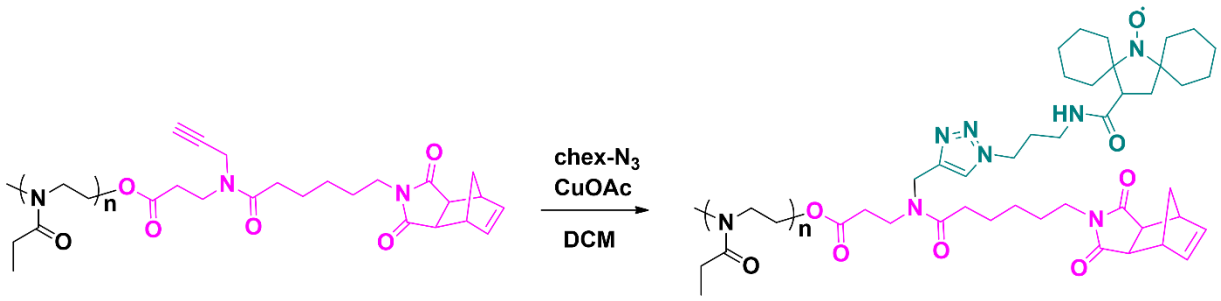

Scheme 22. Synthesis of **chex-PetOx MM**.

The successful introduction of the nitroxide radical to the branched PEtOx MM was confirmed by MALDI, where one main population is observed and the theoretical *m/z* value of the repeating units matches the *m/z* found experimentally (**Figure 74**).

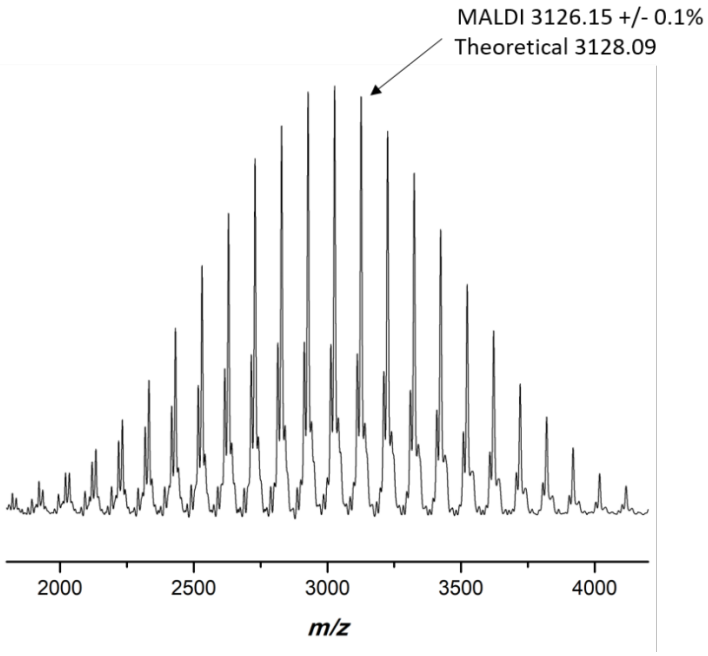

Figure 74. MALDI spectrum of **chex-PEtOx 3kDa.**

The SEC traces obtained from DMAc SEC confirm that the structure of the polymer backbone before and after CuAAC remains unchanged ($M_{n,SEC}$ = 2900 and 3300 g mol^{-1}, respectively), and with low dispersity values ($Đ$ = 1.13) (**Figure 75**).

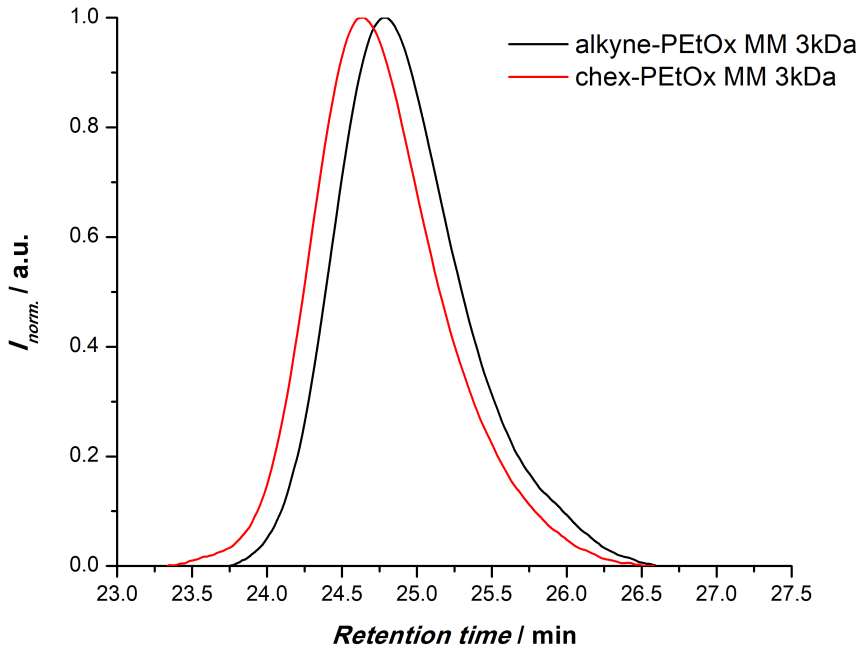

Figure 75. SEC traces of **alkyne-PEtOx MM 3kDa** and the product of the click reaction of it with azide-chex to yield **chex-PEtOx MM 3kDa**.

4.7. Synthesis of functional polymer brushes and BASP-ORCAs

The BASP structure provides the possibility to incorporate molecules at a rigid core shell interface, providing potential benefits such as more stability or activity enhancement. In this case, bottlebrush and BASPs were synthesized from the newly developed **chex-PEtOx MM 3kDa**. To evaluate the properties of the BASPs, a screening of MM-to-**G3** (m) and crosslinker-to-**G3** (N) ratios was carried out (**Table 10**). Similar to the previous BASP synthesis experiment, **chex-PEtOx MM 3kDa** underwent graft-through ROMP using **G3** bis-pyridine initiator. After 20 minutes, the living bottlebrush polymers were crosslinked by addition of N equivalents of crosslinker (**acetal-XL**) to the reaction mixture. The reactions were quenched with excess EVE and samples taken of the resulting bottlebrush polymer and BASP were analyzed by SEC and DLS.

Nearly quantitative conversion was obtained for the formation of bottlebrush polymers from MM and BASPs from bottlebrush polymers, as observed from the SEC traces in DMF (**Figure 76**). The remaining signals can be attributed to unreactive MMs and bottlebrush polymers, similar to traces obtained from previous experiments. These results are in agreement with previous reports of related nitroxide-labeled ROMP polymer systems, proving the high efficiency of the graft-through ROMP process.[201] The M_n values of BASPs obtained with a similar crosslinker-to-catalyst ratio (N = 20) but varying the size of the bottlebrush polymer (m = 7 or 10) are relatively similar (5 or 5.9 x10^5 g mol^{-1}). Conversely, by keeping bottlebrush size constant (m = 10) but increasing N from 20 to 30, the M_n exhibits an approximately 2-fold increase (5.9 to 10.8 x10^5 g mol^{-1}), evidence of the influence of N on the size of the resulting BASPs (**Table 10**). A similar behavior was observed from the BASP-ORCA diameters determined by DLS. The largest BASP diameter (27 nm) was observed from N = 30, compared to diameters from BASPs with N = 20 from similar bottlebrush size (21 nm) (**Table 10**). Compared to the PEG-based BASPs analogues with similar N and m values, PEtOx-based BASPs are approximately 10 nm more compact in diameter.[197]

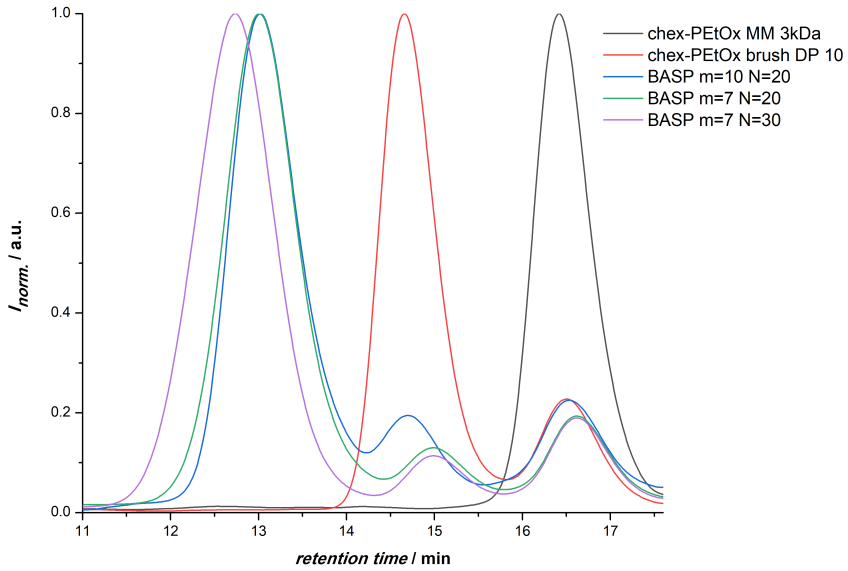

Figure 76. SEC traces in DMF of **chex-PEtOx 3kDa,** the chex-bottlebrush polymer with DP 10, and BASP-ORCAs obtained varying MM-to-G3 ratio (m) and crosslinker-to-G3 ratio (N).

4.8. Characterization of PEtOx-based BASP-ORCA magnetic properties

4.8.1. Electron paramagnetic resonance spectroscopy

Electron paramagnetic resonance spectroscopy (EPR) was used to confirm the presence of **chex** and to characterize the spin concentration in the produced bottlebrush polymer and BASP-ORCAs. The EPR spectra of **chex**-MM, bottlebrush, and BASP-ORCAs were normalized and are shown in **Figure 77**. The spectra of bottlebrush polymer and BASP-ORCAs are significantly broader than **chex**-MM, which is attributed to the high nitroxide density near the poly(norbornene) backbone. Additionally, for BASP-ORCAs, the signal broadening is more intense due to the larger and more rigid BASP structure where **chex** is at the dense interface between the crosslinked core and the PEtOx shell. In all cases, the spin concentrations measured were > 85%, similar to the observed values for the PEG-based BASP-ORCAs reported.[197,201]

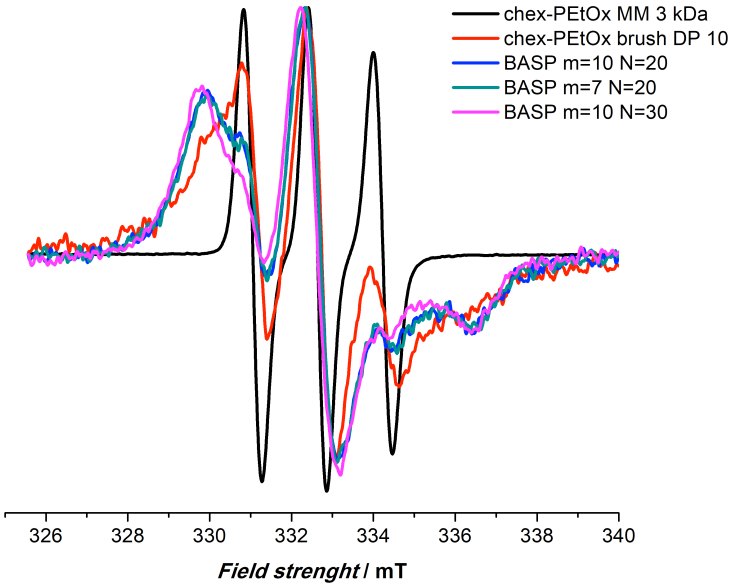

Figure 77. Electron paramagnetic resonance (EPR) spectra of **chex-PEtOx MM 3kDa**, chex-PEtOx brush DP 10, and BASP-ORCAs obtained varying MM-to-G3 ratio (m) and crosslinker-to-G3 ratio (N).

4.8.2. Relaxivity studies

The longitudinal (r_1) and transverse (r_2) relaxivities of the resulting BASP-ORCAs were measured using a Bruker 7 T MRI scanner. The r_1 values obtained as a function of m and N ranged from 0.17 to 0.19 $mM^{-1}s^{-1}$, showing no variation when modifying the polymer architecture from MM to bottlebrush. Furthermore, these values are similar to the r_1 values obtained from nitroxide CP-3, but below what is reported for chex-PEG macromonomer (r_1 values of 0.15 and 0.21, respectively). Nevertheless, the r_2 values for BASPs ranged from 1.83 to 2.28 $mM^{-1}s^{-1}$, which is in average ~2.5-fold greater than the reported r_2 of chex-PEG bottlebrush polymers[201] and ~11- to ~13.5-fold greater than nitroxide 3-CP. However, the r_2 values obtained are below those reported for the analogue PEG-based BASP-ORCAs which range from 4.67 to 7.40 $mM^{-1}s^{-1}$.[197] Further screening of synthetic parameters such as MM-to-catalyst and bottlebrush polymer-to-catalyst ratios could potentially modify the resulting relaxivity to values comparable to the already reported PEG-based BASP-ORCAs. Besides relaxivity enhancement, it is fundamental to reduce the rapid reduction of the nitroxide in biologically relevant conditions. Therefore, the stability *in vivo* of the PEtOx-based BASP-ORCAs should be evaluated and compared to the available PEG-based MRI probes. Additionally, cytotoxicity studies are necessary to ensure the viability of PEtOx-based nanoparticles in biological systems.

Table 10. Characterization data for BASP-ORCAs

	m	N	r_1 ($mM^{-1}s^{-1}$)	r_2 ($mM^{-1}s^{-1}$)	D_h (nm)	M_n (× 10^5 g mol^{-1})	M_w (× 10^5 g mol^{-1})	$Đ$
MM	1	0	0.14	0.17	n.d.	0.0527	0.0544	1.03
Brush	10	0	0.16	0.58	10 ± 4	0.373	0.374	1.01
BASP	10	20	0.19	1.83	18 ± 4	5.04	6.00	1.19
	7	20	0.17	1.96	21 ± 6	5.89	8.25	1.40
	7	30	0.19	2.28	27 ± 9	10.8	15.9	1.47

4.9. Conclusion

The successful synthesis of the first PEtOx-based macromonomers for ROMP was achieved using the termination step of the CROP of 2-oxazolines to introduce a norbornene moiety. The obtained polymers were fully characterized by SEC, MALDI-ToF mass spectrometry, and ^{1}H NMR spectroscopy, to confirm end group fidelity with the targeted molar masses and narrow dispersities ($Đ$ < 1.15). The viability of the new **PEtOx MM** to form bottlebrush copolymers and BASPs by graft-through ROMP was tested. Quantitative conversions from MM to bottlebrush were obtained for all MMs, as observed from an increase in M_n on the SEC traces. In addition, a preliminary test to form BASPs from **PEtOx MM 3kDa** resulted in increased M_n and diameter, indicating the successful formation of the desired architecture. We combined the newly synthesized **PEtOx MMs** with a previously reported strategy to form bivalent macromonomers where one domain contains a linear polymer and the second a functional moiety of interest (e.g., anti-cancer drugs or imaging agents).[194] To achieve this, the termination step of the CROP of EtOx was carried out with an alkyne-branched-norbornene moiety, followed by the attachment of the paramagnetic nitroxide **chex** by CuAAC click reaction. Characterization of the polymers by SEC, MALDI-ToF spectrometry, and ^{1}H NMR spectroscopy revealed defined narrow molar mass distributions and the integrity of the end group and polymer backbone after functionalization. The successful synthesis of bottlebrush polymers and BASPs from the **chex**-functionalized PEtOx MMs by graft-through ROMP was carried out with the screening of various MM-to-catalyst and crosslinker-to-catalyst ratios. Characterization of the resulting polymers by SEC revealed nearly quantitative conversion from monomer to bottlebrush, and from bottlebrush to BASP, as observed from the M_n increase. Furthermore, DLS measurements evidenced an increase in diameter after crosslinking indicating the successful formation of BASPs. Additionally, the size range of the measured BASPs is suitable for *in vivo* administration, since polymer-conjugated particles of similar sizes show enhanced circulation times in blood and selective tumor uptake. The magnetic properties of the produced BASP-ORCAs were measured and showed improved transverse relaxivity values (r_2) of up to ~13.5-fold when compared to the conventional nitroxide CP-3, and up to ~2.5-fold compared to the analogue **chex**-PEG bottlebrush previously reported.[201] However, the relaxivity values obtained are still

below what is reported for PEG-based BASP-ORCA analogues, which can increase r_2 up to 44 times compared to CP-3. Optimization of synthetic parameters, as well as stability and cytotoxicity assessments should be conducted to demonstrate the viability of PEtOx-based BASP-ORCAs in biologically relevant environments. Nevertheless, the newly synthesized metal-free PEtOx-based MRI probes have potential for further development as an alternative to the previously reported PEG-based MRI probes.

5

PNAM and POEGMA conjugates as alternatives to protein PEGylation

5.1. Introduction[3]

The use of recombinant enzymes in the biotechnological field is rapidly increasing due to the wide range of applications available, from biocatalysis to textile, food, and pharmaceutical industries. Particularly, the use of protein- or peptide-based drugs has benefited the pharmaceutical market, since these bring specificity for molecular targets in the body, while exhibiting reduced side effects.[297] The complex molecular structure of proteins provides the specificity required from a drug, however, it also brings a series of challenges such as instability, often poor solubility, and an immune response from the body that results in short circulation times.[298–300]

[3] The project described in this chapter was done in collaboration with the group of Prof. Juergen Hubbuch from the Institute of Engineering in Life Sciences, KIT. The conjugation, separation, activity, and phase diagram experiments, as well as characterization by capillary gel electrophoresis and size exclusion chromatography of proteins were done by Josefine Morgenstern and Nicolai Bluthardt.

A strategy to improve the properties of the pharmaceutical active is the generation of polymer-protein conjugates by covalent attachment of a polymer to the protein of interest.[299,301,302] The potential polymer should fulfill requirements such as high solubility in aqueous environments and biocompatibility, and should bear a functional group available for conjugation to the protein.[303]

As previously mentioned in other sections (**2.1.1**), PEG is the gold standard, FDA-approved, most commonly used hydrophilic polymer in biomedical applications. Among the many advantages, PEGylated proteins possess increased stability,[304] solubility,[305] and circulation time.[306] However, the huge amount of exposure of humans to PEG for the last decades has also lead to the formation of antibodies against PEG,[10,12,307–310] which as a consequence, decreases the circulation time of PEGylated actives,[311] defeating the purpose of conjugation. In addition, depending on the PEG size, larger conjugates cannot be excreted from the body, and these accumulate as vacuoles in the liver, kidneys, or spleen.[13,312] As a result of these findings, there is an increasing interest in the development of alternative polymers for biomedical applications. Among the many polymer systems available, synthetic polymers are an attractive possibility.[313–315] The recently developed RDRP techniques, allow the development of a wide range of architectures, with defined polymer sizes, narrow distributions, and the possibility to add desired functional groups on the end chains.[302] In addition, by varying the monomer choice, the resulting properties of the resulting polymer system can be tuned.[316]

The optimization of the biological and physicochemical properties of conjugates depends on the careful selection of the type of polymer bound, its size, and the number of chains attached to the protein.[302] However, so far there is no available tool to quantify the influence of the mentioned parameters on the properties of the polymer-protein conjugates. In this chapter, poly(*N*-acryloylmorpholine) (PNAM) and poly(oligo(ethylene glycol) methyl ether methacrylate) (POEGMA) of varied sizes were synthesized by RAFT polymerization and conjugated to different degrees to a model protein. The influence of the polymer used, its size, and conjugation degree, on the physicochemical properties of the resulting conjugates was investigated using high-

throughput screening. The properties investigated are aggregation behavior, solubility, and remaining activity of a model protein (**Figure 78**).

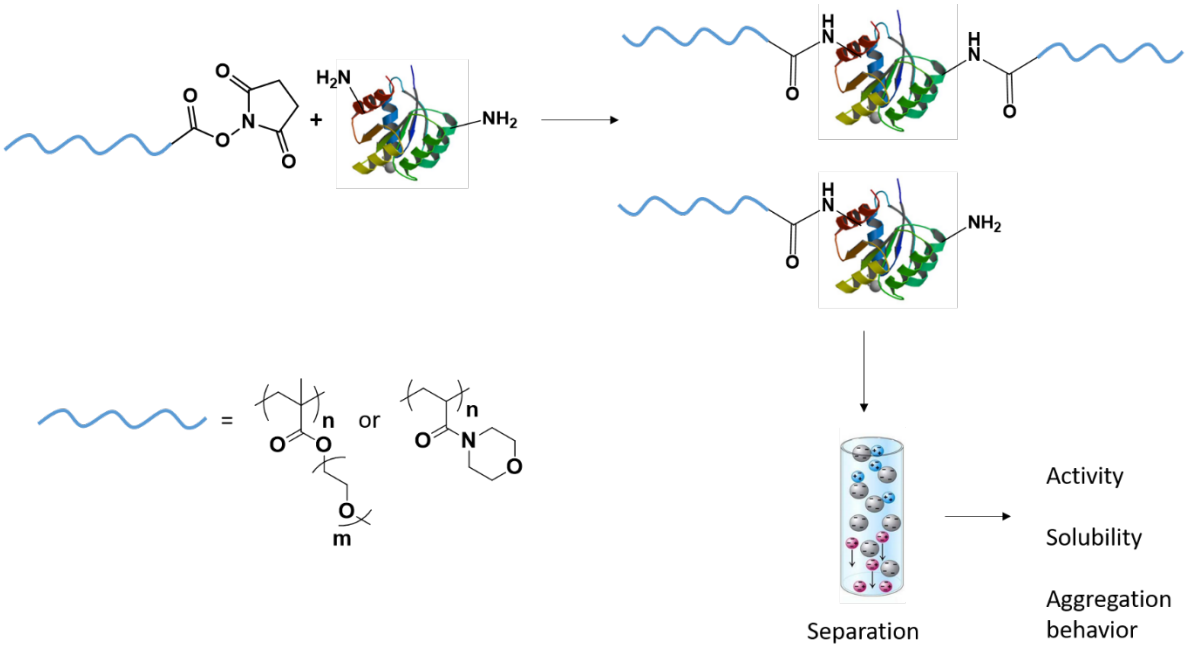

Figure 78. Strategy for the formation of polymer-protein conjugates and its separation for high-throughput screening of physicochemical properties.

5.2. Synthesis of PNAM and POEGMA by RAFT polymerization

The search for alternatives to PEG for therapeutic purposes makes synthetic polymers such as PNAM and POEGMA an interesting choice to explore (**Figure 79**). PNAM is a water-soluble bi-substituted acrylamide derivative. It has been synthesized by RAFT polymerization and modified for selective attachment to surfaces, as well as enzymes, showing a reduced immunogenicity.[78] For instance, drug-PNAM conjugates have been reported for doxorubicin and amoxicillin, although without further evaluation.[79] In addition, PNAM conjugation to the enzyme Candida lipase resulted in hybrids with a higher solubility in organic solvents and higher remaining activity when compared to its reported PEG analogue.[79] POEGMA, on the other hand, is a hydrophilic, PEG-based comb-like polymer, that has been extensively studied for potential biomedical applications. POEGMA can be synthesized by RDRP techniques such as ATRP or RAFT polymerization, and can be modified to add special functionalities to the polymeric chain ends depending on the initiator or transfer agent used.[22–24] POEGMA has been grafted from model proteins using modified ATRP initiators in aqueous medium,[23,68,69] with the advantage of specificity on the conjugation site (either *N* or *C* terminus). In addition, *in vivo* studies showed an increased circulation time of 15-50 times, as well as increased tumor accumulation when compared to the native protein, lysozyme.[13] Both polymer systems share characteristics such as high solubility in water and other polar solvents, as well as low toxicity. In addition, both can be synthesized with relative ease by RAFT polymerization, which brings all the advantages of RDRP techniques, with the possibility to add a linking functionality for conjugation on the end chain by careful selection of the RAFT agent.

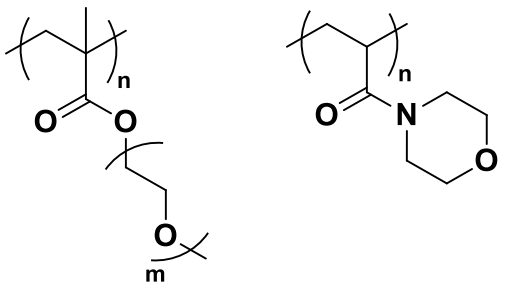

Figure 79. Structures of poly(oligo(ethylene glycol) methyl ether methacrylate) (POEGMA) (left) and poly(*N*-acryloylmorpholine) (PNAM) (right).

For this project it was decided to form the conjugates with the activated ester – lysine methodology, by direct incorporation to the polymer chain of an activated NHS ester present in a functionalized CTA (**Figure 80**) during the RAFT polymerization. A description of the NHS-lysine binding for conjugation was given in section **2.5**. For each monomer selected, two different sizes were targeted so that the influence of polymer size could be analyzed.

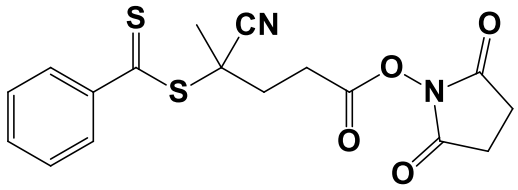

Figure 80. RAFT agent used in the present study 4-cyano-4-(phenylcarbonothioylthio)pentanoic acid *N*-succinimidyl ester.

The polymers were synthesized using conditions adapted from the literature,[317,318] and after purification were analyzed by ^{1}H NMR and SEC. The ^{1}H NMR spectra obtained show the polymer backbone signals expected, as well as the side chain (**Figure 81**, **Figure 82**, **Figure 83**, and **Figure 84**). Importantly, signals corresponding to the aromatic (at approximately 7.3-8.0 ppm) and NHS groups (at approximately 2.8 ppm) of the RAFT agent can also be observed, which gives an indication of the quantitative survival of the CTA. The aromatic signals were used to calculate $M_{n,NMR}$ by comparing the integration values to those of the signals that correspond to the repeating unit of the polymer (approximately at 3.2-3.9 ppm for the morpholine repeating unit of PNAM, and 3.9-4.2 ppm for the methylene protons adjacent to ester bond of POEGMA). In each case, the target was to have two different molar masses for each polymer that could then be compared after conjugation. PNAM and POEGMA of approximately 3.5 kDa and 7 kDa were obtained according to the values calculated by ^{1}H NMR, through integration of chain end and backbone peaks.

Table 11. Summary of the characterization of the four polymers synthesized for this study.

Polymer	$M_{n,NMR}$ (g mol^{-1})	$M_{n,SEC}$ (g mol^{-1})	$Đ$
$PNAM_{3.5kDa}$	3500	1900	1.08
$PNAM_{7kDa}$	7100	3800	1.09
$POEGMA_{3.5kDa}$	3600	3400	1.10
$POEGMA_{7.5kDa}$	7600	6700	1.10

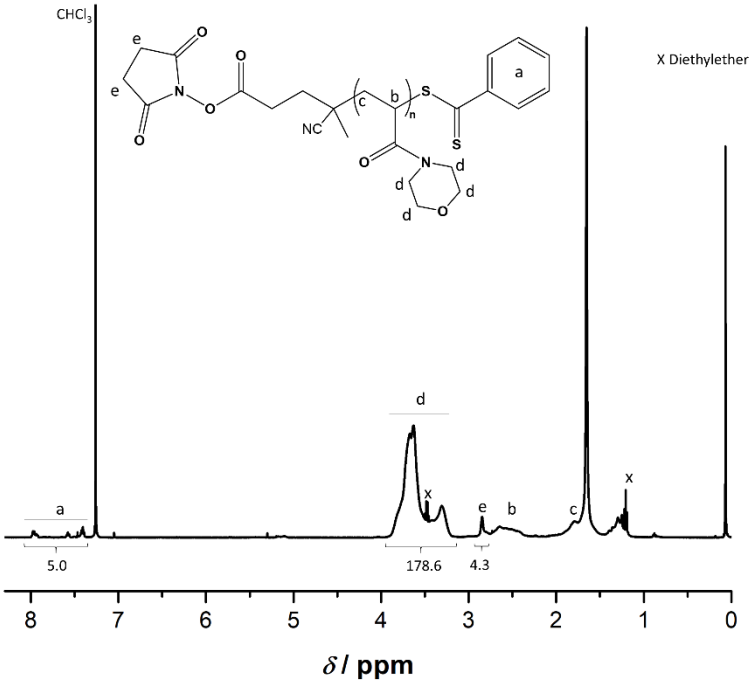

Figure 81. ^{1}H NMR spectrum of the purified $PNAM_{3.5kDa}$.

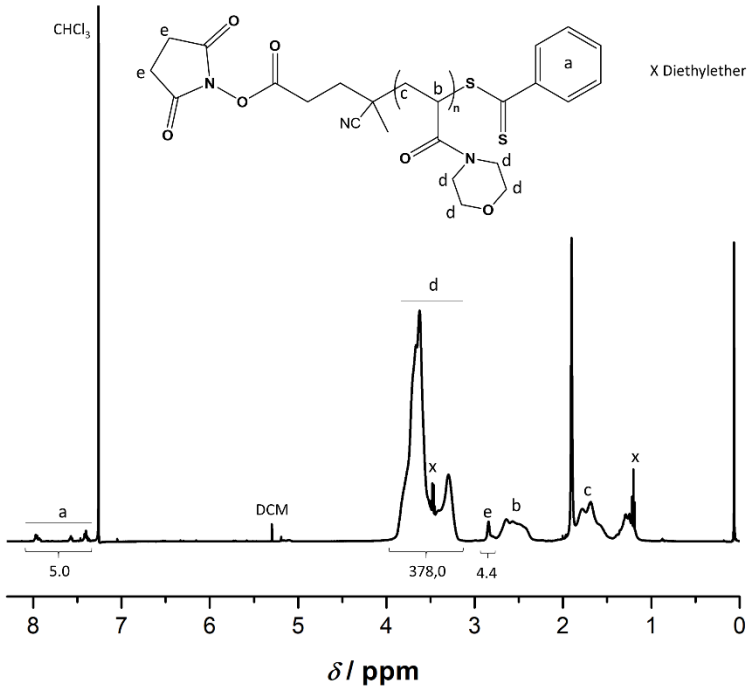

Figure 82. ^{1}H NMR spectrum of the purified $PNAM_{7kDa}$.

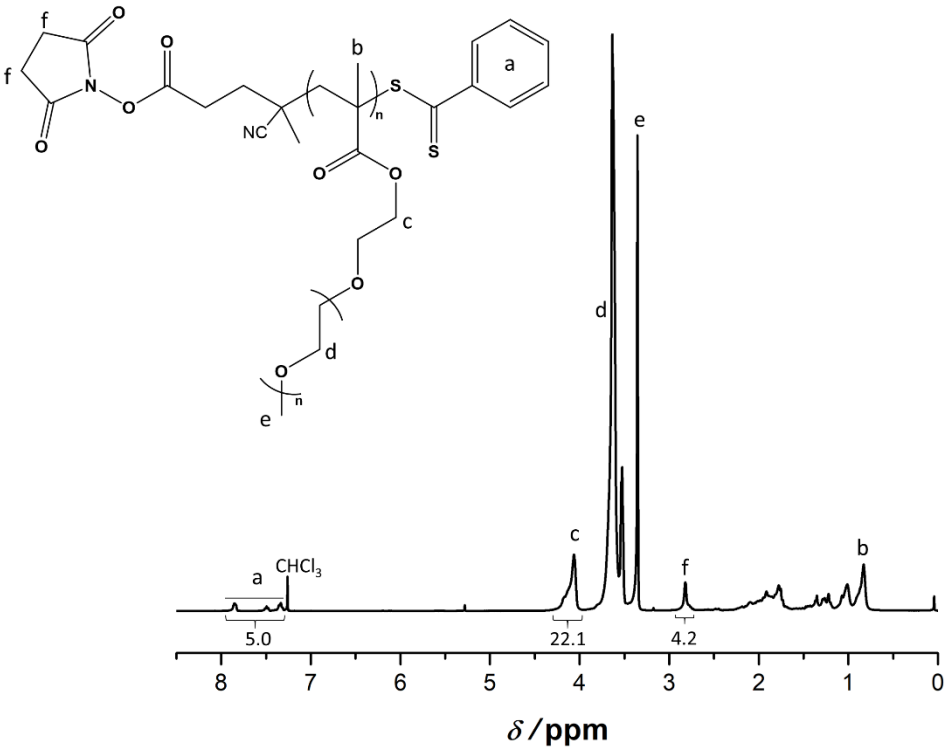

Figure 83. ^{1}H NMR spectrum of the purified $POEGMA_{3.5kDa}$.

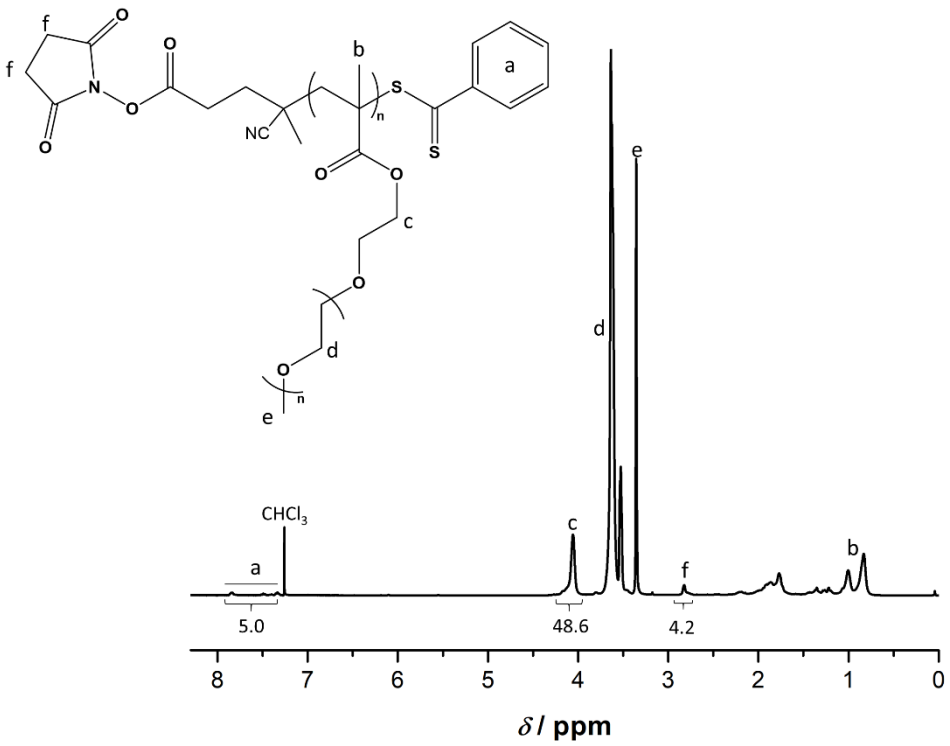

Figure 84. ^{1}H NMR spectrum of the purified POEGMA$_{7.5kDa}$.

The SEC traces of all polymers in THF gave dispersity values *Đ* below 1.1, which, as expected, indicates a narrow distribution typical of a controlled polymerization (**Figure 85**). The $M_{n,SEC}$ values were calculated based on PMMA standards and therefore do provide accurate estimates. The obtained $M_{n,SEC}$ values increased proportionally with target polymer size. MALDI-ToF analyses, shown in **Figure 87** (**a** and **c**) and **Figure 88** (**a** and **c**) confirmed the defined size with narrow dispersities of the obtained polymers. **Table 11** summarizes the characterization of the polymers used for conjugation.

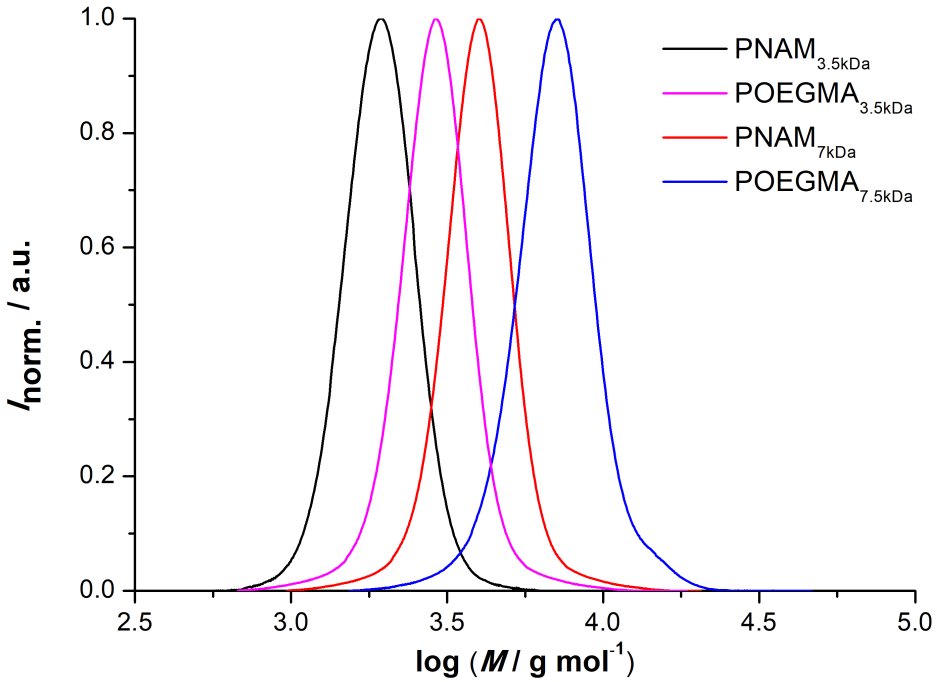

Figure 85. Size-exclusion chromatograms in THF of the synthesized polymers.

5.3. Protein conjugation and purification

The conjugation reaction was carried out for each of the polymers using lysozyme of chicken egg white as model protein. The extensive research on conjugates from this protein, due to the availability of lysine residues, make it a suitable prospect for the study. The conjugation reaction was performed using a 2-fold excess polymer at pH 7.2 in a phosphate buffer for 1 hour at room temperature.

The species present in the mixture were separated by preparative cation exchange chromatography (CEX) for subsequent analysis of each fraction. The chromatograms presented in **Figure 86** were obtained from diluted batches (1:12) of the original reaction mixture. The first 50 ml correspond to the loading phase carried out with a 50 mL loop and are, therefore, not displayed on the chromatograms. The separation was monitored using two different wavelengths: 280 nm for the detection of both polymer and protein, and 320 nm for polymer detection exclusively, thanks to the characteristic absorption of the dithiobenzoate group in the CTA (see experimental section for UV spectra). The difference in absorption of polymer and protein at the designated wavelengths facilitated a first assumption on the nature of each species on the chromatogram. A high absorption at 280 nm, with little to none at 320 nm, can be expected from native lysozyme, and as the 320 nm:280 nm absorption ratio increases, higher conjugation degrees are expected. This would mean that native lysozyme has the highest binding affinity to the column and is the last species to be eluted, while the addition of polymer chains to the protein decreases the binding affinity, resulting in faster elution. The attachment of the polymer on the surface of the protein weakens the electrostatic interaction between the protein surface and the charged column material.[319–321] This assumption can be corroborated by comparison of the results obtained with the reported chromatograms of the purification of PEGylated lysozyme,[305] where a similar pattern was obtained.

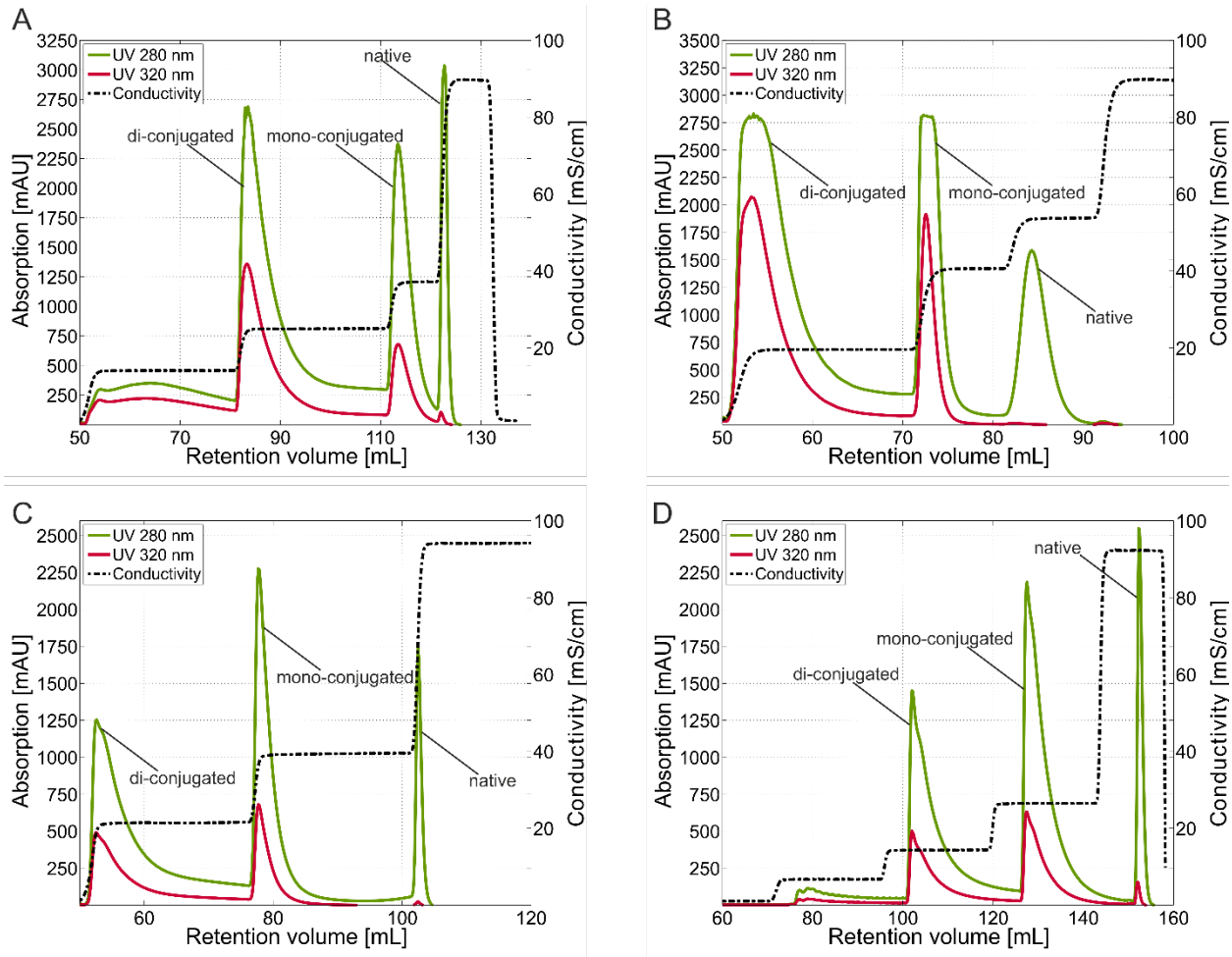

Figure 86. CEX chromatograms of 1:12 diluted conjugation batches (2-fold polymer excess, pH 7.2, 1 h) for (A) $PNAM_{3.5kDa}$, (B) $PNAM_{7kDa}$, (C) $POEGMA_{3.5kDa}$, and (D) $POEGMA_{7.5kDa}$.

The collected fractions, as well as a sample of the raw mixture, were analyzed using MALDI-ToF to confirm the nature of each peak on the chromatogram. The obtained spectra are shown in **Figure 87** (**b** and **d**) and **Figure 88** (**b** and **d**). Three main distributions are visible on the MALDI spectra of all raw reaction mixtures, before purification by CEX. The very narrow distribution at *m/z* = 14.3 kDa corresponds to remaining unreactive lysozyme, while higher *m/z* values can be associated to the conjugated species obtained.

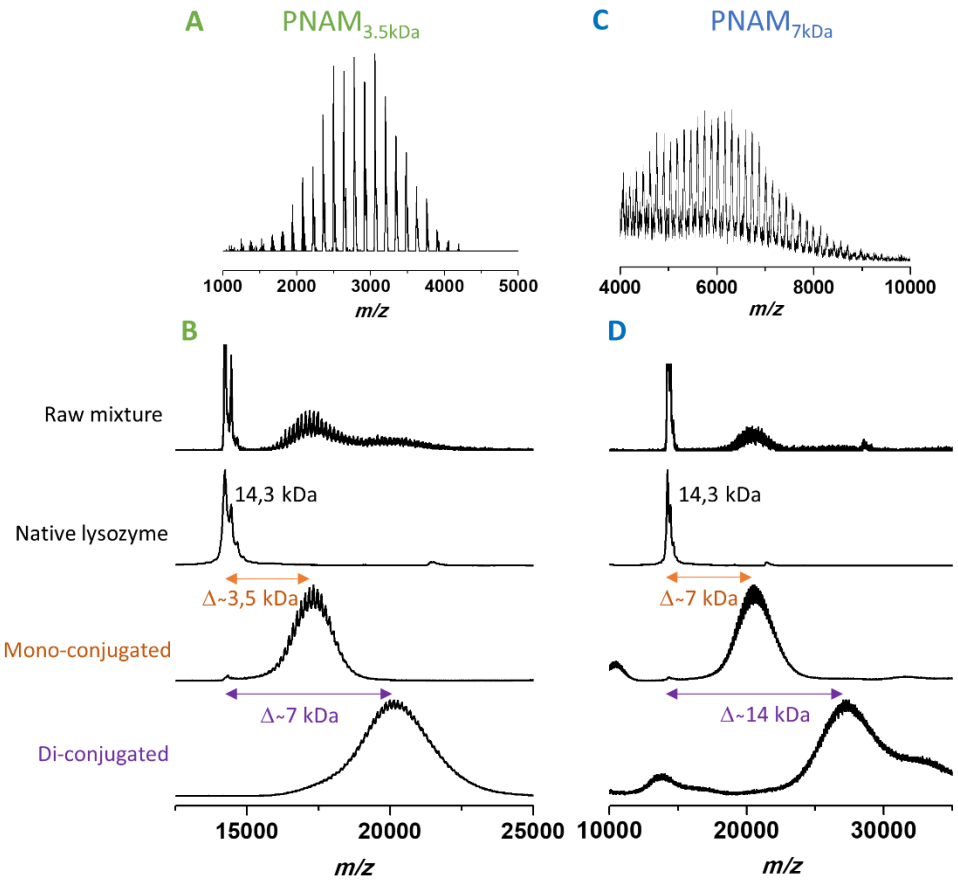

Figure 87. MALDI-ToF spectra of the synthesized PNAM with two different chain lengths (A and C), and the conjugated fractions separated using CEX chromatography (B and D).

MALDI-ToF analysis confirmed the purification of the PNAM conjugates. Fractions collected by CEX give one (almost pure) distribution in mass spectrometry, that corresponds to either the native protein or the protein with one or two polymer chains, respectively (**Figure 87**). However, in the case of POEGMA, despite the good separation obtained on CEX, surprisingly, all MALDI spectra of the collected fractions from CEX show the characteristic signal of the native protein, besides the expected population of conjugates (**Figure 88**). Further characterization of the conjugated species carried out by capillary gel electrophoresis and size-exclusion chromatography show one distribution on each case (**Figure 89**, **Figure 90**, and **Figure 91**), confirming the purity of the conjugated POEGMA fractions. The drastic difference in the results

obtained from MALDI may come from the high ionization capability of lysozyme which, even in trace amounts, would create a much stronger signal than the conjugated protein.

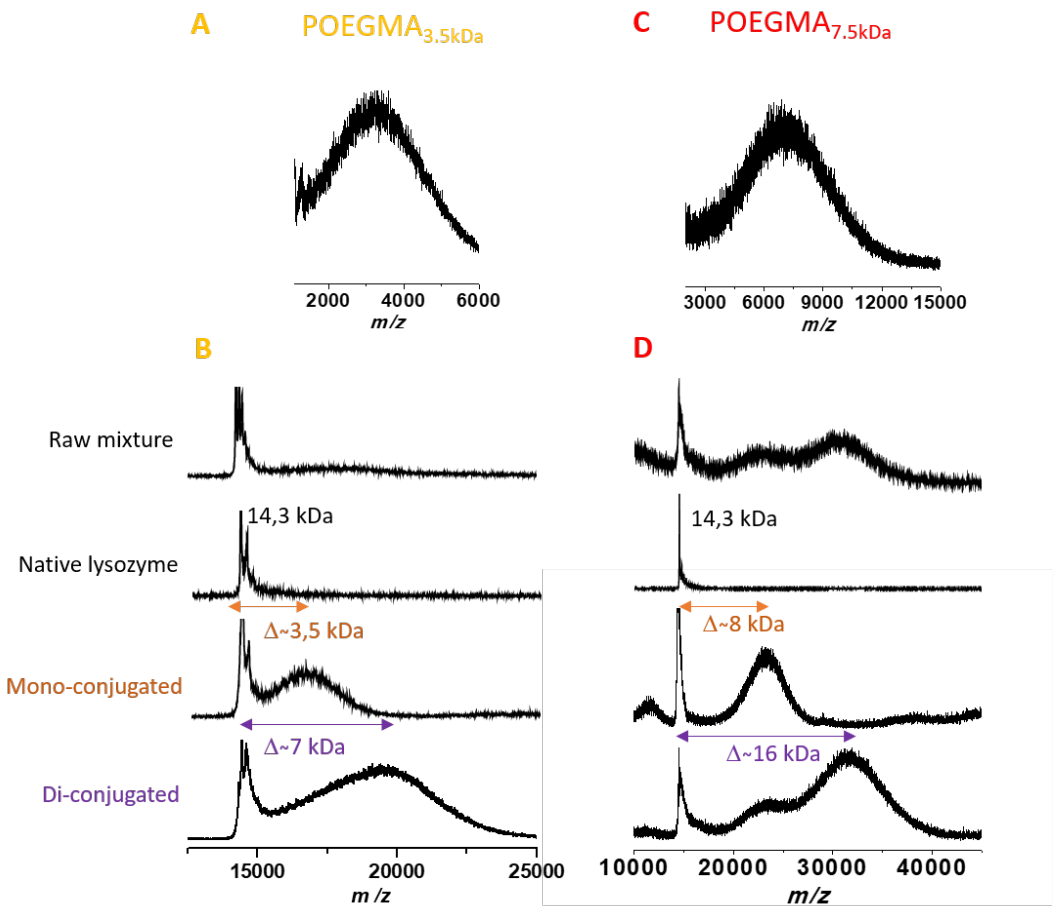

Figure 88. MALDI spectra of the synthesized POEGMA (a and c) and the conjugated fractions separated using CEX chromatography (b and d).

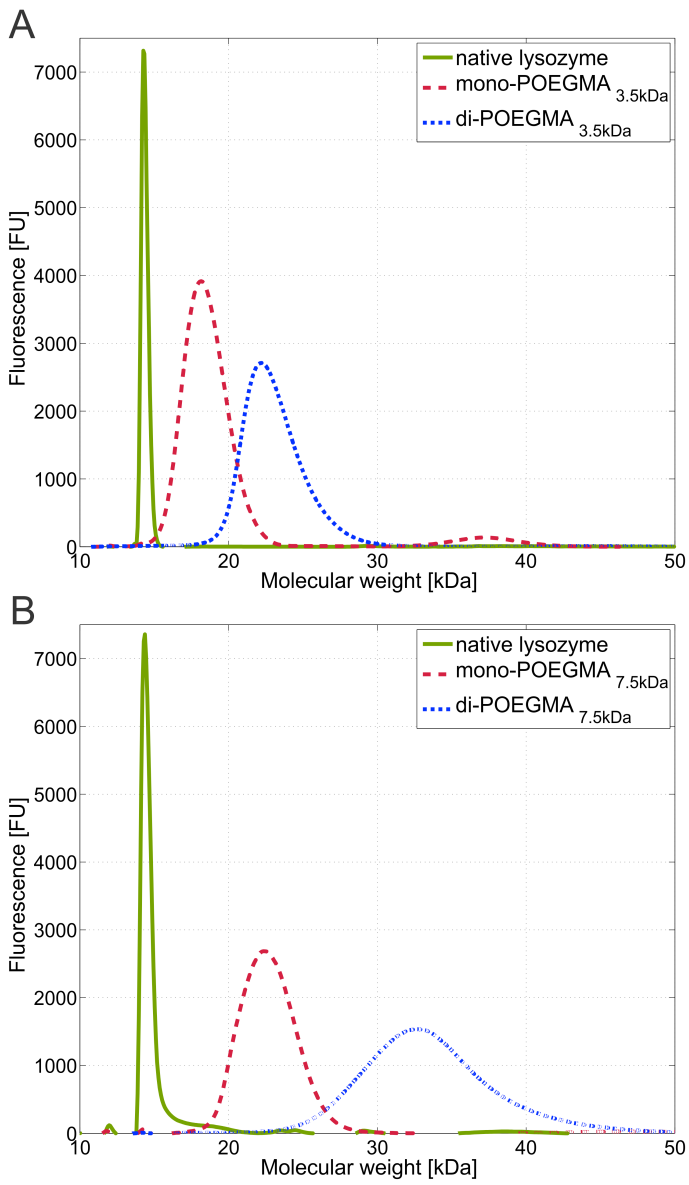

Figure 89. Analysis of the purified $POEGMA_{7.5kDa}$-lysozyme conjugates using high-throughput capillary gel electrophoresis (HT-CGE), according to reference [322].

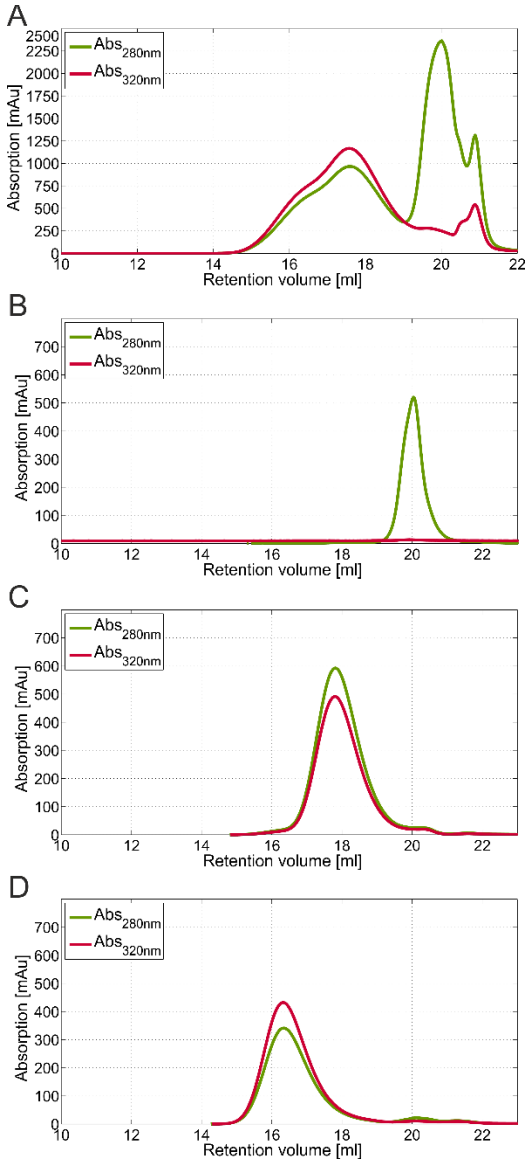

Figure 90. SEC chromatograms of (A) POEGMA$_{3.5kDa}$ conjugation batch, and the purified species of (B) native lysozyme, (C) mono-conjugated lysozyme, and (D) di-conjugated lysozyme.

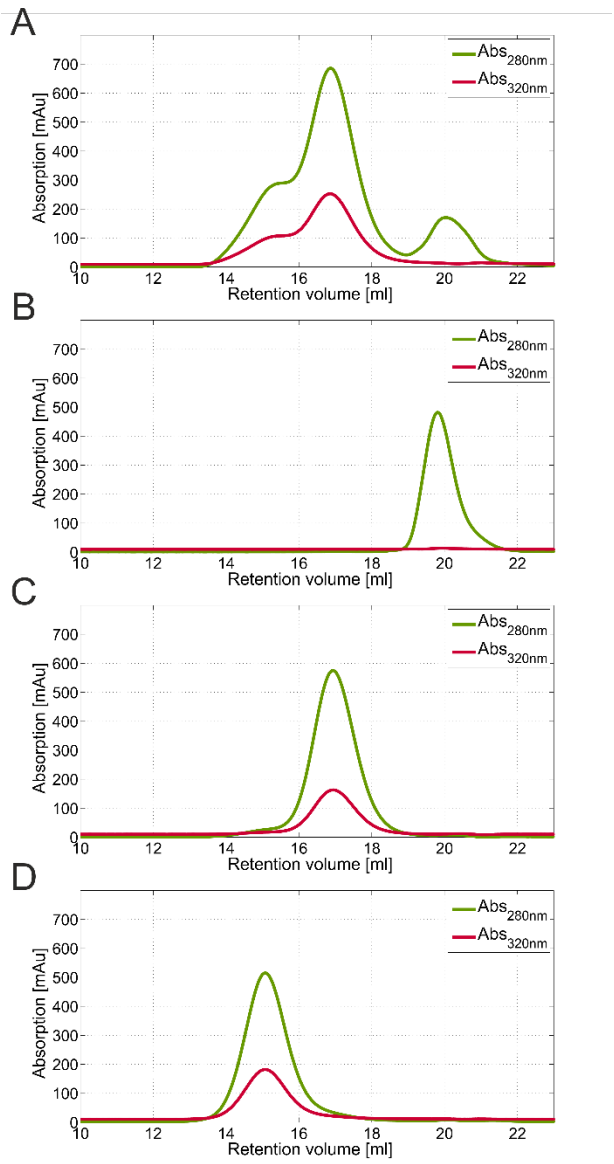

Figure 91. SEC chromatograms of (A) $POEGMA_{7.5kDa}$ conjugation batch, and the purified species of (B) native lysozyme, (C) mono-conjugated lysozyme, and (D) di-conjugated lysozyme.

5.4. Stability assessment

5.4.1. Functional stability

The functional stability of polymer-protein conjugates refers to the analysis of the residual activity of a protein after conjugation. In this project, the assay to calculate the residual activity was based on the lysis of *M. lysodeikticus* by lysozyme.[305] The cell density decrease leads to a clearer solution monitored by an absorbance measurement at 450 nm.

The results of the assay for both polymer systems and native lysozyme are shown in **Figure 92**. The residual activity of the mono conjugates using the smaller polymer chain length, mono-PNAM$_{3.5kDa}$ylated and mono-POEGMA$_{3.5kDa}$ylated lysozyme, was higher or at least equal to that of the native protein. For the rest of the tested conjugates, the remaining activity was lower compared to the native protein.

For both polymer systems, when keeping the conjugation degree constant, higher molar mass polymer-conjugates exhibit lower activity. A similar decrease in activity arises when increasing the conjugation degree and maintaining the molar mass constant. This drastic change in activity may be assigned to the hindering of the active site of the protein by the polymer, as higher molar mass polymers, or an increased conjugation degree cover larger portions of the protein surface, thereby decreasing or even halting its activity.

When directly comparing PNAM conjugates to POEGMA counterparts at equal size or conjugation degree, PNAMylated conjugates show a higher residual activity. In this case, it appears that the nature of the side chain plays an important role on the changes observed of residual activity. Since POEGMA is a comb-like polymer, the conformation these polymers adopt in solution is different from the linear chain of PNAM. It can be assumed in this case that the brush covers a larger surface area of the protein, probably close to the catalytic site, that results in the observed decrease of the activity. The molecular flexibility of the linear PNAM might result in a less hindered conjugate, which causes a less dramatic decrease in activity.

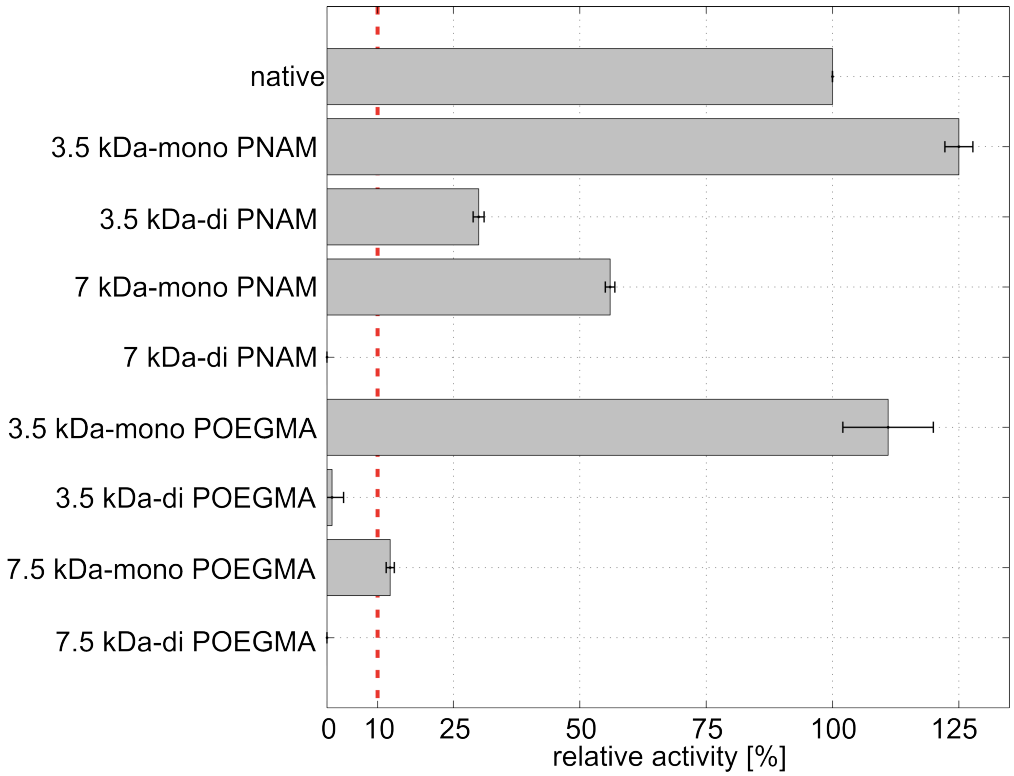

Figure 92. Residual lysozyme activity (%) of protein-polymer conjugates towards the substrate *M. lysodeikticus*. The indicated activity values refer to native lysozyme as reference.

For further analyses, the di-conjugated species of POEGMA and $PNAM_{7.5kDa}$ were not considered due to the very low activity values obtained (below 10%).

5.4.2. Colloidal stability

Physicochemical properties of the obtained conjugates such as solubility and phase behavior, were investigated as well.

For colloidal stability, phase diagrams were created for monoconjugates of each available polymer ($PNAM_{3.5kDa}$, $PNAM_{7kDa}$, $POEGMA_{3.5kDa}$, and $POEGMA_{7.5kDa}$) and di-conjugated $PNAM_{3.5kDa}$. Conjugate solutions of different concentrations at pH 3 were prepared. NaCl in varied concentrations was used as precipitating agent. The solutions were mixed and transferred to a 96-well plate to create a binary phase diagram screening conjugate concentrations ranging from 0.17 to 1.52 M, and salt concentrations from 0 to 2.5 M (**Figure**

93). The experiment was transferred to a stable 25 °C atmosphere for 40 days (17 days for mono-POEGMA$_{3.5kDa}$, due to thesis submission deadline) where photographs of each well were taken by an automated imaging system. The evaluation of the phase diagrams is based on visual analysis where the observed possibilities were precipitation, crystallization, or gelation. The results were compared to the previously reported native lysozyme phase diagram.[323]

For all conjugates, the soluble area was extended as a result of a reduced propensity to protein aggregation. For instance, in the case of mono-PNAM$_{3.5kDa}$ylated lysozyme, the phase transition was reached using twice the salt concentration compared to native protein. The largest soluble area was obtained with the mono-POEGMA$_{7.5kDa}$ylated lysozyme conjugate, where phase transition was induced using four times the salt concentration necessary to destabilize the native protein. This effect is a result of a shielding phenomenon created by the hydrophilic polymers that decreases the interaction between the protein surface and the surrounding ions of the medium, requiring higher amounts of precipitating agent (NaCl) to reach a phase transition.

Although the phase diagrams of both PNAM$_{3.5kDa}$ylated lysozyme show similar characteristics, visually, the aggregates formed are quite different (see **Figure 93** inserts B and C). Mono-PNAM$_{3.5kDa}$ylated lysozyme produces dark precipitates, while di-PNAM$_{3.5kDa}$ylated lysozyme forms mainly gels, and a light precipitate. At higher salt concentrations, the protein is at a ersaturated state and because of the attachment of a single polymer chain (in the case of mono-PNAM$_{3.5kDa}$ylated lysozyme) lysozyme cannot have ordered nucleation and crystal growth, leading instead into a direct transition to precipitation. By adding two polymer chains, not only precipitation is favored but the propensity of the PNAM to create physically crosslinked hydrogels[324,325] is showcased, observed by the formation of gels and a light precipitate. By increasing the conjugation degree of the conjugate, the resulting properties are influenced by the inherent properties of the polymer used.

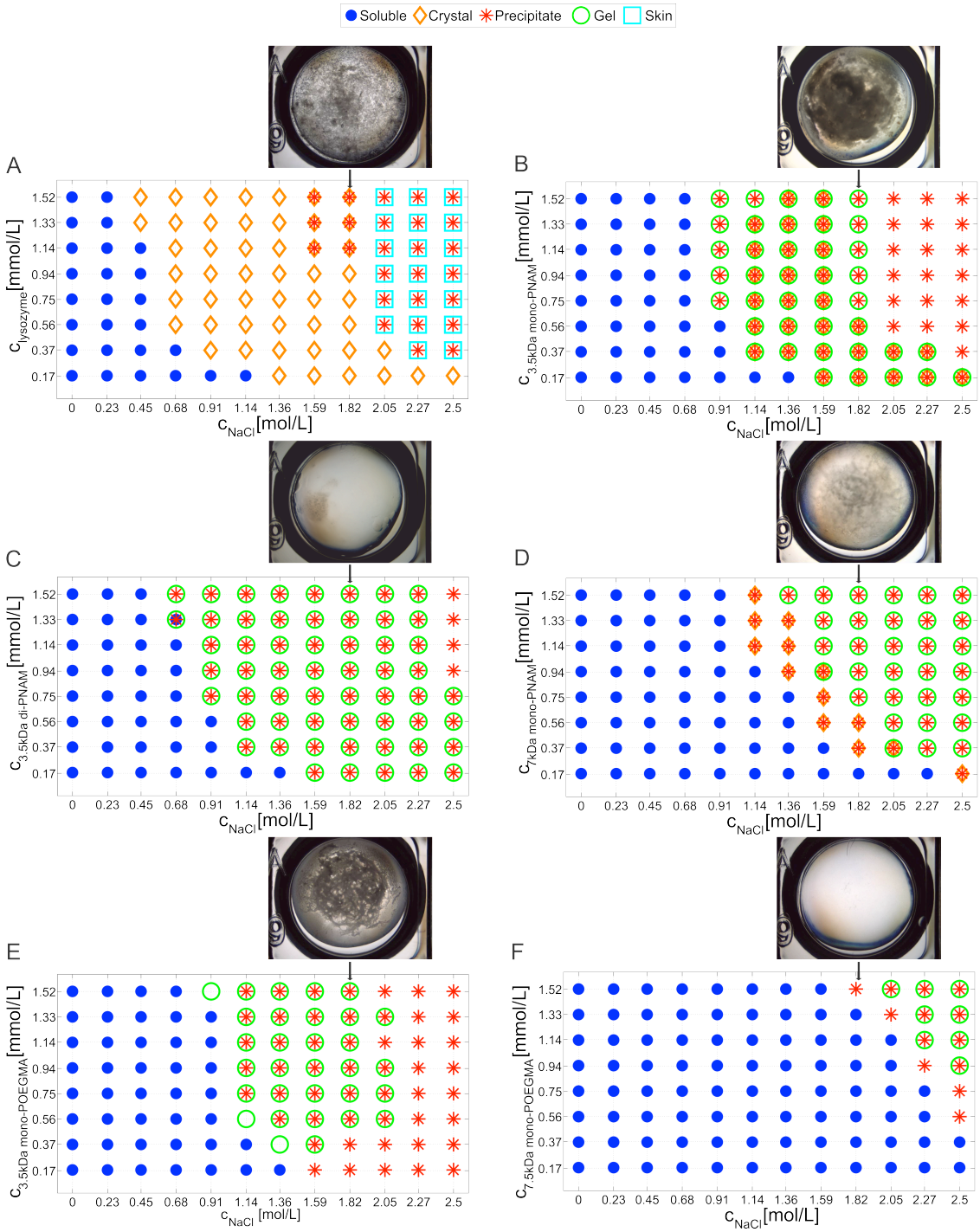

Figure 93. Phase diagrams for (A) native lysozyme, (B) mono-PNAM$_{3.5kDa}$ylated, (C) di-PNAM$_{3.5kDa}$ylated, (D) mono-PNAM$_{7kDa}$ylated, (E) mono-POEGMA$_{3.5kDa}$lated, and (F) mono-POEGMA$_{7.5kDa}$lated lysozyme with sodium chloride (NaCl) as precipitant at pH 3. Phase diagrams of native lysozyme was taken from reference [323]. Inserts show pictures taken after 40 days of wells with conjugate and salt concentrations of 1.52 M and 1.82 M, respectively, for comparison of the aggregates formed.

Although an excellent solubility is achieved with the mono-POEGMA$_{7.5kDa}$ conjugate, the poor remaining activity eclipses the promising results. This exemplifies the compromise that must exist between molar mass, conjugation degree, and choice of monomer when selecting the conjugate to use for the desired application. The mono-POEGMA$_{3.5kDa}$ conjugate shows a larger soluble area compared to its mono-PNAM$_{3.5kDa}$ analogue, indicating the influence of polymer structure on the solubility of the conjugates. Although its soluble area is reduced compared to mono-POEGMA$_{7.5kDa}$, out of the evaluated conjugates, mono-POEGMA$_{3.5kDa}$ shows the largest increase in soluble area while at the same time conserving activity comparable to native lysozyme.

A quantitative method was used to evaluate the increase in solubility of the developed conjugates. The concentration of remaining soluble conjugates in the supernatant from the previous experiment after 40 days was measured. The solubility curves obtained were compared to those previously reported for the native lysozyme[326] and its PEGylated analogue (**Figure 94**).[305] Unfortunately, the solubility curve of mono-POEGMA$_{3.5kDa}$ could not be included since by the time this thesis was submitted, the required 40 days this experiment takes had not passed yet.

All analyzed conjugates display, in general, higher solubility compared to the native protein, as expected. The mono-PNAM$_{7kDa}$ylated conjugate shows a similar behavior to the PEG analogue, despite the lower M_n used for PEG. The different conformation in the solvent adopted by PEG and PNAM can potentially be the reason why a larger PNAM chain is necessary to shield with the same magnitude as a shorter PEG chain. Although solubility increases when conjugating the protein to PNAM, it was unusual to find that at lower salt concentrations the di-conjugate version of the lysozyme has a lower solubility than the mono-conjugated analogue, although as NaCl concentration increased the difference became less apparent.

Mono-POEGMA$_{7.5kDa}$ showed the highest solubility increase of all analyzed conjugates, including the reference linear PEG$_{2kDa}$ conjugate. In this case, it is the higher molar mass and the brush architecture that provide the higher solubility. However, it is those same characteristics that quantitatively suppress the activity.

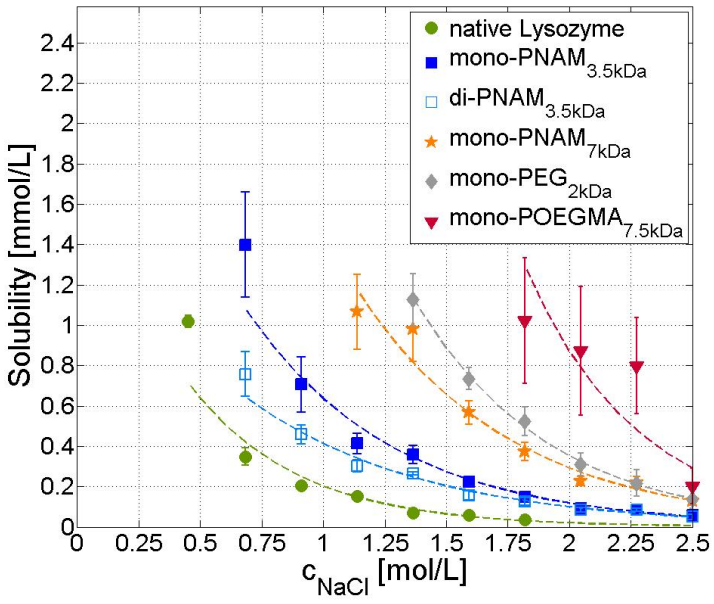

Figure 94. Solubility lines of unmodified lysozyme,[326] mono-PNAM$_{3.5kDa}$ylated lysozyme, di-PNAM$_{3.5kDa}$ylated lysozyme, mono-PNAM$_{7kDa}$ylated lysozyme, mono-POEGMA$_{7.5kDa}$ lysozyme, and mono-PEG$_{2kDa}$ylated lysozyme[305] at pH 3. The solubility curve for mono-POEGMA$_{3.5kDa}$ lysozyme is in preparation.

5.5. Conclusion

PNAM and POEGMA of different chain lengths were synthesized by RAFT polymerization and conjugated to the model protein lysozyme from chicken egg white. The properties of the resulting conjugates are influenced by both the native protein and the polymer properties. It was observed that for the mono-conjugates with lower molar mass polymer (both PNAM and POEGMA), the activity of the conjugated protein was equal or higher than native lysozyme. For the rest of the conjugates, the remaining activity decreased, product of possible shielding of the polymer on the catalytic site. In all cases, the equilibrium solubility increased under the influence of high salt concentrations (NaCl up to 2 M) and acidic pH, when compared to the native protein. These are promising results in the case of mono-conjugates with the small molar mass, where both increased (or equal) activity and higher solubility than those of the native enzyme were achieved. However, in the case of PNAM, already reported PEG-conjugates remains the better option since it has been proved these show a higher solubility increase. On the other hand, $POEGMA_{7.5kDa}$ shows a better solubility when compared to PEG-based conjugates, but at the cost of a significant decrease in activity (less than 10%).

From the results obtained, it can be concluded that depending on the desired application of the conjugate, a compromise between enhanced physicochemical properties and activity has to be found. The physicochemical properties of the resulting conjugate can be shaped depending on the choice of polymer, its size, and the number of attached chains. The presented preparative and analytical methods are a helpful tool for the optimization of these parameters. Furthermore, the robustness of the method allows the potential extrapolation of the method to assess the physicochemical properties of conjugates using other biocompatible polymers alternative to PEG.

6

Conclusion

The biocompatible polymers synthesized for this thesis show promising results on each case study. The synthetic versatility of PAOx, PNAM, and POEGMA was showcased for the incorporation of functional groups on the chain ends of well-defined polymers. The reactive groups introduced allow the incorporation of molecules of interest (including proteins and imaging agents), the attachment of the polymer to a functionalized surface, and the formation of complex architectures such as bottlebrush and arm-star polymers. Nevertheless, further biological studies are still necessary to ensure PAOx, PNAM, and POEGMA can be a useful alternative and a complementary polymer to PEG.

In Chapter 3, a new strategy to obtain maleimide and thiol α-functionalized PAOx was established using nosylate initiators. The novel initiators bear either a furan-protected maleimide moiety or a protected thiol group in the form of thioacetate. For **FurMalNos 4**, thermal and solubility limitations required polymerization conditions with lower monomer concentration and temperature. In the case of **ThioAcNos 8**, its simpler synthetic strategy, good solubility, and compatibility with microwave-assisted polymerization provided a straightforward path to well-defined polymers. Polymers with molar masses relevant for either bioconjugation

or surface functionalization were obtained from the synthesized initiators. The strategy described provides the possibility to functionalize the ω-chain end and obtain bifunctional telechelic polymers by appropriate termination. However, this route can potentially lead to the presence of proton-initiated chains (in the case of **FurMalNos 4,** for instance), via H transfer, or to discrepancies on the expected molar mass as a result of lower efficiency of the initiator. The described approach can potentially have applications in the development of bifunctional linkers for surface biofunctionalization, stealth surfaces, or the construction of artificial protein dimers.

Chapter 4 described the successful synthesis of the first PEtOx-based macromonomers for ROMP to develop a metal-free PEtOx-based MRI probe. New branched and linear PEtOx macromonomers were obtained taking advantage of the termination step of the CROP of EtOx to introduce norbornene or dual norbornene-alkyne moieties. Bivalent alkyne-PEtOx macromonomers were functionalized with the paramagnetic nitroxide **chex,** used as MRI contrast enhancement agent, by CuAAC click reaction. The synthesis of bottlebrush polymers and BASPs from linear and **chex**-functionalized PEtOx MMs by graft-through ROMP was carried out screening different MM-to-catalyst, and crosslinker-to-catalyst ratios. Nearly quantitative conversion from monomer to bottlebrush and from bottlebrush to BASP was observed from SEC characterization. The magnetic properties of the synthesized PEtOx-based BASP-ORCAs showed an improved transverse relaxivity (r_2) of up to ∼13.5 times higher when compared to nitroxide CP-3, and up to ∼2.5-fold compared to the analogue **chex**-PEG bottlebrush previously reported.[201] However, the relaxivity values observed are below what is reported for the PEG-based analogue BASP, which increases r_2 up to 44 times compared to CP-3. Nevertheless, the novel metal-free PEtOx-based MRI probes have potential for further development as an alternative to the previously reported PEG-based MRI probes, after screening of further synthetic parameters is performed.

In Chapter 5, the evaluation of the physicochemical properties of PNAM- and POEGMA-conjugated lysozyme provided information on the extent polymer type, size, and conjugation degree affect the properties of the conjugates. The drastic effect of molar mass and conjugation degree on the activity of the conjugates was evident considering the activity of the

set of 3 kDa mono-conjugates (both PNAM and POEGMA) increased or was equal to that of the native protein, while to higher molar mass and conjugation degree polymer-protein conjugates that showed lower activity. This is caused by a shielding phenomenon of the polymer on the active site of the protein. The equilibrium solubility increased for all conjugates in high salt concentrations (NaCl up to 2.5 M) at pH 3 with respect to the native protein. $POEGMA_{7.5kDa}$ showed the highest increase in solubility of all tested conjugates. However, the improved solubility is eclipsed by the minimal activity observed (less than 10%). The results lead to the conclusion that depending on the desired application of the conjugate, a compromise should exist between enhanced solubility and activity. The high-throughput method developed provides a systematic evaluation of the properties of polymer-protein conjugates. Its robustness allows the potential extrapolation to assess other available biocompatible polymers.

7

Experimental Section

7.1. Maleimide- and thiol-functionalized initiators for the polymerization of 2-oxazolines

7.1.1. Materials and instrumentation

Materials

Maleic anhydride (99%, Bernd Kraft), furan (99%, Acros), allyl alcohol (99%, Sigma), ethanolamine (99%, Acros), 4-toluenesulfonyl chloride (99%, Acros), 4-nitrobenzenesulfonyl chloride (97%, Sigma-Aldrich), pyridine (99%, Roth), benzene (99%, Sigma), cyclohexane (VWR), benzoin (98%, Acros), 4-dimethylaminopyridine (DMAP; 99%, Aldrich), triazabicyclodecene (TBD, Sigma), dimethylphenylphosphine (DMPP; 99%, Sigma), sodium chloride (99.8%, Roth), thioacetic acid (98%, Acros), sodium hydroxide (99%, Roth), tetramethylammonium hydroxide (25 wt% in methanol, Acros), bovine serum albumin (BSA; Sigma), toluene (Fisher), petroleum ether (Acros), ethanol (99.8%, Acros), acetone (Fisher), tetrahydrofuran (THF; VWR), diethyl ether (99.5%, Roth), and dichloromethane (DCM; VWR) were used as received. Acetonitrile

(MeCN; Sigma-Aldrich) was dried in a solvent purification system (JC Meyer) before use as a polymerization solvent. 2-ethyl-2-oxazoline (EtOx; Aldrich) was distilled over barium oxide and stored under argon.

Characterization techniques

All polymer solutions and samples were prepared in a VIGOR Sci-Lab SG 1200/750 Glovebox System with a water concentration ≤ 0.1 ppm. Polymerization reactions assisted by microwave irradiation were performed in capped vials in a microwave reactor (Biotage) equipped with an infrared (IR) temperature sensor.

Gas chromatography (GC)

Monomer conversion was determined by GC. Samples were measured on a 7890A from Agilent Technologies with an Agilent J&W Advanced Capillary GC column (30 m, 0.320 mm, and 0.25 lm). Injections were operated with an Agilent Technologies 7693 auto sampler.

^{1}H nuclear magnetic resonance (NMR) spectroscopy

Measurements were performed on a Bruker AM 500 spectrometer (500 MHz). All compounds were dissolved in either $CDCl_3$ or DMSO-d6 and the residual solvent peak was employed for shift correction (7.26 ppm for $CDCl_3$ and 2.50 ppm for DMSO-d6).

Size-exclusion chromatography (SEC)

SEC was used with *N*,*N*-dimethylacetamide (DMAc) as eluent with a sample concentration of 2 g L^{-1} on a Polymer Laboratories PL-GPC 50 Plus Integrated system comprising an autosampler, a PLgel 2,5 µm bead-size guard column (50 × 7.5 mm) followed by three PLgel 5 µm MixedC columns (300 × 7.5 mm), and a flow rate of 1 mL min^{-1}. The SEC system was calibrated against linear poly(methyl methacrylate) standards with molar masses ranging from 700 to 2 × 10^6 Da. The samples were filtered through PTFE membranes with a pore size of 0.2 µm prior to injection.

Electrospray ionization mass spectrometry (ESI-MS)

Spectra were recorded on an LXQ mass spectrometer (Thermo Fisher Scientific, San Jose, CA) equipped with an atmospheric pressure ionization source operating in the nebulizer assisted electrospray mode. The instrument was calibrated in the *m/z* range 195−1822 using a standard containing caffeine, Met-Arg-Phe-Ala acetate (MRFA), and a mixture of fluorinated phosphazenes (Ultramark 1621) (all from Aldrich). A constant spray voltage of 4.5 kV was used. Nitrogen at a dimensionless sweep gas flow rate of 2 (approximately 3 L min^{-1}) and a dimensionless sheath gas flow rate of 5 (approximately 0.5 L min^{-1}) was applied. The capillary voltage, the tube lens offset voltage, and the capillary temperatures were set to 34 V, 90 V, and 275 °C, respectively. The samples were dissolved at a concentration of 0.1 mg mL^{-1} in a mixture of THF and MeOH (3:2 v/v) containing sodium trifluoroacetate (0.14 µg L^{-1}).

Sodium dodecyl sulfate polyacrylamide gel electrophoresis (SDS-PAGE)

Protein-polymer conjugates were analyzed on 12% SDS-PAGE under non-reducing conditions, using standard molecular biology techniques, followed by Coomassie Brilliant Blue staining.

Fast protein liquid chromatography (FPLC)

FPLC was performed for the preparative separation of BSA conjugates. An ÄTKA purifier system equipped with an autosampler A-905 and a Fraction Collector Frac-950 (GE Healthcare) was used. The separation of BSA-PEtOx conjugates was performed on a Superdex 200 10/300 GL (GE Healthcare) SEC column using a 0.05 M phosphate buffer (pH 7.0) and 0.15 M NaCl solution. The column was loaded with 300 µL of sample and the system was run at a flow rate of 0.5 mL min^{-1}. Fractions of 250 µL were collected into a 96-well plate. A UV detector continuously measured the relative absorbance of the mobile phase at 280 nm. The yields were not optimized.

Matrix-assisted laser desorption ionization coupled to time-of-flight (MALDI-ToF) mass spectrometry

Mass spectra were acquired with a 4800 Proteomics Analyzer (Applied Biosystems, Foster City, CA, USA) in positive ion linear mode and a mass range of 60000 to 80000 Da. The laser intensity was set to 4700. The spectra obtained represent the average of laser shots taken by an automatic scheme measuring spectra over the whole spot.

X-Ray Photoelectron Spectroscopy (XPS)

XPS investigation was performed in a K-Alpha+ spectrometer (ThermoFisher Scientific, East Grinstead, UK) using a microfocused, monochromated Al Kα X-ray source (150 μm and 400 μm spot size). The kinetic energy of the electrons was measured by a 180° hemispherical energy analyzer operated in the constant analyzer energy mode (CAE) at 50 eV pass energy for elemental spectra. The K-Alpha+ charge compensation system was employed during analysis, using electrons of 8 eV energy, and low-energy argon ions to prevent any localized charge build-up. Data acquisition and processing using the Thermo Avantage software is described elsewhere.[327] The spectra were fitted with one or more Voigt profiles (BE uncertainty: +0.2eV) and Scofield sensitivity factors were applied for quantification.[328] All spectra were referenced to the C 1s peak (C-C, C-H) at 285.0 eV binding energy controlled by means of the well-known photoelectron peaks of Cu, Ag, and Au respectively.

7.1.2. Syntheses

Synthesis of maleimide-functionalized initiators

3a,4,7,7a-Tetrahydro-4,7-epoxyisobenzofuran-1,3-dione (1)

Maleic anhydride (30.0 g, 306 mmol) was suspended in toluene (150 mL) in a 250 mL round-bottom flask. This mixture was heated to 80 °C. Furan (33.4 mL, 459 mmol) was added dropwise with a syringe. After stirring for 6 h, the mixture was cooled to ambient temperature and then

left in the freezer overnight. The resulting crystals were collected by filtration and washed with petroleum ether (3 × 30 mL). **1** was obtained as white crystals after drying under reduced pressure (41.7 g, 82%).

^{1}H NMR ($CDCl_3$, 500 MHz, δ): 6.58 (s, 2H), 5.47 (s, 2H), 3.18 (s, 2H) ppm.

2-(2-Hydroxyethyl)-3a,4,7,7a-tetrahydro-1H-4,7-epoxyisoindole-1,3(2H)-dione (2)

The anhydride **1** (10.0 g, 60.2 mmol) was dissolved in ethanol (15 mL) in a 100 mL two-neck round-bottom flask. A solution of ethanolamine (3.75 mL, 62.1 mmol) in ethanol (5 mL) was added dropwise. The resulting solution was stirred and heated under reflux for 4 h. Subsequently, the solution was kept at –20 °C overnight. The obtained white solid was filtered, recrystallized in ethanol, and dried under reduced pressure to yield **2** as a white powder (4.34 g, 34%).

^{1}H NMR ($CDCl_3$, 500 MHz, δ): 6.53 (s, 2H), 5.29 (s, 2H), 3.76-3.79 (m, 2H), 3.70-3.72 (m, 2H), 2.90 (s, 2H) ppm.

2-(1,3-dioxo-1,3,3a,4,7,7a-hexahydro-2H-4,7-epoxyisoindol-2-yl)ethyl-4-methylbenzene-sulfonate (FurMalTos 3)

A solution of compound **2** (1.0 g, 4.8 mmol) and pyridine (0.75 g, 9.5 mmol) in THF (7 mL) was prepared in a 50 mL round-bottom flask cooled to 0 °C, before a solution of 4-toluenesulfonyl chloride (1.82 g, 9.5 mmol) in THF (5 mL) was added dropwise. The mixture was then stirred at ambient temperature overnight. The remaining solution was filtered and the solvent was removed under reduced pressure. The product was dissolved in DCM and the mixture was washed with saturated $NaHCO_3$ and water, before being dried over $MgSO_4$. The solvent was removed under vacuum and the residual white powder was recrystallized in an ethanol/acetone mixture (2:1 v/v). After filtration and drying under reduced pressure, **3** was obtained as white crystals (1.10 g, 63%).

^{1}H NMR ($CDCl_3$, 500 MHz, δ): 7.75-7.73 (d, 2H), 7.31-7.33 (d, 2H), 6.50 (s, 2H), 5.22 (s, 2H), 4.17 (t, 2H), 3.73 (t, 2H), 2.84 (s, 2H), 2.42 (s, 3H) ppm.

^{13}C NMR ($CDCl_3$, 125 MHz, δ): 21.75, 37.77, 47.63, 65.51, 80.94, 128.05, 129.99, 132.74, 136.61, 145.15, 175.86 ppm.

ESI-MS (*m/z*): $[M+Na]^+$ calc.: 386.067, found: 386.066 amu.

2-(1,3-dioxo-1,3,3a,4,7,7a-hexahydro-2H-4,7-epoxyisoindol-2-yl)ethyl-4-nitrobenzene sulfonate (FurMalNos 4)

A solution of compound **2** (1.0 g, 4.8 mmol) and pyridine (0.75 g, 9.5 mmol) in THF (7 mL) prepared in a 50 mL round-bottom flask was cooled to 0 °C. To this, a solution of 4-nitrobenzenesulfonyl chloride (2.12 g, 9.5 mmol) in THF (5 mL) was added dropwise. The mixture was then stirred at ambient temperature overnight, after which the produced solid was filtered. The obtained solid was dissolved in DCM, washed with saturated $NaHCO_3$ and water, before being dried over $MgSO_4$. After filtering off the drying agent, the solvent was removed. The residual white powder was recrystallized in an acetone/methanol mixture (3:1 v/v). After filtration and drying under reduced pressure, **4** was recovered as a white powder (0.55 g, 29%).

^{1}H NMR ($CDCl_3$, 500 MHz, δ): 8.38-8.40 (d, 2H), 8.09-8.11 (d, 2H), 6.52 (s, 2H), 5.24 (s, 2H), 4.32 (t, 2H), 3.80 (t, 2H), 2.88 (s, 2H) ppm.

^{13}C NMR ($CDCl_3$, 125 MHz, δ): 37.09, 47.11, 67.49, 80.35, 125.04, 129.32, 136.47, 140.11, 150.78, 176.12 ppm.

ESI-MS (*m/z*): $[M-Na^+]$ calc.: 417.036, found: 417.035 amu.

Allyl tosylate (5)

To a mixture of allyl alcohol (10.0 g, 0.17 mol) and *p*-toluenesulfonyl chloride (16.70 g, 0.10 mol) in a 250 mL two-neck round-bottom flask equipped with a dropping funnel was added 5 N aqueous sodium hydroxide solution (50 mL) below 15 °C. Additional tosyl chloride (16.70 g, 0.10 mol) and then 5 N aqueous NaOH (50 mL) were added consecutively to the reaction mixture. An organic layer was extracted with toluene, washed with 10% aqueous NaOH, and then dried over

potassium carbonate. Evaporation of solvent produced liquid allyl tosylate **5**, which was purified by Kugelrohr distillation (110 °C, 0.15 mmHg) (15.4 g, 43%).

^{1}H NMR ($CDCl_3$, 500 MHz, δ): 7.76-7.78 (d, 2H), 7.32-7.34 (d, 2H), 5.75-5.88 (m, 1H), 5.28-5.31 (d, 1H), 5.24-5.22 (d, 1H), 4.50-4.51 (d, 2H), 2.43 (s, 3H) ppm.

S-(3-(tosyloxy)propyl) ethanethioate (ThioAcTos 6)

Allyl tosylate (**5**) from the above reaction (5.00 g, 23.6 mmol) was mixed with thioacetic acid (5.38 g, 70.7 mmol) and benzoin (0.100 g, 0.47 mmol). The mixture was flushed with N_2 and then irradiated for 1 h using a 36 W compact low-pressure fluorescent lamp (Philips CLEO Compact PL-L, λ_{max} = 355 nm). The product was dissolved in DCM and the mixture was washed with saturated $NaHCO_3$ and water, and dried over $MgSO_4$. After removal of the solvent, the product was purified by column chromatography (silica gel, EtOAc to cyclohexane). The initiator (**6**) was obtained as a pale yellow oil (5.3 g, 78%).

^{1}H NMR ($CDCl_3$, 500 MHz, δ): 7.77-7.79 (d, 2H), 7.34-7.36 (d, 2H), 4.06-4.08 (t, 2H), 2.85-2.88 (t, 2H), 2.45 (s, 3H), 2.29 (s, 3H), 1.89-1.95 (m, 2H) ppm.

^{13}C NMR ($CDCl_3$, 125 MHz, δ): 195.33, 144.76, 132.66, 129.75, 127.75, 68.50, 30.43, 28.77, 24.95, 21.51 ppm.

ESI-MS (*m/z*): [M-Na^+] calc.: 311.0383, found: 311.0378 amu.

S-(3-hydroxypropyl) ethanethioate (7)

Allyl alcohol (5.7 g, 98.1 mmol) and thioacetic acid (8.21 g, 107.9 mmol) were mixed with benzoin (0.417 g, 2 mmol) and stirred. The mixture was flushed with nitrogen and then irradiated for 1 h using a 36 W compact low-pressure fluorescent lamp (Philips CLEO Compact PL-L, λ_{max} = 355 nm). The product (**7**) was dissolved in DCM and the mixture was washed with saturated $NaHCO_3$ and water, and dried over $MgSO_4$. The excess solvent was removed under reduced pressure to obtain 10.7 g. (81% yield).

^{1}H NMR ($CDCl_3$, 500 MHz, δ): 3.61-3.63 (t, 2H), 2.96-2.98 (t, 3H), 2.33 (s, 3H), 1.77-1.82 (m, 2H) ppm.

S-(3-(((4-nitrophenyl)sulfonyl)oxy)propyl) ethanethioate (ThioAcNos 8)

In a 250 mL round-bottom flask compound **(7)** (3.62 g, 27.0 mmol) and DMAP (3.96 g, 32.4 mmol) were dissolved in DCM (40 mL). Subsequently, a solution of 4-nitrobenzenesulfonyl chloride (6 g, 27.0 mmol) in DCM (40 mL) was added dropwise at 0° C. After stirring for 2 h the reaction was quenched by adding cold water (60 mL) and DCM (60 mL) and stirred for 10 minutes. The mixture was washed with water (2x) and brine (2x). The remaining solvent was evaporated under reduced pressure. The product was precipitated in hexane and recrystallized from ethanol. (7.84 g, 74%)

^{1}H NMR ($CDCl_3$, 500 MHz, δ): 8.41-8.42 (d, 2H), 8.11-8.13 (d, 2H), 4.18-4.21 (t, 2H), 2.88-2.91 (t, 2H), 2.30 (s, 3H), 1.95-2.00 (m, 2H) ppm.

^{13}C NMR ($CDCl_3$, 125 MHz, δ): 194.95, 141.51, 129.09, 124.34, 69.58, 30.42, 28.81, 24.73 ppm.

ESI-MS (*m/z*): [M-Na^+] calc.: 342.0077, found: 342.0069 amu.

7.1.3. CROP of 2-oxazolines

CROP of EtOx using furan-protected maleimide initiators

The furan-protected maleimide initiators were dissolved in MeCN in glass vials at different monomer-to-initiator ratios ([M]/[I] = 20, 40, and 60) at a monomer concentration of 1.5 M. The vials were capped under inert conditions in a glove box. The capped vials were heated to 50 °C with constant stirring under inert atmosphere. Samples for GC and SEC analysis were taken periodically using a syringe, quenched by the addition of water, and injected without further purification in order to monitor kinetics and molar mass distributions. For further experiments, the polymerization was terminated by addition of tetramethylammonium hydroxide. After

evaporation of the solvent under reduced pressure and dissolving the residue in DCM, the polymer was precipitated in diethyl ether, centrifuged, separated, and dried under vacuum. The dry product was analyzed by DMAc SEC, ESI-MS, and ^{1}H NMR spectroscopy.

CROP of EtOx using thioacetate initiators

The thiol-containing initiators were dissolved in acetonitrile in microwave vials at different monomer-to-initiator ratios ([M]/[I] = 20, 40, and 60) and a monomer concentration of 4 M. The vials were crimped air-tight under inert conditions inside a glove box (Vigor Gas Purification Technologies). The capped vials were heated to 140 °C under microwave irradiation with constant stirring under inert atmosphere. For kinetic investigations of the polymerization, a stock solution of the polymerization mixture was prepared in a glovebox and divided into individual vials before transfer to the microwave reactor. After microwave irradiation the polymerization mixtures were cooled to ambient temperature and quenched by addition of water. Samples of the reaction mixture were taken for GC and DMAc SEC without further purification.

For further experiments, the polymerization was terminated through the addition of sodium carbonate and heated to 80 °C in a microwave for 12 h. After evaporation of the solvent under reduced pressure and dissolving the residue in DCM, the polymer was precipitated in diethyl ether, centrifuged, separated, and dried under vacuum. The dry product was analyzed by DMAc SEC, ESI-MS, and ^{1}H NMR spectroscopy.

7.1.4. Deprotection and modification of FurMal-PEtOx and ThioAc-PEtOx

Deprotection of the maleimide end group (Mal-PEtOx)

In a 25 mL round-bottom flask, 100 mg of a furan-protected maleimide end-functionalized polymer **FurMal-PEtOx** ($M_{n,SEC}$ = 6500 g mol^{-1}, $Đ$ = 1.20, $M_{n,NMR}$ = 4400 g mol^{-1}) were dissolved in toluene (10 mL). This solution was then heated to 110 °C for 4 h. After evaporation of the solvent under reduced pressure and dissolving the residue in DCM, the product was

precipitated in diethyl ether, centrifuged, separated, and dried under vacuum. The dry product **Mal-PEtOx** was analyzed by DMAc SEC, ESI-MS, and ^{1}H NMR spectroscopy.

Deprotection of the thioacetate end group (Thiol-PEtOx)

In a 25 mL round-bottom flask, 200 mg of a thiol end-functionalized polymer **ThioAc-PEtOx** ($M_{n,SEC}$ = 5800 g mol^{-1}, $Đ$ =1.09, $M_{n,NMR}$ = 4100 g mol^{-1}) was dissolved in methanol (5 mL). 0.8 mg (0.1 equivalent) of TBD was added and the mixture was then heated to 65 °C for 4 h. After evaporation of the solvent under reduced pressure and dissolving the residue in DCM, the product was precipitated in diethyl ether, centrifuged, separated, and dried under vacuum. The dry product **Thiol-PEtOx** was analyzed by DMAc SEC, ESI-MS, and ^{1}H NMR spectroscopy.

Model Michael addition of Mal-PEtOx with benzyl mercaptan

In a 25 mL round-bottom flask, deprotected **Mal-PEtOx** (30 mg) was dissolved in DCM (10 mL), then mixed with a 10-fold excess of benzyl mercaptan and 0.1 equivalent of triethylamine. The mixture was stirred overnight at room temperature. After evaporation of the solvent under reduced pressure and dissolving the residue in DCM, the product was precipitated in diethyl ether, centrifuged, separated, and dried under vacuum. The dry product was analyzed by ESI-MS, SEC, and ^{1}H NMR spectroscopy.

Model Michael addition of Thiol-PEtOx with butyl acrylate, acrylic acid *N*-hydroxysuccinimide ester, and furfuryl methacrylate

In a 25 mL round-bottom flask, **Thiol-PEtOx** (30 mg) was dissolved in acetone (10 mL), then mixed with a 3-fold excess of either butyl acrylate, acrylic acid *N*-hydroxysuccinimide ester, or furfuryl methacrylate, and 0.3 equivalent of DMPP. The mixture was stirred for 3 h at room temperature. After evaporation of the solvent under reduced pressure and dissolving the residue in DCM, the product was precipitated in diethyl ether, centrifuged, separated, and dried under vacuum. The dry product was analyzed by ESI-MS and DMAc SEC.

7.1.5. Bioconjugation of FurMal-PEtOx with BSA

Three solutions at different polymer-to-protein molar ratios were prepared (5, 10, and 15). A solution of 100 mM PBS was degassed by bubbling nitrogen for 30 min. 3 mL of oxygen-free water was transferred via a degassed syringe into a sealed vial equipped with a rubber septum, containing 40 mg of BSA and either 18.75, 37.5, or 56.5 mg of **MalPEtOx** ($M_{n,SEC}$ = 10600 g mol^{-1}, $Đ$ = 1.13, $M_{n,NMR}$ = 5500 g mol^{-1}) stored under a nitrogen atmosphere. After 18 h, several aliquots were taken for SDS-PAGE. For the sample with the polymer-to-protein ratio of 5:1, preparative FPLC was carried out and a relevant fraction was analyzed by MALDI-ToF mass spectrometry.

7.1.6. Surface modification procedures

Acrylate-modified surfaces

Silicon wafers (1 × 1 cm^2) were cleaned by 3 cycles of 15 min sonication with dichloromethane, acetone, and MilliQ water, in this order. Surfaces were then activated by immersion into acidic piranha solution (H_2SO_4:H_2O_2, 3:1) for 40 min at room temperature. Caution: piranha solution is an extremely strong oxidant and should be handled very carefully! After rinsing the substrates twice with MilliQ water, they were dried under a stream of N_2 and used immediately. Wafers were immersed in a 1% (v/v) solution of 3-(trimethoxysilyl)propyl acrylate in dry toluene and the reaction was carried out for 2 hours at 50 °C and then overnight at room temperature. Finally, surfaces were washed by rinsing sequentially 3 times with toluene, acetone, and MilliQ water solutions, and blow-dried with N_2. All these steps were followed and characterized by XPS.

Spotting setup

The patterning of **Thiol-PEtOx** was performed on a NLP 2000 system (NanoInk, USA) with oxygen plasma activated (0.2 mbar O_2, 2 min) SPT probes (SPT-S-C10S, BioForce Nanosciences, USA). The ink mixture was prepared by admixing 1 µl thiol-PEtOx solution (2.5 mg mL^{-1} in DMSO) with 0.2 µl of DMPP and 1 µl of glycerol. Glycerol was added to prevent the premature

drying of the ink on the SPT. Probes were filled with 0.4 µL ink, mounted onto the probe holder and used directly for spotting on acrylate-modified silicon wafers. Spotting was performed at 50% relative humidity. All patterning procedures were carried out with the sample stage tilted by 8° with respect to the SPT tip to minimize the probability of a contact between the ink reservoir and the sample surface. The pattern was done using a 30 µm spacing between dots. Unreactive material was removed The wafers were washed 3x with water and ethanol. Samples were analyzed by XPS.

7.2. Poly(2-ethyl-2-oxazoline) macromonomers for the synthesis of functional bottlebrush polymers

7.2.1. Materials and characterization techniques

Materials

Tetrahydrofuran (THF), ethyl vinyl ether, diethyl ether, acetonitrile, and trimethylamine, were purchased from commercial suppliers and used without further purification. Grubbs III bispyridyl initiator,[329] norbornene-hexanoic acid,[286] norbornene-hexanoic acid-alkyne,[194] chex nitroxide,[201] and cross-linker Acetal-XL[285] were provided and prepared according to literature procedures. Methyl tosylate and 2-ethyl-2-oxazoline were distilled over calcium anhydride.

Instrumentation

^{1}H and ^{13}C nuclear magnetic resonance (NMR) spectroscopy

The spectra were recorded on Bruker AVANCE-400 NMR spectrometer in the Department of Chemistry Instrumentation Facility at the Massachusetts Institute of Technology (MIT). All compounds were dissolved in $CDCl_3$ and the residual solvent peak was employed for shift correction (7.26 ppm).

Matrix-assisted laser desorption ionization mass spectrometry (MALDI-ToF MS)

The measurements were conducted on a Bruker model MicroFlex instrument using sinapic acid as matrix with NaTFA as dopant. In a typical experiment, 2.0 mg of polymer sample were dissolved in 500 μL of acetonitrile, then mixed with the matrix solution (1:2 vol/vol), and 1 μL was spotted on the MALDI plate for analysis.

Size exclusion chromatography (SEC)

Polymer molar masses and dispersity values were determined using DMAc, THF, or DMF as solvent. SEC with *N*,*N*-dimethylacetamide (DMAc) as eluent was performed with a sample concentration of 2 g L^{-1} on a Polymer Laboratories PL-GPC 50 Plus Integrated system comprising

an autosampler, a PLgel 2,5 µm bead-size guard column (50 × 7.5 mm) followed by three PLgel 5 µm MixedC columns (300 × 7.5 mm), and a flow rate of 1 mL min^{-1}. The SEC system was calibrated against linear poly(methyl methacrylate) standards with molar masses ranging from 700 to 2 × 10^6 Da. The samples were filtered through PTFE membranes with a pore size of 0.2 µm prior to injection. When tetrahydrofuran (THF) was the eluent, an HP series 1100 GPC system was used. Polystyrene standards were used for calibration and at a flow rate of 1.0 mL min^{-1}. DMF Size exclusion chromatography (SEC) analyses were performed on an Agilent 1260 Infinity setup with two Shodex KD-806M columns in tandem and a 0.025 M LiBr DMF mobile phase run at 60 °C. The differential refractive index (dRI) of each compound was monitored using a Wyatt Optilab T-rEX detector and the light scattering (LS) signal was acquired with a Wyatt Dawn Heleos-II detector. A differencial refractive index (*dn/dc*) of 0.0600 measured for PEtOx was used for the calculation of M_n and *Đ*.

Dynamic light scattering (DLS)

The measurements were performed using a Wyatt Technology Mobius DLS instrument. The sample solution was passed through a 0.4 µm Teflon syringe filter directly into the cuvette. Measurements were made in sets of 10 acquisitions and the average hydrodynamic diameters were calculated using the DLS correlation function via a regularization fitting method (Dynamics 7.3.1.15 software package from Wyatt Technology).

Preparative gel-permeation chromatography (prep-GPC)

Prep-GPC was performed on a JAI Preparative Recycling HPLC (LaboACE-LC-5060) system equipped with either 2.5HR and 2HR columns in series (20 mm ID x 600 mm length) using $CHCl_3$ as the eluent.

Relaxivity measurements by magnetic resonance imaging (MRI)

Phantom MRI data were acquired in a 12 cm outer diameter birdcage transceiver for imaging in a 20 cm bore Bruker 7 T Avance III MRI scanner. Samples at varying concentrations (0 up to 5 mM) in PBS buffer were loaded into the wells of a 384-well clear polystyrene plate (Thermo

Scientific Nunc), which had been pre-cut in half to optimally fit the coil. Unused wells were filled with PBS buffer. 2 mm slices were imaged through the samples with the field of view of 5 x 5 cm and the data matrices were 256 x 256 points. Longitudinal (r_1) and transverse (r_2) relaxivity measurements were acquired using multi-spin multi-echo (MSME) sequences (flip angle = 180°). r_1; TE = 12 ms, TR = 300, 350, 400, 450, 500, 600, 800, 1000, 1200, 1500, 3000, 5000, 10000 ms. r_2; TR = 5000 ms, TE = 12, 24, 36, 48, 60, 72, 84, 96, 108, 120, 132, 144, 156, 168, 280, 192, 204, 216, 228, 240, 252, 264, 276, 288, 300, 312, 324, 336, 348, 360 ms. Custom routines written in Matlab (Mathworks, Natick, MA) were used to reconstruct the images and compute relaxation time constants by fitting image intensity data to exponential decay curves.

Electron Paramagnetic Resonance (EPR)

Spectra were acquired at the University of Nebraska using a Bruker CW X-band spectrometer equipped with a frequency counter. The spectra were obtained using a dual mode cavity; all spectra were recorded using an oscillating magnetic field perpendicular (TE102) to the swept magnetic field. DPPH powder (g = 2.0037) was used as a g-value reference.

The reference for spin concentration was 0.50 mM Proxyl in phosphate-buffered saline (PBS) (pH 7.2). This reference was always stored in dry ice, except during measurements, and occasionally re-checked for spin concentration decay.

7.2.2. Synthesis of PEtOx macromonomers

Synthesis of norbornene-PEtOx macromonomers (PEtOx MM) and norbornene-branched-alkyne PEtOx macromonomers (Alkyne-PEtOx MM)

All polymerizations were performed in capped vials in a microwave reactor (Biotage) equipped with an infrared (IR) temperature sensor. Methyl tosylate was dissolved in acetonitrile in microwave vials at different monomer-to-initiator ratios ([M]/[I] = 15, 30, and 45) and a monomer concentration of 4 M. The vials were crimped air-tight under inert conditions inside a glove box. The capped vials were heated to 140 °C under microwave irradiation with constant

stirring under inert atmosphere. After microwave irradiation the polymerization was terminated through the addition of 1.5 equivalents of norbornene-hexanoic acid (or 2 equivalents of norbornene-hexanoic acid-branch-alkyne for **Alkyne-PEtOx MM**) and 2 equivalents of TEA. The mixture was stirred overnight. After evaporation of the solvent under reduced pressure and dissolving the residue in DCM, the polymer was precipitated in diethyl ether, centrifuged, separated, and dried under vacuum. The dry product was analyzed by SEC, MALDI-ToF MS, and ^{1}H NMR spectroscopy.

Synthesis of norbornene-branched-chex PEtOx macromonomers (chex-PEtOx MM)

Alkyne-PEtOx MM (114.4 mg, 1 eq) was added to a vial with bi-spirocyclohexylnitroxide-propyl-azide (14.6 mg, 1.1 eq) and 3 mL of dry DCM under N_2. A spatula tip of CuOAc was added. The mixture was stirred for 2 h. The entire reaction mixture was dried on a rotary evaporator, redissolved in $CHCl_3$ and cleaned using preparative GPC. The pure fractions containing **chex-PEtOx MM** were condensed with a rotary evaporator. The resulting residue was dried overnight and analyzed via MALDI-ToF MS, DMAc SEC, and ^{1}H NMR.

7.2.3. Formation of brush copolymers using PEtOx MM

All syntheses were performed in a glove box. **PEtOx MM** was added to a 2 mL vial containing a stir bar. THF was added to the vial followed by a freshly prepared solution of Ru catalyst G3 bispyridyl in THF (7 mg mL^{-1} THF, amount added to give desired **PEtOx MM**:**G3**) such that the total concentration of **PEtOx MM** was 0.05 M. For kinetic studies, samples were taken at established times, and ethyl vinyl ether (EVE) was added to quench the polymerization. To screen DPs, the reactions ran overnight and then were quenched with EVE. The resulting samples were analyzed by DMAc SEC.

7.2.4. Brush-arm star polymer (BASP) formation

Here is a representative procedure for BASP synthesis with brush length of 7.0 (m) and 20 equivalents (N) of cross-linker Acetal-XL (BASP, m = 7.07, N = 20). Polymers with other degrees of polymerization can be readily prepared by varying the crosslinker-to-initiator or macromonomer-to-initiator ratios. In a 2 mL vial, a suspension of acetal-XL (20.0 eq) in THF was prepared to afford a concentration of 0.1 M acetal-XL. To a second 2 mL vial containing a stir bar, either **PEtOx MM** or **chex-PEtOx MM** (7.0 eq) was added. In a third vial, a solution of Grubbs 3rd generation bispyridyl catalyst (**G3**, 7 mg/mL in THF) was freshly prepared. The corresponding amount of THF from vial 3 was then added to the **PEtOx MM** or **chex-PEtOx MM** vial, to give the desired MM:G3 ratio of 7:1 achieving a total MM concentration of 0.05 M. The reaction mixture was stirred for 30 min at room temperature before an aliquot (~5 μL) was taken out and quenched with 1 drop of ethyl vinyl ether for GPC analysis. The acetal-XL suspension was then added dropwise (in aliquots of 5 eq, or ~70 μL, every 5 minutes) over the course of 20 min into the MM vial, and the polymerizing mixture was allowed to stir overnight at room temperature. To quench the polymerization, a drop of ethyl vinyl ether was added. The reaction mixture was transferred to a 5kD molecular weight cutoff dialysis tubing (Spectrum Laboratories) in 10 mL nanopure water, and the solution was dialyzed against water (500 mL X 3, solvent exchange every 6 h). The resulting BASPs were analyzed by SEC and DLS.

7.3. PNAM and POEGMA conjugates as alternatives to protein PEGylation

7.3.1. Materials and instrumentation

Materials

N-acryloylmorpholine (Sigma, 97%), 1,4-dioxane (Sigma, 99%), dichloromethane (DCM; VWR), diethyl ether (99.5%, Roth), sinapic acid (Sigma, 98%), 2,2'-azobis(2-methylpropionitrile) (AIBN, Aldrich, 98%), 4-cyano-4-(phenylcarbonothioylthio)pentanoic acid *N*-succinimidyl ester (Aldrich), oligo(ethylene glycol) methyl ether methacrylate (OEGMA; M_n=300 g mol^{-1}, Sigma), *trans*-2-[3-(4-*tert*-butylphenyl)-2-methyl-2-propenylidene]malononitrile (DCTB, 99%), and acetonitrile (anhydrous, 99.8%, Sigma) were used as received. The used buffer substances were sodium citrate tribasic dihydrate (Sigma Aldrich) for pH 3, sodium acetate trihydrate (Sigma Aldrich) for pH 5, and sodium phosphate monobasic dihydrate (Sigma Aldrich) and disodium hydrogen phosphate dihydrate (Merck) for pH 7.

Instrumentation

^{1}H nuclear magnetic resonance (NMR) spectroscopy

Measurements were performed on a Bruker AM 500 spectrometer (500 MHz). All compounds were dissolved in $CDCl_3$ and the residual solvent peak was used for shift correction (7.26 ppm).

Matrix-assisted laser desorption ionization coupled to time-of-flight (MALDI-ToF) mass spectrometry

Mass spectra were acquired with a 4800 Proteomics Analyzer (Applied Biosystems, Foster City, CA, USA) in positive ion linear mode and a mass range of 1000 to 40000 Da. The laser intensity was set to 4800. The spectra obtained represent the average of laser shots taken by an automatic scheme measuring spectra over the whole spot. The matrices used were sinapic acid for conjugated proteins and DCTB for the polymer samples. Peak lists were generated using Data Explorer Software 4.0 (Applied Biosystems).

Size exclusion chromatography (SEC)

The measurements were performed on a TOSOH EcoSEC HLC-8320 GPC System, comprising an autosampler, a SDV 5 µm bead size guard column (50x8 mm, PSS) followed by three SDV 5 µmm columns (300x7.5 mm, subsequently 100 Å, 1000 Å and 10^5 Å pore size, (PSS)), and a differential refractive index (DRI) detector using THF as eluent at 30 °C with a flow rate of 1 mL/min. The SEC system was calibrated using linear polystyrene standards ranging from 266 to 252x10^6 g mol^{-1}. Before injection the samples were filtered using a 0.2 µm filter.

7.3.2. Polymer synthesis

RAFT polymerization of *N*-acryloylmorpholine

In a 250 mL round-bottom flask 4-cyano-4-(phenylcarbonothioylthio)pentanoic acid *N*-succinimidyl ester were mixed with AIBN (0.3 equivalents) and NAM (34 or 68 equivalents). Trioxane was used added to be used as reference. The mixture was then dissolved in 1,4-dioxane to a monomer final concentration of 1.6 M, and flushed with nitrogen for 30 minutes. The polymerization mixture was heated to 70 °C and monitored by ^{1}H NMR spectroscopy until the target conversion values (70%) were reached. The polymerization was stopped by cooling the reaction flask. After evaporation of the solvent under reduced pressure and dissolving the residue in DCM, the polymer was precipitated in diethyl ether, centrifuged, separated, and dried under vacuum. The dry product was analyzed by SEC, MALDI-ToF, and ^{1}H NMR spectroscopy.

RAFT Polymerization of oligo(ethylene glycol) methyl ether methacrylate

In a 250 mL round-bottom flask 4-cyano-4-(phenylcarbonothioylthio)pentanoic acid *N*-succinimidyl ester was mixed with AIBN (0.2 equivalents) and OEGMA (20 or 40 equivalents). The mixtures were dissolved in acetonitrile to a RAFT agent final concentration of 16 mM, and flushed with nitrogen for 30 minutes. The polymerization mixtures were then heated to 70 °C and monitored by ^{1}H NMR until the target conversion values (50%) were reached. The

polymerization was stopped by cooling the reaction flask. After evaporation of the solvent under reduced pressure and dissolving the residue in DCM, the polymers were precipitated in a 1:1 mixture of petroleum ether and diethyl ether, separated, and dried under vacuum. The dry products were analyzed by SEC, MALDI-ToF, and ^{1}H NMR spectroscopy.

7.3.3. Protein conjugation

Conjugation experiments were performed batch-wise in 50 mL Falcon Tubes (BD Biosciences). For conjugation, lysozyme and the respective polymer were dissolved in 25 mM sodium phosphate buffer at pH 7.2. The concentration of lysozyme was set to 0.28 mmol L^{-1}. PNAM and POEGMA were added based on a molar polymer-to-protein ratio of 2. For the reaction, the tube was continuously shaken in an overhead shaker (LabincoLD79, Labinco BV) for 1 h at room temperature.

7.3.4. Protein purification

The preparative separation of protein conjugates with varying numbers of attached polymer molecules was performed on an AKTA purifier system equipped with a fraction collector Frac-950 (GE Healthcare). As stationary phase, a 5 ml prepacked Toyopearl GigaCap S-650M cation exchange (CEX) column (TOSOH Bioscience) was used. For column loading, the system was equilibrated in 10 mM sodium acetate buffer (pH 5). In order to reduce the influence of unbound polymer on the binding behavior of the conjugates to the CEX resin, the conjugation batch was diluted 1:6 in 10 mM sodium acetate buffer (pH 5). Injection of the diluted batch was performed using a 50 mL super loop (GE Healthcare). Elution was performed by applying an NaCl step gradient with an elution buffer containing 1 M sodium chloride in 10 mM sodium acetate buffer (pH 5). The NaCl molarities used for the step elution of the different conjugates are displayed in **Table 12** in dependence of the attached polymer. The flow rate for equilibration, binding, and elution was set to 1 ml min^{-1}. To monitor the process, absorption at

wavelengths of 280 nm (for protein) and 320 nm (for polymer) as well as conductivity were detected continuously. From each chromatographic separation, fractions of 2 mL were collected into a 96-well plate (VWR, USA). To obtain sufficient sample for stability assessment of the different conjugate species, the corresponding fractions of multiple chromatographic runs were pooled. Peak allocation to the different conjugate species were performed by MALDI-ToF.

Table 12. NaCl eluent solution gradient (in mol L^{-1}) used for the elution of different conjugate species from Toyopearl GigaCap S-650M at pH 5 in dependency of the attached polymer

Polymer used	Native Lysozyme	Mono-conjugated lysozyme	Di-conjugated lysozyme
$PNAM_{3.5kDa}$	1	0.36	0.23
$PNAM_{7.5kDa}$	1	0.4	0.175
$POEGMA_{3.5kDa}$	1	0.37	0.19
$POEGMA_{7.5kDa}$	1	0.24	0.12

7.3.5. Conditioning and quantification of protein conjugates

The separation of protein-polymer conjugates led to fractions containing different NaCl concentrations. Characterizing the isolated conjugates with regard to activity and phase behavior thus required a sample conditioning consisting of buffer exchange (resp. pH change) and concentration increase. Buffer exchange was carried out using Slide-A-Lyzer™ Dialysis Cassettes (Thermo Fisher Scientific) with a molecular weight cut-off of 2 kDa. Concentrating of protein samples was performed by evaporation using a vacuum concentration unit RVC 2-33CDplus (Martin Christ Gefriertrocknungsanlagen GmbH) operated at 24 mbar. Concentrations of unmodified lysozyme were determined by measuring the absorption at 280 nm using a NanoDrop 2000c UV-Vis spectroscopic device (Thermo Fisher Scientific) and an extinction coefficient of $\varepsilon_{280nm,lyzozyme}^{1\%}$ = 22.00.[326] To convert mass concentrations into molar

concentrations, a molecular weight of lysozyme of 14.3 kDa was used.[330] Since the two polymers PNAM and POEGMA also absorb at 280 nm, the total absorption at 280 nm (A_{280nm}) is described for protein-polymer conjugates by:

$$A_{280nm} = A_{280nm,lysozyme} + A_{280nm,polymer}$$

In order to quantify the molar concentration of the protein-polymer conjugates, measurements solely at 280 nm are therefore not sufficient. For the quantification of protein-polymer conjugates, a method based on the differences in the spectra of protein and polymer was applied. At 320 nm, the two polymers absorb light due to the RAFT group,[331] while lysozyme does not. Thus, by measuring the absorption at 320 nm and comparing it to a calibration of polymer solutions, it is possible to quantify how much polymer is bound to a protein. For polymer calibration, absorption spectra between 240 nm and 340 nm were recorded for polymer solutions (in conjugation buffer) at 10 concentrations between 0.1 and 1.0 mg mL^{-1} using a NanoDrop 2000c UV-Vis spectroscopic device (Thermo Fisher Scientific) (**Figure 95**). Using the respective molar mass of the polymer, the mass concentrations were converted to molar concentrations.

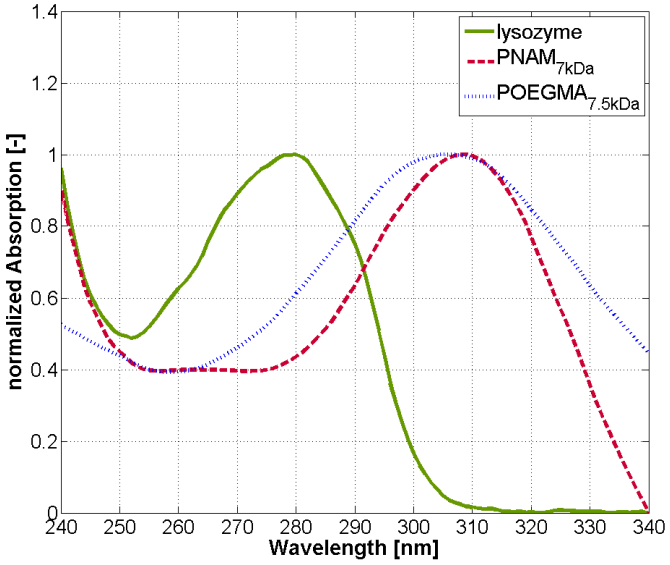

Figure 95. Absorption spectra of lysozyme, $PNAM_{7kDa}$, and $POEGMA_{7.5kDa}$ normalized to their absorption maximum.

From the recorded polymer spectra, the absorption values were extracted for 280 nm and 320 nm. By implementing the proportionality

$$K = A_{280nm,polymer}/A_{320nm,polymer}$$

it is possible to calculate the absorption $A_{280nm,lysozyme}$ as

$$A_{280nm,lysozyme} = A_{280nm} - K \cdot A_{320nm,polymer}$$

For the K value, the mean value of all K values of the 10 measured polymer concentrations was used. In order to convert the calculated absorption $A_{280nm,lysozyme}$ into a concentration, the extinction coefficient of $\varepsilon_{280nm,lyzozyme}^{1\%}$ = 22.00 was used as for unmodified lysozyme. All concentration measurements were performed as triplicates.

7.3.6. Stability assessment

Functional stability

In order to evaluate the residual activity of the protein-polymer conjugates after conjugation and separation, a *Micrococcus lysodeikticus*-based activity assay was performed according to Morgenstern et al.[305] The kinetic assay is based on the lysis of bacterial cells by the enzyme. The decrease in cell density results in a decrease in turbidity over time, which was monitored by measuring the absorbance at 450 nm. To allow a comparison for different conjugated species, the derived activities were normalized to the activity of native lysozyme.

Colloidal stability

Using a protocol reported by Baumgartner et al.,[323] a total of five protein phase diagrams for mono-PNAM$_{3.5kDa}$ylated lysozyme, di-PNAM$_{3.5kDa}$ylated lysozyme, mono-PNAM$_{7kDa}$ylated lysozyme, monoPOEGMA$_{3.5kDa}$ylated, and monoPOEGMA$_{7.5kDa}$ylated lysozyme, were generated on an automated liquid handling station (Freedom EVO®200 from Tecan). The pH value was adjusted to 3 using a buffer system of citric acid monohydrate (Merck) and sodium citrate

tribasic dihydrate (Sigma Aldrich, USA) and a total buffer capacity of 100 mM. The purified conjugated species were concentrated to 3.04 ± 0.07 mM (corresponds to 43.5 ± 1 mg mL^{-1} unmodified protein) and dialyzed into 100 mM citric buffer (pH 3) (= protein stock solution). Eight protein dilution steps between 0.35 and 3.04 mM were prepared by mixing protein stock solution and 100 mM citric buffer (pH 3) on a protein plate. As precipitant, sodium chloride was used. Twelve salt concentrations between 0 and 5 M were created. Binary phase diagrams were generated by mixing 12 µL of each diluted protein solution with 12 µL of each prepared salt concentration on a crystallization plate (Swissci) resulting in 96 batch systems with varying composition. As a result, the protein concentrations varied from 0.17 to 1.52 mM and the salt concentrations from 0 M to 2.5 M. Evaluation of phase states was conducted based on photographs taken by the Rock Imager 182/54 automated imaging system (Formulatrix). In order to determine solubility lines, the protein concentration in the supernatant of batch systems where a phase transition occurred was determined after 40 days using a NanoDrop 2000c UV–Vis spectroscopic device.

Bibliography

(1) Nair, L. S.; Laurencin, C. T. *Prog. Polym. Sci.* **2007**, *32*, 762–798.

(2) Teo, A. J. T.; Mishra, A.; Park, I.; Kim, Y.-J.; Park, W.-T.; Yoon, Y.-J. *ACS Biomater. Sci. Eng.* **2016**, *2*, 454–472.

(3) Duncan, R. *Nat. Rev.* **2003**, *2*, 347–360.

(4) Turecek, P. L.; Bossard, M. J.; Schoetens, F.; Ivens, I. A. *J. Pharm. Sci.* **2016**, *105*, 460–475.

(5) Soo, J.; Xu, Q.; Kim, N.; Hanes, J.; Ensign, L. M. *Adv. Drug Deliv. Rev.* **2016**, *99*, 28–51.

(6) Roberts, M. J.; Bentley, M. D.; Harris, J. M. *Adv. Drug Deliv. Rev.* **2012**, *64*, 116–127.

(7) David, P.; Morbidelli, M. *J. Control. Release* **2014**, *180*, 134–149.

(8) Kolate, A.; Baradia, D.; Patil, S.; Vhora, I.; Kore, G.; Misra, A. *J. Control. Release* **2014**, *192*, 67–81.

(9) Wenande, E.; Garvey, L. H. *Clin. Exp. Allergy* **2016**, *46*, 907–922.

(10) Schellekens, H.; Hennink, W. E.; Brinks, V. *Pharm. Res.* **2013**, *30*, 1729–1734.

(11) Garay, R. P.; El-Gewely, R.; Armstrong, J. K.; Garratty, G.; Richette, P. *Expert Opin. Drug Deliv.* **2012**, *9*, 1319–1323.

(12) Richter, A. W.; Åkerblom, E. *Int. Arch. Allergy Immunol.* **1984**, *74*, 36–39.

(13) Qi, Y.; Chilkoti, A. *Curr. Opin. Chem. Biol.* **2015**, *28*, 181–193.

(14) Conover, C.; Lejeune, L.; Linberg, R.; Shum, K.; Shorr, R. G. L. *Artif. Cells. Blood Substit. Immobil. Biotechnol.* **1996**, *24*, 599–611.

(15) Murdock, N.; Weissig, W.; Pettinger, T. K. *Int. J. Nanomedicine* **2014**, *9*, 4357–4373.

(16) Broyer, R. M.; Grover, G. N.; Maynard, H. D. *Chem. Commun.* **2011**, *47*, 2212.

(17) Shipp, D. A. *Polym. Rev.* **2011**, *51*, 99–103.

(18) Moad, G.; Rizzardo, E.; Thang, S. H. *Acc. Chem. Res.* **2008**, *41*, 1133–1142.

(19) Matyjaszewski, K. *Macromolecules* **2012**, *45*, 4015–4039.

(20) Moad, G.; Rizzardo, E.; Thang, S. H. *Aust. J. Chem* **2005**, *58*, 379–410.

(21) Li, C. *Adv. Drug Deliv. Rev.* **2002**, *54*, 695–713.

(22) Qi, Y.; Amiram, M.; Gao, W.; McCafferty, D. G.; Chilkoti, A. *Macromol. Rapid Commun.* **2013**, *34*, 1256–1260.

(23) Bontempo, D.; Maynard, H. D. *J. Am. Chem. Soc.* **2005**, *127*, 6508–6509.

(24) Yu, S. H.; Hu, J.; Ercole, F.; Truong, N. P.; Davis, T. P.; Whittaker, M. R.; Quinn, J. F. *ACS Macro Lett.* **2015**, *4*, 1278–1282.

(25) Gorman, M.; Chim, Y. H.; Hart, A.; Riehle, M. O.; Urquhart, A. J. *J. Biomed. Mater. Res. A* **2013**, *102*, 1809–1815.

(26) Kainthan, R. K.; Janzen, J.; Levin, E.; Devine, D. V; Brooks, D. E. *Biomacromolecules* **2006**, *7*, 703–709.

(27) Kopec, P.; Minko, T.; Lu, Z. *Eur. J. Pharm. Biopharm.* **2000**, *50*, 61–81.

(28) Souza, A. J. M. D.; Schowen, R. L.; Topp, E. M. *J. Control. Release* **2004**, *94*, 91–100.

(29) De La Rosa, V. R. *J. Mater. Sci. Mater. Med.* **2014**, *25*, 1211–1225.

(30) Tomalia, D. A.; Sheetz, D. P. *J. Polym. Sci. A Polym. Chem.* **1966**, *4*, 2253–2265.

(31) Levy, A.; Litt, M. *Polym. Lett.* **1967**, *5*, 871–879.

(32) Seeliger, W.; Aufderhaar, E.; Diepers, W.; Feinauer, R.; Nehring, R.; Thier, W.; Hellmann,

H. *Angew. Chem. Int. Ed.* **1966**, *5*, 875–888.

(33) Kagiya, T.; Maeda, T.; Fukui, K.; Narisawa, S. *Polym. Lett.* **1966**, *4*, 441–445.

(34) Adams, N.; Schubert, U. S. *Adv. Drug Deliv. Rev.* **2007**, *59*, 1504–1520.

(35) Rossegger, E.; Schenk, V.; Wiesbrock, F. *Polymers.* **2013**, *5*, 956–1011.

(36) Verbraeken, B.; Monnery, B. D.; Lava, K.; Hoogenboom, R. *Eur. Polym. J.* **2016**, *88*, 451–469.

(37) Lava, K.; Verbraeken, B.; Hoogenboom, R. *Eur. Polym. J.* **2015**, *65*, 98–111.

(38) Langer, R.; Tirrell, D. A. *Nature* **2004**, *428*, 487–492.

(39) Lutz, J.-F.; Bo, H. G.; Weichenhan, K. *Macromolecules* **2006**, *39*, 6376–6383.

(40) Maeda, H.; Bharate, G. Y.; Daruwalla, J. *Eur. J. Pharm. Biopharm.* **2009**, *71*, 409–419.

(41) Zalipsky, S. *Bioconjug. Chem.* **2000**, *4*, 296–299.

(42) Troiber, C.; Wagner, E. *Bioconjug. Chem.* **2011**, *22*, 1737–1752.

(43) Viegas, T. X.; Bentley, M. D.; Harris, J. M.; Fang, Z.; Yoon, K.; Dizman, B.; Weimer, R.; Mero, A.; Pasut, G.; Veronese, F. M. *Bioconjug. Chem.* **2011**, *22*, 976–986.

(44) Salmaso, S.; Caliceti, P. *J. Drug Deliv.* **2013**, *19*, 1–19.

(45) Torchilin, V. P.; Trubetskoy, V. S. *Adv. Drug Deliv. Rev.* **1995**, *16*, 141–155.

(46) Pasut, G.; Veronese, F. M. *Adv. Drug Deliv. Rev.* **2009**, *61*, 1177–1188.

(47) Knop, K.; Hoogenboom, R.; Fischer, D.; Schubert, U. S. *Angew. Chemie - Int. Ed.* **2010**, *49*, 6288–6308.

(48) Veronese, F. M.; Pasut, G. *Drug Discov. Today* **2005**, *10*, 1451–1458.

(49) Tong, R.; Gabrielson, N. P.; Fan, T. M.; Cheng, J. *Curr. Opin. Solid State Mater. Sci.* **2013**, *16*, 323–332.

(50) Zhang, T.; She, Z.; Huang, Z.; Li, J.; Luo, X.; Deng, Y. *Asian J. Pharm. Sci.* **2014**, *9*, 75–81.

(51) Veronese, F. M. *Biomaterials* **2001**, *22*, 405–417.

(52) Abuchowski, A.; Mccoy, J. R.; Palczuk, N. C.; Es, T. V. A. N.; Davis, F. F. *J. Biol. Chem.* **1977**, *252*, 3582–3586.

(53) Biondi, O.; Motta, S.; Mosesso, P. *Mutagenesis* **2002**, *17*, 261–264.

(54) Alconcel, S.; Baas, A.; Maynard, H. D. *Polym. Chem.* **2011**, *2*, 1442–1448.

(55) Mosbah, I. B.; Abdennebi, H. B.; Hernandez, R.; Escolar, G.; Saidane, D.; Peralta, C. *Transplant. Proc.* **2006**, *38*, 1229–1235.

(56) Convergence, F.; Labaratory, T.; Hospital, A. *J. Bioact. Compat. Polym.* **2009**, *24*, 316–328.

(57) Yu, J.; Xu, X.; Yao, F.; Luo, Z.; Jin, L.; Xie, B.; Shi, S. *Int. J. Pharm.* **2014**, *470*, 151–157.

(58) Jun-ichi Tsuji; Katsumi Hirose; Etsuko Kasahara; Maki Naitoh; Itary Yamamoto. *Int. J. Immunopharmacol.* **1985**, *7*, 725–730.

(59) Fox, M. E.; Szoka, F. C.; Frechet, J. M. J. *Acc. Chem. Res.* **2009**, *42*, 1141–1151.

(60) Herold, D. A.; Keil, K.; Bruns, D. E. *Biochem. Pharmacol.* **1989**, *38*, 73–76.

(61) Obst, M.; Steinbu, A. *Biomacromolecules* **2004**, *5*, 1166–1176.

(62) Cavallaro, G.; Craparo, E. F.; Sardo, C.; Lamberti, G.; Barba, A. A.; Dalmoro, A. *Int. J. Pharm.* **2015**, *495*, 719–727.

(63) Metselaar, J. M.; Bruin, P.; De Boer, L. W. T.; De Vringer, T.; Snel, C.; Oussoren, C.; Wauben, M. H. M.; Crommelin, D. J. A.; Storm, G.; Hennink, W. E. *Bioconjug. Chem.* **2003**, *14*, 1156–1164.

(64) Birke, A.; Ling, J.; Barz, M. *Prog. Polym. Sci.* **2018**, 1–46.

(65) Pytela, J.; J, S. *J. Control. Release* **1989**, *10*, 17–25.

(66) Romberg, B.; Metselaar, J. M.; Baranyi, L.; Snel, C. J.; Rolf, B.; Hennink, W. E.; Szebeni, J.; Storm, G. *Int. J. Pharm.* **2007**, *331*, 186–189.

(67) Li, C.; Wallace, S. *Adv. Drug Deliv. Rev.* **2008**, *60*, 886–898.

(68) Gao, W.; Liu, W.; Mackay, J. A.; Zalutsky, M. R.; Toone, E. J.; Chilkoti, A. *PNAS* **2009**, *106*, 15231–15236.

(69) Gao, W.; Liu, W.; Christensen, T.; Zalutsky, M. R.; Chilkoti, A. *PNAS* **2010**, *107*, 16432–16437.

(70) Jiang, S.; Cao, Z. *Adv. Mater.* **2010**, *22*, 920–932.

(71) Kane, R. S.; Deschatelets, P.; Whitesides, G. M. *Langmuir* **2003**, *19*, 2388–2391.

(72) Keefe, A. J.; Jiang, S. *Nat. Chem.* **2012**, *4*, 59–63.

(73) Imran, M.; Lai, B. F. L.; Kizhakkedathu, J. N. *Biomaterials* **2012**, *33*, 9135–9147.

(74) Harth, E.; Spears, B. R.; Waksal, J.; Mcquade, C.; Lanier, L.; Harth, E. *Chem. Commun.* **2013**, *49*, 2394–2396.

(75) Wurm, F.; Dingels, C.; Frey, H.; Klok, H. *Biomacromolecules* **2012**, *13*, 1161–1171.

(76) Khandare, J.; Minko, T. *Prog. Polym. Sci.* **2006**, *31*, 359–397.

(77) Scales, C. W.; Vasilieva, Y. A.; Convertine, A. J.; Lowe, A. B.; Mccormick, C. L. *Biomacromolecules* **2005**, *6*, 1846–1850.

(78) Veronese, F. M.; Schiavon, O.; Caliceti, P.; Sartore, L.; Ranucci, E.; Ferruti, P. Google Patents 1997.

(79) Veronese, F. M.; Schiavon, O.; Sartore, L.; Ranucci, E.; Ferruti, P. Polymers of N-acryloyl morpholine activated at one end and conjugates with bioactive materials and surfaces. 5,629,384, 2000.

(80) Torchilin, V. P. *J. Microencapsul.* **2008**, *15*, 1–19.

(81) Ray, B.; Kotani, M.; Yamago, S. *Macromolecules* **2006**, *39*, 5259–5265.

(82) Schiavon, O.; Veronese, F. M. *J. Bioact. Compat. Polym.* **1995**, *10*, 103–120.

(83) Sedlacek, O.; Monnery, B. D.; Mattova, J.; Kucka, J.; Panek, J.; Janouskova, O.; Hocherl, A.; Verbraeken, B.; Vergaelen, M.; Zadinova, M.; Hoogenboom, R.; Hruby, M. *Biomaterials* **2017**, *146*, 1–12.

(84) Hoogenboom, R. *Angew. Chem. Int. Ed.* **2009**, *48*, 7978–7994.

(85) Luxenhofer, R.; Han, Y.; Schulz, A.; Tong, J.; He, Z.; Kabanov, A. V.; Jordan, R. *Macromol. Rapid Commun.* **2012**, *33*, 1613–1631.

(86) Hoogenboom, R.; Schlaad, H. *Polym. Chem.* **2017**, *8*, 24–40.

(87) Weber, C.; Hoogenboom, R.; Schubert, U. S. *Prog. Polym. Sci.* **2012**, *37*, 686–714.

(88) Bauer, M.; Lautenschlaeger, C.; Kempe, K.; Tauhardt, L.; Schubert, U. S.; Fischer, D. *Macromol. Biosci.* **2012**, *12*, 986–998.

(89) Konradi, R.; Acikgoz, C.; Textor, M. *Macromol. Rapid Commun.* **2012**, *33*, 1663–1676.

(90) Konradi, R.; Pidhatika, B.; Mühlebach, A.; Textor, M. *Langmuir* **2008**, *24*, 613–616.

(91) Webster, O. W. *Science (80-.).* **1991**, *251*, 887–893.

(92) Guillerm, B.; Monge, S.; Lapinte, V.; Robin, J. J. *Macromol. Rapid Commun.* **2012**, *33*, 1600–1612.

(93) Glassner, M.; D'Hooge, D. R.; Park, J. Y.; Van Steenberge, P. H. M.; Monnery, B. D.;

Reyniers, M.-F.; Hoogenboom, R. *Eur. Polym. J.* **2015**, *65*, 298–304.

(94) Saegusa, T.; Ikeda, H. *Macromolecules* **1973**, *6*, 808–811.

(95) Hoogenboom, R.; Paulus, R. M.; Fijten, M. W. M.; Schubert, U. S. *J. Polym. Sci. Part A Polym. Chem.* **2005**, *43*, 1487–1497.

(96) Hoogenboom, R.; Schubert, U. S.; Fijten, M. W. M. *J. Polym. Sci. Part A Polym. Chem.* **2008**, *46*, 4804–4816.

(97) Wiesbrock, F.; Hoogenboom, R.; Leenen, M. A. M.; Meier, M. A. R.; Schubert, U. S. *Macromolecules* **2005**, *38*, 5025–5034.

(98) Hoogenboom, R.; Fijten, M. W. M.; Paulus, R. M.; Thijs, H. M. L.; Hoeppener, S.; Kickelbick, G.; Schubert, U. S. *Polymer (Guildf).* **2006**, *47*, 75–84.

(99) Baeten, E.; Verbraeken, B.; Hoogenboom, R.; Junkers, T. *Chem. Commun.* **2015**, *51*, 11701–11704.

(100) Litt, M.; Levy, A.; Herz, J. *J. Macromol. Sci. Part A - Chem.* **1975**, *9*, 703–727.

(101) Warakomski, J. M.; Thill, B. P. *J. Polym. Sci. A Polym. Chem.* **1990**, *28*, 3551–3563.

(102) Nuyken, O.; Maier, G.; Groß, A.; Fischer, H. *Macromol. Chem. Phys.* **1996**, *197*, 83–95.

(103) de la Rosa, V. R.; Tempelaar, S.; Dubois, P.; Hoogenboom, R.; Mespouille, L. *Polym. Chem* **2016**, *7*, 1559–1568.

(104) Kobayashi, S.; Masuda, E.; Shoda, S. ichiro; Shimano, Y. *Macromolecules* **1989**, *22*, 2878–2884.

(105) Okada, M.; Aoi, K. *Prog. Polym. Sci.* **1996**, *21*, 151–208.

(106) Park, J. S.; Akiyama, Y.; Winnik, F. M.; Kataoka, K. *Macromolecules* **2004**, *37*, 6786–6792.

(107) Volet, G.; Lav, T. X.; Babinot, J.; Amiel, C. *Macromol. Chem. Phys.* **2011**, *212*, 118–124.

(108) Volet, G.; Deschamps, A.-C.; Amiel, C. *Am. Chem. Soc. Polym. Prepr. Div. Polym. Chem.* **2008**, *49*, 2247–2485.

(109) Cesana, S.; Auernheimer, J.; Jordan, R.; Kessler, H.; Nuyken, O. *Macromol. Chem. Phys.* **2006**, *207*, 183–192.

(110) Chujc, Y.; Ihara, E.; Ihara, H.; Saegusa, T. *Macromolecules* **1989**, *22*, 2040–2043.

(111) Hoogenboom, R.; Fijten, M. W. M.; Meier, M. A. R.; Schubert, U. S. *Macromol. Rapid Commun.* **2003**, *24*, 92–97.

(112) Luxenhofer, R.; Jordan, R. *Macromolecules* **2006**, *39*, 3509–3516.

(113) Cirpan, A.; Alkan, S.; Toppare, L.; David, G.; Yagci, Y. *Eur. Polym. J.* **2001**, *37*, 2225–2229.

(114) David, G.; Alupei, V.; Simionescu, B. C. *Eur. Polym. J.* **2001**, *37*, 1353–1358.

(115) Woodle, M. C.; Engbers, C. M.; Zalipsky, S. *Bioconjug. Chem.* **1994**, *5*, 493–496.

(116) David, G.; Ioanid, A. *J. Appl. Polym. Sci.* **2001**, *80*, 2191–2199.

(117) Weber, C.; Krieg, A.; Paulus, R. M.; Lambermont-Thijs, H. M. L.; Becer, C. R.; Hoogenboom, R.; Schubert, U. S. *Macromol. Symp.* **2011**, *308*, 17–24.

(118) Miyamoto, M.; Naka, K.; Tokumizu, M.; Saegusa, T. *Macromolecules* **1989**, *22*, 1604–1607.

(119) Mero, A.; Fang, Z.; Pasut, G.; Veronese, F. M.; Viegas, T. X. *J. Control. Release* **2012**, *159*, 353–361.

(120) Kobayashi, S.; Uyama, H.; Narita, Y. *Macromolecules* **1990**, *23*, 353–354.

(121) Fijten, M. W. M.; Haensch, C.; van Lankvelt, B. M.; Hoogenboom, R.; Schubert, U. S. *Macromol. Chem. Phys.* **2008**, *209*, 1887–1895.

(122) Guillerm, B.; Darcos, V.; Lapinte, V.; Monge, S.; Coudane, J.; Robin, J.-J. *Chem. Commun.*

2012, *48* (23), 2879.

(123) Obeid, R.; Scholz, C. *Biomacromolecules* **2011**, *12*, 3797–3804.

(124) Reif, M.; Jordan, R. *Macromol. Chem. Phys.* **2011**, *212*, 1815–1824.

(125) England, R. M.; Hare, J. I.; Kemmitt, P. D.; Treacher, K. E.; Waring, M. J.; Barry, S. T.; Alexander, C.; Ashford, M. *Polym. Chem.* **2016**, *7*, 4609–4617.

(126) Fik, C. P.; Krumm, C.; Muennig, C.; Baur, T. I.; Salz, U.; Bock, T.; Tiller, J. C. *Biomacromolecules* **2012**, *13*, 165–172.

(127) Yu, Y. C.; Cho, H. S.; Yu, W. R.; Youk, J. H. *Polymer.* **2014**, *55*, 5986–5990.

(128) Hoogenboom, R.; Fijten, M. W. M.; Kickelbick, G.; Schubert, U. S. *Beilstein J. Org. Chem.* **2010**, *6*, 773–783.

(129) Hoogenboom, R.; Thijs, H. M. L.; Wouters, D.; Hoeppener, S.; Schubert, U. S. *Soft Matter* **2008**, *4*, 103–107.

(130) Diab, C.; Akiyama, Y.; Kataoka, K.; Winnik, F. M. *Macromolecules* **2004**, *37*, 2556–2562.

(131) Demirel, A. L.; Meyer, M.; Schlaad, H. *Angew. Chemie - Int. Ed.* **2007**, *46*, 8622–8624.

(132) Uyama, H.; Kobayashi, S. *Chemistry Letters*. 1992, pp 1643–1646.

(133) Meyer, M.; Antonietti, M.; Schlaad, H. *Soft Matter* **2007**, *3*, 430.

(134) Christova, D.; Velichkova, R.; Loos, W.; Goethals, E. J.; Du Prez, F. *Polymer.* **2003**, *44*, 2255–2261.

(135) Hoogenboom, R.; Thijs, H. M. L.; Jochems, M. J. H. C.; Lankvelt, B. M. Van; Fijten, W. M.; Schubert, U. S. *Chem. Commun.* **2008**, 5758–5760.

(136) Park, J.; Kataoka, K. *Macromolecules* **2007**, *40*, 3599–3609.

(137) Weber, C.; Neuwirth, T.; Kempe, K.; Ozkahraman, B.; Tamahkar, E.; Mert, H.; Becer, C. R.; Schubert, U. S. *Macromolecules* **2012**, *45*, 20–27.

(138) Del Rio, E.; Lligadas, G.; Ronda, J. C.; Galia, M.; Cadiz, V. *J. Polym. Sci. Part A Polym. Chem.* **2011**, *49*, 3069–3079.

(139) Hoogenboom, R.; Schubert, U. S. *Green Chem.* **2006**, *8*, 895.

(140) Bloksma, M. M.; Weber, C.; Perevyazko, I. Y.; Kuse, A.; Baumgärtel, A.; Vollrath, A.; Hoogenboom, R.; Schubert, U. S. *Macromolecules* **2011**, *44*, 4057–4064.

(141) Cesana, S.; Kurek, A.; Baur, M. A.; Auernheimer, J.; Nuyken, O. *Macromol. Rapid Commun.* **2007**, *28*, 608–615.

(142) Lobert, M.; Thijs, H. M. L.; Erdmenger, T.; Eckardt, R.; Ulbricht, C.; Hoogenboom, R.; Schubert, U. S. *Chem. - A Eur. J.* **2008**, *14*, 10396–10407.

(143) Kempe, K.; Hoogenboom, R.; Schubert, U. S.; Lobert, M. *J. Polym. Sci. Part A Polym. Chem.* **2009**, *47*, 3829–3838.

(144) Lüdtke, K.; Jordan, R.; Hommes, P.; Nuyken, O.; Naumann, C. A. *Macromol. Biosci.* **2005**, *5*, 384–393.

(145) Miyamoto, M.; Aoi, K.; Saegusa, T. *J. Polym. Sci. Part A Polym. Chem.* **1997**, *35*, 933–945.

(146) Miyamoto, M.; Shimakura, M.; Tsutsui, K.; Hasegawa, K.; Aoi, K.; Yamaga, S.; Saegusa, T. *Macromolecules* **1993**, *26*, 7116–7124.

(147) Levy A,Bassiri, L.; Bassiri, L.; Levy, A.; Litt, M. *J.Polym.Sci.PartB:Polym.Lett* **1968**, *5*, 2253–2265.

(148) Kempe, K. *J. Comb. Chem. Chem.* **2009**, *11*, 274–280.

(149) Glaied, O.; Delaite, C.; Hurtrez, G.; Joubert, M.; Dumas, P. *J. Polym. Sci. Part A Polym. Chem.* **2005**, *43*, 2440–2447.

(150) Hochwimmer, G.; Nuyken, O.; Schubert, U. S. *Macromol. Rapid Commun.* **1998**, *19*, 309–313.

(151) Mees, M. A.; Hoogenboom, R. *Macromolecules* **2015**, *48*, 3531–3538.

(152) Foertig, A.; Jordan, R.; Graf, K.; Tanaka, M. *Macromol. Symp.* **2004**, *210*, 329–338.

(153) Chujo, Y.; Saegusa, T. *Macromolecules* **1993**, *26*, 5681–5686.

(154) Kempe, K.; Killops, K. L.; Poelma, J. E.; Jung, H.; Bang, J.; Hoogenboom, R.; Tran, H.; Hawker, C. J.; Schubert, U. S.; Campos, L. M. *ACS Macro Lett.* **2013**, *2*, 267–682.

(155) Voit, B.; Shevtsova, G.; Rueda, J. C.; Komber, H. *Macromol. Chem. Phys.* **2003**, *204*, 947–953.

(156) Christova, D.; Velichkova, R.; Goethals, E. J. *Macromol. Rapid Commun.* **1997**, *18*, 1067–1073.

(157) Velander, W. H.; Madurawe, R. D.; Subramanian, A.; Kumar, G.; Sinai-Zingde, G.; Riffle, J. S.; Orthner, C. L. *Biotechnol. Bioeng.* **1992**, *39*, 1024–1030.

(158) Li, J.; Zhou, Y.; Li, C.; Wang, D.; Gao, Y.; Zhang, C.; Zhao, L.; Li, Y.; Liu, Y.; Li, X. *Bioconjug. Chem.* **2015**, *26*, 110–119.

(159) Gao, Y.; Li, Y.; Li, Y.; Yuan, L.; Zhou, Y.; Li, J.; Zhao, L.; Zhang, C.; Li, X.; Liu, Y. *Nanoscale* **2015**, *7*, 597–612.

(160) Canal, F.; Sanchis, J.; Vicent, M. J. *Curr. Opin. Biotechnol.* **2011**, *22*, 894–900.

(161) Krishnan, S.; Weinman, C. J.; Ober, C. K. *J. Mater. Chem.* **2008**, *18*, 3405.

(162) Wang, H.; Li, L.; Tong, Q.; Yan, M. *ACS Appl. Mater. Interfaces* **2011**, *3*, 3463–3471.

(163) William, A.; Merck, N. G. M. United States Patent 2,721,189, 1955.

(164) Press, P.; Britdn, G. *Tetrahedron Lett.* **1967**, *34*, 3327–3329.

(165) Schrock, R. R. *Angew. Chem. Int. Ed.* **2006**, *45*, 3748–3759.

(166) Grubbs, R. H. *Angew. Chem. Int. Ed.* **2006**, *45*, 3760–3765.

(167) Sutthasupa, S.; Shiotsuki, M.; Sanda, F. *Polym. J.* **2010**, *42*, 905–915.

(168) Calderon, B. N.; Ofstead, E. A. *Angew. Chem. Int. Ed.* **1976**, *15*, 401–409.

(169) Chauvin, Y.; Herisson, J.-L. *Makromol. Chemie* **1970**, *141*, 161–176.

(170) Bielawski, C. W.; Grubbs, R. H. *Prog. Polym. Sci.* **2007**, *32*, 1–29.

(171) Vougiokalakis, G. C.; Grubbs, R. H. *Chem. Rev.* **2010**, *110*, 1746–1787.

(172) Rodgers, A. S.; Shaw, R.; Walsh, R. *Chem. Rev.* **1969**, *69*, 279–324.

(173) Matyjaszewski, K. *Macromolecules* **1993**, *26*, 1787–1788.

(174) Truett, W. L.; Johnson, D. R.; Robindon, I. M.; Montague, B. A. *J. Am. Chem. Soc.* **1960**, *82*, 2337–2340.

(175) Dall'Asta, G.; Mazzanti, G.; Natta, G.; Porri, L. *Macromol. Chem. Phys.* **1962**, *56*, 224–227.

(176) Calderon, N.; Ofstead, E. A.; Judy, W. A. *J. Polym. Sci. Part A Polym. Chem.* **1967**, *5*, 2209–2217.

(177) Trnka, T. M.; Grubbs, R. H. *Acc. Chem. Res.* **2001**, *34*, 18–29.

(178) Grubbs, R. H.; Gilliom, L. R. *J. Am. Chem. Soc.* **1986**, *108*, 733–742.

(179) Risse, W.; Wheeler, D. R.; Cannizzo, L. F.; Grubbs, R. H. *Macromolecules* **1989**, *22*, 3205–3210.

(180) Cannizzo, L. F.; Grubbs, R. H. *Macromolecules* **1988**, *21*, 1961–1967.

(181) Wallace, K. C.; Liu, A. H.; Dewan, J. C.; Schrock, R. R. *J. Am. Chem. Soc.* **1988**, *110*, 4964–4977.

(182) Wallace, K. C.; Schrock, R. R. *Macromolecules* **1987**, *20*, 448–450.

(183) Schrock, R. R.; Feldman, J.; Cannizzo, L. F.; Grubbs, R. H. *Macromolecules* **1987**, *20*, 1169–1172.

(184) Donoghue, M. B. O.; Schrock, R. R.; Lapointe, A. M.; Davis, W. M. *Organometallics* **1996**, *15*, 1334–1336.

(185) Schrock, R. R.; Murdzek, J. S.; Bazan, G. C.; Robbins, J.; Dimare, M.; Regan, M. O. *J. Am. Chem. Soc.* **1990**, *112*, 3875–3886.

(186) Khosravi, E.; Al-hajaji, A. A. *Polymer.* **1998**, *39*, 5619–5625.

(187) Trzaska, S. T.; Lee, L. W.; Register, R. A. *Macromolecules* **2000**, *33*, 9215–9221.

(188) Perrott, M. G.; Novak, B. M. *Macromolecules* **1995**, *28*, 3492–3494.

(189) Wu, Z.; Benedicto, A. D.; Grubb. *Macromolecules* **1993**, *26*, 4975–4977.

(190) Beckman, M.; Ziller, J. W. *J. Am. Chem. Soc.* **1993**, *115*, 9858–9859.

(191) Leitgeb, A.; Wappel, J.; Slugovc, C. *Polymer.* **2010**, *51*, 2927–2946.

(192) Moerdyk, J. P.; Bielawski, C. W. *Architectures of Polymers Synthesized using ROMP*; Elsevier B.V., 2012; Vol. 4.

(193) Kiessling, L. L.; Mangold, S. L. *Current and Forthcoming Applications of ROMP Polymers - Biorelated Polymers*; Elsevier B.V., 2012; Vol. 4.

(194) Johnson, J. A.; Lu, Y. Y.; Burts, A. O.; Xia, Y.; Durrell, A. C.; Tirrell, D. A.; Grubbs, R. H. *Macromolecules* **2010**, *43*, 10326–10335.

(195) Lienkamp, K.; Madkour, A. E.; Musante, A.; Nelson, C. F.; Nüsslein, K.; Tew, G. N. *J. Am. Chem. Soc.* **2008**, *130*, 9836–9843.

(196) Allen, M. J.; Raines, R. T.; Kiessling, L. L. *J. Am. Chem. Soc.* **2006**, *128*, 6534–6535.

(197) Nguyen, H. V. T.; Chen, Q.; Paletta, J. T.; Harvey, P.; Jiang, Y.; Zhang, H.; Boska, M. D.; Ottaviani, M. F.; Jasanoff, A.; Rajca, A.; Johnson, J. A. *ACS Cent. Sci.* **2017**, *3*, 800–811.

(198) Shibuya, Y.; Johnson, J. A. *ACS Macro Lett.* **2017**, *6*, 963–968.

(199) Peer, D.; Karp, J. M.; Hong, S.; Farokhzad, O. C.; Margalit, R.; Langer, R. *Nat. Nanotechnol.* **2007**, *2*, 751–760.

(200) Ai, B. H.; Flask, C.; Weinberg, B.; Shuai, X.; Pagel, M. D.; Farrell, D.; Duerk, J.; Gao, J. *Adv. Mater.* **2005**, *17*, 1949–1952.

(201) Sowers, M. A.; Mccombs, J. R.; Wang, Y.; Paletta, J. T.; Morton, S. W.; Dreaden, E. C.; Boska, M. D.; Ottaviani, M. F.; Hammond, P. T.; Rajca, A.; Johnson, J. A. *Nat. Commun.* **2014**, *5*, 1–9.

(202) Stenzel, M. H.; Barner-kowollik, C. *Mater. Horizons* **2016**, *3*, 471–477.

(203) Braunecker, W. A.; Matyjaszewski, K. *Prog. Polym. Sci.* **2007**, *32*, 93–146.

(204) Szwarc, M.; Levy, M.; Milkovich, R. *Nature* **1956**, *78*, 2656–2657.

(205) Nicolas, J.; Guillaneuf, Y.; Lefay, C.; Bertin, D.; Gigmes, D.; Charleux, B. *Prog. Polym. Sci.* **2013**, *38*, 63–235.

(206) Rizzardo, E.; Solomon, D. H.; Organic, A. *Polym. Bull.* **1988**, *534*, 529–534.

(207) Tebben, L.; Studer, A. *Angew. Chem. Int. Ed.* **2011**, *50*, 5034–5068.

(208) Simula, A.; Aguirre, M.; Ballard, N.; Veloso, A.; Leiza, J. R.; van Es, S.; Asua, J. M. *Polym. Chem.* **2017**, *8*, 1728–1736.

(209) Wang, J. S.; Matyjaszewski, K. *J. Am. Chem. Soc.* **1995**, *117*, 5614–5615.

(210) Braunecker, W. A.; Brown, W. C.; Morelli, B. C.; Tang, W.; Poli, R.; Matyjaszewski, K. *Macromolecules* **2007**, *40*, 8576–8585.

(211) Ran, J.; Wu, L.; Zhang, Z.; Xu, T. *Prog. Polym. Sci.* **2014**, *39*, 124–144.

(212) Siegwart, D. J.; Oh, J. K.; Matyjaszewski, K. *Prog. Polym. Sci.* **2012**, *37*, 18–37.

(213) Zhao, W.; Liu, F.; Chen, Y.; Bai, J.; Gao, W. *Polymer.* **2015**, *66*, A1–A10.

(214) Hussain, A. F.; Rune, H.; Kampmeier, F.; Weissbach, T.; Licha, K.; Kratz, F.; Haag, R.; Caldero, M.; Barth, S. *Biomacromolecules* **2013**, *14*, 2510–2520.

(215) Cacioli, P.; Hawthorne, D. G.; Laslett, R. L.; Rizzardo, E.; Solomon, D. H.; Hawthorne, D. G.; Laslett, R. L.; Rizzardo, E.; Solomon, D. H. *J. Macromol. Sci. Part A - Chem.* **2006**, *23*, 839–852.

(216) Moad, G.; Chiefari, J.; Chong, B. Y. K.; Krstina, J.; Mayadunne, R. T. A.; Postma, A.; Rizzardo, E.; Thang, S. H. *Polym. Int.* **2000**, *49*, 993–1001.

(217) Mayadunne, R. T. A.; Rizzardo, E.; Chiefari, J.; Chong, Y. K.; Moad, G.; Thang, S. H. *Macromolecules* **1999**, *32*, 6977–6980.

(218) Moad, G.; Rizzardo, E.; Thang, S. H. *Polymer.* **2008**, *49*, 1079–1131.

(219) Wang, Y. S.; Youngster, S.; Bausch, J.; Zhang, R.; McNemar, C.; Wyss, D. F. *Biochemistry* **2000**, *39*, 10634–10640.

(220) Pepinsky, R. B.; LePage, D. J.; Gill, A.; Chakraborty, A.; Vaidyanathan, S.; Green, M.; Baker, D. P.; Whalley, E.; Hochman, P. S.; Martin, P. *J. Pharmacol. Exp. Ther.* **2001**, *297*, 1059–1066.

(221) Soyez, H.; Schacht, E.; Vanderkerken, S. *Adv. Drug Deliv. Rev.* **1996**, *21*, 81–106.

(222) Grover, G. N.; Maynard, H. D. *Curr. Opin. Chem. Biol.* **2010**, *14*, 818–827.

(223) McDowall, L.; Chen, G.; Stenzel, M. H. *Macromol. Rapid Commun.* **2008**, *29*, 1666–1671.

(224) Ladmiral, V.; Monaghan, L.; Mantovani, G.; Haddleton, D. M. *Polymer.* **2005**, *46* (19 SPEC.

ISS.), 8536–8545.

(225) Ruehl, J.; Morimoto, C.; Stevens, D. J.; Braslau, R. *React. Funct. Polym.* **2008**, *68*, 1563–1577.

(226) Tao, L.; Liu, J.; Xu, J.; Davis, T. P. *Org. Biomol. Chem.* **2009**, *7*, 3481–3485.

(227) Sayers, C. T.; Mantovani, G.; Ryan, S. M.; Randev, R. K.; Keiper, O.; Leszczyszyn, O. I.; Blindauer, C.; Brayden, J.; Haddleton, D. M. *Soft Matter* **2009**, *5*, 3038–3046.

(228) Goodson, R. J.; Katre, N. V. *Bio/Technology* **1990**, *8*, 343–346.

(229) Shiu, H. Y.; Chan, T. C.; Ho, C. M.; Liu, Y.; Wong, M. K.; Che, C. M. *Chem. - A Eur. J.* **2009**, *15*, 3839–3850.

(230) Jung, B.; Theato, P. *Adv. Polym. Sci.* **2013**, *253*, 37–70.

(231) Bays, E.; Tao, L.; Chang, C. W.; Maynard, H. D. *Biomacromolecules* **2009**, *10*, 1777–1781.

(232) Mantovani, G.; Lecolley, F.; Tao, L.; Haddleton, D. M.; Clerx, J.; Cornelissen, J. J. L. M.; Velonia, K. *J. Am. Chem. Soc.* **2005**, *127*, 2966–2973.

(233) Le Droumaguet, B.; Nicolas, J. *Polym. Chem.* **2010**, *1*, 563.

(234) Bontempo, D.; Heredia, K. L.; Fish, B. A.; Maynard, H. D. *J. Am. Chem. Soc.* **2004**, *126*, 15372–15373.

(235) Liu, J.; Bulmus, V.; Barner-Kowollik, C.; Stenzel, M. H.; Davis, T. P. *Macromol. Rapid Commun.* **2007**, *28*, 305–314.

(236) Heredia, K. L.; Bontempo, D.; Ly, T.; Byers, J. T.; Halstenberg, S.; Maynard, H. D. *J. Am. Chem. Soc.* **2005**, *127*, 16955–16960.

(237) Boyer, C.; Bulmus, V.; Liu, J.; Davis, T. P.; Stenzel, M. H.; Barner-Kowollik, C. *J. Am. Chem. Soc.* **2007**, *129*, 7145–7154.

(238) Tasdelen, M. A.; Kahveci, M. U.; Yagci, Y. *Prog. Polym. Sci.* **2011**, *36*, 455–567.

(239) Saegusa, T.; Kobayashi, S.; Yamada, A. *Makromol. Chem.* **1976**, *177*, 2271–2283.

(240) Hoogenboom, R.; Fijten, M. W. M.; Schubert, U. S. *J. Polym. Sci. Part A Polym. Chem.* **2004**, *42*, 1830–1840.

(241) Mueller, P.; Woerner, C.; Muelhaupt, R. *Macromol. Chem. Phys.* **1995**, *196*, 1929–1936.

(242) Delaittre, G.; Guimard, N. K.; Barner-Kowollik, C. *Acc. Chem. Res.* **2015**, *48*, 1296–1307.

(243) Gandini, A. *Prog. Polym. Sci.* **2013**, *38*, 1–29.

(244) Hall, D. J.; Van Den Berghe, H. M.; Dove, A. P. *Polym. Int.* **2011**, *60*, 1149–1157.

(245) Sanyal, A. *Macromol. Chem. Phys.* **2010**, *211*, 1417–1425.

(246) Dietrich, M.; Delaittre, G.; Blinco, J. P.; Inglis, A. J.; Bruns, M.; Barner-Kowollik, C. *Adv. Funct. Mater.* **2012**, *22*, 304–312.

(247) Pfeifer, S.; Lutz, J.-F. *Chem. Eur. J.* **2008**, *14*, 10949–10957.

(248) Lowe, A. B. *Polym. Chem.* **2010**, *1*, 17–36.

(249) Melandri, D.; Montevecchi, P. C.; Navacchia, M. L.; O, C. *Tetrahedron* **1999**, *55*, 12227–12236.

(250) Boyer, C.; Boutevin, G.; Robin, J. J.; Boutevin, B. *Polymer.* **2004**, *45*, 7863–7876.

(251) Carrot, G.; Hilborn, J.; Hedrick, J. L.; Trollsås, M. *Macromolecules* **1999**, *32*, 5171–5173.

(252) Roth, P. J.; Boyer, C.; Lowe, A. B.; Davis, T. P. *Macromol. Rapid Commun.* **2011**, *32*, 1123–1143.

(253) Matsumura, S.; Hlil, A. R.; Lepiller, C.; Gaudet, J.; Guay, D.; Shi, Z.; Holdcroft, S.; Hay, A. S. *Am. Chem. Soc. Polym. Prepr. Div. Polym. Chem.* **2008**, *49*, 511–512.

(254) Wendler, F.; Rudolph, T.; Görls, H.; Jasinski, N.; Trouillet, V.; Barner-kowollik, C.; Schacher, F. H. *Polym. Chem* **2016**, *7*, 2419–2426.

(255) Stanford, M. J.; Pflughaupt, R. L.; Dove, A. P. *Macromolecules* **2010**, *43*, 6538–6541.

(256) Pounder, R. J.; Stanford, M. J.; Brooks, P.; Richards, S. P.; Dove, A. P. *Chem. Commun.* **2008**, 5158–5160.

(257) Nawroth, J. F.; Mcdaniel, J. R.; Chilkoti, A.; Jordan, R.; Luxenhofer, R. *Macromol. Biosci.* **2016**, *16*, 322–333.

(258) Mantovani, G.; Lecolley, F.; Tao, L.; Haddleton, D. M.; Clerx, J.; Cornelissen, J. J. L. M.; Velonia, K. *J. Am. Chem. Soc.* **2005**, *127*, 2966–2973.

(259) Shimano, Y.; Sato, K.; Kobayashi, S. *J. Polym. Sci. Part A Polym. Chem.* **1995**, *33*, 2715–2723.

(260) Hsiue, G.; Chiang, H.; Wang, C.; Juang, T. *Bioconjug. Chem.* **2006**, *17*, 781–786.

(261) De La Rosa, V. R.; Zhang, Z.; De Geest, B. G.; Hoogenboom, R. *Adv. Funct. Mater.* **2015**, *25*, 2511–2519.

(262) Hartlieb, M.; Floyd, T.; Cook, A. B.; Sanchez-cano, C.; Catrouillet, S.; Burns, J. A.; Perrier, S. *Polym. Chem* **2017**, *8*, 2041–2054.

(263) Koshkina, O.; Westmeier, D.; Lang, T.; Bantz, C.; Hahlbrock, A.; Würth, C.; Resch-Genger, U.; Braun, U.; Thiermann, R.; Weise, C.; Eravci, M.; Mohr, B.; Schlaad, H.; Stauber, R. H.; Docter, D.; Bertin, A.; Maskos, M. *Macromol. Biosci.* **2016**, 1287–1300.

(264) Koshkina, O.; Lang, T.; Thiermann, R.; Docter, D.; Stauber, R. H.; Secker, C.; Schlaad, H.; Weidner, S.; Mohr, B.; Maskos, M.; Bertin, A. *Langmuir* **2015**, *31*, 8873–8881.

(265) Lehmann, T.; Rühe, J. *Macromol. Symp.* **1999**, *142*, 1–12.

(266) Goethals, F.; Frank, D.; Du Prez, F. *Prog. Polym. Sci.* **2017**, *64*, 76–113.

(267) Alvaradejo, G. G.; Glassner, M.; Hoogenboom, R.; Delaittre, G. *RSC Adv.* **2018**, *8*, 9471–9479.

(268) Bouten, P. J. M.; Hertsen, D.; Vergaelen, M.; Monnery, B. D.; Boerman, M. A.; Goossens, H.; Catak, S.; van Hest, J. C. M.; Van Speybroeck, V.; Hoogenboom, R. *Polym. Chem.* **2015**, *6*, 514–518.

(269) Miyamoto, M.; Naka, K.; Shiozaki, M.; Chujo, Y.; Saegusa, T. *Macromolecules* **1990**, *23*, 3201–3205.

(270) Tong, J.; Luxenhofer, R.; Yi, X.; Jordan, R.; Kabanov, A. V. *Mol. Pharm.* **2010**, *7*, 984–992.

(271) Bontempo, D.; Heredia, K. L.; Fish, B. A.; Maynard, H. D. *J. Am. Chem. Soc.* **2004**, *126*, 15372–15373.

(272) Morgese, G.; Benetti, E. M. *Eur. Polym. J.* **2017**, *88*, 470–485.

(273) Tauhardt, L.; Kempe, K.; Gottschaldt, M.; Schubert, U. S. *Chem. Soc. Rev.* **2013**, *42*, 7998–8011.

(274) Hyon, S.; Cha, W.; Ikada, Y. *Polym. Bull.* **1987**, *29*, 119–126.

(275) Mansfield, E. D. H.; Sillence, K.; Hole, P.; Williams, A. C.; Khutoryanskiy, V. V. *Nanoscale* **2015**, *7*, 13671–13679.

(276) Haensch, C.; Erdmenger, T.; Fijten, M. W. M.; Hoeppener, S.; Schubert, U. S. *Langmuir* **2009**, *25*, 8019–8024.

(277) Yoshikawa, S.; Tsubokawa, N. *Polym. J.* **1996**, *28*, 317–322.

(278) Yoshikawa, S.; Tsubokawa, N.; Fujiki, K.; Sakamoto, M. *Compos. Interfaces* **1999**, *6*, 395–407.

(279) Hoogenboom, R. *Macromol. Chem. Phys.* **2007**, *208*, 18–25.

(280) Groß, A.; Maier, G.; Nuyken, O. *Macromol. Chem. Phys.* **1996**, *197*, 2811–2826.

(281) Kobayashi, S.; Kaku, M.; Sawada, S.; Saegusa, T. *Polym. Bull.* **1985**, *13*, 447–451.

(282) Weber, C.; Babiuch, K.; Rogers, S.; Perevyazko, I. Y.; Hoogenboom, R.; Schubert, U. S. *Polym. Chem.* **2012**, *3*, 2976.

(283) Shoda, S. -I; Masuda, E.; Furukawa, M.; Kobayashi, S. *J. Polym. Sci. Part A Polym. Chem.* **1992**, *30*, 1489–1494.

(284) Weber, C.; Remzi Becer, C.; Guenther, W.; Hoogenboom, R.; Schubert, U. S. *Macromolecules* **2010**, *43*, 160–167.

(285) Gao, A. X.; Liao, L.; Johnson, J. A. *ACS Macro Lett.* **2014**, *3*, 854–857.

(286) Liu, J.; Burts, A. O.; Li, Y.; Zhukhovitskiy, A. V.; Ottaviani, M. F.; Turro, N. J.; Johnson, J. A. *J. Am. Chem. Soc.* **2012**, *134*, 16337–16344.

(287) Matsumoto, K. I.; Hyodo, F.; Matsumoto, A.; Koretsky, A. P.; Sowers, A. L.; Mitchell, J. B.; Krishna, M. C. *Clin. Cancer Res.* **2006**, *12*, 2455–2462.

(288) Zhelev, Z.; Bakalova, R.; Aoki, I.; Matsumoto, K. I.; Gadjeva, V.; Anzai, K.; Kanno, I. *Mol. Pharm.* **2009**, *6*, 504–512.

(289) Keana, J. F. W.; Pou, S.; Rosen, G. M. *Magn. Reson. Med.* **1987**, *5*, 525–536.

(290) Swaminathan, S.; Horn, T. D.; Pellowski, D.; Abul-Ezz, S.; Bornhorst, J. A.; Viswamitra, S.; Shah, S. V. *N. Engl. J. Med.* **2007**, *357*, 720–722.

(291) Hyodo, F.; Matsumoto, K. I.; Matsumoto, A.; Mitchell, J. B.; Krishna, M. C. *Cancer Res.* **2006**, *66*, 9921–9928.

(292) Rajca, A.; Wang, Y.; Boska, M.; Paletta, J. T.; Olankitwanit, A.; Swanson, M. A.; Mitchell, D. G.; Eaton, S. S.; Eaton, G. R.; Rajca, S. *J. Am. Chem. Soc.* **2012**, *134*, 15724–15727.

(293) Burts, A. O.; Li, Y.; Zhukhovitskiy, A. V.; Patel, P. R.; Grubbs, R. H.; Ottaviani, M. F.; Turro, N. J.; Johnson, J. A. *Macromolecules* **2012**, *45*, 8310–8318.

(294) Xia, Y.; Grubbs, R. H. *Macromolecules* **2009**, *50*, 197–198.

(295) Davis, R. M.; Matsumoto, S.; Bernardo, M.; Sowers, A.; Matsumoto, K. I.; Krishna, M. C.; Mitchell, J. B. *Free Radic. Biol. Med.* **2011**, *50*, 459–468.

(296) Rajca, A.; Wang, Y.; Boska, M.; Paletta, J. T.; Olankitwanit, A.; Swanson, M. A.; Mitchell, D. G.; Eaton, S. S.; Eaton, G. R.; Rajca, S. *J. Am. Chem. Soc.* **2014**, *136*, 3318.

(297) EvaluatePharma. Evaluate Pharma 2015.

(298) Harris, J. M.; Martin, N. E.; Modi, M. *Clin. Pharmacokinet.* **2001**, *40*, 539–551.

(299) Harris, J. M.; Chess, R. B. *Nat. Rev. Drug Discov.* **2003**, *2*, 214–221.

(300) Manning, M. C.; Patel, K.; Borchardt, R. T. *Pharm. Res.* **1989**, *6* , 903–918.

(301) Biedermann, F.; Rauwald, U.; Zayed, J. M.; Scherman, O. A. *Chem. Sci.* **2011**, *2*, 279–286.

(302) Lucius, M.; Falatach, R.; McGlone, C.; Makaroff, K.; Danielson, A.; Williams, C.; Nix, J. C.; Konkolewicz, D.; Page, R. C.; Berberich, J. A. *Biomacromolecules* **2016**, *17*, 1123–1134.

(303) Katre, N. V. *Adv. Drug Deliv. Rev.* **1993**, *10*, 91–114.

(304) da Silva Freitas, D.; Abrahao-Neto, J. *Int. J. Pharm.* **2010**, *392*, 111–117.

(305) Morgenstern, J.; Baumann, P.; Brunner, C.; Hubbuch, J. *Int. J. Pharm.* **2017**, *519*, 408–417.

(306) Abuchowski, A.; van Es, T.; Palczuk, N. C.; Davis, F. F. *J. Biol. Chem.* **1977**, *252*, 3578–3581.

(307) Richter, A. W.; Åkerblom, E. *Int. Arch. Allergy Immunol.* **1983**, *70*, 124–131.

(308) Sundy, J. S.; Ganson, N. J.; Kelly, S. J.; Scarlett, E. L.; Rehrig, C. D.; Huang, W.; Hershfield, M. S. *Arthritis Rheumatol.* **2007**, *56*, 1021–1028.

(309) Garay, R. P.; El-Gewely, R.; Armstrong, J. K.; Garratty, G.; Richette, P. *Expert Opinion on Drug Delivery*. 2012, pp 1319–1323.

(310) Seyfried, B. K.; Marchetti-Deschmann, M.; Siekmann, J.; Bossard, M. J.; Scheiflinger, F.; Turecek, P. L.; Allmaier, G. *Biotechnol. J.* **2012**, *7*, 635–641.

(311) Armstrong, J. K.; Hempel, G.; Koling, S.; Chan, L. S.; Fisher, T.; Meiselman, H. J.; Garratty, G. *Cancer* **2007**, *110*, 103–111.

(312) Ulbricht, J.; Jordan, R.; Luxenhofer, R. *Biomaterials 35*, 4848–4861.

(313) Pelegri-ODay, E. M.; Lin, E.-W.; Maynard, H. D. *J. Am. Chem. Soc.* **2014**, *136*, 14323–14332.

(314) Knop, K.; Hoogenboom, R.; Fischer, D.; Schubert, U. S. 6288–6308.

(315) Ozer, I.; Chilkoti, A. **2017**.

(316) Krishna, O. D.; Kiick, K. L. *Pept. Sci.* **2010**, *94*, 32–48.

(317) Favier, A.; Charreyre, M. T.; Pichot, C. *Polymer.* **2004**.

(318) Karagoz, B.; Esser, L.; Duong, H. T.; Basuki, J. S.; Boyer, C.; Davis, T. P. *Polym. Chem.* **2014**, *5*, 350–355.

(319) Seely, J. E.; Richey, C. W. *J. Chromatogr. A* **2001**, *908*, 235–241.

(320) Yoshimoto, N.; Yamamoto, S. *Biotechnol. J.* **2012**, *7*, 592–593.

(321) Morgenstern, J.; Wang, G.; Baumann, P.; Hubbuch, J. *Biotechnol. J.* **2017**.

(322) Morgenstern, J.; Busch, M.; Baumann, P.; Hubbuch, J. *J. Chromatogr. A* **2016**, *1462*, 153–164.

(323) Baumgartner, K.; Galm, L.; Nötzold, J.; Sigloch, H.; Morgenstern, J.; Schleining, K.; Suhm, S.; Oelmeier, S. A.; Hubbuch, J. *Int. J. Pharm.* **2015**, *479*, 28–40.

(324) Hennink, W. E.; Nostrum, C. F. Van. *Adv. Drug Deliv. Rev.* **2012**, *64*, 223–236.

(325) Hoffman, A. S. *Adv. Drug Deliv. Rev.* **2012**, *64*, 18–23.

(326) Galm, L.; Morgenstern, J.; Hubbuch, J. *Int. J. Pharm.* **2015**, *494*, 370–380.

(327) McArthur, S. L. *Surf. Interface Anal.* **2006**, *38*, 1380–1385.

(328) Scofield, J. H. *J. Electron Spectros. Relat. Phenomena* **1976**, *8*, 129–137.

(329) Love, J. A.; Morgan, J. P.; Trnka, T. M.; Grubbs, R. H. *Angew. Chemie - Int. Ed.* **2002**, *41*, 4035–4037.

(330) Smith, R. D.; Loo, J. A.; Edmonds, C. G.; Barinaga, C. J.; Udseth, H. R. *Anal. Chem.* **1990**, *62*, 882–899.

(331) Skrabania, K.; Miasnikova, A.; Bivigou-Koumba, A. M.; Zehm, D.; Laschewsky, A. *Polym. Chem.* **2011**, *2*, 2074–2083.

Abbreviation List

a.u.	arbitraty units
AIBN	2,2'-azobis(2-methylpropionitrile)
anti-PEG	antibodies against PEG
ATRP	atom transfer radical polymerization
b	block
BASP	brush-arm star polymer
BSA	Bovine serum albumin
C	Celsius
CROP	cationic ring-opening polymerization
CT	camptothecin
CTA	chain transfer agent
CuAAC	copper-catalyzed azide–alkyne cycloaddition
Đ	dispersity
Da	Dalton
DCM	dichloromethane
DLS	dynamic light scattering
DMAc	dimethylacetamide
DMAP	4-dimethylaminopyridine
DMF	dimethylformamide
DMPP	dimethylphenylphosphine

DNA	deoxyrribonucleic acid
DOX	doxorubicin
DP	degree of polymerization
DTB	dithiobenzoate
ESI-MS	electrospray ionization mass spectrometry
EtOx	2-ethyl-2-oxazoline
EVE	ethyl vinyl ether
FDA	Food and Drug Administration
HPMA	*N*-(2-hydroxypropyl) methacrylamide
k_p	propagation rate constant
LCST	lower critical solution temperature
M	molar
MM	macromonomer
M_n	number-average molar mass
MRI	magnetic resonance imaging
M_w	number-average molecular weight
NAP	natural antimicrobial peptides
NHS	*N*-hydroxysuccinimide
NMP	nitroxide-mediated polymerization
NMR	nuclear magnetic resonance
ORCA	organic radical contrast agent
PAOx	poly(2-alkyl-2-oxazoline)s

PCBMA	poly(carboxybetaine methacrylate)
PEG	polyethylene glycol
PEGA	poly(ethylene glycol acrylate)
PEtOx	poly(2-ethyl-2-oxazoline)
PG	polyglycerol
PGA	polyglutamic acid
PHEA	poly(hydroxyethyl-*L*-asparagine)
PHEG	poly(hydroxyethyl-*L*-glutamine)
PHPMA	poly(*N*-(2-hydroxypropyl)methacrylamide)
PISA	polymerization induced self-assembly
PLA	polylactic acid
PMeOx	poly(2-methyl-2-oxazoline)
PNAM	poly(*N*-acryloyl morpholine)
POEGMA	poly(oligo(ethylene glycol) methyl ether methacrylate)
ppm	part per million
PRE	persistent radical effect
PSA	polysialic acid
pSar	poly(sarcosine)
PSBMA	poly(sulfobetaine methacrylate)
PVP	poly(vinylpyrrolidone)
RAFT	reversible addition-fragmentation chain transfer
RDRP	reversible deactivation radical polymerization

RNA	ribonucleic acid
ROMP	ring-opening metathesis polymerization
RT	room temperature
SEC	size exclusion chromatography
SDS-PAGE	sodium dodecyl sulfate polyacrylamide gel electrophoresis
TEA	triethylamine
THF	tetrahydrofuran
wt%	weight%
XPS	X-ray photoelectron spectroscopy
δ	chemical shift
λ	wavelength

List of Figures

List of Schemes

List of Tables

Publications

Publications arising from the present thesis

- Gabriela Gil Alvaradejo, Hung V.T. Nguyen, Guillaume Delaittre, Jeremiah A. Johnson. Polyoxazoline- and nitroxide-based macromolecular contrast agents. *In preparation*
- Gabriela Gil Alvaradejo, Mathias Glassner, Sylwia Sekula-Neuner, Vanessa Trouillet, Michael Hirtz, Richard Hoogenboom, Guillaume Delaittre. Thioacetate-based initiators for the synthesis of thiol-capped poly(2-oxazoline)s. *In preparation*.
- Gabriela Gil Alvaradejo, Josefine Morgenstern, Nicolai Bluthardt, Guillaume Delaittre, Jürgen Hubbuch. PNAM and POEGMA conjugates as alternatives to protein PEGylation. *In preparation*.
- Gabriela Gil Alvaradejo, Mathias Glassner, Richard Hoogenboom, Guillaume Delaittre. Maleimide end-functionalized poly(2-oxazoline)s by the functional initiator route: synthesis and (bio)conjugation. *RSC Adv.* 2018, DOI: 10.1039/c8ra00948a

Additional publications

- Gil-Alvaradejo, G., Ruiz-Arellano, R., Owen, C. Rodríguez-Romero, A., Rudiño-Piñera, E., Antwi, M., Stojanoff, V., and Moreno, A. Novel Protein Crystal Growth Electrochemical Cell for Applications in X-ray Diffraction and Atomic Force Microscopy. *Crystal Growth & Design*. 2011, 11 (9), 3917–392.

Conference contributions

- "Maleimide- and thiol-functionalized poly(2-oxazoline)s for bioconjugation and surface functionalization". **12th international conference on Advance Polymers via Macromolecular Engineering**. Gent, Belgium (May, 2017). Poster presenter.
- "Heterotelechelic poly(2-oxazoline)s towards the immobilization of biomolecules" **252nd American Chemical Society Meeting and Exposition**. Philadelphia, PA. USA (August, 2016). Poster presenter.
- "Polymer linkers towards the controlled immobilization of enzymes" Invited speaker at the **Mexikanische Woche der Wissenschaft und Technologie**. Student representative in the natural sciences area. Embassy of Mexico in Berlin (June, 2016). Talk.
- "Polymer linkers for the controlled immobilization of enzymes". **Innovation Match MX 2015-2016. International Forum of Mexican Talents.** Guadalajara, Mexico (March, 2016). Talk.

Acknowledgements

I want to thank Guillaume for his supervision over the last three and a half years of my PhD. Thanks for your guidance, advice, and support during this time. It has been great to be part of your group and I feel very grateful for the opportunity.

Prof. Barner-Kowollik is thanked for his constant support.

I am grateful to CONACyT for a PhD scholarship.

I am grateful to the Karlsruhe House of Young Scientists for a travel grant to visit the Johnson group at MIT.

Thanks to Jeremiah Johnson and his group at MIT. Visiting and working at MIT was a very inspiring, productive, and certainly unforgettable experience. Special thanks to Hung, Deb, Dr. Eileen, and Dr. Nate.

Thanks to Prof. Hoogenboom, and his group at Ghent University, for the great collaboration. Special thanks to Dr. Mathias Glassner for the guidance and help in the lab.

Thanks to Prof. Jürgen Hubbuch and Dr. Josefine Morgenstern, Dr. Sylwia Sekula-Neuner, Dr. Michael Hirtz, and Vanessa Trouillet. I am very grateful to you all for our collaborations.

Thanks to all members of AKGD, you guys made these last years a great experience in and out of the lab. I want to specially thank the original members of the Gryffindor Lab, Dr. Ana and Divya: we made a great team! Dr. Dao, Lin Chiang, and Ted, my lunch partners and friends, thanks for being so interesting, awesome, and so fun to be around. Thanks to Tobi, Aaron, Remi, and Moana for the good times in the office. Thanks to my master students, Nicolai Bluthard and Arijeta Osmani, for the hard work.

Thanks to all Macroarc members. Special thanks also to Hatice M., Dr. Eva, Dr. Siham, and Dr. Charlotte.

Gracias a mis padres, Lourdes Alvaradejo y Mario Gil. No estaría aquí sin su esfuerzo por darnos lo mejor. Mamá, gracias por tu fuerza, motivación, y por inspirarme siempre para luchar por lo que creo. Papá, sé que estarías aun más orgulloso de mí. Te extraño mucho. Gracias a mi hermana, Lulú Gil, por ser mi ejemplo a seguir y mejor amiga. Gracias, familia, siempre están conmigo sin importar la distancia. Los amo.

Huey Wen, thanks for your patience, love, and great sense of humor. I love you, my rainbow-infused unicorn.

Carol and Diogo, you guys made life in Karlsruhe so much better and I am so grateful we met.

Thanks to my friends scattered around the world (you know who you are). It is great to have you all in my life. It is a small world after all.

Gracias a las familias Ochoa Magana y Camarena por el apoyo siempre.

Thanks, Sara Bareilles.